

***An in vivo and in vitro* study of stress-induced
senescence in neurones and its role in
neurodegeneration**

by

Irina Vázquez-Villaseñor

(BSc, MSc)

Submitted for the degree of Doctor of Philosophy, PhD

Sheffield Institute for Translational Neuroscience

The University of Sheffield



Abstract

Cellular senescence, characterised by the development of a toxic secretory phenotype in response to persistent DNA damage, has been studied in proliferating cells but is not well understood in post-mitotic neurones. Recent evidence showed a neuronal senescent-like state in response to persistent DNA damage *in vivo*, which could contribute to neuronal dysfunction in aging and neurodegeneration. The current study hypothesised that oxidative stress, a hallmark of neurodegeneration, activates a persistent DNA damage response and promotes neuronal senescence. To investigate this, activation of senescence in response to oxidative DNA damage was studied in human post-mitotic neurones in culture, as well as in the brains of control and ALS/MND donors.

For the *in vitro* study, post-mitotic LUHMES were stressed with a double dose of 50 μM H_2O_2 , which caused a persistent DNA damage in the form of double-strand breaks that was detectable 96 hours' post-stress. Expression of the "classical" senescence marker SA- β -gal and formation of senescence-associated heterochromatin foci (SAHF) were evaluated at the 96 hours-timepoint, using cytochemical methods. A co-culture system of double stressed LUHMES and healthy LUHMES was developed to study DNA damage propagation; gene expression profiling was used to investigate changes in known senescence pathways in 96 hours-double stressed LUHMES. Results from this study revealed a highly variable SA- β -gal activity in healthy and double stressed LUHMES; SAHF were not present in these cells and propagation of DNA damage was not seen in the co-culture system. Transcriptomic analysis of double stressed LUHMES revealed dysregulation of the APC/C:Cdh1 cell cycle regulatory pathway, ATR signalling and

mitochondrial complex I activity, which could be related to oxidative stress but not to senescence.

The current work also investigated the relevance of neuronal senescence in neurodegeneration. “Classical” senescence (SA- β -gal, p16 and p21) and oxidative DNA damage markers (8-OHdG and γ H2AX) were investigated in the motor cortex, spinal cord and frontal association cortex of ALS/MND and control donors using immunohistochemistry. Transcriptome analysis of LCM neurones obtained from the frontal cortex of control and ALS/MND donors was used to investigate early changes in gene expression that could be linked to a senescent-like state.

Transcriptomic analysis suggested dysregulation of DDR, cell cycle and oxidative phosphorylation pathways as a consequence of the persistent oxidative DNA damage, but no of “classical” senescence was found in the *in vitro* neuronal model. *In vivo*, p21 expression was found in neurones and glia, whereas p16 was exclusively expressed in glial cells. A significantly higher percentage of p21⁺ neurones was detected in the frontal association cortex of ALS/MND donors. Transcriptome analysis showed alteration of DDR pathways and mitochondrial function in these neurones, but did not reveal dysregulation of “classical” senescence pathways.

Neurones may activate a senescent-like state in response to persistent DNA damage but signalling pathways involved in this mechanism may differ from the ones described in mitotic cells. Thus, “classical” senescence markers should be used cautiously when studying neuronal senescence, as they could reflect induction of related but different mechanisms in these cells. In order to study neuronal senescence, it is necessary to understand first the cell cycle regulatory mechanisms that occur in neurones as part of the DDR.

Acknowledgements

I would like to thank my supervisor, Prof Steve Wharton, for his guidance and endless support. Thank you for trusting me to take this project forward. Under your supervision, I have acquired invaluable knowledge and skills that have helped me to improve as a scientist and as a person.

Many thanks to my second supervisor, Dr Julie Simpson. Thank you for sharing your knowledge with me, for your support and for your words of encouragement; you made me feel more confident when things were not going as planned.

I would also like to thank Dr Paul Heath for his guidance throughout my PhD, but specially during the last year. I really enjoyed this last experimental phase of my project and gained valuable knowledge on transcriptome analysis thanks to your support.

Thanks to Claire, Sarah and Laura, for your help in the lab and for your invaluable friendship.

Thank you to the Neuropathology group and to the SITraN technical team for your support during my PhD.

Special thanks go to my parents and grandparents. I would not have been able to complete this huge task without your constant encouragement and immeasurable love. Thank you also to my family in Mexico. There was not a day that I did not receive a message that reminded me of your love and support.

Thank you to my friends in Sheffield, whom I now call my family as well. Being miles away from Mexico was much easier having you around.

Thank you to Israel for accompanying me in this adventure, even when it meant leaving for a while something that I know you love deeply. It has not been easy, but your love and words of wisdom always warmed my heart, cleared my mind and inspired me to keep going.

I am grateful to Consejo Nacional de Ciencia y Tecnología (CONACyT), México and Dirección General de Relaciones Internacionales de la Secretaría de Educación Pública (DGRI SEP), México, for sponsoring my postgraduate studies.

Publications

Publications

Vazquez-Villaseñor I., Garwood C.J., Heath P.R., Simpson J.E., Ince P.G., Wharton S.B. (2018) Expression of cell cycle inhibitor p21 may indicate early activation of senescence pathways in neurons in MND. *In preparation.*

Morgan S.V., Garwood C.J., Simpson J.E., Heath P.R., Mihaylov S., **Vazquez-Villasenor I.**, Ince P.G., Dickman M., Hautbergue G.M., Wharton S.B. (2018) Proteomic analysis and localisation studies suggest non-tight junction cytoplasmic and nuclear roles for occludin in astrocytes. *In preparation.*

Ratcliffe L.E., **Vázquez-Villaseñor I.**, Jennings L., Heath P.R., Mortiboys H., Schwartzentruber A., Karyka E., Simpson J.E., Ince P.G., Garwood G.J., Wharton S.B. (2017) Loss of IGF1R in human astrocytes alters complex I activity and support for neurons. *Submitted for peer review.*

Garwood, C.J., Ratcliffe, L.E., Morgan, S. V., Simpson, J.E., Owens, H., **Vazquez-Villaseñor, I.**, Heath, P.R., Romero, I.A., Ince, P.G., and Wharton, S.B. (2015). Insulin and IGF1 signalling pathways in human astrocytes in vitro and in vivo; characterisation, subcellular localisation and modulation of the receptors. *Mol. Brain* 8.

Abstracts

Vazquez-Villasenor I., Simpson J.E., Garwood, C.J., Heath P. Ince P.G., Wharton S.B. Neuronal senescence as a contributor to neurodegeneration. (2017), Poster Abstracts. *Neuropathol Appl Neurobiol*, 43: 32–57.

Vazquez-Villasenor I., Simpson J.E., Garwood, C.J., Heath P. Ince P.G., Wharton S.B. Neuronal senescence as a contributor to neurodegeneration. (2016), *Amyotroph Lateral Scler Frontotemporal Degener*, 18(sup2).

Vazquez-Villasenor I., Simpson J.E., Garwood, C.J., Heath P. Ince P.G., Wharton S.B. Neuronal senescence as a contributor to neurodegeneration. (2016), 117th Meeting of the British Neuropathological Society Royal College of Physicians. *Neuropathol Appl Neurobiol*, 42: 5–10.

Vazquez-Villasenor I., Simpson J.E., Garwood, C.J., Heath P. Ince P.G., Wharton S.B. Neuronal senescence as a contributor to neurodegeneration. (2015), Poster Presentations. *Neuropathol Appl Neurobiol*, 41: 30–58.

TABLE OF CONTENTS

Abstract	I
Acknowledgements	III
Publications	V
List of Figures	XIV
List of Tables	XIX
List of Abbreviations	XXIII
Chapter 1. General introduction	1
1.1. The biology of cellular senescence	1
1.1.1. Characteristics of senescent cells: effector pathways and the SASP.....	2
1.1.1.1. Senescence-associated cell cycle arrest induction via p53/p21 and p16/pRB signalling	3
1.1.1.2. The senescence-associated secretory phenotype (SASP)	7
1.1.2. Biomarkers of cellular senescence	12
1.1.2.1. DNA damage, DDR and cell cycle arrest markers	12
1.1.2.2. Senescence-associated- β -galactosidase	13
1.1.2.3. Senescence-associated heterochromatin foci (SAHF)	14
1.2. Senescence in ageing and age-related diseases	16
1.2.1. Senescence in brain ageing and in neurodegeneration	19
1.2.1.1. Senescence in astrocytes and microglia.....	19
1.2.1.2. The paradox of neuronal senescence	20
1.3. Amyotrophic Lateral Sclerosis	24
1.4. Hypothesis	27
1.4.1. Aims	27
Chapter 2. Development and characterisation of an <i>in vitro</i> model of oxidative DNA damage in human neurones	28
2.1. Introduction	28
2.2. Aims and objectives	30
2.3. Materials and Methods	30
2.3.1. LUHMES cell culture optimisation.....	30
2.3.1.1. LUHMES maintenance and differentiation: Optimisation of cell culture conditions.....	31
2.3.1.2. MTT reduction assay	34
2.3.2. Characterisation of differentiated neurones by immunocytochemistry.....	34

2.3.3. Optimisation of H ₂ O ₂ treatments.....	38
2.3.3.1. Cell viability assays to assess H ₂ O ₂ -induced toxicity.....	38
2.3.3.2. Immunocytochemical detection of double strand breaks (DSBs).....	39
2.3.4. Double stress model.....	39
2.3.4.1. H ₂ O ₂ clearance: pHPA extracellular H ₂ O ₂ assay.....	39
2.3.4.2. Induction of a persistent oxidative DNA damage.....	43
2.3.5. Statistical analysis.....	44
2.4. Results.....	45
2.4.1. Optimisation of LUHMES culturing conditions.....	45
2.4.2. LUHMES can be successfully differentiated into post-mitotic neurones following a two-step differentiation protocol.....	49
2.4.3. Induction of oxidative stress in post-mitotic LUHMES in vitro.....	53
2.4.3.1. Assessing cell viability and metabolic activity in H ₂ O ₂ -treated LUHMES.....	53
2.4.3.1.1. H ₂ O ₂ induced oxidative DNA damage is repaired in differentiated LUHMES.....	56
2.4.4. Development of a persistent DNA damage model in post-mitotic LUHMES.....	59
2.4.4.1. H ₂ O ₂ clearance by LUHMES.....	59
2.4.4.2. A second H ₂ O ₂ treatment causes a persistent decrease in LUHMES' viability for up to 96 hours.....	62
2.4.4.3. A second H ₂ O ₂ treatment causes persistent DSBs in differentiated LUHMES.....	63
2.5. Discussion.....	65
2.5.1. Optimisation of LUHMES cell culture.....	65
2.5.2. Following a 2-step differentiation protocol, LUHMES reach a complete post-mitotic phenotype.....	68
2.5.3. Development of an in vitro model of oxidative stress in differentiated LUHMES.....	70
2.5.4. Establishment of a model of persistent DNA damage in LUHMES using H ₂ O ₂	73
2.6. Main conclusions.....	75
Chapter 3. Investigating induction of senescence in the LUHMES single and double stress models.....	77
3.1. Introduction.....	77
3.2. Aims and objectives.....	78
3.3. Materials and methods.....	78
3.3.1. Double –stress model in post-mitotic LUHMES.....	79
3.3.2. Detection of common senescence markers in single/double stressed LUHMES.....	79
3.3.2.1. Senescence associated – β – galactosidase (SA- β - gal) activity.....	80
3.3.2.2. Immunocytochemistry.....	80
3.3.2.2.1. Detection of senescence-associated heterochromatin foci (SAHF).....	80
3.3.3. Induction of a SASP.....	81

3.3.3.1. Effect of stressed cells conditioned media on viability of healthy LUHMES	81
3.3.3.2. Effect of stressed cells conditioned media on neurite outgrowth of healthy LUHMES	82
3.3.3.3. Healthy GFP-LUHMES/stressed LUHMES co-culture	82
3.3.3.3.1. GFP-LUHMES production	82
3.3.3.3.2. GFP-LUHMES/non-transduced LUHMES co-culture optimisation	83
3.3.3.3.3. Neurite outgrowth assays in GFP-LUHMES co-cultured with stressed LUHMES	83
3.3.3.3.4. Detection of DSBs formation in GFP-LUHMES co-cultured with stressed LUHMES	84
3.3.4. Statistical analysis	84
3.4. Results.....	84
3.4.1. SA- β -gal activity in differentiated LUHMES	84
3.4.2. Formation of heterochromatin foci (SAHFs) in single/double stressed LUHMES.....	88
3.4.3. DS-LUHMES have a detrimental effect on healthy LUHMES suggesting propagation of injury	90
3.4.4. GFP-LUHMES/non-transduced LUHMES co-culture optimisation.....	93
3.4.5. Neurite outgrowth assays in GFP-LUHMES co-cultured with stressed LUHMES.....	94
3.4.6. DNA damage under co-culture conditions	96
3.5. Discussion	98
3.5.1. SA- β -gal activity is present in untreated and stressed LUHMES	98
3.5.2. Heterochromatin foci (SAHFs) are not present in SS or DS-LUHMES	101
3.5.3. Do LUHMES develop a secretory phenotype in response to persistent DNA damage?..	103
3.6. Main conclusions.....	108
Chapter 4. Transcriptome analysis of single and double stressed LUHMES	109
4.1. Introduction	109
4.2. Aims and objectives	111
4.3. Materials and methods	112
4.3.1. Transcriptome analysis of stressed LUHMES	112
4.3.2. Trizol RNA extraction.....	112
4.3.2.1. RNA amplification and microarray hybridisation	113
4.3.2.2. Microarray data quality control	115
4.3.2.3. Microarray data analysis.....	115
4.3.2.4. qRT-PCR validation of microarray genes of interest	115
4.3.2.5. Functional validation of microarray genes of interest	118
4.3.2.5.1. Detection of Ki67 and MCM2 expression in DS-LUHMES	118
4.3.2.5.2. Investigating Complex I activity in DS-LUHMES	119
4.4. Results.....	121
4.4.1. Integrity of purified RNA from control and stressed LUHMES	121
4.4.2. RNA preparation for microarray analysis	123

4.4.3. Microarray data quality control (QC) overview	126
4.4.3.1. Sample quality	127
4.4.3.1.1. Labelling controls	127
4.4.3.1.2. 3'/5' ratio for β -actin and GAPDH	129
4.4.3.2. Hybridisation and signal quality	130
4.4.3.2.1. Spike-in eukaryotic hybridisation controls	130
4.4.3.2.2. Percent present (% P).....	131
4.4.3.3. Signal comparability.....	132
4.4.4. Microarray data analysis	133
4.4.4.1. Clustering Analysis	133
4.4.5. Candidate analysis.....	137
4.4.5.1. Functional Enrichment Analysis using DAVID Bioinformatics Tool.....	137
4.4.5.2. Pathway enrichment analysis using IMPaLA.....	142
4.4.6. Pathways of interest	146
4.4.6.1. Cell cycle.....	146
4.4.6.2. DNA damage response	148
4.4.6.3. Metabolism.....	149
4.4.6.4. Inflammation and immune response.....	150
4.4.6.5. Cellular responses to stress.....	152
4.4.7. Validation of candidate genes by qRT-PCR	153
4.4.7.1. Validation of DNA damage response genes	154
4.4.7.2. Validation of APC/C:Cdh1 complex genes.....	155
4.4.7.3. Validation of oxidative phosphorylation genes	155
4.4.7.4. Validation of RIG-I-like signalling pathway genes	156
4.4.8. Functional validation of dysregulated pathways	157
4.4.8.1. Assessing cell cycle re-activation in DS-LUHMES	157
4.4.8.2. Assessing complex I dysfunction in DS-LUHMES	159
4.5. Discussion	160
4.5.1. H ₂ O ₂ induces changes in the transcriptome of DS-LUHMES.....	160
4.5.1.1. DNA damage response and cell cycle regulation	162
4.5.1.1.1. ATR-signalling pathway.....	162
4.5.1.1.2. Cell cycle regulation: APC/C-Cdh1 complex.....	166
4.5.1.2. Mitochondrial dysfunction	168
4.5.1.3. Immune response.....	171
4.6. Main conclusions.....	174
Chapter 5. Relevance of neuronal senescence <i>in vivo</i>: DNA damage and senescence in the brain of ALS/MND patients.....	175
5.1. Introduction	175

5.2. Aims and objectives	176
5.3. Materials and methods	177
5.3.1.1. Human Brain Tissue	177
5.3.1.1.1. Classification of ALS/MND cases based on p62 pathology in the FACx	180
5.3.1.2. Detection of senescence associated- β -galactosidase (SA- β -gal) activity in post-mortem tissue	180
5.3.1.3. Immunohistochemistry	181
5.3.1.3.1. Senescence markers p16 and p21	181
5.3.1.3.1.1. Double labelling to identify the cell type expressing p16 and p21	182
5.3.1.3.2. Oxidative DNA damage markers 8-OHdG and γ H2AX.....	184
5.3.1.3.3. MHC class II and CD68 staining	184
5.3.1.4. Quantitative analysis	185
5.3.1.4.1. p21 ⁺ , p16 ⁺ and 8-OHdG ⁺ cells	185
5.3.1.4.2. Quantification of γ H2AX ⁺ cells.....	186
5.3.1.4.3. Quantification of MHC class II and CD68 staining.....	187
5.3.1.5. Statistical analysis of immunohistochemical staining	187
5.3.2. Transcriptome analysis of FACx neurones from ALS/MND and control donors.....	188
5.3.2.1. Checking for RNA quality from tissue for microarray.....	188
5.3.2.2. Laser capture microdissection (LCM) of neurones from the FACx	189
5.3.2.3. RNA isolation from LCM samples.....	190
5.3.2.3.1. Confirmation of neuronal enrichment.....	190
5.3.2.4. RNA amplification and microarray hybridisation	191
5.3.2.5. Microarray data quality control	192
5.3.2.6. Microarray data analysis.....	193
5.3.2.7. qRT-PCR validation of microarray genes of interest	193
5.4. Results.....	195
5.4.1. Classification of ALS/MND cases according to the p62 pathology is not linked to expression of senescence and DNA damage markers in ALS/MND cases.....	195
5.4.2. SA- β -gal activity is a feature of brains from ALS/MND and control donors	197
5.4.3. Expression of p16 is exclusive to glial cells.....	203
5.4.4. Expression of p21 is detected in glial and neuronal nuclei	206
5.4.5. Expression of p16 and p21 in the occipital cortex of ALS/MND and control donors	211
5.4.6. Detection of DNA damage and DNA damage response markers	213
5.4.6.1. γ H2AX expression in ALS/MND and control brains.....	213
5.4.6.2. 8-OHdG expression in ALS/MND and control brains	215
5.4.6.3. Association between DNA damage and senescence markers in neurones	217
5.4.7. Microglial activation in the FACx of ALS/MND cases.....	220
5.4.8. p62 pathology is not linked to the of senescence and DNA damage markers in ALS/MND cases	222

5.4.9. Microarray analysis of the neuronal transcriptome in the frontal cortex of MND patients.	225
5.4.9.1. Integrity of purified RNA from frozen tissue	225
5.4.9.2. RNA integrity from LCM neurone enriched RNA samples	227
5.4.9.3. Confirmation of neuronal enrichment in LCM samples	229
5.4.9.4. RNA preparation for microarray analysis	230
5.4.9.5. Microarray data quality control (QC) overview	232
5.4.9.5.1. Sample quality	233
5.4.9.5.1.1. Labelling controls	233
5.4.9.5.1.2. 3'/5' ratio for β -actin and GAPDH	234
5.4.9.5.2. Hybridisation and signal quality	235
5.4.9.5.2.1. Spike-in eukaryotic hybridisation controls	235
5.4.9.5.2.2. Percent present (% P)	236
5.4.9.5.3. Signal comparability	237
5.4.9.6. Microarray data analysis	239
5.4.9.6.1. Clustering Analysis	239
5.4.9.6.2. Functional annotation and pathway enrichment analysis	241
5.4.9.6.2.1. Functional Enrichment Analysis using DAVID Bioinformatics Tool	241
5.4.9.6.2.2. Pathway enrichment analysis using IMPaLA	246
5.4.9.6.2.3. Summary of DAVID and IMPaLA results	250
5.4.9.6.3. Analysis of single dysregulated transcripts with fold change $FC \geq 2.0$	252
5.5. Discussion	259
5.5.1. Oxidative DNA damage, DDR and senescence in ALS/MND	259
5.5.1.1. SA- β -gal activity is present in neurones and glia of ALS/MND and control brains	260
5.5.1.2. Expression of p16 and p21 in ALS/MND and control brains	262
5.5.1.2.1. Expression of p16 and p21 in astrocytes suggests activation of glial senescence in ALS/MND and control brains	262
5.5.1.2.2. Expression of p21 in neurones of ALS/MND and control brains	264
5.5.1.2.3. Expression of senescence markers is significantly higher in the FACx of ALS/MND brains	265
5.5.1.3. Oxidative DNA damage and the DNA damage response in ALS/MND	266
5.5.1.4. No evidence of microglial activation in the FACx of ALS/MND donors	268
5.5.2. Microarray analysis of the transcriptome of FACx neurones in ALS/MND	268
5.6. Main conclusions	272
Chapter 6. General discussion	274
6.1. Summary of major findings and limitations of the study	274
6.2. Conclusions	280
6.3. Future work	281

6.3.1. Characterisation of the ATR and the APC/C:Cdh1 complex in DS-LUHMES	281
6.3.2. Investigating a toxic secretory phenotype in DS-LUHMES	281
6.3.3. Confirmation of qRT-PCR validation results for the in vivo study	282
6.3.4. Investigating the origin of p21 expression in ALS/MND	282
6.3.5. Investigating astrocyte senescence in ALS/MND.....	283
6.3.6. Directly reprogrammed human neurones to study ageing and senescence in vitro.....	283
6.3.7. Transcriptomic analysis of LCM neurones from young and old donors	284
References.....	285
Appendices.....	314

List of Figures

Figure 1.1 Senescence inducers and signalling pathways.	6
Figure 1.2 Autocrine and paracrine effects of the SASP.	11
Figure 1.3 Classical markers of cellular senescence.	15
Figure 1.4 Hypothetical mechanism of neuronal senescence induction.	23
Figure 2.1 Optimisation of LUHMES cell culture conditions.	33
Figure 2.2 Removal of extracellular H ₂ O ₂ by LUHMES: Examples of standard curves and plots used for kobs determination.	42
Figure 2.3 LUHMES were cultured in 2 different cell culture media and differentiated using different protocols to determine the optimal culture conditions for future experiments.	48
Figure 2.4 Successful differentiation of LUHMES into post-mitotic neurones using a 2-step differentiation protocol.	51
Figure 2.5 LUHMES successfully exit the cell cycle and differentiate into post-mitotic neurones using a 2-step differentiation protocol.	52
Figure 2.6 The effect of increasing concentrations of H ₂ O ₂ on the viability of differentiated LUHMES.	55
Figure 2.7 Formation and repair of DSBs after treatment with H ₂ O ₂	57
Figure 2.8. Formation and repair of DSBs after treatment with H ₂ O ₂ (Higher power images).	58
Figure 2.9 Clearance of extracellular H ₂ O ₂ by LUHMES.	61
Figure 2.10 A second H ₂ O ₂ treatment induces a persistent decrease in metabolic activity.	62

Figure 2.11 γ H2AX foci are detectable in the double stressed LUHMES for up to 96 hours after stress.	64
Figure 3.1 SA- β -gal activity in single/double stressed LUHMES.....	86
Figure 3.2 SA- β -gal activity increases with passage number in differentiated LUHMES. A.....	87
Figure 3.3 H3K9me3 expression in stressed LUHMES.	89
Figure 3.4 Incubation of healthy LUHMES with SS and DS-CM has a small significant effect on cell metabolism of healthy LUHMES.	91
Figure 3.5 Incubation in SS and DS-CM impaired neurite outgrowth of healthy differentiating LUHMES.	92
Figure 3.6 Optimisation of healthy GFP-LUHMES/stressed LUHMES co-culture.....	93
Figure 3.7 DS-LUHMES impair neurite outgrowth significantly of differentiating GFP-LUHMES in a co-culture system.....	95
Figure 3.8 96 hours DS-LUHMES did not cause DNA damage on healthy LUHMES....	97
Figure 4.1 RNA integrity of control and SS/DS-LUHMES.	122
Figure 4.2 Assessing fragmentation of ss-cDNA.	126
Figure 4.3 Poly-RNA controls for 96 hours control and SS/DS LUHMES.	128
Figure 4.4 Housekeeping (HK) genes GAPDH and β -actin signal ratios for 96 hours control and SS/DS LUHMES arrays.....	129
Figure 4.5 Eukariotic hibridisation controls for 96 hours control and SS/DS LUHMES.	130
Figure 4.6 Percentage of probes present in the 96 hours control and SS/DS LUHMES array.	131
Figure 4.7 Signal histogram for the 96 hours control and SS/DS LUHMES arrays.	132

Figure 4.8 Relative log expression (RLE) box plots for the 96 hours control and SS/DS LUHMES arrays.	133
Figure 4.9 Clustering analysis of 96 hours control LUHMES compared to 96 hours SS and DS-LUHMES – Multi Group Comparison.	134
Figure 4.10 Clustering analysis of 96 hours control LUHMES compared to 96 hours SS and DS-LUHMES – Two Group Comparison.	136
Figure 4.11. Validation of DNA damage response genes by qRT-PCR.	154
Figure 4.12 Validation of APC/C:Cdh1 complex genes by qRT-PCR.	155
Figure 4.13 Validation of oxidative phosphorylation genes by qRT-PCR.	156
Figure 4.14 Validation of RIG-I-like signalling pathway genes by qRT-PCR.	157
Figure 4.15 Assessing expression of Ki67 and MCM2 in SS and DS-LUHMES.	158
Figure 4.16 Assessing mitochondrial Complex I activity in stressed LUHMES.	159
Figure 5.1 Grid used for quantitative analysis of p21, p16 and 8-OHdG staining.	186
Figure 5.2. Classification of ALS/MND cases according to p62 pathology.	196
Figure 5.3 Representative images of SA- β -gal activity in brains of two control donors.	199
Figure 5.4 Representative images of SA- β -gal activity in brains of two ALS/MND donors.	200
Figure 5.5 Representative images of SA- β -gal activity in the white matter of control and ALS/MND donors.	202
Figure 5.6 Representative images of p16 staining in control and ALS/MND brains.	204
Figure 5.7 Representative images of dual immunostaining for p16/GFAP.	205
Figure 5.8 Quantitative analysis of p16+ glial cells in control and ALS/MND brains. ..	205
Figure 5.9 p21 staining on controls and ALS/MND brains (Mex, Fcx, Sc).	208
Figure 5.10 Representative images of dual immunostaining for p21/GFAP.	209

Figure 5.11 Representative images of double fluorescence immunostaining for p21/NeuN.	209
Figure 5.12 Quantitative analysis of p21+ glial and neuronal cells in control and ALS/MND brains.....	210
Figure 5.13 Representative images of p16 and p21 staining in the OCx of ALS/MND and control donors.	211
Figure 5.14 Quantitative analysis of p16 and p21 immunohistochemistry in the OCx...212	
Figure 5.15 Representative images γ H2AX staining in the MCx and FACx of ALS/MND donors.....	213
Figure 5.16 Quantitative analysis of γ H2AX+ cells.	214
Figure 5.17 Representative images of 8-OHdG in ALS/MND and controls.....	215
Figure 5.18 Quantitative analyses of 8-OHdG+ neurones.....	216
Figure 5.19 Association between 8-OHdG+ and γ H2AX+ neurones in ALS/MND brains.	218
Figure 5.20 Association between p21+ and γ H2AX+ neurones in ALS/MND brains....	218
Figure 5.21 Association between p21+ and 8-OHdG+ neurones in ALS/MND brains. .	219
Figure 5.22 Representative images of CD68+ microglia in the FACx of ALS/MND and control donors.	220
Figure 5.23 Representative images of MHC II+ microglia in the FACx of ALS/MND and control donors.	221
Figure 5.24 Quantitative analysis of CD68 and MHC class II expression in the FACx of controls and ALS/MND donors.	221
Figure 5.25 Analysis of p16 and p21 expression in glial cells of FTLD-TDP B cases...223	
Figure 5.26 Analysis of p21 expression in neurones of FTLD-TDP B cases.....	223

Figure 5.27 Analysis of γ H2AX and 8-OHdG expression in neurones of FTL-D-TDP B cases.	224
Figure 5.28 RNA integrity from FACx frozen tissue.	226
Figure 5.29 RNA integrity from FACx frozen tissue.	228
Figure 5.30 Enrichment of LCM samples with a population of neuronal cells.	229
Figure 5.31 Assessing fragmentation of ss-cDNA.	232
Figure 5.32 Poly-RNA controls for neurone RNA enriched samples from controls and ALS/MND cases.	233
Figure 5.33 Housekeeping (HK) genes GAPDH and β -actin signal ratios.....	234
Figure 5.34 Eukariotic hibridisation controls for FACx neurone arrays.	235
Figure 5.35 Percentage of probes present in the 96 hours control and SS/DS LUHMES array.	236
Figure 5.36 Signal histogram forALS/MND and control FACx neurones arrays.	237
Figure 5.37 Relative log expression (RLE) box plots for the ALS/MND and control FACx neurones arrays.....	238
Figure 5.38 Clustering analysis of ALS/MND FACx neurones compared to Control FACx neurones – Two groups analysis.	240
Figure 5.39 p53 signalling pathway (KEGG pathways).....	251
Figure 5.40 Validation of candidate genes by qRT-PCR.	258

List of Tables

Table 2.1 Pre-differentiated LUHMES densities used for cell culture optimisation.	32
Table 2.2 Primary antibodies used for immunocytochemistry.	37
Table 2.3 Fluorescent secondary antibodies used for immunocytochemistry.	37
Table 2.4 H ₂ O ₂ clearance rates of differentiated LUHMES.	60
Table 4.1 PrimeTime ® qPCR assays used for validation of the candidate gene expression changes in control, SS and DS-LUHMES.	117
Table 4.2 Primary antibodies used for immunocytochemistry.	119
Table 4.3 Primary antibodies used for immunocytochemistry.	119
Table 4.4 Initial concentrations of RNA in untreated control, SS and DS-LUHMES samples.	121
Table 4.5 Initial concentrations of RNA in untreated control, single and double stressed LUHMES samples.	123
Table 4.6 Initial concentrations of cRNA in untreated control, single and double stressed LUHMES samples.	124
Table 4.7 Initial concentrations of ds-cDNA in untreated control, single and double stressed LUHMES samples.	125
Table 4.8 Number of differentially expressed transcripts for each of the 3 comparisons computed by Qlucore Omics Explorer and used for the pathway enrichment analysis. .	136
Table 4.9 DAVID Functional Enrichment analysis of the total number of differentially expressed transcripts in stressed LUHMES.	139
Table 4.10 DAVID Functional Enrichment analysis of the UP-REGULATED transcripts in stressed LUHMES.	140

Table 4.11 DAVID Functional Enrichment analysis of the DOWN-REGULATED transcripts in stressed LUHMES.....	141
Table 4.12 IMPaLA Pathway Analysis of the total number of differentially expressed transcripts in stressed LUHMES.....	143
Table 4.13 IMPaLA Pathway Analysis of the UP-REGULATED transcripts in stressed LUHMES.	144
Table 4.14 IMPaLA Pathway Analysis of the DOWN-REGULATED transcripts in stressed LUHMES.	145
Table 4.15 Genes involved in cell cycle regulation in SS and DS-LUHMES.....	147
Table 4.16 Genes involved in DNA damage response pathways in SS and DS-LUHMES.	148
Table 4.17 Genes involved in senescence and cellular responses to stress in SS and DS-LUHMES.	149
Table 4.18 Genes involved in immune response in SS and DS-LUHMES.	151
Table 4.19 Genes involved in senescence and cellular responses to stress in SS and DS-LUHMES.	152
Table 4.20 Genes selected for qRT-PCR validation.....	153
Table 5.1 Number of cases available for each brain region studied from controls and ALS/MND donors.....	178
Table 5.2 Clinical and demographic data for the control and ALS/MND donors.	179
Table 5.3 Antibodies used for immunohistochemistry experiments.	183
Table 5.4 Effect size Cohen's guidelines.....	187
Table 5.5 Control and ALS/MND cases that were selected for LCM isolation of neurones from the FACx.	189

Table 5.6. Gene specific primers used to confirm neuronal enrichment of LCM samples.	191
Table 5.7 Amplification reaction protocol.....	191
Table 5.8 Control and ALS/MND selected qRT-PCR validation.....	194
Table 5.9 PrimeTime ® qPCR assays used for validation of the transcripts of interest in control, SS and DS-LUHMES.	194
Table 5.10 Classification of ALS/MND cases according to their p62 pathology.	195
Table 5.11 Initial concentrations of RNA in FACx frozen tissue samples.	225
Table 5.12 RNA concentration and quality in neurone enriched samples.....	227
Table 5.13 Concentrations of cRNA obtained after ss-cDNA synthesis.	230
Table 5.14. Concentration of ds-cDNA obtained after the 2nd amplification cycle.	231
Table 5.15 Number of differentially expressed transcripts in ALS/MND FACx neurones.	241
Table 5.16 DAVID Functional and Pathway Enrichment analysis of the total number of differentially expressed transcripts in the ALS/MND FACx neurones	243
Table 5.17 DAVID Functional and Pathway Enrichment analysis of the UP-REGULATED transcripts in the ALS/MND FACx neurones.....	244
Table 5.18 DAVID Functional and Pathway Enrichment analysis of the DOWN-REGULATED transcripts in the ALS/MND FACx neurones.....	245
Table 5.19 IMPaLA Pathway Analysis of the total number of differentially expressed transcripts in ALS/MND FACx neurones.....	247
Table 5.20 IMPaLA Pathway Analysis of the UP-REGULATED transcripts in ALS/MND FACx neurones.	248
Table 5.21 IMPaLA Pathway Analysis of the DOWN-REGULATED transcripts in ALS/MND FACx neurones.	249

Table 5.22 Genes involved in p53 pathway in ALS/MND FACx neurones.	250
Table 5.23 UP-REGULATED transcripts with FC \geq 2.0 in the ALS/MND FACx neurones.	255
Table 5.24 DOWN-REGULATED transcripts with FC \geq 2.0 in the ALS/MND FACx neurones.	256
Table 5.25 Genes selected for qRT-PCR validation.	257

List of Abbreviations

% P	Percent present
8-OHdG	8-hydroxy-2'-deoxyguanosine
AB	avidin-biotin
ABC-AP	avidin biotinylated alkaline phosphatase
ABC-HRP	avidin-biotin horseradish peroxidase
AD	Alzheimer's disease
ALS	Amyotrophic Lateral Sclerosis
ANOVA	analysis of variance
APE 1	apurinic/ apyrimidinic endonuclease 1
ATM	ataxia telangiectasia mutated
ATR	ataxia-telangiectasia-mutated and Rad-3 related
AU	absorbance units
BafA1	Bafilomycin A1
BER	base excision repair
bFGF	basic fibroblast growth factor
BG Avg	Average background intensity
BRAF^{V600E}	serine/threonine-protein kinase B-Raf
BrdU	bromodeoxyuridine
BSA	bovine serum albumin
cdk	cyclin-dependent kinase
cDNA	complimentary DNA
CFAS	Cognitive Function and Ageing Studies
Chk1	checkpoint kinases 1
Chk2	checkpoint kinases 2
CM	conditioned media
CMV	cytomegalovirus
CNS	central nervous system
cRNA	complimentary RNA
CSF	cerebrospinal fluid
Ct	cycle threshold
DAB	3,3'-Diaminobenzidine

DAPI	4',6-diamidino-2-phenylindole
DAVID	Database for annotation, Visualization and Integrated Discovery
DDR	DNA damage response
DEPC	diethyl pyrocarbonate
DMEM	Dulbecco's Modified Enriched Media
DMF	dimethylformamide
DN	dystrophic neurites
DNA	deoxyribonucleic acid
DNA-PK	DNA dependent kinase
DS	double stressed
DSBs	double-strand breaks
ds-cDNA	double-stranded-cDNA
DS-LUHMES	double stressed LUHMES
E2F1	E2F1 transcription factor
EDTA	ethylenediaminetetraacetic acid
EGF	epidermal growth factor
ER	endoplasmic reticulum
ETC	electron transport chain
EthD-1	ethidium homodimer-1
F	forward primer
FACx	frontal association cortex
fALS	familial Amyotrophic lateral sclerosis
FBS	foetal bovine serum
FC	fold change
FFPE	formalin-fixed paraffin-embedded
FGF	fibroblast growth factor
FI	fluorescence intensity
FTLD	Frontotemporal lobar degeneration
FU	fluorescence unit
G1	Gap 1 phase
GAPDH	glyceraldehyde 3-phosphate dehydrogenase
GCI	glial cytoplasmic inclusions
GDNF	glial cell-derived neurotrophic factor
GFAP	glial fibrillary acidic protein
GFP	green Fluorescent Protein

GFP-LV	GFP-expressing lentivirus
H2AX	histone 2AX
H₂O₂	hydrogen peroxide
HBSS	Hank's Balanced Salt Solution
HEK 293	human embryonic kidney cells 293
HEPES	4(-2-hydroxyethyl)-1-piperazineethansulfonic acid
HK	housekeeping gene
HMGA	high mobility group A
HOCl	hypochlorous acid
HR	homologous recombination
HRP	horseradish peroxidase
hTRT	human telomerase reverse transcriptase catalytic subunit
HUVECs	Human umbilical vein endothelial cells
IFN	interferon
IGF-1	insulin-like growth factor-1
IGFBP-5	insulin-like growth factor binding protein-5
IGFBP-6	insulin-like growth factor binding protein-6
IL-6	interleukin-6
IL-7	interleukin-7
IL-8	interleukin-8
IMPala	Integrated Molecular Pathway Level Analysis
iPSC	induced pluripotent stem cell
IVT	<i>In Vitro</i> Transcription
JEV	Japanese encephalitis virus
KEGG	Kyoto encyclopedia of genes and genomes
LCM	laser capture microdissection
LFS	Li-Fraumeni syndrome
LUHMES	Lund Human Mesencephalic
MAP2	Microtubule-associated protein 2
MAPK	Mitogen-Activated Protein Kinases
MAS 5.0	MicroArray Suite 5.0
MC	minimal changes
MCM	minichromosome maintenance
Mcm2	minichromosome Maintenance Component 2
MCx	motor cortex

MDA	malondialdehyde
MHC	major histocompatibility complex
MK2	mitogen-activated protein kinase-activated protein kinase 2
mM	millimolar
MND	motor neuron disease
mOD	micro optical density
MRC	Medical Research Council
MRN	MRE11–RAD50–NBS1
mRNA	messenger RNA
MTT	3-(4,5-dimethylthiazol-2-yl)-2,5-diphenyltetrazolium
NAD⁺	oxidized nicotinamide adenine dinucleotide
NADH	reduced nicotinamide adenine dinucleotide
NBS1	nibrin
NCI	neuronal cytoplasmic inclusions
NEMO	NF- κ B Essential Modulator
NFTs	neurofibrillary tangles
ng	nanogram
NHEJ	non-homologous end-joining
NI	neuronal intranuclear inclusions
Nox4	NADPH oxidase 4
NSCs	neural stem cells
O₂⁻	superoxide anion
OCx	occipital cortex
OIS	oncogene-induced senescence
PAI-1	Plasminogen activator inhibitor-1
PBS	phosphate buffered saline
PCA	principal component analysis
PCNA	proliferating cell nuclear antigen
PCR	Polymerase chain reaction
PD	Parkinson's disease
Pen/Strep	Penicillin/Streptomycin
PFA	paraformaldehyde
pHPA	<i>para</i> -hydrophenylacetic acid
PIKK	3-kinase-like kinases
pLo	poly-L-ornithine hydrobromide

PMD	post mortem delay
PrECs	prostate epithelial cells
PSD	postsynaptic density
PTEN	phosphatase and tensin homolog
QC	quality control
qRT-PCR	quantitative real-time PCR
R	reverse primer
RIG-I	retinoic acid-inducible gene I
RIN	RNA integrity number
RLE	Relative Log Expression
RMA	Robust Multi-Array Average
RNA	ribonucleic acid
ROS	reactive oxygen species
RPA	Replication protein A
rRNA	ribosomal RNA
RT	room temperature
S – phase	synthesis phase
SAHF	senescence-associated heterochromatic foci
sALS	sporadic Amyotrophic Lateral Sclerosis
SASP	senescence-associated secretory phenotype
SA-β-gal	senescence-associated-β-galactosidase
SBTB	Sheffield Brain Tissue Bank
Sc	spinal cord
SDS	sodium dodecyl sulphate
SEM	standard error of the mean
shRNA	short hairpin RNA
SIPS	stress-induced premature senescent
SS	single stressed
SSBs	single-strand breaks
ss-cDNA	single-stranded-cDNA
SS-LUHMES	single stressed LUHMES
T2D	type 2 diabetes
TBS	tricarboxylic acid
TCA	Tris-buffered saline
TdT	terminal deoxynucleotidyl transferase

TE	Tris-EDTA
tet	tetracycline hydrochloride
TGF- β	transforming growth factor- β
Tipin	TIMELESS Interacting protein
TLR3	Toll-like receptor 3
tTA	tetracycline-controlled transactivator
UDG	uracil-DNA glycosylase
UVB	ultraviolet B
VEGF	vascular endothelial growth factor
W1	wash buffer 1
W2	wash buffer 2
γH2AX	phosphorylated histone H2AX
μl	microlitre
μm	micrometer
μM	micromolar
$\Delta\Delta$Ct	delta delta cycle threshold
\bulletOH	hydroxyl radical

Chapter 1. General introduction

1.1. The biology of cellular senescence

Cellular senescence was first described by Hayflick and Moorhead in 1961; their experiments in human foetal lung fibroblasts provided strong evidence of the limited proliferative capacity of mitotic cells in culture (Hayflick and Moorhead, 1961). In a later study, Hayflick also reported that human foetal fibroblasts stopped dividing after a specific amount of time; their growth arrest was not caused by culture conditions but depended on the number of doublings that fibroblasts went through, rather than on the sub-culturing ratio. He referred to this mechanism as replicative senescence and suggested that limited proliferative capacity could be affected by the age of the cell's donor (Hayflick, 1965). Even though Hayflick's experiments did not confirm this last belief, research carried out by Hayflick and colleagues shed a light on what could be occurring to cells *in vivo* and proposed replicative senescence as a mechanism that could influence the lifespan of an organism.

Telomere shortening was later described as the event causing replicative senescence *in vitro*, but it was soon revealed that oncogene expression and genotoxic stress were involved in the induction of a similar mechanism. This phenotype was characterised by a stable permanent cell cycle arrest and by the development of a senescence-associated secretory phenotype (SASP). Early studies of senescence suggested a main role as a tumour suppressor mechanism, but at the same time, evidence proposed senescence as a contributor to the gradual decline in organ function that characterises ageing. More recent reports have also shown that cellular senescence plays a role in embryonic

development, tissue remodelling and wound healing (Demaria et al., 2014; Muñoz-Espín et al., 2013; Storer et al., 2013)

The biology of cellular senescence is very complex and it involves activation of signalling cascades that participate in the induction and maintenance of a senescent phenotype in the form of a permanent cell cycle arrest, and the reinforcement and spread of the senescent state through the SASP. These cascades and their intricate interactions are discussed in the following section.

1.1.1. Characteristics of senescent cells: effector pathways and the SASP

Senescence can be activated by different stimuli and is classified accordingly in replicative senescence, oncogene-induced senescence (OIS), and stress-induced senescence. Replicative senescence as described by Hayflick and Moorhead, was later linked to a telomere shortening dependent mechanism. Work conducted by Bodnar et al. in retinal pigment cells and foreskin fibroblasts in culture showed that the expression of the human telomerase reverse transcriptase catalytic subunit (hTERT) in these cells prolonged their lifespan in culture. Compared to hTERT⁻ clones, cells expressing the enzyme had longer telomeres and were able to continue dividing in culture; this evidence suggested a link between telomere attrition and loss of replicative capacity *in vitro* (Bodnar et al., 1998). OIS was first described in human and mice fibroblasts in culture exposed to prolonged expression of oncogenic *Ras*, which caused a permanent cell cycle arrest in G1 (Gap 1 phase) (Serrano et al., 1997). Other studies have also shown that expression of BRAF^{V600E} (serine/threonine-protein kinase B-Raf) oncogene (Cisowski et al., 2016; Michaloglou et al., 2005), as well as loss of tumour suppressor PTEN (phosphatase and tensin homolog) also activate senescence-associated growth arrest

(Alimonti et al., 2010; Chen et al., 2005b). Finally, stressed-induced senescence results from the exposure to sub-lethal stresses, including oxidative stress, UVB (ultraviolet B) light and ionising radiation (Barascu et al., 2012; Coleman et al., 2013; Liao et al., 2014; De Magalhães et al., 2002; Parrinello et al., 2003). While specific characteristics have been seen for each of these 3 mechanisms, one main event is involved in the induction of a permanent growth arrest in all of them: a persistent DNA damage and a DNA damage response (DDR). A persistent DDR orchestrates the permanent cell cycle arrest and promotes the development of the SASP through two main effector pathways, the p53/p21 and the p16/pRB pathways (**Figure 1.1**).

1.1.1.1. Senescence-associated cell cycle arrest induction via p53/p21 and p16/pRB

signalling

DNA damage, mainly in the form of double strand breaks (DSBs), activates a DDR and leads to repair, apoptosis or senescence, depending on the intensity of the damage. DSBs are detected by the highly conserved protein kinases ataxia-telangiectasia mutated (ATM) and ATM-and Rad3-related (ATR) (Bensimon et al., 2010; Kozlov et al., 2016; Matsuoka et al., 2007); this event initiates the DDR. After sensing DNA damage and in order to maintain genome integrity, ATM/ATR trigger a complex response through phosphorylation of their downstream targets Chk1 (checkpoint kinase 1), Chk2 (checkpoint kinase 2) and MK2 (mitogen-activated protein kinase-activated protein kinase 2); this response involves the recruitment of the DNA repair machinery, control of cell cycle checkpoints and changes in gene expression (Han et al., 2014; Liu et al., 2007, 2000; Sørensen et al., 2005). To allow for the damage to be repaired, a transient cell cycle arrest is mediated by stabilisation of p53 directly by ATM (ataxia telangiectasia mutated) or through Chk2 (Hirao et al., 2002; Mak, 2000), followed by activation of the cyclin-

dependent kinase (cdk) inhibitor p21. P21 induces the arrest at G1 thanks to the inhibition of cyclin-cdk2/4 complexes, E2F transcription factors that regulate expression of replication and cell cycle progression genes, and proliferating cell nuclear antigen (PCNA) (Chang et al., 2000; Wade Harper et al., 1993; Waga et al., 1994). This temporary growth arrest is necessary for cells to activate the appropriate repair mechanisms in response to DNA lesions and to prevent the propagation of the damage to the next generation of cells. However, under prolonged expression of p21, this arrest can turn into a permanent event, and promote the development of senescence.

The mechanisms that control the transition from a temporary to an irreversible cell cycle arrest are still not well understood. However, it has been shown that activation of the p53/p21 axis alone is not enough to promote a state of permanent cell cycle and that activation of p16 is necessary to accomplish this important characteristic of the senescent phenotype. Cdk inhibitor p16 also prevents cell proliferation and participates in the maintenance of senescence. The role of p16 in cell cycle arrest is accomplished through inhibition of cyclin D/CDK4 and cyclin D/CDK6 complexes; this action prevents inactivation of the phosphorylated retinoblastoma protein (pRB) and results in the repression of E2F dependent-transcription of cell proliferation genes (Li et al., 1994).

The interaction between p21 and p16 pathways in senescence is complex: they have differential roles in the induction and maintenance of the cell cycle arrest and the development of the SASP, but can also activate senescence independently. Stein et al. (1999) studied the role of both effector pathways in senescent human lung fibroblasts through the dynamics of the cell cycle arrest. Their experiments revealed different levels of accumulation of p16 and p21 in senescent fibroblasts as they halted proliferation. p53-

dependent activation of p21 resulted in the initial and temporary cell cycle arrest, after which p21 levels started to decrease; in contrast, p16 expression increased after the arrest and remained elevated for a 2 months, suggesting that p21 is necessary for the induction of cell cycle arrest but p16 is crucial for its long term maintenance (Stein et al., 1999). In later studies, serial passageing and oncogene activation did not cause senescence in mice fibroblasts obtained from a p16/p21 double knock-down model, while some features of senescence were detected in p16 and p21 knock-outs and wild type fibroblasts, suggesting a cooperative action of p16/p21 in senescence *in vitro* (Takeuchi et al., 2010). More recent reports show the involvement of other pathways in maintaining an irreversible cell cycle arrest. *In vitro* studies conducted by Demidenko et al. (2010) and Korotchkina et al. (2010) demonstrate that activation of mTOR signalling promotes p53-mediated irreversible senescence and that its inhibition leads to quiescence instead, despite p53 being active (Demidenko et al., 2010; Korotchkina et al., 2010). A more in depth analysis of p53-mTOR signalling revealed an important role for Akt activation mediated by mTOR in the induction of an irreversible cell cycle arrest *in vitro*, as well as in the development of other features of senescence, including the SASP (Kim et al., 2017).

In summary, a persistent DDR is the key mechanism required to induce a senescence-associated cell cycle arrest through its effector cascades p53/p21 and p16/pRB. Interestingly, senescence can also be induced independently of these pathways, a phenomenon that has been mainly seen in oncogene-induced senescence *in vitro* models (Bryson et al., 2017; Olsen et al., 2002).

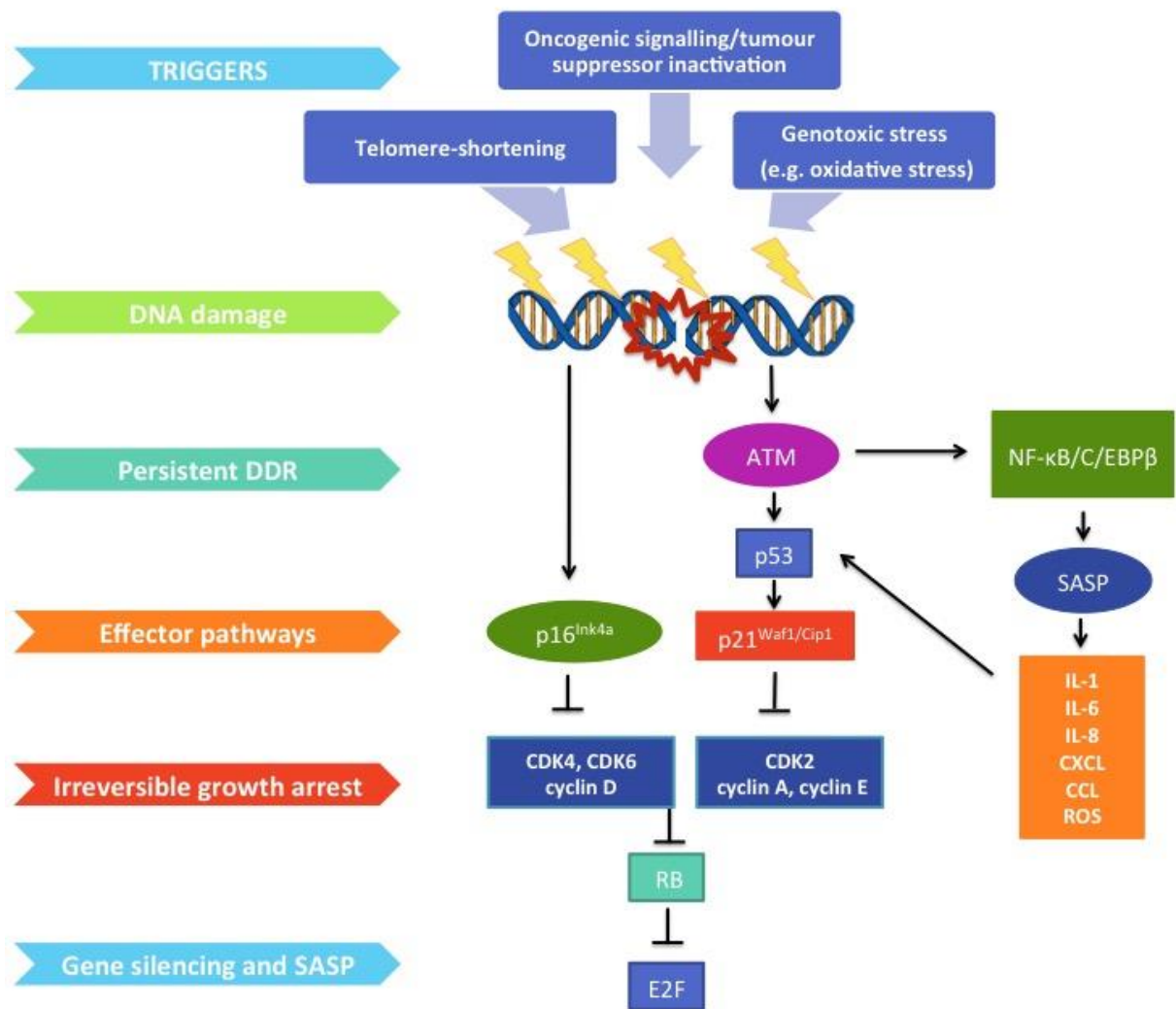


Figure 1.1 Senescence inducers and signalling pathways.

Telomere-shortening, oncogenic signalling and genotoxic stress, such as oxidative stress, drive senescence through the activation of a persistent DDR. The p53/p21 and p16/pRb pathways are activated by the DDR and together promote an irreversible cell cycle arrest, which is accompanied by repression of proliferation genes and by the development of a toxic secretory phenotype.

1.1.1.2. The senescence-associated secretory phenotype (SASP)

As part of the senescent program, cells develop a senescence-associated secretory phenotype (SASP) characterised by the secretion of cytokines, chemokines, growth factors and proteases. The SASP promotes a pro-inflammatory and pro-oxidant environment that can reinforce the senescent state in already damaged cells and can also spread DNA damage to neighbouring cells (Coppé et al., 2010; Kuilman and Peeper, 2009). These characteristics may reflect the role that the SASP has in the ageing process and in the pathophysiology of age-related diseases (**Figure 1.1** and **Figure 1.2**).

Coppé et al. (2008) first described the SASP in cultured pre-senescent and senescent human fibroblasts from different strains and human prostate epithelial cells (PrECs). Conditioned media from these cells was analysed using modified antibody arrays and revealed secretion of high levels of inflammatory cytokines, immune modulators, growth factors, cell surface proteins and survival factors, by senescent cultures. The components of the SASP varied between strain and cell types, although the study identified a core group of molecules to be highly expressed in all senescent cultures, including interleukin-6 (IL-6), interleukin-8 (IL-8) and CXCL1 (Coppé et al., 2008). Different studies have since then identified various molecules and pathways associated to the SASP. For instance, the retinoic-acid-inducible-gene-1 (RIG-1) signalling pathway, which is known to participate in the immune response against viruses, was shown to regulate expression of IL-6 and IL-8 in senescent human fibroblasts and umbilical vein endothelial (HUVEC) cells (Liu et al., 2011).

It is of importance to consider that, despite a number of common SASP factors have been identified in different studies on senescence, its composition is highly dependent on the

type of cell and the time at which SASP expression is analysed. In a recent report, the heterogeneity of the SASP was investigated using a gene expression profiling approach in which whole-transcriptome datasets were used to identify transcriptomic signatures associated with specific senescence-inducing stresses in fibroblasts, keratinocytes and melanocytes. Interestingly, results showed a high variability in the expression of SASP components, such as *IL1*, *IL6*, *IL11*, *IGFBP2*, *CXCL8*, *VEGFA*, *MMP1*, *CCL2* and *CCL5*, between cell types and time-points at which the experiments were performed, thus highlighting the relevance of time and cell identity in the composition of the SASP (Hernandez-Segura et al., 2017).

Further studies have investigated the regulatory mechanisms of the SASP. These reports have shown that the SASP develops over several days, rather than being activated immediately after cell cycle arrest; most importantly, a DDR signalling is necessary for the initiation of the SASP and does not depend directly on the p53/p21 or p16/pRb pathways (Coppé et al., 2008, 2010; Rodier et al., 2009). Loss of ATM, NBS1 (nibrin, a component of the MNR complex that interacts with ATM) or CHK2 reduced the expression of core SASP components IL-6 and IL-8 in human fibroblasts in culture, whereas p53 deficient fibroblasts still induced a SASP in the absence of cell cycle arrest and p16 expression without DNA damage did not induce the phenotype (Rodier et al., 2009). Thus, expression of the SASP is mainly dependent on the activation of a persistent DDR.

Transcriptional regulation of the SASP components is linked to activity of the NF- κ B and C/EBP β transcription factors (Acosta et al., 2008, 2013; Chien et al., 2011). Kuilman et al. (2008) confirmed IL-6 and IL-8 to be a direct transcriptional target of C/EBP β in

human senescent fibroblasts; together, IL-6 and C/EBP β participated in a positive-feedback loop that promoted the maintenance of a senescence-growth arrest and SASP. C/EBP β depletion resulted in inhibition of IL-6 and IL-8 expression, while depletion of IL-6, C/EBP β and IL-8 levels also showed a marked decrease; both events promoted senescence bypass and inhibited expression of SASP components (Kuilman et al., 2008). In a different study, ectopic expression of IL-1 α was shown to trigger senescence by induction of oxidative DNA damage, a DDR and p53/p21 signalling activation, together with IL-6 and IL-8 expression (Acosta et al., 2013). More recent studies that explore the SASP have strengthened the evidence on NF- κ B-dependent regulation of IL-6 and IL-8 secretion as part of the SASP. Using a computational model and publically available gene interaction data, Meyer et al. (2017) were able to predict in-silico knock-outs that could inhibit IL-6 and IL-8 secretion in response to a persistent DNA damage. One of the principal knock-out candidates was the NF- κ B Essential Modulator (NEMO); validation studies in murine dermal fibroblasts confirmed the depletion of NEMO inhibited expression of IL-6 and IL-8 at the messenger RNA (mRNA) and protein levels (Meyer et al., 2017).

It has been shown that cells undergoing different forms of senescence (oncogene, replicative and drug-induced senescence) have the ability to promote reactive oxygen species (ROS)-mediated DNA damage and a DDR in neighbouring cells; as a consequence, bystander cells activate TGF β /SMAD and IL-1/NF- κ B signalling pathways that when inhibited, suppressed the DDR (Hubackova et al., 2012). Experiments performed in human lung fibroblasts showed increased ROS production after activation of the NADPH oxidase 4 (Nox4) enzyme as part of the oncogenic-induced senescence program (Kodama et al., 2013). Stimulation with IL-6 also caused a pro-oxidant effect on

human fibroblasts and the induction of senescence characterised by oxidative DNA, p53-dependent growth arrest and up-regulation of IL-1 α/β , IL-6 and CXCL8 transcripts 4 days after IL-6 stimulation (Kojima et al., 2012).

Expression of SASP factors has been detected in senescent cells *in vivo*. NF- κ B, IL-1 α and major SASP components (IL-6, IL-8, MCP-1, PAI-1, PAI-2 and TNF α) were up-regulated in enriched populations of myeloid cells and osteocytes obtained from ageing mice (Farr et al., 2016). Gene expression analysis in samples from human breast cancer and prostate cancer tumours also showed expression of the SASP-related transcripts *IL1A*, *IL1B*, *IL6*, and *IL8* (Capell et al., 2016). Furthermore, SASP cytokines such as IL-6, IL-8, VEGF (vascular endothelial growth factor) and PAI-1 (plasminogen activator inhibitor), were detected in the vitreous humour of patients with proliferative diabetic retinopathy (Oubaha et al., 2016) and up-regulation of *TNF* and *CCL2* mRNA, two pro-inflammatory cytokines associated with the SASP, was detected in adipose tissue from diabetic patients (Minamino et al., 2009).

All these data together suggest that SASP is not a homogeneous paracrine mechanism, as it varies between cell types and also depends on the conditions that trigger the DDR. The SASP program may not only be reinforcing the senescence state in already growth arrested cells, but it could also be promoting damage and senescence activation in surrounding cells through an oxidative and pro-inflammatory environment.

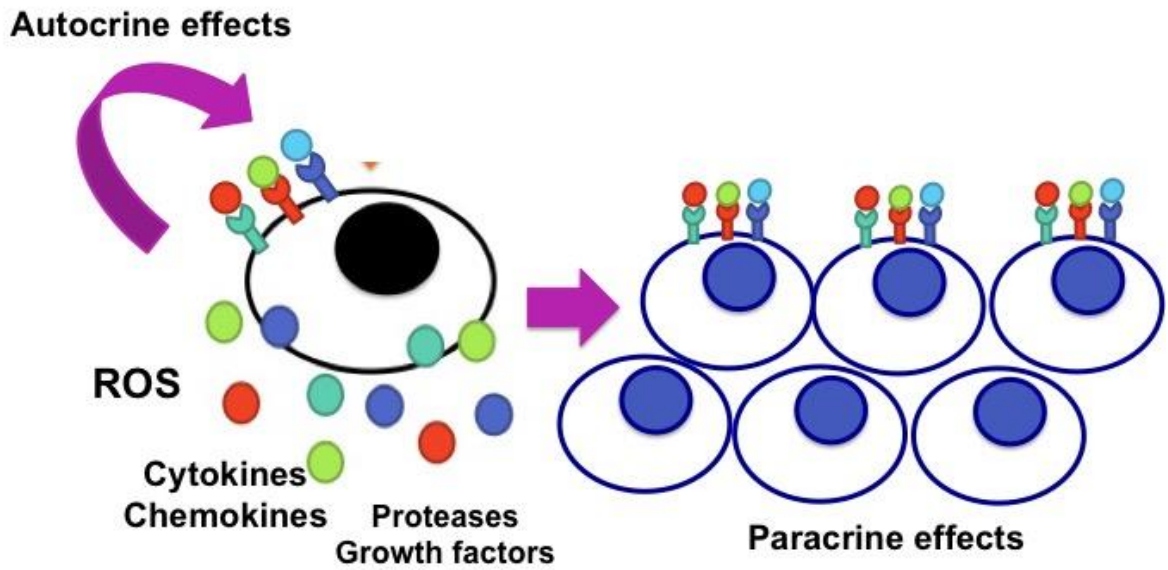


Figure 1.2 Autocrine and paracrine effects of the SASP.

Through the increase in ROS production and the release of cytokines, chemokines, proteases, growth factors the senescent cells reinforce the senescent state (autocrine SASP) at the same time that they induce a senescent-associated growth arrest in neighbouring cells. These events are useful in the context of cancer and the anti-tumorigenic role of senescence in young organisms, however, in an ageing context, the SASP promotes cellular dysfunction and contributes to degenerative processes.

1.1.2. Biomarkers of cellular senescence

Cellular senescence in *in vitro* models is accompanied by morphological changes in the cells that are not seen in senescence *in vivo*. These changes are detectable as an enlarged and flattened cell body, vacuolisation and accumulation of stress granules (Muñoz-Espín et al., 2013; Serrano et al., 1997). Since these characteristics are exclusive of *in vitro* models of senescence, research has focused on the study of biomarkers that can facilitate *in vitro* and *in vivo* identification of senescence activation. To date, a specific marker of senescence is still lacking, thus investigation of this mechanism relies on a group of markers that are associated with the effector mechanisms of senescence and that in combination suggest senescence induction (**Figure 1.3**).

1.1.2.1. DNA damage, DDR and cell cycle arrest markers

Examination of the gene and protein expression mediators of the DDR and the p53/p21 and p16/pRB signalling pathways can partially help in the identification of senescent cells in culture and in tissue. For instance, detection of DNA damage and activation of a DDR can be achieved using known DNA damage markers, such as phosphorylated histone H2AX (γ H2AX), which correlates with the formation of DSBs (Mariotti et al., 2013; Rogakou et al., 1998). Analysis of the expression of ATM, p16, p53 and p21 has also been used to detect senescence-associated cell cycle arrest in response to DDR activation (Dungan et al., 2017; Herbig et al., 2004; Hewitt et al., 2012; Kim et al., 2017). Moreover, the use of proliferation markers, such as Ki67, and proliferation assays like bromodeoxyuridine (BrdU) labelling, can be used to confirm growth arrest in cells suspected of senescence activation (Biran et al., 2017; Lawless et al., 2010; Serrano et al., 1997).

1.1.2.2. Senescence-associated- β -galactosidase

One of the first markers to be described for the *in vitro* detection of senescent cells was the increased activity of a lysosomal β -galactosidase at pH6 (Dimri et al., 1995; Lee et al., 2006). Senescence-associated- β -galactosidase (SA- β -gal) results from the expression of the *GLB1* gene, which encodes for a β -D-galactosidase. The activity of this enzyme is optimal at pH4-4.5, but in senescent cells, increased expression of the mRNA and protein allows its detection at suboptimal pH conditions (Kurz et al., 2000; Lee et al., 2006). SA- β -gal activity can be detected *in vivo* and in cultured cells by incubating fixed samples with the enzyme substrate, which results in either the precipitation of a coloured compound or in the emission of a fluorescent signal, both detectable by microscopy (Debacq-Chainiaux et al., 2009).

The role of SA- β -gal in senescence is still not well understood, although it is known that its activity in senescent cells results from an increased lysosomal content (Kurz et al., 2000; Lee et al., 2006) that could be linked to up-regulation of autophagy (Gerland et al., 2003; Narita et al., 2011). To date, SA- β -gal activity is one of the main indicators of senescence and is usually included in the panel of markers used to identify replicative, oncogene and stress-induced senescence (Chan et al., 2016; Gao et al., 2016; Singh et al., 2016). However, several reports, starting with early studies by Dimri et al. (1995), have suggested that SA- β -gal activity is not a universal marker of senescence, and that its activity could vary depending on the cell type or tissue that is being investigated (Dimri et al., 1995; De Magalhães et al., 2004; Piechota et al., 2016; Yegorov et al., 1998). These limitations will be discussed in more detail in Chapters 3, 5 and 6 of this thesis.

1.1.2.3. Senescence-associated heterochromatin foci (SAHF)

Senescence is also characterised by changes in chromatin structure that can be identified as senescence-associated heterochromatin foci (SAHF). Narita et al. (2003) described SAHF formation in senescent human fibroblasts using electron and confocal microscopy to localise heterochromatin sites within the nuclei of the cells. Their studies showed formation of dense DAPI (4',6-diamidino-2-phenylindole) positive foci in replicative, oncogene-induced and stress-induced senescent cells *in vitro* but not in quiescent cells; SAHF development was dependent on activation of the p16/pRB signalling cascade, since inactivation of this pathway prevented SAHF formation (Narita et al., 2003). Each heterochromatin focus corresponds to one chromosome region that is identified by the accumulation of heterochromatin proteins and histone modifications known to be involved in gene repression. SAHF components include macroH2A, a histone variant known to participate in gene silencing, high mobility group A (HMGA) proteins, which induce SAHF formation through p16 activation, and the heterochromatin markers di- or tri-methylated lysine 9 histone H3 (H3K9Me_{2/3}) and bound HP1 proteins (Funayama et al., 2006; Narita et al., 2003, 2006; Zhang et al., 2005). Taking this data into account, it has been suggested that SAHF could contribute to the irreversibility of the cell cycle arrest in senescent cells by silencing expression of proliferative genes, including E2F targets (Narita et al., 2003; Zhang et al., 2005).

Detection of SAHF formation could be helpful in the detection of senescent cells (Aird and Zhang, 2013). However, as it occurs with SASP components, SAHF formation could also depend on cell type and the stimuli that activates senescence (Kosar et al., 2011; Di Micco et al., 2011), thus, SAHF development or absence *in vivo* and *in vitro* need to be interpreted carefully.

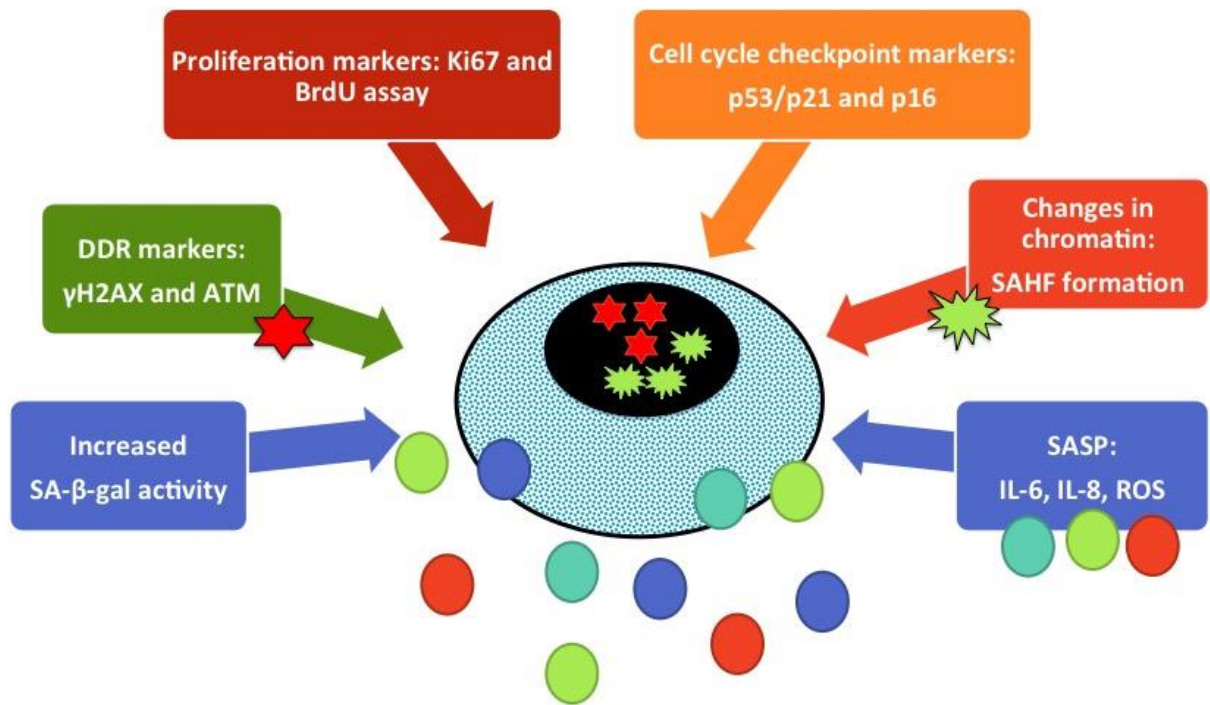


Figure 1.3 Classical markers of cellular senescence.

Identification of senescent cells *in vivo* and *in vitro* relies in a panel of markers that in combination suggest activation of senescence. This panel comprises the detection of increased SA- β -gal activity, expression of the DDR markers γ H2AX (red star) and/or ATM, confirmation of cell cycle arrest through proliferation marker Ki67 and BrdU assay, expression of the main proteins involved in the p53/p21 and p16/pRb signalling cascades, changes in chromatin organisation in the form of SAHF (senescence-associated heterochromatin foci) (green star) and secretion of SASP-related cytokines and increased ROS.

1.2. Senescence in ageing and age-related diseases

Ageing is characterised by the progressive loss of physiological functions that ultimately results in tissue dysfunction of an organism. Deterioration of the normal physiological processes increases our vulnerability to environmental factors, which can lead to the development of age-related diseases, such as cardiovascular disease, type 2 diabetes (T2D), cancer and neurodegenerative diseases (Loaiza and Demaria, 2016; Niccoli and Partridge, 2012; Stefanatos and Sanz, 2017). The underlying mechanisms of ageing are not clearly understood, however, several cellular and molecular hallmarks have been shown to contribute to this mechanism, including cellular senescence (López-Otín et al., 2013).

Cellular senescence is recognised as an anti-tumorigenic mechanism that prevents tumour development early in life (Braig et al., 2005; Chen et al., 2005b; Katlinskaya et al., 2016; Serrano et al., 1997). However, senescence can become detrimental with age and can contribute to the development of age-related pathologies. Hayflick and Moorhead findings on senescence were the first to suggest a link between senescence and ageing (Hayflick, 1965; Hayflick and Moorhead, 1961). Further work identified accumulation of senescent cells in tissue from ageing mammals. Krishnamurthy et al. (2004) assessed accumulation of p16⁺ cells in the tissue of young and old rodents; their results indicated an age-associated increase in the expression of p16 in different organs, which correlated with increased SA-β-gal activity (Krishnamurthy et al., 2004). Moreover, clearance of p16⁺ cells in a progeroid murine model delayed the onset of age-related phenotypes that are known to occur in this model, including cataract and sarcopenia development (Baker et al., 2011). In humans, accumulation of senescent cells has been implicated in various age-related pathologies, including pulmonary fibrosis (Minagawa et al., 2011; Schafer et

al., 2017), obesity, type 2 diabetes and metabolic syndrome (Aravinthan et al., 2014; Kim et al., 2006; Markowski et al., 2013), cardiovascular disease (Minamino et al., 2002) cancer (Demaria et al., 2017; Dou et al., 2017; Lugo et al., 2016) and neurodegeneration (Al-Mashhadi et al., 2015; Bhat et al., 2012; Simpson et al., 2010, 2014). Telomere shortening is one of the factors that could be promoting senescence in ageing. Together, this evidence suggests an important role of senescence in the ageing and in the development and progression of age-related diseases.

Telomere-attrition and oncogene activation could be implicated in the induction of senescence in ageing. It is known that a decrease in telomere-length occurs naturally as part of the DNA replication mechanism over continuous cellular divisions. This event leads to accumulation of un-repairable DNA damage, activation of a DDR and a senescence-associated cell cycle arrest (Fumagalli et al., 2012; Herbig et al., 2004; Hewitt et al., 2012). Oncogenes also trigger a DNA damage response as a consequence of replication stress and, interestingly, ROS accumulation, which leads to the activation of senescence pathways (Bartkova et al., 2006; Di Micco et al., 2006, 2011; Ogrunc et al., 2014).

Apart from age-related telomere shortening and oncogene expression, strong genotoxic stress, such as oxidative stress, can also damage telomeric and non-telomeric DNA regions, causing a persistent DDR response and driving senescence (Brandl et al., 2011; Crowe et al., 2016; Kurz, 2004; Venkatachalam et al., 2017). Accumulation of unreparable DSBs in non-telomeric regions has been shown in senescent human and mice fibroblasts in culture (Sedelnikova et al., 2004); DNA damage accumulation could result from a constant exposure to an oxidative environment.

ROS are known signalling molecules that participate in physiological functions under normal conditions but are also the bypass products of cellular metabolism (Ray et al., 2012; Schieber and Chandel, 2014). An imbalance between ROS production and the anti-oxidant mechanisms of the cells can cause oxidative stress and promote oxidative damage to proteins, lipids and nucleic acids. Evidence of increased ROS and oxidative DNA damage has been reported in human ageing organs, including the brain (Al-Mashhadi et al., 2015; Guest et al., 2014; Massudi et al., 2012; Mecocci et al., 1999; Simpson et al., 2014). The age-related increase in ROS could cause DNA damage accumulation and drive senescence. ROS have been implicated in the induction of senescence and in the autocrine and paracrine effects of the SASP. Both telomere-shortening and oncogenic signalling have been shown to promote senescence activation via ROS accumulation (Ameziane-El-Hassani and Dupuy, 2017; Lee et al., 1999; Passos et al., 2010) however, oxidative stress can directly cause oxidative DNA damage as well. For instance, sub-lethal concentrations of H₂O₂ can cause oxidative DNA damage in myoblasts *in vitro* and drive senescence through the p53/p21 axis; moreover, senescence induction is accompanied by increased SA-β-gal activity and SAHF formation (Venkatachalam et al., 2017). In a different report, persistent exposure to low levels of H₂O₂ caused long-term increased p21 expression in head and neck squamous carcinoma cells (Fitzgerald et al., 2015). Interestingly, long-term expression of p21 causes mitochondrial dysfunction and ROS accumulation, which reinforce the senescent phenotype by generating oxidative DNA damage and maintaining a persistent DDR (Passos et al., 2010).

In summary, a persistent DNA damage response and the induction of senescence could be mediated by ROS accumulation, a hallmark of the ageing process. This event could

contribute to tissue dysfunction through the SASP and promote the development of age-related pathologies, including neurodegeneration.

1.2.1. Senescence in brain ageing and in neurodegeneration

Cellular senescence could contribute to brain ageing and disease. In recent years, several reports have revealed evidence of cellular senescence in the brain, mainly in proliferation-competent cells, but also in post-mitotic neurones. The implications of neuronal senescence in ageing and in the neuronal dysfunction that characterises disorders such as Alzheimer's disease (AD), Parkinson's disease (PD) and amyotrophic lateral sclerosis (ALS; or motor neurone disease, MND) are still not clear. However, investigation of this mechanism could reveal a novel pathogenic process involved in age-related brain dysfunction and could extend our understanding of neurodegenerative diseases.

1.2.1.1. Senescence in astrocytes and microglia

Astrocytes and microglia have been shown to senesce in culture and *in vivo* through activation of stress-induced or replicative senescence. Induction of replicative senescence has been described in rat microglial cells *in vitro* and *in vivo* (Flanary and Streit, 2003, 2004). More recently, an age-dependent increase in myelin fragmentation in the white matter of ageing mice was reported, which caused formation of insoluble lysosomal microglial inclusions that contributed to microglial dysfunction and senescence, suggesting that microglia also activate a senescent program in response to stress (Safaiyan et al., 2016). Contradicting evidence was shown in a different study, where detection of SA- β -gal in the white matter of an ageing cohort did not colocalise with microglial marker CD68 (Al-Mashhadi et al., 2015); however, it is possible that senescence induction in microglia depends on whether these cells are in a quiescent state

or express a reactive proliferative phenotype. Taking this into account, a more thorough study of the mechanisms that drive microglial senescence and its implications in neurodegeneration is still needed.

Current evidence on astrocyte senescence is more compelling and suggests that astrocytes can activate senescence through the same signalling pathways that have been described in other cell types, including fibroblasts. For instance, cultured human and rat astrocytes developed a p21 and pRb-dependent senescence-associated growth arrest in response to oxidative stress; moreover, these cells underwent chromatin remodelling and increased ROS generation that probably related to gene silencing and the development of a SASP (Bitto et al., 2010). Subsequent studies confirmed these findings and expanded the evidence on astrocyte senescence *in vitro* and *in vivo*. Analysis of the transcriptome of senescent human astrocytes revealed downregulation of cell cycle genes and of transcripts implicated in the protective functions of astrocytes (Crowe et al., 2016). Moreover, presence of astrocytes expressing p16 and increased SA- β -gal activity was demonstrated in the white matter of the ageing human brain (Al-Mashhadi et al., 2015). This data suggest that age-related induction of senescence in astrocytes could affect their functionality and impact progression of neurodegeneration.

1.2.1.2. The paradox of neuronal senescence

Contrary to astrocytes and microglia, neurones exist in a state of natural cell cycle arrest and would not be predicted to activate senescence. However, in the past few years, several studies have shown the induction of neuronal senescence both *in vitro* and *in vivo* and have challenged the idea of senescence being limited to proliferating cells and have proposed a role for neuronal senescence in age-related neuronal dysfunction.

In 2010, Uday Bhanu et al. reported increased SA- β -gal activity in long-term cultured rat cerebellar granule neurones. Their finding correlated with impaired base-excision (BER) and non-homologous end-joining (NHEJ) DNA damage repair mechanisms (Uday Bhanu et al., 2010), suggesting that accumulation of DNA damage could drive senescence in neurones *in vitro*. Increased SA- β -gal activity was also seen in rat hippocampal neurones kept in culture for up to 30 days; the increase in the enzyme activity was accompanied by a significant rise in ROS generation which originated from mitochondrial dysfunction (Dong et al., 2011). While these findings proposed a link between SA- β -gal activity and the accumulation of DNA damage and mitochondrial dysfunction, they did not confirm activation of senescence.

In 2012, however, Jurk et al. provided evidence of senescent Purkinje and cortical neurones in the brains of old mice. These neurones showed increased lipid and protein peroxidation and γ H2AX foci, confirming the involvement of a DDR in response to oxidative damage, and expression of p21 and macroH2A, markers of senescence signalling and SAHF formation, respectively; SA- β -gal activity and increased ROS production and IL-6 expression were also observed, suggesting activation of a p21-dependent senescent-like state, accompanied by a SASP in mice post-mitotic neurones. Moreover, this phenotype was aggravated by telomere dysfunction (Jurk et al., 2012). Overall, this work suggested that accumulation of oxidative DNA damage and telomere dysfunction could result in the development of a senescent-like phenotype in post-mitotic neurones. More importantly, this phenotype could potentially contribute to neuronal dysfunction through a pro-inflammatory and pro-oxidant mechanism, similar to the SASP.

Despite this evidence, the activation of senescence in neurones seems contradictory. The fact that neurones are terminally differentiated questions whether they can actually induce senescence through the same mechanisms as mitotic cells do. A possible answer to this relates to the cell cycle regulatory mechanisms that have been implicated in the neuronal DDR and repair mechanisms. In recent reports, it has been shown that DNA damage causes re-activation of the neuronal cell cycle, which resulted necessary for the activation of the proper repair mechanisms. As part of this cell cycle reactivation program, cell cycle arrest occurs prior to S-phase transition, otherwise aberrant DNA replication could occur and lead the neurones to apoptosis (Kruman et al., 2004; Schwartz et al., 2007; Tomashevski et al., 2010). Taking this evidence into account, cell cycle reactivation in damaged neurones could resemble an active proliferative state as seen in mitotic cells. Under these circumstances, a persistent DNA damage could cause an aberrant cell cycle arrest, which instead of directing cells to re-enter a post-mitotic state or to die by apoptosis, it could promote activation of senescence pathways and the development of a senescent phenotype, including a SASP (**Figure 1.4**).

Taking all this evidence into account, further work should be done to confirm Jurk et al. (2011) findings in human neurones and to determine the repercussions of a senescent-like phenotype in neurodegeneration. Part of this project focused on determining the relevance of neuronal senescence *in vivo* in the brains of ALS/MND donors. As it will be explained in the final section of this chapter, oxidative stress and cumulative DNA damage have been shown to be involved in ALS/MND, thus providing an interesting option to investigate activation of senescence in neurones in response to oxidative stress.

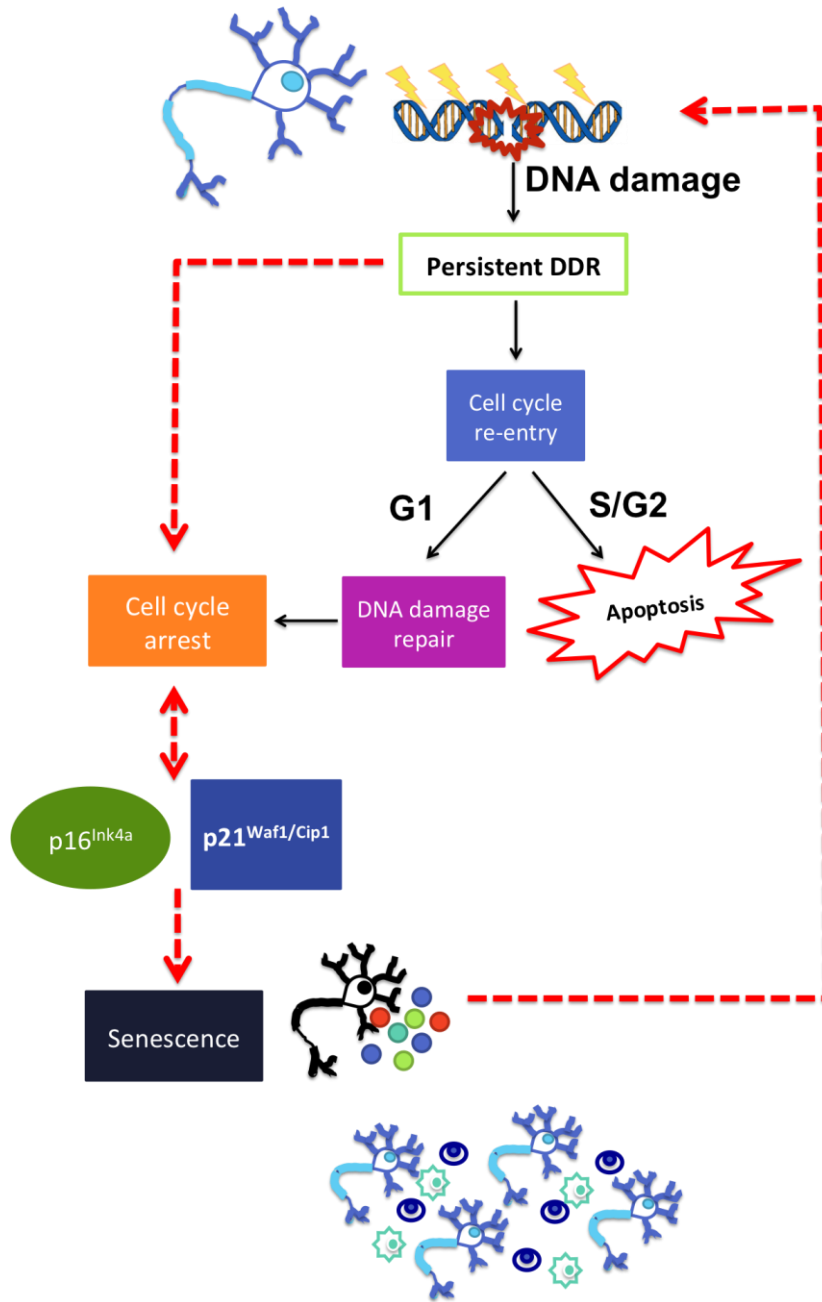


Figure 1.4 Hypothetical mechanism of neuronal senescence induction.

DNA damage in neurones could re-enter their cell cycle as part of the DDR. Neurones would undergo G1 transition, activate repair mechanisms and arrest their cell cycle once the DNA damage is repaired. However, if neurones are undergoing a persistent DDR, these cell cycle arrest signals could induce expression of p16 and p21 senescence effector pathways and promote the development of a senescent phenotype, including a SASP. Paracrine SASP would generate a pro-inflammatory and pro-oxidant environment that would reinforce the DDR and contribute to neuronal dysfunction.

1.3. Amyotrophic Lateral Sclerosis

Neurons are especially vulnerable to oxidative stress due in part to their post-mitotic nature, their high metabolic rate, their polyunsaturated fatty acids enriched cell membrane and their poor antioxidant mechanisms (Friedman, 2011). Therefore, oxidative stress could be the ideal culprit behind a persistent neuronal DNA damage response and senescence in the ageing brain and in neurodegeneration. Numerous evidence of oxidative damage in neurodegeneration has been shown in AD (Lee et al., 2013; Scheff et al., 2016), PD (Choi et al., 2005; Deas et al., 2016) and ALS/MND (Li et al., 2011; Nagase et al., 2016).

Amyotrophic lateral sclerosis (ALS), also referred to as motor neuron disease (MND) or Lou Gehrig's disease, is an adult-onset neurodegenerative disorder of rapid progression characterised by the degeneration of motor neurones from the motor cortex (MCx), brainstem and spinal cord (Sc) (Kiernan et al., 2011). Motor neuron dysfunction in ALS/MND leads to progressive muscle atrophy, weakness, paralysis, and death, usually by respiratory failure, within 2-5 years after diagnosis; although age and site of onset, as well as severity, are highly variable (Kiernan et al., 2011; Traxinger et al., 2013). ALS/MND cases are classified in sporadic (sALS/MND) and familial (fALS/MND) forms. The latter are associated with inheritable genetic mutations that are predominantly autosomal dominant, and account for approximately 5-10% of the cases, although some of these mutations are also present in sALS forms (Al-Chalabi et al., 2013).

The gene encoding for the copper/zinc superoxide dismutase (*Cu/Zn SOD*, *SOD1*) was the first gene to be associated to fALS/MND, representing 20% of the familial cases of ALS/MND (Rosen et al., 1993). Currently, there are 29 known gene mutations that have

been linked to the disease and that alter proteins involved in a variety of cell functions. *TARDBP*, *FUS/TLS*, *HNRNPA2/B1*, *ELP3*, *HNRNPA1*, *STX* and *ATXN2* are involved in RNA metabolism, while *ALS2*, *VABP*, *CHMP2B*, *FIG4*, *OPTN* are linked to vesicle trafficking and *UBQLN2* and *VCP* to proteosomal function (Chen et al., 2013). The hexanucleotide expansion in *C9orf72* has been implicated in the pathology of ALS-FTD (fronto-temporal dementia) (DeJesus-Hernandez et al., 2011; Mori et al., 2013; Renton et al., 2011). The most recent gene associated to fALS/MND is *TBK1*, which encodes for a TANK-binding kinase involved in autophagy and the immune response (Freischmidt et al., 2015, 2016).

Due to its complexity, the exact processes through which ALS/MND originates, develops and progresses are still not well understood, however, several mechanisms have been suggested to contribute to the pathology. These mechanisms comprise defects in RNA processing, protein aggregation, excitotoxicity, endoplasmic reticulum (ER) stress, disrupted axonal trafficking, mitochondrial dysfunction and oxidative stress (Barber and Shaw, 2010).

Numerous studies have shown increased oxidative nuclear and mitochondrial DNA damage in ALS/MND *in vivo*. This evidence suggests that oxidative DNA damage is involved in the pathogenesis of the disease and might reflect mitochondrial alterations and neuronal dysfunction. For instance, early studies by Ferrante et al. (1997) reported increased levels of 8-OHdG, a marker of DNA oxidation, in the MCx and Sc of sALS patients, while in fALS cases, this increase was only detected in the MCx (Ferrante et al., 1997). In a different study, assessment of 8-OHdG levels in cerebrospinal fluid (CSF), urine and plasma of ALS/MND patients revealed significantly higher levels in patients

when compared to controls; additionally, a disease-severity dependent rate of increase in 8-OHdG levels was detected in urine (Bogdanov et al., 2000). Studies in the SOD1^{G93A} mutant mice have shown formation of single-strand (SSBs) and DSBs in neuronal and mitochondrial DNA, which increased with the progression of the disease (Martin et al., 2007). A more recent study has measured 8-OHdG levels, along with other markers of oxidative stress such as malondialdehyde (MDA), as well as IL-6 and IL-8 levels in a cohort of 10 ALS donors and 10 controls. A significant increase in MDA and 8-OHdG was detected in ALS patients, together with increased concentrations of IL-6 and IL-8 cytokines, which indicated alterations in the redox biology of ALS patients and alterations in the inflammatory response (Blasco et al., 2016). Accumulation of DNA damage in ALS/MND has also been linked to the *C9orf72* hexanucleotide expansion. Lopez-Gonzalez et al. (2016) also showed an age-dependent increase in DNA damage in induced pluripotent stem cells (iPSCs) motor neurones derived from *C9orf72* patients, which correlated with high levels of oxidative stress and was linked to an ATR/p53-dependent DDR (Lopez-Gonzalez et al., 2016). Moreover, a recent report suggests *C9orf72* hexanucleotide expansions disrupt ATM-mediated DNA damage repair *in vitro* and *in vivo*, in the spinal cord of *C9orf72* patients, suggesting DNA damage accumulation and genomic instability as contributors to the disease (Walker et al., 2017).

Overall, oxidative stress and DNA damage are both implicated in the pathogenesis of ALS/MND. More importantly, DNA damage has been shown to accumulate in the disease, which opens the possibility for neurones to activate a senescent-like state.

1.4. Hypothesis

Neurones undergo a senescent-like state in response to oxidative DNA damage and a persistent DNA damage response. They also develop a secretory phenotype characterised by the release of pro-inflammatory and pro-oxidant factors that contributes to neuronal dysfunction in neurodegeneration.

1.4.1. Aims

Using two experimental approaches, this study aimed to determine:

1. *In vitro* approach

- a. Whether cultured human neurones exposed to oxidative stress could develop a persistent DNA damage.
- b. Whether this damage caused activation of a “classical” senescent phenotype, including activation of senescence pathways, expression of senescence markers and development of a SASP.

2. *In vivo* approach

- a. Whether senescent neurones were present in brains with neurodegeneration. For this project, ALS/MND was considered a paradigm of neurodegeneration.
- b. Whether senescent neurones in ALS/MND correlated with DNA damage and a DNA damage response.
- c. Whether senescent neurones in ALS/MND exhibited a senescent phenotype.

Chapter 2. Development and characterisation of an *in vitro* model of oxidative DNA damage in human neurones

2.1. Introduction

Normal cellular metabolism results in the formation of oxygen metabolites with oxidising potential, also known as reactive oxygen species (ROS) (Birben et al., 2012; Dringen et al., 2005; Mittal et al., 2014). The main endogenous oxidants are the hydroxyl radical ($\bullet\text{OH}$), the superoxide anion (O_2^-), hydrogen peroxide (H_2O_2) and hypochlorous acid (HOCl), and they are predominantly generated by the mitochondrial electron transport chain (ETC) as well as by cytochrome P450 activity (Davalli et al., 2016; Mittal et al., 2014). H_2O_2 originates from superoxide, through the action of superoxide dismutases (SODs), and can generate $\bullet\text{OH}$ through the Fenton reaction (Birben et al., 2012; Dringen et al., 1999, 2005). In neurones, low levels of H_2O_2 , and ROS in general, have a role in cell signalling and inter-cellular communication (Hohnholt et al., 2015; Schieber and Chandel, 2014); however, an imbalance between the formation and breakdown of ROS can lead to accumulation of these molecules which then cause damage to lipids, proteins, RNA and DNA in the cell. Alteration of the balance between oxidant-antioxidant mechanisms is known as oxidative stress (Davalli et al., 2016).

Oxidative stress is a common characteristic of ageing and has been widely investigated as a mechanism of neurodegeneration (Jiang et al., 2016; Schriener, 2005). Oxidative stress has also been linked to the induction of senescence in mitotic cells as a result of DNA damage (Pole et al., 2016; Zhang et al., 2017). Oxidative stress related senescence has also been studied in the ageing brain; astrocytes have been shown to develop features of senescence, including a SASP, in response to chronic oxidative stress (Bitto et al., 2010;

Crowe et al., 2016), but whether a similar phenotype could develop in post-mitotic cells such as neurones is not known.

To address this question, an *in vitro model* of neuronal oxidative DNA damage was developed using the Lund Human Mesencephalic (LUHMES) cell line. LUHMES are conditionally immortalised human dopaminergic neuronal precursor cells that can be differentiated into post-mitotic neurones through the addition of tetracycline and other specific factors. LUHMES are a subclone of the MESII(1)C2.10 cell line, which was obtained from an 8-week-old human embryo (Lotharius et al., 2002). LUHMES were immortalised with a LINX *v-myc* retroviral vector containing a tetracycline-controlled transactivator (tTA) (Hoshimaru et al., 1996; Lotharius et al., 2002). In this system, the absence of tetracycline (tet) allows tTA to activate transcription of the *v-myc* gene from a CMV promoter, thus maintaining LUHMES in a proliferative state. When tet is added to the culture media it binds to tTA and represses *v-myc* expression. This action induces cell cycle arrest and initiates differentiation.

This chapter focuses on the optimisation of the culturing conditions for the LUHMES and the characterisation of their post-mitotic phenotype. To model oxidative DNA damage in LUHMES, H₂O₂ was used. This chapter also describes the experiments performed to establish the concentration of H₂O₂ that would induce DNA damage. The data suggest that a single bolus of H₂O₂ causes acute damage in the form of double strand breaks (DSBs) but is not enough to induce a persistent DNA damage in LUHMES. A protocol was therefore developed using a repeat dosing of differentiated LUHMES with H₂O₂, which caused chronic DNA damage that was detectable 96 hours post-stress.

2.2. Aims and objectives

- 1) Induce a persistent DNA damage response in human neuronal cells to determine if this could stimulate aspects of a senescent phenotype in post-mitotic neurones.
 - a) Optimise the cell culture conditions for the LUHMES and confirm their successful differentiation into post-mitotic neurones.
 - b) Characterise the response of post-mitotic LUHMES to an extracellular source of oxidative stress through incubation in different concentrations of H₂O₂.
 - c) Determine the optimal conditions to cause a persistent oxidative DNA damage in LUHMES.

2.3. Materials and Methods

All chemicals were obtained from Sigma-Aldrich (St Louis, MO, USA) unless stated. Solutions required for the experiments described in this chapter were prepared as specified in **Appendix A**.

2.3.1. LUHMES cell culture optimisation

NunclonTM cell culture plastic flasks (ThermoFisher Scientific, Boston, MA, USA) and GreinerTM multiwell plates (Sigma-Aldrich, St Louis, MO, USA) were pre-coated with a solution of 50 µg/ml poly-L-ornithine hydrobromide (pLo) (Sigma-Aldrich) and 1 µg/ml fibronectin (Sigma-Aldrich) from human plasma in distilled water (dH₂O). Flasks/plates were pre-coated with the pLo/fibronectin solution at 37 °C for at least 3 hours. After incubation, the coating solution was removed and culture flasks/plates were washed once with 1x sterile phosphate buffered saline (PBS) before cell seeding.

Optimisation of the LUHMES cell culture conditions involved the assessment of two types of media: GlutaMAX media (DMEM/F-12 [Dulbecco's Modified Eagle Medium/Nutrient Mixture F-12] Gibco®) GlutaMAX [ThermoFisher Scientific] + 1x N2-supplement [ThermoFisher Scientific] + 1% Penicillin/Streptomycin [Pen/Strep] [Lonza Group Ltd, Basel, Switzerland], and Advanced media (Advanced DMEM/F12 [Gibco®] + 1x N2-Supplement + 2 mM L-glutamine [Lonza Group Ltd] + 1% Pen/Strep). For proliferating cells, 40 ng/ml of recombinant basic fibroblast growth factor (bFGF) (Peprotech EC Ltd, Rocky Hill, NJ, USA) was added to both versions of cell culture media just prior to cell seeding. For LUHMES differentiation protocol two media compositions were assessed. The first version (+/+) consisted of GlutaMAX or Advanced media with 1 µg/ml tetracycline hydrochloride (tet) (Sigma-Aldrich) and 2 ng/ml recombinant human GDNF (Peprotech EC Ltd); the second version (+/-) omitted the addition of human GDNF. **Figure 2.1A** contains a summary of the cell culture media and factors used for the optimisation of the LUHMES culturing conditions.

2.3.1.1. LUHMES maintenance and differentiation: Optimisation of cell culture conditions

LUHMES were cultured in GlutaMAX or Advanced proliferation media and maintained at 37 °C with 5% CO₂. Cells were enzymatically dissociated using 1x trypsin versene (Lonza Group Ltd) and passaged when they reached 80% confluency. For differentiation, the two-step protocol developed by Scholz et al. was followed (**Figure 2.1B**) (Scholz et al., 2011). Briefly, proliferating LUHMES were seeded on to pre-coated T75 flasks at a density of 3x10⁶ cells/flask in GlutaMAX or Advanced proliferation media. Differentiation was started 24 hours after seeding (Day 0) by changing to GlutaMAX/Advanced (+/+) or (+/-) differentiation medium. After 2 days of pre-differentiation, cells were trypsinised and replated onto pre-coated 24 and 6-well plates,

as well as 10 cm dishes. Cell densities are specified in **Table 2.1**. Cells were maintained in differentiation media for further 3 days for cells to reach a fully differentiated state. A visual assessment of the cells during the differentiation protocol was performed to detect abnormal cell detachment and cell death under the culturing conditions already described.

Plate or dish format	Cell density (cells/well or dish)
24-well plate	3.5×10^5 and 5×10^5
6-well plate	1.5×10^6
10 cm dish	2.5×10^6

Table 2.1 Pre-differentiated LUHMES densities used for cell culture optimisation.

Different plating formats were assessed for LUHMES cell culture. A visual assessment of cell health (proliferation, cell death, neurite development and morphology) was conducted in LUHMES plated in 6-well and 24-well plates, as well as in 10 cm dishes. Cells seeded in 24-well plates were used for the MTT assays described in this chapter.

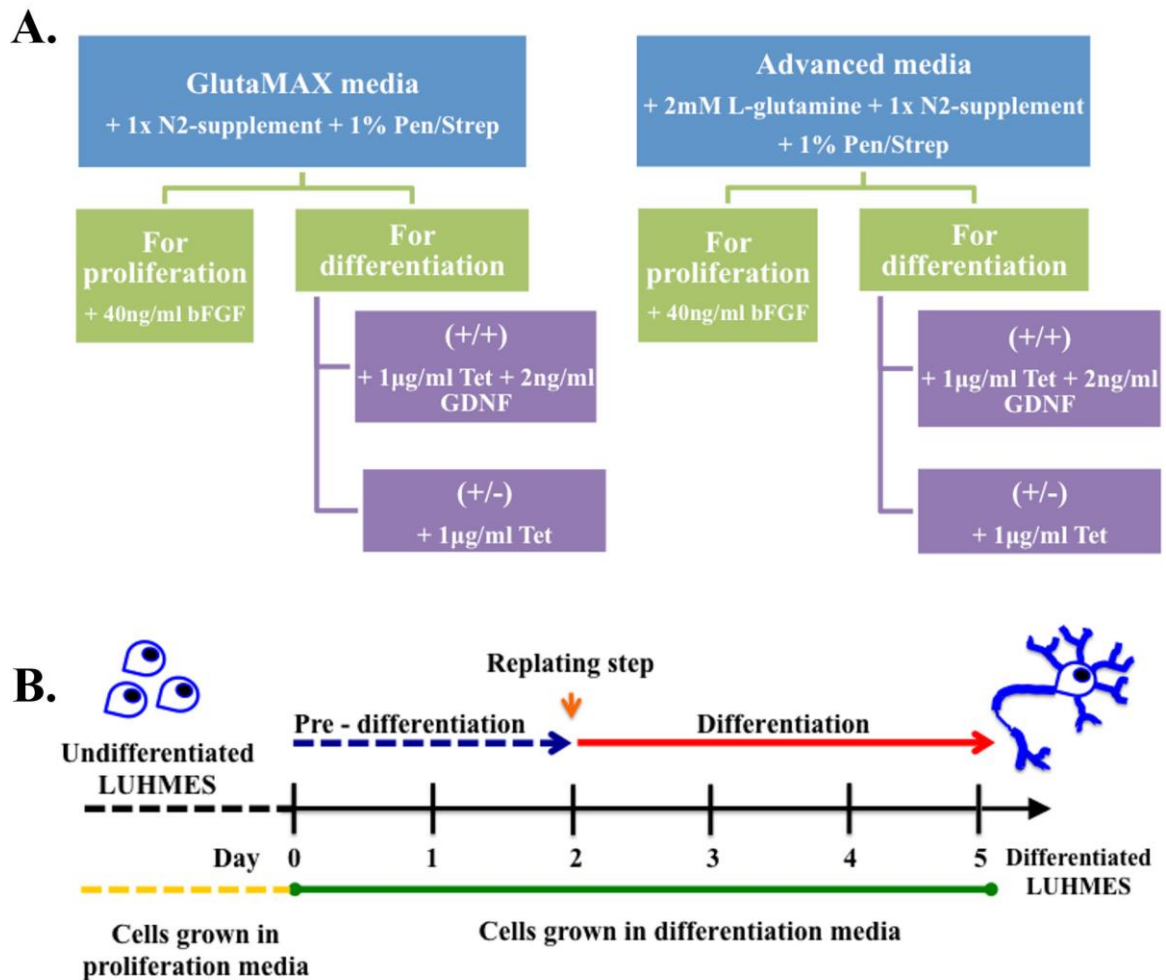


Figure 2.1 Optimisation of LUHMES cell culture conditions.

A. Two different media compositions (Advanced and GlutaMAX) were assessed for culturing LUHMES. In addition, 2 combinations of differentiation factors (tetracycline [Tet] and GDNF) were used to differentiate LUHMES into mature neurones. **B.** The 2-step differentiation protocol (Scholz et al., 2011) included a pre-differentiation step, where proliferating LUHMES were incubated with differentiation media for 2 days, followed by a re-plating step at day 2. After re-plating, LUHMES were kept in differentiation media for 3 more days

2.3.1.2. MTT reduction assay

To determine the optimal cell culture conditions for LUHMES, their health was monitored under the conditions summarised in **Figure 2.1A** using the MTT reduction assay. The MTT reduction assay has been widely used to measure cell proliferation and cytotoxicity in cells in culture. Cell health was assessed in normal differentiated LUHMES as well as LUHMES incubated with 100 μM H_2O_2 , to investigate vulnerability of LUHMES to an external stress when cultured in the 2 different culture medias.

Differentiated LUHMES plated in 24-well plates were treated with 100 μM H_2O_2 for 24 hours. Control cells were treated with the same volume of 1x sterile PBS (vehicle) and a medium-only control was included in all experiments (background). 24 hours after stressing the cells, 50 μl of MTT (Sigma-Aldrich, MA, USA) solution were added to each well and cells were incubated for 3 hours at 37 $^\circ\text{C}$ to promote the formation of formazan crystals. To solubilise the crystals, 550 μl of SDS/DMF solution was added to each well and the plates were incubated for 30 minutes at room temperature (RT), in darkness and with constant agitation. The final solubilised solution was homogenised by pipetting it up and down gently; three 200 μl samples were taken from each well and transferred to a 96-well plate. Absorbance was read at 595 nm in a PHERAStar microplate reader (BMG Labtech, Ortenberg, Germany). For data analysis, the absorbance value (AU) from the medium-only control (background) was subtracted from the values of the control and treated samples. Data was expressed as percentage (%) of viable cells.

2.3.2. Characterisation of differentiated neurones by immunocytochemistry

Scholz et al. characterised differentiated LUHMES using several approaches, including quantification of mRNA of cell cycle control related genes, immunocytochemical

detection of neuronal differentiation markers and time-lapse microscopy to assess neurite outgrowth (Scholz et al., 2011). To confirm that we could successfully replicate the differentiation of LUHMES, we investigated the expression of neuronal and cell cycle markers in proliferating, differentiating and differentiated LUHMES by immunocytochemistry. All experiments from this point on were performed using Advanced proliferation media and using Advanced (+/+) media for differentiation.

For immunocytochemistry experiments, cells were plated at a density of 2.5×10^5 cells/well onto pre-coated glass coverslips, in 24-well plates. Cells were fixed with 4% paraformaldehyde (PFA) at days 0, 1, 2, 3, 4 and 5 of the differentiation process. Cells were permeabilised by incubating them in 0.3% Triton-X100 (Sigma-Aldrich) for 3 minutes, followed by 3 washes with 1x PBS. Cells were then blocked in 3% bovine serum albumin (BSA) blocking solution for 30 minutes and then single labelled for β -III-tubulin, MAP-2 and PSD95. Details for the antibodies used as well as incubation conditions are described in **Table 2.2**. Cells were washed 3 times with 1x PBS and incubated with the corresponding secondary antibodies, as detailed in **Table 2.3**. Cells were washed 3 times with 1x PBS and incubated for 10 minutes in Hoechst 33342 dye (Sigma-Aldrich), followed by 3 further washes with 1x PBS. Coverslips were mounted in Flouromount™ Aqueous Mounting medium (Sigma-Aldrich). Omission of the primary antibody (Negative control) and incubation with rabbit/mouse isotype controls (IgG controls) were included in all experiments. Images of the cells were taken with a Nikon ECLIPSE Ni microscope (Nikon Instruments, Amsterdam, Netherlands).

Dual labelling was performed for Ki67 and E2F1 (E2F transcription factor 1) with the cytoskeletal marker β -III-tubulin. For this, cells were fixed, permeabilised and blocked as

explained before. After incubation with the primary antibodies against Ki67 and E2F1 (**Table 2.2**), cells were washed 3 times with 1x PBS and incubated with the respective secondary antibody, as described in **Table 2.3**. From this point on, the staining protocol was performed under darkness. Cells were washed 3 times with 1x PBS and blocked again, for 30 minutes. Cells were incubated with the primary anti- β -III-tubulin overnight at 4 °C. Cells were washed 3 times with 1x PBS and incubated with the goat anti-chicken fluorescent secondary antibody (**Table 2.3**). Cells were washed 3 times with 1x PBS and incubated in Hoechst 33342 dye for 10 minutes, followed by 3 washes with 1x PBS. Coverslips were mounted and visualised as explained previously for the single labelled samples.

Antibody	Species	Clone	Dilution and incubation conditions	Source	Catalog number
Ki67	Mouse monoclonal	MM1	1:50 (overnight at 4 °C)	Leica Microsystems, Wetzlar, Germany.	NCL-L-Ki67-MM1
E2F1	Rabbit polyclonal	-	1:100 (2 hours, RT)	Proteintech, Rosemont, IL, USA	12171-1-AP
β -III-tubulin	Chicken polyclonal	-	1:1000 (2 hours, RT)	Merck Millipore, Darmstadt, Germany.	AB9354
PSD95	Mouse monoclonal	K28/43	1:1000 (2 hours, RT)	Merck Millipore, Darmstadt, Germany.	MABN68
γ H2AX (Ser 139)	Mouse monoclonal	JBW301	1:1000 (2 hours, RT)	Merck Millipore, Darmstadt, Germany.	05-636

Table 2.2 Primary antibodies used for immunocytochemistry.

Primary antibodies, dilutions and incubation conditions used for single and double labelling of proliferating and differentiating LUHMES.

Antibody	Species	Dilution and incubation conditions	Source	Catalog number
488 Alexa Fluor [®] anti-chicken	Goat	1:1000 (1 hour, RT)	Thermo Fisher Scientific, Waltham, MA, USA	A-11039
568 Alexa Fluor [®] anti-rabbit	Donkey	1:1000 (1 hour, RT)		A10042
568 Alexa Fluor [®] anti-mouse	Goat	1:1000 (1 hour, RT)		A-11004

Table 2.3 Fluorescent secondary antibodies used for immunocytochemistry.

Secondary antibodies, dilutions and incubation conditions used for visualisation of proteins labelled by immunocytochemistry in proliferating and differentiating LUHMES.

2.3.3. Optimisation of H₂O₂ treatments

Pre-differentiated LUHMES were re-plated into 24 well plates for the cell viability assays, and on to glass coverslips for the immunocytochemistry experiments, at a density of 3.5×10^5 cells/well. Cells were incubated for further 3 days before H₂O₂ exposure. On the 5th day after differentiation, cells were incubated with 10, 25, 50, 75 and 100 μ M H₂O₂ for 1, 2, 4, 6 and 24 hours. Cell viability and induction of DNA damage were assessed as described next.

2.3.3.1. Cell viability assays to assess H₂O₂-induced toxicity

To assess cell viability and cell health under these conditions, metabolic activity of the cells was monitored using the MTT reduction and the Ethidium homodimer-1 (EthD-1) staining protocol. The MTT assay was performed as described in **section 2.3.1.2**. The EthD-1 staining protocol is described below.

EthD-1 is a cell-impermeant fluorescent dye that binds to DNA and is used to label and detect dying or dead cells, since it can only enter cells with a compromised membrane. After treatment with H₂O₂ cell culture medium was removed and replaced with 250 μ l of 2 μ M EthD-1 (Sigma-Aldrich) solution and 250 μ l of Advanced (+/+) medium per well. Cells were incubated at 37°C for 1 hour after which fluorescence was read on a PHERAStar spectrophotometer at Ex570/Em610. The plates were stored at -20 °C overnight and then thawed to cause membrane rupture in all the cells. 500 μ l of 2 μ M EthD-1 solution were added to each well and the plates were incubated for 1 hour at 37 °C. Fluorescence was read using the same parameters as already described and the results were used to normalise the data to the number of total cells/well.

2.3.3.2. Immunocytochemical detection of double strand breaks (DSBs)

Immunocytochemistry against γ H2AX was performed to detect oxidative DNA damage in the form of DSBs in LUHMES exposed to H_2O_2 . The formation of DSBs was investigated at 1, 2, 4, 6 and 24 hours after H_2O_2 treatment in order to study the kinetics of the formation of γ H2AX foci and of the DNA repair machinery when LUHMES were exposed to the different H_2O_2 concentrations described previously. The fixation, immunocytochemistry and mounting protocols were performed as described in **section 2.3.2**. The primary and secondary antibodies used for these experiments are listed in **Table 2.2** and **Table 2.3**, respectively.

2.3.4. Double stress model

To develop a persistent oxidative DNA damage model, a double H_2O_2 stress protocol was established by exposing previously stressed LUHMES to a second H_2O_2 insult. Before doing this, the clearance rate of extracellular H_2O_2 was assessed in LUHMES incubated with 50 μ M H_2O_2 to quantitatively determine the ability of LUHMES to remove H_2O_2 from the culture media.

2.3.4.1. H_2O_2 clearance: pHPA extracellular H_2O_2 assay

Pre-differentiated LUHMES were replated onto pre-coated 96-well plates at 3 different densities: 2×10^4 , 3×10^4 and 4×10^4 cells/well. Cells were kept in differentiation media for 3 more days and H_2O_2 clearance assays were performed on day 5 of the differentiation protocol.

H_2O_2 clearance rate was determined following the method described by Wagner et al. (2013). This assay allows for the determination of the rate of removal of extracellular

H₂O₂ by cells in culture. For this, cells were incubated with a known concentration of H₂O₂. Addition of H₂O₂ was done at intervals of 30 seconds - 5 minutes to consecutive wells; once H₂O₂ was added to the last set of wells, a stopping solution containing horseradish peroxidase (HRP) and pHPA was added to all wells. The HRP in the stopping solution reacts with the remaining H₂O₂ and active HRP oxidises pHPA, a reagent that emits fluorescence under these conditions. Under these conditions, fluorescence intensity (FI) is proportional to the concentration of H₂O₂ present in the culture media. A set of H₂O₂ standards was included in every experiment which were used to create a standard curve to calculate H₂O₂ concentration in the samples (Wagner et al., 2013).

Prior to the start of experiments cells were washed and media was replaced with Gibco® Hank's Balanced Salt Solution (HBSS; Thermo Fisher Scientific). Standard stock solutions of H₂O₂/HBSS were prepared before use at increasing concentrations of 0, 2, 4, 8, 12, 16, 20, 24, 28, 32, 40, 48, 60, 70, 80 and 100 µM H₂O₂. These were then added to wells containing 50 µl of HBSS to make a final volume of 100 µl/well and final standard concentrations of 0, 1, 2, 4, 6, 8, 12, 16, 20, 24, 30, 35, 40 and 50 µM H₂O₂. All standards were run in triplicate and were used to create a standard curve of remaining H₂O₂ in the medium. Parallel to the preparation of standards, 50 µl of 0 µM and 100 µM H₂O₂ solutions were added to wells containing cells, in triplicate, to make final concentrations of 0 µM and 50 µM in 100 µl/well. H₂O₂ was added at 5 minutes intervals for 30 minutes. Immediately after adding the H₂O₂ to the final wells, 100 µl of stopping solution were added to all the wells, including standards. The stopping solution was added to all wells, including standards. Blank wells (standards with no H₂O₂) were included in every plate. Fluorescence was then read using a PHERAStar multiplate reader (Ex345/Em425) at intervals of 5 minutes for 30 minutes. These readings were performed to ensure that

results remained stable over the specified period of time, but only one reading was used for the final analysis. Each experiment consisted of LUHMES samples and standards run in triplicate; 3 independent experiments were performed for the final analysis.

For data analysis the mean value of the blanks was subtracted from standards and LUHMES samples. A standard curve was created using the fluorescence intensity values from the H₂O₂ standards (**Figure 2.2A**) and this was then used to determine the remaining extracellular H₂O₂ concentration ([H₂O₂]/ μ M) in the LUHMES samples. A graphic depiction of the removal of extracellular H₂O₂ was obtained by plotting [H₂O₂]/ μ M versus time (minutes) (**Figure 2.9**). The observed first-order rate constant (k_{obs}) was given by the slope of ln[H₂O₂] versus time (seconds) (**Figure 2.2B**). The observed rate constant for each cell (k_{cell}) was obtained using the formula

$$k_{cell} = k_{obs}/(\text{cells L}^{-1})$$

where (cells L⁻¹) is the number of cells in one well divided by the volume of media (in liters) in that same well (before the addition of the stopping solution). The rate of removal of extracellular H₂O₂ was then calculated with

$$\text{rate} = -k_{cell} [\text{H}_2\text{O}_2] (\text{cells L}^{-1})$$

The half-life of 50 μ M H₂O₂ was determined using the formula

$$t_{1/2} = 0.693/(k_{cell} (\text{cells L}^{-1}))$$

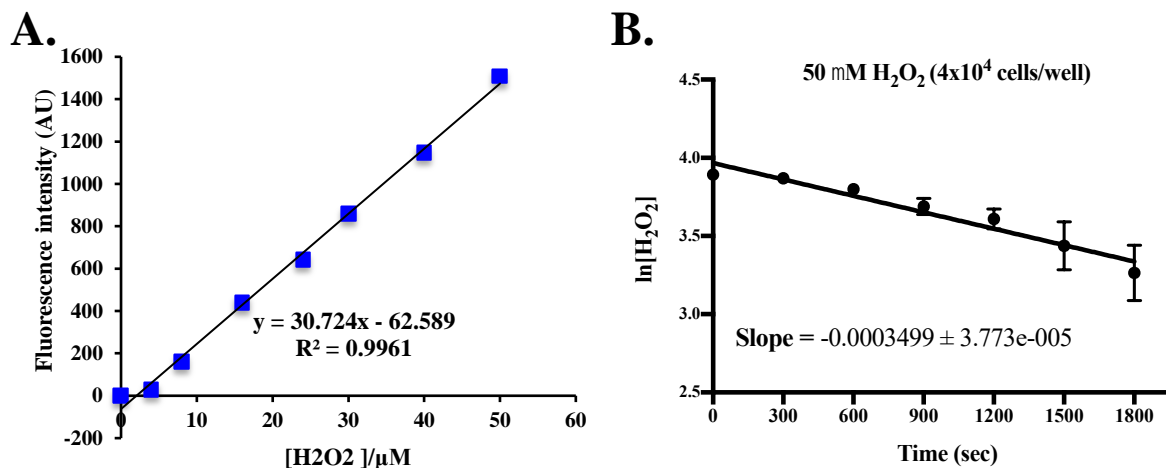


Figure 2.2 Removal of extracellular H₂O₂ by LUHMES: Examples of standard curves and plots used for k_{obs} determination.

A. Representative standard curve used for the pHPA H₂O₂ clearance assay. Standards (0 - 50 μM H₂O₂) were included in every experiment, in triplicate. Fluorescence values for the standards were used to calculate the concentration of H₂O₂ in the cell culture media of LUHMES samples. **B.** Representative plot of $\ln[H_2O_2]$ versus time (seconds) in LUHMES samples with 4×10^4 cells/well. The slope provides the value of the first-order rate constant k_{obs} that is required to calculate the clearance rate for a specific cell density and sample volume.

2.3.4.2. Induction of a persistent oxidative DNA damage

Based on H₂O₂ clearance results, as well as on results obtained from the MTT and EthD-1 assays and the detection of DSBs, the second H₂O₂ insult was applied 6 hours after LUHMES were incubated in H₂O₂ for the first time. For this, differentiated LUHMES (3.5x10⁵ cells/well) plated onto coated 24-well plates were incubated with 50 μM H₂O₂ for 6 hours. After this time, the old media was removed and replaced with freshly prepared 50 μM H₂O₂ media. Cells were kept in culture for 96 hours. To ensure that the second stress did not cause considerable negative effects in LUHMES viability, LUHMES health was assessed with the MTT assay 6, 24, 48, 72 and 96 hours after the second stress and compared to LUHMES incubated once with 50 μM H₂O₂. The MTT assay was conducted as explained previously, in **section 2.3.1.2**.

To investigate whether a second H₂O₂ stress caused persistent DNA damage, formation of γH2AX foci was assessed by immunocytochemistry in double stressed (DS) and single stressed (SS) LUHMES 6, 24, 48, 72 and 96 hours after stress, as described in **sections 2.3.2 and 2.3.3.2**. A quantitative analysis of the percentage of neurones that were stained for γH2AX was performed to compare the effects of a double H₂O₂ challenge. For this, five images per coverslip were taken for every condition, from at least 3 coverslips per experiment. The number of γH2AX⁺ neurones per field was manually quantified, plus the number of total nuclei/field. A percentage was obtained by dividing the number of γH2AX⁺ neurones by the number of total nuclei per field. This result was multiplied by 100 and data was expressed as % γH2AX⁺ LUHMES.

2.3.5. Statistical analysis

Data obtained from the MTT, EthD-1 and H₂O₂ clearance assays was analysed with Prism 7.0c (GraphPad Software, Inc., CA, USA). All data is presented as mean \pm standard error of the mean (SEM).

2.4. Results

2.4.1. Optimisation of LUHMES culturing conditions

To assess the best conditions for LUHMES cell culture, cells were grown in two different media formulations which were selected based on previous research on this cell line (Lotharius, 2005; Lotharius et al., 2002; Schildknecht et al., 2009, 2013; Scholz et al., 2011) and the culturing conditions suggested by the supplier. Early observations of proliferating LUHMES in culture did not detect abnormal proliferation, cell death or morphology changes. During pre-differentiation, cells appeared healthy and there was no obvious difference in terms of neurite development between culturing conditions. The number of cells per ml (cells/ml) was determined each time cells were replated after pre-differentiation. The mean number of cells/ml is reported in **Figure 2.3A** (3 independent counts).

LUHMES pre-differentiated in GlutaMAX (+/-) medium had a lower mean number of cells/ml ($2.4 \times 10^6 \pm 145,895$) compared to the LUHMES in Advanced (+/-) ($3.2 \times 10^6 \pm 142,945$) and Advanced (+/+) ($3.5 \times 10^6 \pm 210,621$) medias. Cells pre-differentiated in GlutaMAX (+/+), which contained recombinant GDNF, had significantly more cells/ml ($3 \times 10^6 \pm 77,675$) than the LUHMES grown in GlutaMAX (+/-); however, when compared to the cells grown in Advanced (+/+) media, the mean number of cells/ml was still significantly lower. There was no difference in the mean number of cells/ml between the LUHMES that were pre-differentiated in Advanced (+/-) and (+/+) medias (**Figure 2.3A**).

Pre-differentiated LUHMES were replated onto coated 24, 12 and 6-well plates and 10 cm dishes. Cell detachment was noticeable in the 10 cm dishes on day 4 of

differentiation, irrespective of cell culture conditions. At day 5, cells cultured in 10 cm dishes had detached completely, while the cells plated in multi-well plates showed only minor detachment (cells in the GlutaMAX medium) or no detachment at all (cells in the Advanced medium). Analysis of LUHMES differentiated in Advanced (+/-) or (+/+) revealed that the addition of GDNF during differentiation maintains cell health for further 5 days (d10) after cells have completed the 5 days of differentiation (**Figure 2.3B**). LUHMES differentiated and maintained in Advanced (+/-) media until day 10 (d10) showed a marked decline in metabolically active, as measured by the MTT assay, compared to those that were maintained in GDNF enriched media. These results suggest that the addition of GDNF is not only necessary for the cells to develop a full dopaminergic phenotype, but it also enhances their overall health and survival in culture.

To assess the viability of the cells and their vulnerability to an external stress under these different culturing conditions, LUHMES plated on to 24-well plates at two different densities were exposed to 100 μM H_2O_2 . Cell health as assessed by the MTT assay revealed a higher vulnerability of the LUHMES to 100 μM H_2O_2 when cultured, differentiated and maintained in GlutaMAX (+/-) or (+/+) media (**Figure 2.3C-D**). A significant reduction of 57.73% ($p < 0.0001$) in metabolically active cells was detected in LUHMES cultured in GlutaMAX (+/-) and of 56.1% ($p < 0.0001$) in LUHMES cultured in GlutaMAX (+/+) when plated at 5×10^5 cells/well (**Figure 2.3D**). The effect of the H_2O_2 was more intense when the cell density was reduced to 3.5×10^5 cells/well, with a reduction of 87.74% ($p < 0.0001$) in metabolically active cells cultured in GlutaMAX (+/-) and of 89.4% ($p < 0.0001$) in cells cultured in GlutaMAX (+/+) (**Figure 2.3C**). H_2O_2 did not have an effect on the metabolism of LUHMES cultured and differentiated in Advanced (+/-) and (+/+) when plated at a density of 5×10^5 cells/well (**Figure 2.3D**);

however, there was a significant reduction in cell metabolism when the cells were less dense (Advanced (+/-), 60.3%, $p < 0.0001$; Advanced (+/+), 66%, $p < 0.0001$) (**Figure 2.3C**). Overall there was a greater impact of H₂O₂ on LUHMES metabolic activity in cells cultured in GlutaMAX media, regardless of the cell density, compared to the Advanced media.

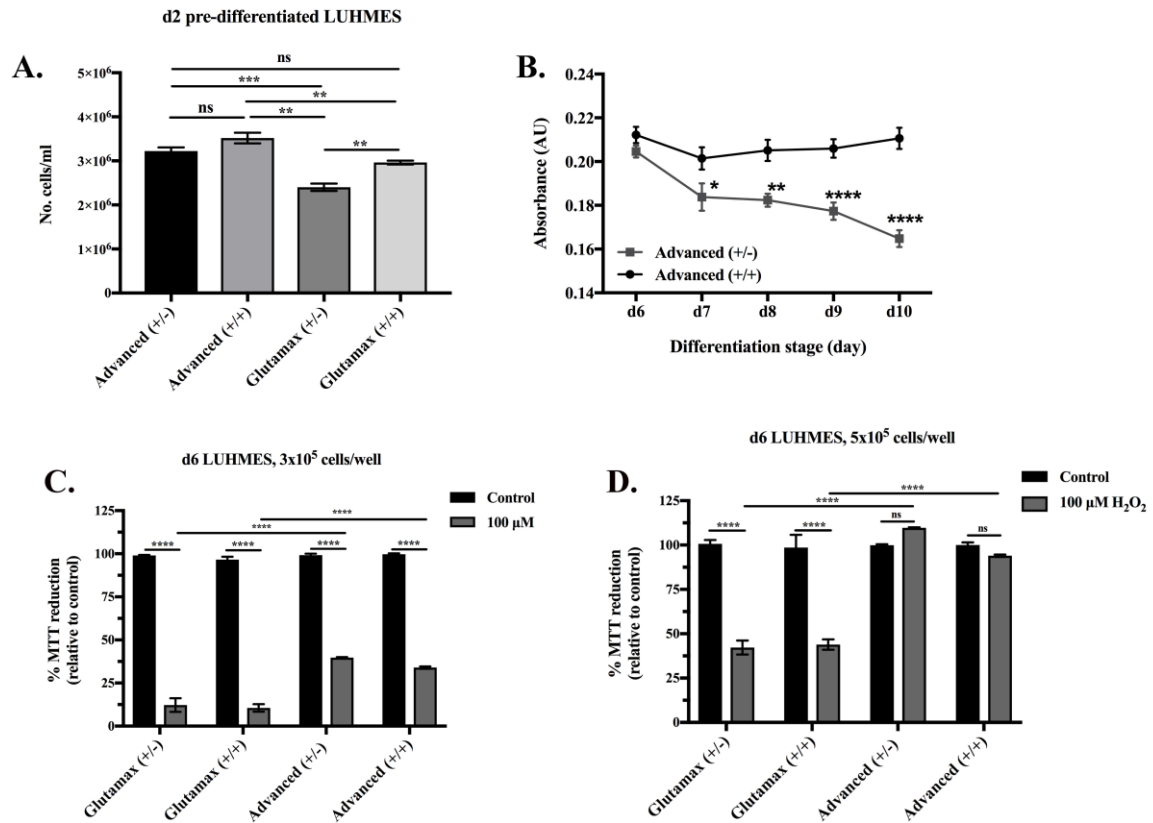


Figure 2.3 LUHMES were cultured in 2 different cell culture media and differentiated using different protocols to determine the optimal culture conditions for future experiments.

A. Determination of the number of cells/ml prior to the re-plating step (d2-LUHMES) showed that there were less cells per ml on average when cultured in GlutaMAX media than those cultured in Advanced media. [(+/+): GDNF and tetracycline; (+/-): only tetracycline]. One-way ANOVA with multiple comparisons, ** $p \leq 0.01$, *** $p \leq 0.001$. **B.** Metabolic activity of control differentiated LUHMES (d6-d10) was assessed using the MTT assay. A significant decrease in metabolic activity over time was detected in control LUHMES differentiated only with tetracycline (Advanced (+/-)), compared to control LUHMES cultured with GDNF and tetracycline (Advanced (+/+)). Since data was obtained from control LUHMES, it was not normalised and is expressed in absorbance units (AU). Two-way ANOVA with multiple comparisons, * $p \leq 0.05$, ** $p \leq 0.01$, **** $p \leq 0.0001$. **C-D.** Differentiated LUHMES (d6) cultured in 4 different media compositions and at different plating densities, were exposed to 100 μM H₂O₂ to determine the vulnerability of the cells to an external stress under these conditions. H₂O₂ was significantly more toxic to differentiated LUHMES maintained in the GlutaMAX media and cells were more vulnerable to stress at lower plating densities. Data was expressed in % metabolically normal cells relative to controls. One-way ANOVA with multiple comparisons, ** $p \leq 0.01$, *** $p \leq 0.001$, **** $p \leq 0.0001$. (Data represents mean \pm SEM. For all experiments: $n=3$, at least 3 replicates/experiment).

2.4.2. LUHMES can be successfully differentiated into post-mitotic neurones following a two-step differentiation protocol

To determine whether the 2-step protocol developed by Scholz et al. would result in fully differentiated neurones, proliferating and post-mitotic LUHMES were characterised by looking at cell cycle and neuronal markers over the course of the differentiation protocol. The most obvious change that proliferating LUHMES go through when they are differentiated into post-mitotic cells is a change in their morphology. In order to track these changes, cells were stained with an anti- β -III-tubulin (Tuj1) primary antibody, which is localised to the cytoskeleton and allowed the visualisation of morphological changes, including neurite development (**Figure 2.4**). β -III-tubulin was present in proliferating LUHMES as well as in 1 and 2-day pre-differentiated LUHMES. During pre-differentiation, the development of short projections was observed. These early structures gave rise to the long neuronal processes that can be identified from day 3 of the differentiation step. By day 3 of the differentiation protocol a reduction in the size of the cell body compared to proliferating cells was observed. Microtubule-associated protein 2 (MAP2) is typically used as a marker of mature neurones as well (Harada et al., 2002; Lee et al., 2016b; Soltani et al., 2005). This protein is involved in the development of dendrites, even though it is found in the axonal projections of certain types of neurones (Binder et al., 1986). Staining for MAP2 in proliferating and pre-differentiated LUHMES (**Figure 2.4**) revealed the formation of neurite precursor structures, although MAP2⁺ neurites in the proliferating LUHMES appeared shorter in length and fewer in number, compared to β -III-tubulin⁺ proliferating LUHMES. Following the replating step, MAP2⁺ staining localised to the long neurites as well. PSD95, a scaffolding protein abundant at the excitatory postsynaptic density (PSD) (Chen et al., 2005a, 2011) was also used as a marker of neuronal maturation in LUHMES. PSD95 expression increased significantly in

LUHMES as the differentiation protocol progressed. PSD95 was only present in the cytoplasm of LUHMES, both in the soma and newly formed neurites.

Cell proliferation markers were also used to assess LUHMES at different stages of differentiation (**Figure 2.5**). A reduction in Ki67⁺ and a change in the localisation of E2F1 were observed in pre-differentiated and fully differentiated LUHMES, which confirmed exit from the cell cycle when LUHMES were cultured in differentiation media. Ki67 antigen is expressed in cycling cells and has been widely used as a proliferation marker; it has recently been shown to localise to heterochromatin and to participate in chromatin organisation (Sobecki et al., 2016). Expression of Ki67 could be detected in the nuclei of all proliferating LUHMES. One day after addition of differentiation media (d1) a number of cells were still Ki67⁺, suggesting they still had an active cell cycle. By day 2 (d2) all cells were negative to Ki67 and this state was maintained throughout the differentiation process. Expression of E2F1, a transcription factor that participates in the regulation of the cell cycle (Iwanaga et al., 2006), was also analysed. E2F1 was found in the nuclei of proliferating and d1 LUHMES; on d2, expression of E2F1 was still localised to the nucleus but by d3, a shift in its localisation, from the nucleus to the cytoplasm, was visible. Cytoplasmic E2F1 was only present in the axon hillock of differentiated LUHMES and its relocalisation was maintained for the rest of the differentiation process.

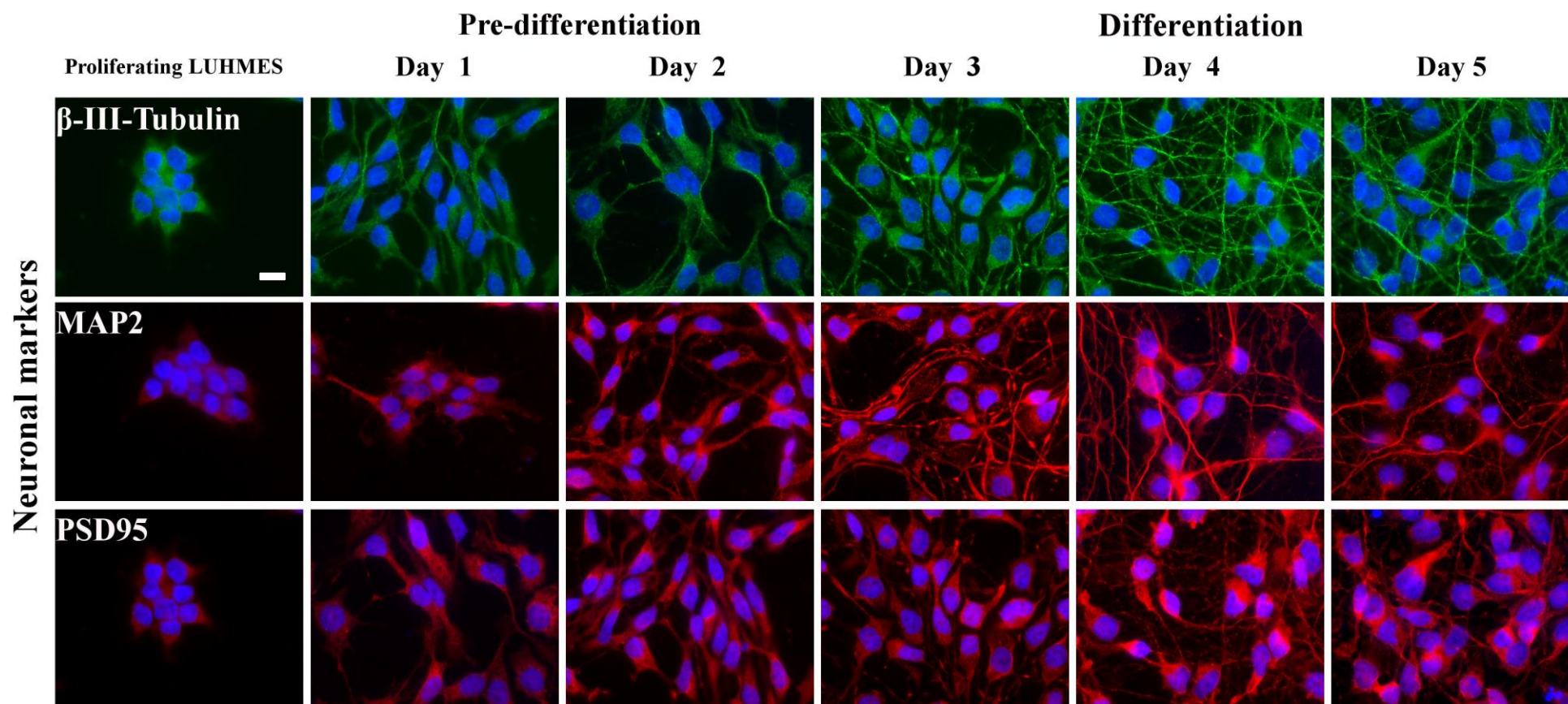


Figure 2.4 Successful differentiation of LUHMES into post-mitotic neurones using a 2-step differentiation protocol.

LUHMES were differentiated in Advanced (+/+) media and fixed at multiple time points to assess changes in cell morphology and maturation. Immunocytochemistry for β -III-tubulin (green) and MAP2 (red) and PSD95 (red), nuclei are labelled with a nuclear dye (Hoechst H3342, blue). Scale bar represents 10 μ m.

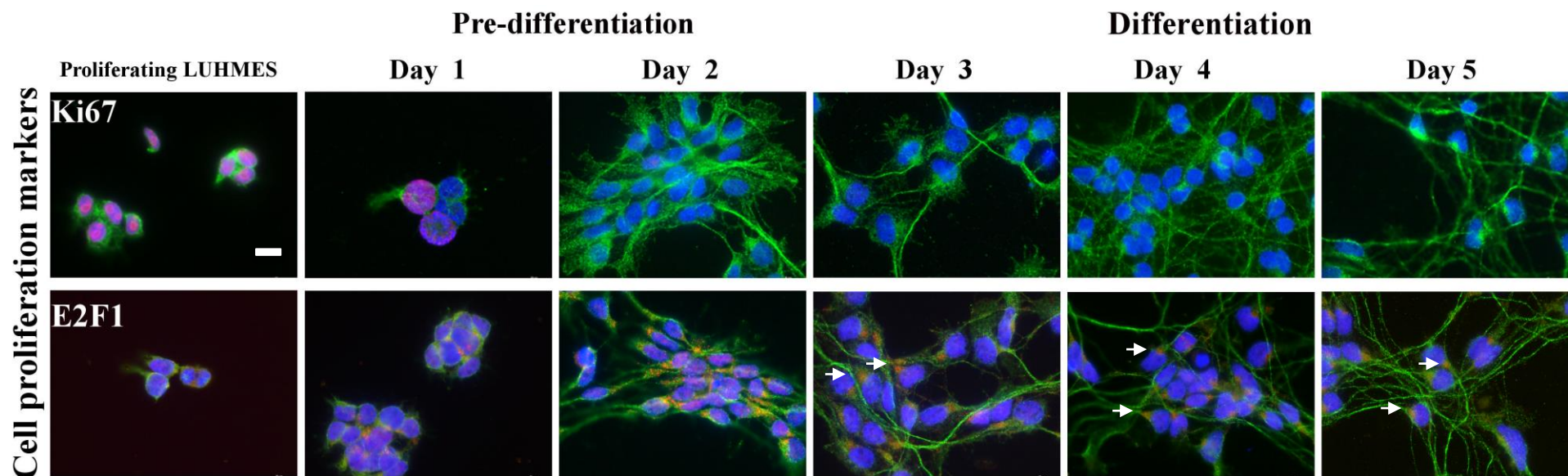


Figure 2.5 LUHMES successfully exit the cell cycle and differentiate into post-mitotic neurones using a 2-step differentiation protocol.

Dual label immunocytochemistry using Ki67 and E2F1 was used to confirm the maturation of LUHMES into post-mitotic neurones. LUHMES were immunostained with Ki67 (red) and β -III-tubulin (green) or with E2F1 (red) and β -III-tubulin (green), nuclei are labelled with Hoechst H3342 (blue). E2F1 presence in the cytoplasm (white arrows) appears as an orange colour (merge) in d3-d5 LUHMES. Scale bar represents 10 μ m.

2.4.3. Induction of oxidative stress in post-mitotic LUHMES in vitro

Oxidative stress has been shown to cause DNA damage and activation of DNA damage response/senescence pathways. A number of methods to model oxidative stress *in vitro* have been documented in the literature, including the use of H₂O₂ (Aksenova et al., 2005; Gille and Joenje, 1992; Lee et al., 2016a; Lehtinen and Bonni, 2006). To induce DNA damage in post-mitotic LUHMES, cells were stressed with H₂O₂. To determine the ideal concentration of H₂O₂, that being one that induces DNA damage without significant cell death, a number of experiments were performed including cell viability, metabolic activity and induction of DNA damage.

2.4.3.1. Assessing cell viability and metabolic activity in H₂O₂-treated LUHMES

To determine the optimal concentration of H₂O₂ that would induce oxidative DNA damage in differentiated LUHMES without any significant cell death, LUHMES were treated with increasing concentrations of H₂O₂ and their cell viability and metabolic activity was assessed with the EthD-1 and MTT assays. EthD-1 is membrane-impermeable and has a high affinity to the DNA; when the cell membrane has been compromised, this dye binds for DNA and emits fluorescence, which is proportional to the number of dead cells present in the sample. The EthD-1 assay results (**Figure 2.6A**) showed that 100 μM H₂O₂ caused significant cell death after 2 hours (16.5% reduction of live cells compared to control, $p \leq 0.01$) and by 24 hours there was an 83.4% reduction of live cells compared to untreated control ($p \leq 0.0001$). Treatment with 75 μM H₂O₂ induced a similar level of cell death at 24 hours (72.8% reduction of live cells compared to control, $p \leq 0.0001$); of the total number of cells had died after 24 hours under these conditions. Treatment with 50 μM H₂O₂ had no significant impact on cell viability at the

earliest timepoint (2 hours) but significant cell death was observed by 24 hours (27.1% reduction compared to control, $p \leq 0.01$). There was no significant cell death when LUHMES were exposed to 10 and 25 μM H_2O_2 .

The MTT assay measures the effect of the H_2O_2 on metabolic function of cells and this can be interpreted as a measure of cell health, although it does not reflect cell death. A significant dysfunction in LUHMES metabolism was seen in cells exposed to 75 and 100 μM H_2O_2 at all timepoints measured with viability declining over time (**Figure 2.6B**). 24 hours after treatment there was a 96.7% and 96.9% reduction in viability compared to control for LUHMES treated with 75 μM and 100 μM respectively ($p \leq 0.0001$). Treatment with lower concentrations of H_2O_2 (10 μM , 25 μM) also significantly affected LUHMES viability at almost all timepoints measured, however at the 24 hour timepoint, more than 50% of the cells showed a normal MTT reduction under these conditions. 50 μM H_2O_2 also had a considerable effect on LUHMES viability, causing a decline in metabolic activity of 46.6% compared to control ($p \leq 0.0001$).

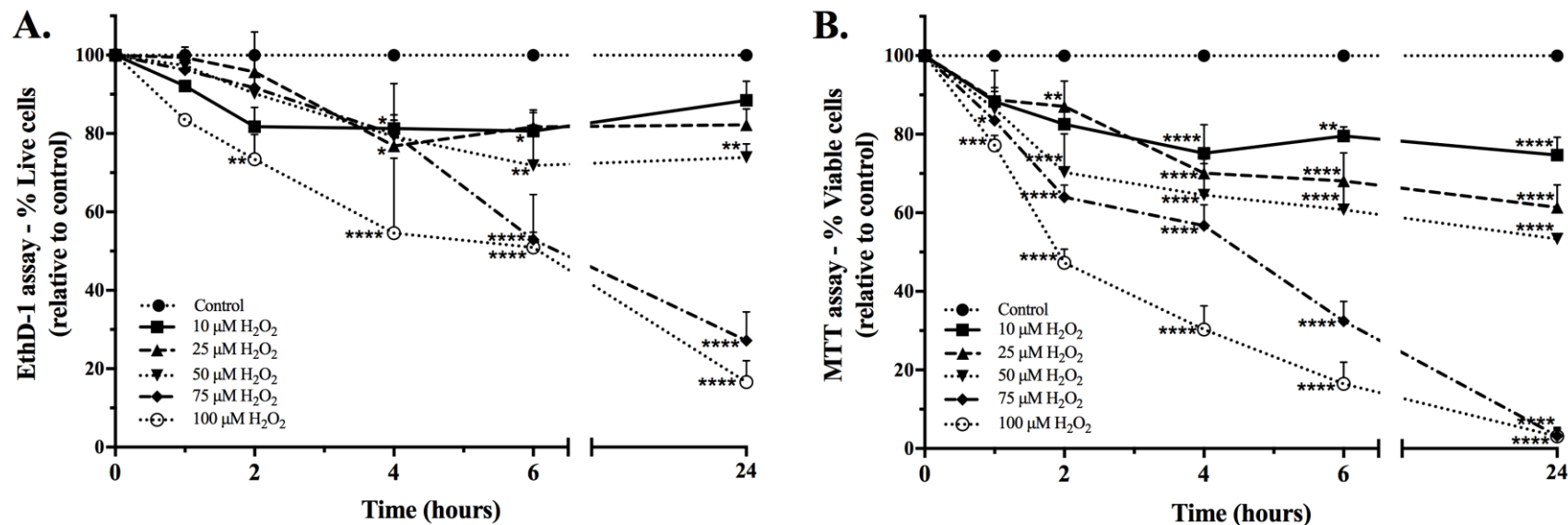


Figure 2.6 The effect of increasing concentrations of H₂O₂ on the viability of differentiated LUHMES.

Differentiated LUHMES were treated with increasing concentrations of H₂O₂ and their viability was assessed with the EthD1 and MTT assays for a period of 24 hours. **A.** Results from the EthD1 assay show significant toxicity of H₂O₂ concentrations $\geq 75 \mu\text{M}$ in differentiated LUHMES; 50 μM has a significant detrimental effect on cell viability without being lethal after 24 hours. Results are expressed in % live cells relative to control. **B.** MTT results show a significant dysfunction in LUHMES exposed to the highest H₂O₂ concentrations; LUHMES viability was significantly affected by 50 μM H₂O₂ and lower concentrations, but to a lesser extent. Results are expressed in % of viable cells relative to controls. Data are mean \pm SEM; 2-Way ANOVA with multiple comparisons, * $p \leq 0.05$, ** $p \leq 0.01$, *** $p \leq 0.001$, **** $p \leq 0.0001$ (N=3, at least 3 replicates, 3 experiments/replicate).

2.4.3.1.1. H₂O₂ induced oxidative DNA damage is repaired in differentiated LUHMES

The effect of H₂O₂ was also assessed in terms of DNA damage by detecting the formation of DSBs after exposure to H₂O₂. To do this immunocytochemistry was carried out with an antibody against the phosphorylated form of histone H2AX. The kinetics of the formation and repair of the DSBs in the form of γ H2AX foci were followed over a period of 24 hours in LUHMES exposed to different concentrations of H₂O₂ (

Figure 2.7 and Figure 2.8). DSBs were detectable 1 hour after treatment with H₂O₂ at all of the concentrations used. The number of γ H2AX⁺ LUHMES declined over time in all cells exposed to H₂O₂ suggesting the activation of DNA repair mechanisms. In cells treated with 10 and 25 μ M H₂O₂ γ H2AX foci disappeared 4 hours after treatment whilst in cells treated with 50 μ M H₂O₂ γ H2AX⁺ foci were still present 6 hours after treatment but were not present after 24 hours. 75 and 100 μ M H₂O₂ solutions were confirmed as lethal, since apoptotic bodies were detected 4 hours after stress and no viable cells were seen after 24 hours.

Together with the EthD-1 and MTT assays results, we confirmed that concentrations \leq 50 μ M H₂O₂ induced oxidative DNA damage without causing considerable cell death. Even though 50 μ M H₂O₂ caused a significant effect in LUHMES MTT reduction capacity, this concentration induced the formation of γ H2AX foci for the longer period of time. Because of this, 50 μ M H₂O₂ was selected as the optimal concentration and was the one used in the double-stressed experiments, as described in the following section.

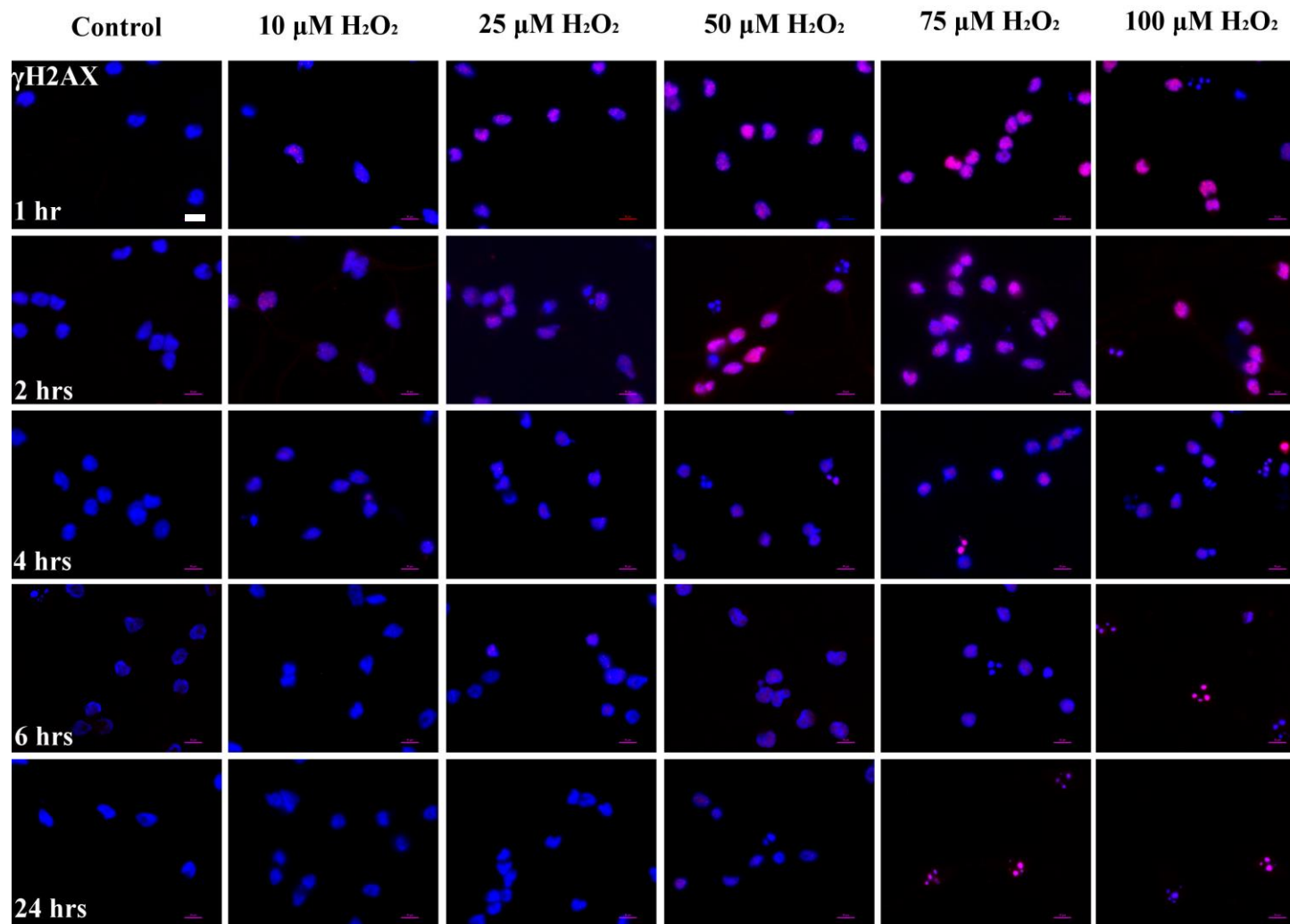


Figure 2.7 Formation and repair of DSBs after treatment with H_2O_2 .

Differentiated LUHMES were fixed at multiple timepoints after treatment with increasing concentrations of H_2O_2 and immunocytochemistry using an antibody against γH2AX (red) was used to identify DSBs. Nuclei were labelled with Hoescht H33342 (blue). Scale bar represents 10 μm

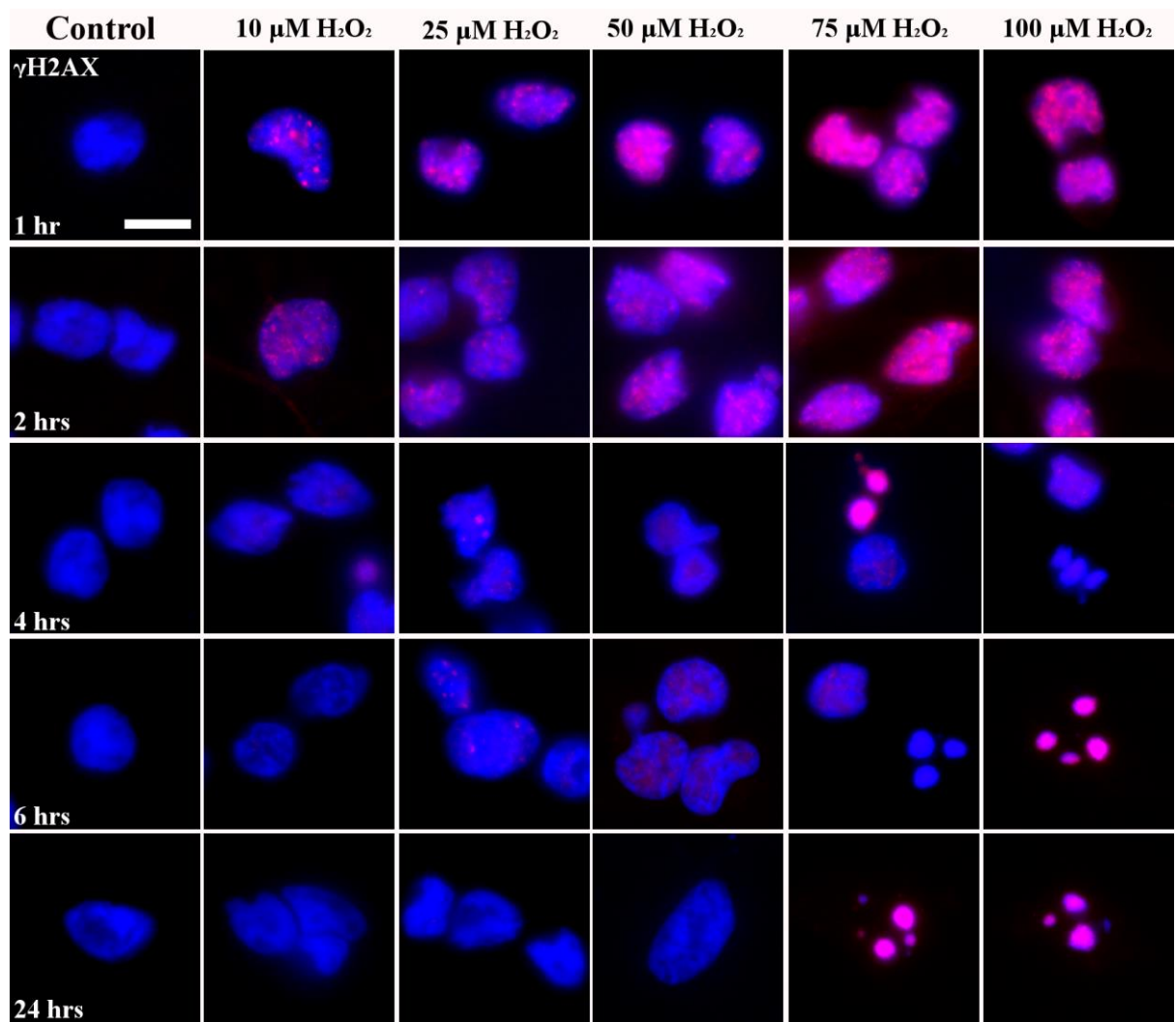


Figure 2.8. Formation and repair of DSBs after treatment with H_2O_2 (Higher power images).

Differentiated LUHMES were fixed at multiple timepoints after treatment with increasing concentrations of H_2O_2 and immunocytochemistry using an antibody against γH2AX (red) was used to identify DSBs. DSBs were detectable 1 hour after stress and decreased in number and size over time. Nuclei were labelled with Hoescht H33342 (blue). Scale bar represents 10 μm (n=3, at least 3 replicates/experiment).

2.4.4. Development of a persistent DNA damage model in post-mitotic LUHMES

The induction of senescence has been linked to the activation of a persistent DNA damage response in mitotic cells. Evidence suggests that activation of senescence pathways in neurones is also associated with chronic stresses that cause DNA damage and activate the DNA damage response. The induction of DSBs in LUHMES exposed to H₂O₂ was investigated by immunocytochemistry to γ H2AX; however, the kinetics of the foci formation showed that the DNA damage induced by H₂O₂ was repaired 24 hours after exposure in LUHMES exposed to 50 μ M H₂O₂ and lower concentrations. Therefore, to promote a chronic oxidative DNA damage, which could potentially lead to the activation of senescence pathways, LUHMES were exposed to a second H₂O₂ dose (double-stress model). For this, the ability of LUHMES to clear extracellular H₂O₂ was assessed to determine how fast LUHMES removed H₂O₂ and to optimise the design of a double-stress model. The MTT assay was also used to assess effects on LUHMES viability when incubated with a second dose of H₂O₂. Finally, the induction of DNA damage was investigated in LUHMES challenged with a second dose of H₂O₂ to determine whether this caused a persistent DNA damage or not.

2.4.4.1. H₂O₂ clearance by LUHMES

H₂O₂ clearance experiments were performed to assess the ability of LUHMES to clear an external source of H₂O₂ from the culture medium. Different densities of differentiated LUHMES were exposed to 50 μ M H₂O₂ and the concentration in the culture medium was then measured every 5 minutes for a period of 30 minutes. Removal of H₂O₂ can be determined by a first-order rate constant (Wagner et al., 2013). In **Table 2.4** the values for k_{obs} , k_{cell} and the half-life ($t_{1/2}$) of H₂O₂ in the medium are presented. Both constants are a measure of the ability of the LUHMES to clear extracellular H₂O₂ from the culture

medium and the $t_{1/2}$ indicates the time that is required for the original concentration of H_2O_2 to decrease by half, when added to a specific cell density.

The capacity of LUHMES to remove extracellular H_2O_2 was dependant on cell density (**Figure 2.9**). Results showed that the rate constants for 50 μM H_2O_2 when added to 4×10^4 cells/well were 1.4 times greater than that for the LUHMES plated at 3×10^4 cells/well and 3.9 to 4 times greater than that of the LUHMES plated at 2×10^4 cells/well and (**Table 2.4**). The half-life of extracellular H_2O_2 also increased as the number of plated cells is reduced. The $t_{1/2}$ for H_2O_2 when added to 4×10^4 cells is 33.01 minutes; when the cell number is decreased to 3×10^4 , the $t_{1/2}$ increases to 48.53 minutes. The $t_{1/2}$ for H_2O_2 when added to 2×10^4 cells increased to 132.88 minutes, as expected.

Cell density (cells/well)	[H_2O_2] (μM)	Observed rate constant k_{obs} (s^{-1})	Observed rate constant for each cell $k_{cell}=k_{obs}/(\text{cell } L^{-1})$	Half life of H_2O_2 (min) ($t_{1/2}=(0.693/(k_{cell}(\text{cells } L^{-1})/60))$)
2×10^4	50	0.00009	4.35×10^{-13}	132.88
3×10^4		0.00024	7.93×10^{-13}	48.53
4×10^4		0.00035	8.75×10^{-13}	33.01

Table 2.4 H_2O_2 clearance rates of differentiated LUHMES.

Differentiated LUHMES seeded at 3 different densities were incubated with 50 μM H_2O_2 . Changes in the H_2O_2 concentration were monitored every 5 minutes for a period of 30 minutes. The slope of $\ln[H_2O_2]$ vs time (seconds) provided the value of k_{obs} , which was used to calculate k_{cell} . The value of k_{cell} was calculated using the formula $k_{cell}=k_{obs}/(\text{cell } L^{-1})$, where $(\text{cell } L^{-1})$ is cells/well divided by the total volume of media/well in litres. H_2O_2 half-life was determined using the formula $t_{1/2}=0.693/(k_{cell}(\text{cells } L^{-1}))$.

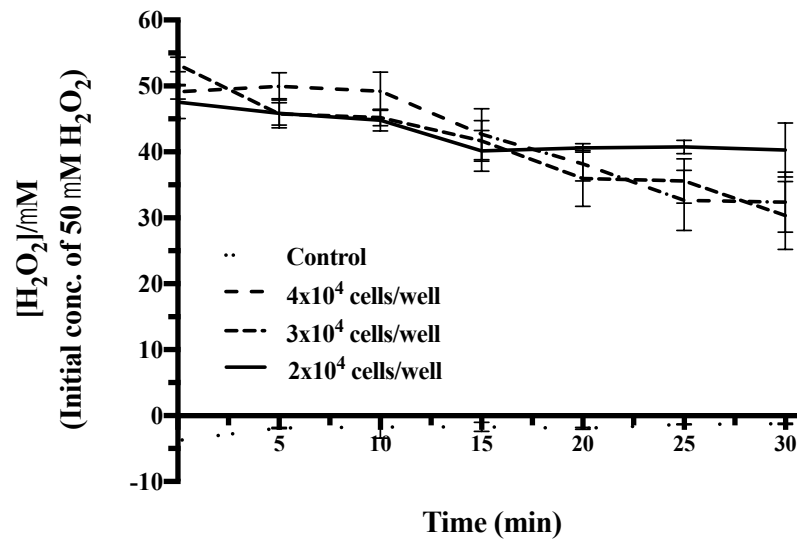


Figure 2.9 Clearance of extracellular H₂O₂ by LUHMES.

Plot depicting the decrease in the extra-cellular H₂O₂ concentration. LUHMES were plated at differing densities (2x10⁴, 3x10⁴ and 4x10⁴ cells/well, respectively) and H₂O₂ concentration was measured over a period of 30 min. Data represents mean ± SEM (n=3, at least 3 replicates/experiment).

2.4.4.2. A second H₂O₂ treatment causes a persistent decrease in LUHMES' viability for up to 96 hours

The effect of this second stress was assessed on the LUHMES' viability over a period of 96 hours, using the MTT assay (**Figure 2.10**). In differentiated LUHMES exposed to a second stress of 50 μ M H₂O₂ there was a significant, persistent impact on metabolic activity as measured by MTT; 24 hours after the second H₂O₂ treatment there was a significant reduction of 30% ($p \leq 0.0001$) in LUHMES viability, which persisted over time (48 hours, 27.2% decrease; 72 hours, 26.1% decrease; 96 hours, 23.9% decrease; all $p \leq 0.0001$) compared to untreated control.

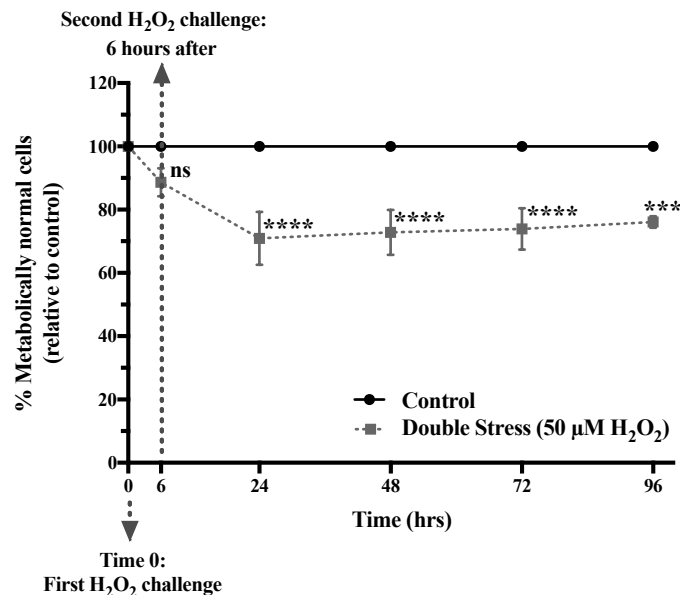


Figure 2.10 A second H₂O₂ treatment induces a persistent decrease in metabolic activity.

Differentiated LUHMES were stressed with a second dose of 50 μ M H₂O₂ 6 hours after the first dose (the dotted arrow lines represent the times at which LUHMES were incubated with 50 μ M H₂O₂). The effect of this second H₂O₂ treatment on LUHMES viability was measured using the MTT assay at 6 (first challenge), 24, 48, 72 and 96 hours. Data represent mean \pm SEM; Two-Way ANOVA with multiple comparisons, *** $p \leq 0.001$, **** $p \leq 0.0001$ (N=3, at least 3 replicates, 3 experiments/replicate).

2.4.4.3. A second H₂O₂ treatment causes persistent DSBs in differentiated LUHMES

After assessing metabolic activity in the double H₂O₂ stress model and confirming that a second H₂O₂ challenge caused a persistent effect on LUHMES metabolism (as measured by MTT) the effect of the single and double stress on DNA damage induction was assessed. For this the formation of γ H2AX foci was tracked over a period of 96 hours. The number of γ H2AX⁺ cells 6, 24, 48, 72 and 96 hours after treatment was quantified and plotted (**Figure 2.11**). As shown previously (**Figure 2.7**), there were γ H2AX foci present 6 hours after treatment with 50 μ M H₂O₂ stress, (55% γ H2AX⁺ LUHMES compared to control). In single stressed LUHMES there was a significant reduction in γ H2AX foci by 24 hours when compared to controls (5% γ H2AX⁺ LUHMES and after 96 hours only 1% of LUHMES are 55% γ H2AX⁺). In the double stress model 18% of the cells were γ H2AX⁺ 24 hours after the second treatment ($p \leq 0.01$) compared to controls and this percentage of positive cells remained constant for the duration of the experiment. The mean percentage of γ H2AX⁺ LUHMES was 12% after 48 hours ($p \leq 0.01$), 22% after 72 hours ($p \leq 0.01$) and 18% after 96 hours ($p \leq 0.01$), compared to controls.

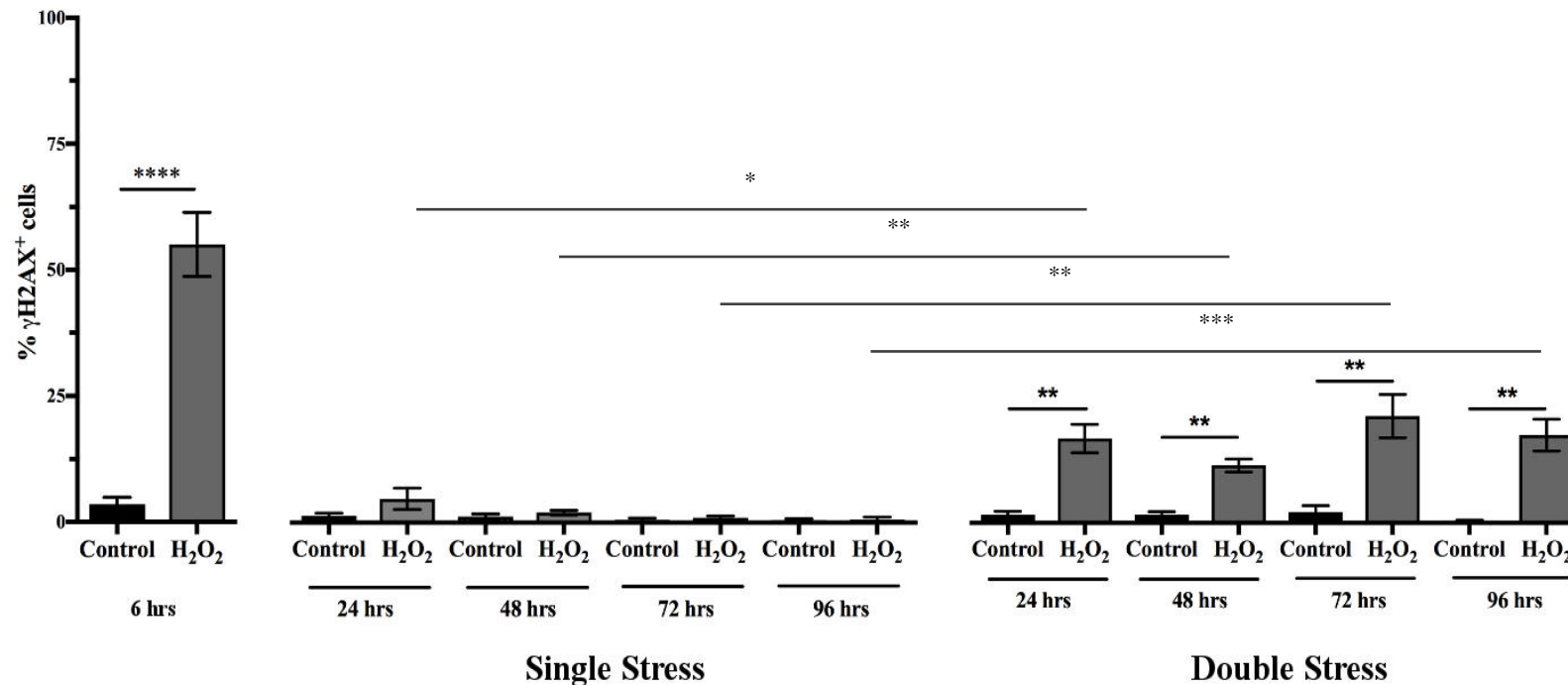


Figure 2.11 γ H2AX foci are detectable in the double stressed LUHMES for up to 96 hours after stress.

Differentiated LUHMES were subjected to either a single 50 μ M H₂O₂ treatment or a double treatment where the cells were given another dose of H₂O₂ 6 hours after the first. Single and double stressed post-mitotic LUHMES were fixed at different time-points to assess the formation of DSBs in the form of γ H2AX foci. Cells were stained with an anti- γ H2AX antibody and fixed. The number of cells positive to γ H2AX was quantified and plotted. This graph represents the % of LUHMES that were stained for nuclear γ H2AX per condition. (Data represent mean \pm SEM; One-Way ANOVA with multiple comparisons, * $p \leq 0.05$, ** $p \leq 0.01$, *** $p \leq 0.001$, **** $p \leq 0.0001$ (N=3, at least 3 replicates, 3 experiments/replicate)).

2.5. Discussion

This chapter describes the optimisation of the LUHMES cell culture and the development of an oxidative stress model in neurones *in vitro*, by stressing LUHMES with H₂O₂. This model will be used to assess the effects of oxidative stress on the induction of senescence in the LUHMES.

2.5.1. Optimisation of LUHMES cell culture

The LUHMES cell line is a sub-clone of the MESC2.10 cells, which were obtained from the ventral mesencephalic tissue of an 8-week old human embryo (Lotharius et al., 2002) and were later characterised by Scholz et al. (2011). These cells can be differentiated into post-mitotic neurones in culture by adding tetracycline to the media, which switches off a *v-myc* transgene, inducing cell cycle arrest and differentiation (Hoshimaru et al., 1996; Lotharius, 2005; Lotharius et al., 2002) The phenotype of these cells is dopaminergic, although expression of dopaminergic markers and electrical activity depends on the differentiation stage of the cells as well as the factors that are used for their differentiation, together with tetracycline (Scholz et al., 2011).

Due to their dopaminergic phenotype, LUHMES were originally used in PD research (Lotharius, 2005; Lotharius et al., 2002; Schildknecht et al., 2009, 2013; Xiang et al., 2013; Zhang et al., 2014b). However, several recent studies report their use for the *in vitro* assessment of neuronal development, neuronal activity, toxicity assays, development of 3D cultures and high-throughput screening in other fields of neuroscience (Hughes et al., 2014; Ilieva et al., 2013; Kurowska et al., 2014; Smirnova et al., 2015; Stępkowski et al., 2017; Tong et al., 2017). The human origin and the ability of these cells to stay in a proliferative state make them advantageous over primary neuronal

murine cultures. Furthermore, because they are not a tumour-derived cell line like other available neuronal cell lines (SH-S5Y5, the NTERA-2 or hNT), they are a suitable model to study changes related to DNA damage and cell cycle regulation, mechanisms that are closely linked with the activation of senescent pathways in mitotic cells.

Before establishing the oxidative stress models in the post-mitotic LUHMES, their culturing conditions were optimised. Studies in embryonic neuronal cells suggest the use of serum-free Dulbecco's Modified Enriched Media (DMEM) with Ham's F12 Nutrient Mixture (1:1) or Neurobasal media for their expansion and maintenance; the addition of supplements, such as N2, and mitogens, such as fibroblast growth factor (FGF) and/or epidermal growth factor (EGF), promote survival of these cell types. The use of N2-supplement instead of 10% FBS (foetal bovine serum) is preferred for neuronal cell culture, since it has been shown that FBS components can reduce growth rate and affect neurite outgrowth of rat neuroblastoma B104 cells (Bottenstein and Sato, 1979). Furthermore, even though N2 also promotes proliferation, adding FGF and/or EGF to the serum-free media accelerates growth rate of neuronal progenitors (Kitchens et al., 1994).

LUHMES cells have been successfully cultured and expanded in serum-free DMEM/F-12 based mediums, containing N2 and basic recombinant human FGF (Ilieva et al., 2013; Lotharius, 2005; Lotharius et al., 2002; Schildknecht et al., 2009, 2013; Scholz et al., 2011; Smirnova et al., 2015). Based on this, two media versions were assessed for LUHMES cell culture for this project: Advanced and GlutaMAX media. Both medias supported survival of proliferating LUHMES; however, an effect on cell proliferation was detectable in cells grown in GlutaMAX when pre-differentiated cells were replated. Quantification of the total number of cells/ml showed that cells cultured in Advanced

media had more cells/ml than cells cultured in GlutaMAX, even when cells for both conditions were seeded at the same density. A visual assessment of cell morphology and overall health during the last days of differentiation identified cell detachment in the GlutaMAX LUHMES, which suggested poor cell health. To confirm this, cells were exposed to H₂O₂ to investigate the vulnerability of post-mitotic LUHMES to an external stress when cultured in these two media. GlutaMAX-cultured LUHMES had less tolerance to H₂O₂ toxicity, as there was a significant reduction in cell health, while Advanced-cultured LUHMES were less susceptible or unaffected by treatment with H₂O₂, depending on their seeding density. This indicated that the Advanced media composition was optimal for LUHMES cell culture. This might be attributed to the extra supplementation of lipids and proteins (AlbuMAX II), insulin and transferrin that this media contains, since these have previously been shown to be crucial for proliferation and maintenance of neural progenitors (Erickson et al., 2008).

The addition of GDNF to the differentiation media, in addition to tetracycline, had no effect on the number of differentiating cells/ml or in the cell health of post-mitotic LUHMES exposed to H₂O₂. However, when the viability of differentiated LUHMES was assessed over a period of 96 hours, the addition of GDNF significantly enhanced cell survival compared to LUHMES differentiated with tetracycline only. These results suggested that GDNF promoted neuronal health and survival, and therefore GDNF was added to the differentiation media for all subsequent experiments. This finding correlates with reports that evidence the neurotrophic nature of GDNF (Jin et al., 2002).

From this point on, proliferating LUHMES were grown in Advanced DMEM/F12 media supplemented with N2 and bFGF. For differentiation, LUHMES were cultured in Advanced DMEM/F12 media, supplemented with N2, tetracycline and GDNF.

2.5.2. Following a 2-step differentiation protocol, LUHMES reach a complete post-mitotic phenotype

Having determined the optimal cell culture conditions for LUHMES proliferation and differentiation, the expression of neuronal and cell proliferation markers was investigated to ensure proper differentiation of these cells.

β -III-tubulin (Tuj1) and MAP2 have been widely used as neuronal markers in both *in vitro* and *in vivo* studies and antibodies against these proteins were used to identify the development of neurites in differentiating LUHMES cultures. β -III-tubulin is one of six tubulin isoforms expressed in the central nervous system (CNS), and is expressed by neurones where it is involved in microtubule assembly (Ludueña, 1998). MAP2 is a member of the MAP family of proteins, whose key function is the stabilisation of microtubules. MAP isoforms 1, 2 and tau are predominantly expressed in neurones, and MAP2 specifically is considered to be a dendritic marker (Caceres et al., 1984), however several reports indicate that this protein also localises to axonal projections. MAP2 axonal expression has been detected in rat hippocampal neurones prior to cell polarisation (Yamamoto et al., 2012), and this agrees with the findings of Scholz et al (2011) in differentiated LUHMES regarding MAP2 axonal expression (Scholz et al., 2011). Both β -III-tubulin and MAP2 allowed the visualisation of the neuritogenesis process in LUHMES before and during differentiation into neurones. PSD95 is a scaffold protein which forms part of the excitatory postsynaptic density complex (Chen et al., 2005a;

Dosemeci et al., 2007) and has an important role in the development and maturation of synapses (Zheng et al., 2012). PSD95 was localised to both the soma and neurites of differentiating LUHMES as they entered into a post-mitotic state, suggesting its synthesis and posterior transport to developing dendrites (Yoshii and Constantine-Paton, 2014; Yoshii et al., 2011).

Alongside the morphological changes that LUHMES undergo in order to reach a post-mitotic phenotype, there are also cellular changes linked to cell cycle control and cellular proliferation. To confirm exit from the cell cycle after exposure to the differentiation factors, LUHMES were stained for the common proliferation and cell cycle markers Ki67 and E2F1. Ki67 is a nuclear antigen that is commonly used in the cancer field, and participates in cell proliferation; however, its function was not well defined until a recent study which showed that Ki67 was involved in heterochromatin organisation and control of gene expression (Sobecki et al., 2016, 2017). The transcription factor E2F1 is a member of the E2F family which controls transcription of cell cycle regulatory genes involved in the G1/S transition in proliferating cells (Sharma et al., 2006; Wu et al., 2001). Undifferentiated LUHMES expressed both markers, confirming their proliferative state. Expression of Ki67 decreased dramatically 2 days after addition of tetracycline and GDNF, indicating cell cycle arrest in these cells and their entry into a quiescent state (Sobecki et al., 2017). Expression of E2F1 re-located from the nucleus to the cytoplasm of the cells, which has been shown to occur during the differentiation of human and mice epidermal keratinocytes *in vitro* and is thought to be necessary to cease expression of genes that are required to maintain a proliferative state (Ivanova et al., 2006, 2007).

Immunocytochemical detection of neuronal and proliferation markers proved to be useful in the identification of neurite formation and to track the development of a post-mitotic phenotype in LUHMES. The use of technologies such as fluorescence-activated cell sorting (FACS) or high content imaging could have also been used to determine the percentage of differentiated LUHMES in the samples at the end of the differentiation process, as well as to track neurite development. For instance, BrdU labelling and FACS could be used to determine the fraction of proliferating cells present in LUHMES samples at different stages of differentiation and complement the information obtained by immunocytochemistry.

2.5.3. Development of an in vitro model of oxidative stress in differentiated LUHMES

This part of the study focused on investigating the effects of H₂O₂ on post-mitotic LUHMES. Different studies have used H₂O₂ to induce oxidative DNA damage in cultured neurones, including LUHMES. A range of concentrations, from 10 to 300 µM, have been assessed to determine the sensitivity of these cells to the peroxide (Fischer et al., 2011; Menges et al., 2017), but there are no reports of the capacity of the LUHMES to remove extracellular H₂O₂. This factor is crucial, since the initial concentration of H₂O₂ added to the cells will not only vary with time, depending on the clearance capacity of the cells, but will also be affected by cell density (Wagner et al., 2013). Extracellular H₂O₂ was efficiently removed from the media by differentiated LUHMES, an effect that was detected by the reduction in H₂O₂ concentration over time. Experiments also confirmed that the clearance rate of H₂O₂, and hence its half-life, was significantly affected by cell density, which correlates with data obtained from rat primary neurones incubated with 100 µM H₂O₂, where the clearance rate was directly proportional to the number of cells present in the sample (Dringen et al., 1999). Even though only two concentrations of

H₂O₂ were assessed for clearance (25 and 50 μM) due to the detection limits of the assay, these results highlighted the importance of maintaining a constant cell density when investigating H₂O₂-induced oxidative stress in differentiated LUHMES.

Exposure to H₂O₂ can affect cells in a number of different ways; although LUHMES were able to remove H₂O₂ from the media and reduce its initial concentration over time, the acute exposure and remaining concentration of H₂O₂ in the media could affect cell metabolism and induce DNA damage. MTT and EthD-1 experiments performed on H₂O₂ treated LUHMES indicated a decline in their viability which was dependant on the concentration of H₂O₂. The MTT analysis is a measure of cell health, since it does not specifically measure cell death, but metabolic dysfunction (Präbst et al., 2017; Riss et al., 2013). This colorimetric assay relies on the conversion of the tetrazolium compound 3-(4,5-Dimethyl-2-thiazolyl)-2,5-diphenyl-2H-tetrazolium bromide into its formazan product, resulting in the formation of a purple-blue precipitate within the cells (Riss et al., 2013). Several studies have shown that reduction of the MTT tetrazolium salt provides information on cell metabolism rather than cell survival or cell proliferation, as usually expressed (Berridge et al., 2005; Galluzzi et al., 2009; van Tonder et al., 2015). It has been shown that mitochondrial succinate dehydrogenase participates in MTT reduction; however, NAD(P)H oxidoreductases present in the cytoplasm and non-mitochondrial membranes, such as the plasma membrane, also reduce the compound and to a greater extent when compared to mitochondrial dehydrogenase (Berridge and Tan, 1993; Stockert et al., 2012). So the MTT assay can reflect changes in any or all of these enzymes. For this reason, the EthD-1 assay, which measures cell death directly, was used in parallel with the MTT assay. Both the Eth-D1 and MTT assays reflected a similar trend in the effect of H₂O₂ in LUHMES viability. Concentrations of 50 μM H₂O₂ or lower

induced modest levels of toxicity (less than 50% reduction in cell metabolic activity after 24 hours) whereas 75 and 100 μ M induced toxicity in the majority of cells. Other studies have reported similar H₂O₂ concentrations, ranging between 75 and 300 μ M, to be lethal to mice primary neurones (Coombes et al., 2011) and rat primary cortical neurons (Whittemore et al., 1995); however, as mentioned before, this will vary depending on the time of exposure and the number of cells that are incubated with the peroxide.

Although measures of H₂O₂ clearance and cell toxicity were critical in determining the tolerance range of differentiated LUHMES to oxidative stress, the aim of this study was to induce a persistent DDR. To measure this, the expression of γ H2AX was examined in LUHMES exposed to H₂O₂. Double strand breaks (DSBs) are one type of DNA lesion that if unrepaired, can compromise genome integrity (Lees-Miller and Meek, 2003). DSBs can be caused by oxidation of DNA bases under oxidative stress conditions (Shu et al., 2015; Woodbine et al., 2011). In response to these lesions, the cell activates a DNA damage response (DDR) that senses DSBs and activates the appropriate signalling cascade to promote DNA repair, cell cycle arrest and senescence or apoptosis (Ciccia and Elledge, 2010). Phosphorylation of histone H2AX at serine 139 is one of the earliest changes to occur in response to DSBs formation; phosphorylated H2AX (γ H2AX) recruits the DDR machinery to chromatin domains (foci) close to the site of lesion (Paull et al., 2000; Rogakou et al., 1998). γ H2AX foci detection is a useful tool to investigate DSBs formation in response to a specific stress (Sharma et al., 2012). Exposure to 50 μ M H₂O₂ induced detectable DNA damage after 1hr of exposure and this remained detectable for 6 hours after exposure. This suggests that H₂O₂ causes DNA damage soon after exposure and that the ability of the cells to repair depends on the concentration of the H₂O₂. Lethal concentrations are likely causing irreparable DNA damage and activating

apoptosis pathways, which is evidenced by the detection of apoptotic bodies in samples exposed to 75 and 100 μM H_2O_2 after 4 hours.

Together the cell viability and metabolic activity assays and the kinetics of the DSBs generation in H_2O_2 -treated LUHMES suggested that 50 μM H_2O_2 was the optimal concentration to use in order to alter cell metabolism and induce DNA damage without causing considerable cell death. However, DSBs in 50 μM H_2O_2 -treated LUHMES were repaired after 24 hours and therefore this was not a suitable model to study a persistent DNA damage response and activation of senescence-related pathways and an alternative approach was sought.

2.5.4. Establishment of a model of persistent DNA damage in LUHMES using H_2O_2

Cellular senescence has been described as an anti-tumorigenic mechanism, which in response to persistent DNA damage, causes cell cycle arrest and prevents proliferation of damaged cells in cancer (Rodier et al., 2009). In ageing and age-related pathologies, senescence can be induced by chronic stresses such as the accumulation of ROS, and these become detrimental due to a loss of tissue-repair capacity and the development of the SASP (Childs et al., 2015; Davalli et al., 2016).

A common feature of senescence is that it is preceded, activated and maintained by a persistent stress. As described above, an acute exposure to 50 μM H_2O_2 affected cell metabolism and caused DSBs in LUHMES, but this damage was repaired within 24 hours. To model persistent DNA damage, LUHMES were exposed to a second H_2O_2 stress 6 hours after the first treatment. This time-point was chosen based on the results obtained from the detection of γH2AX , which showed γH2AX foci were present up to 6

hours after H₂O₂ treatment. This second H₂O₂ treatment, at this timepoint, was intended to reinforce the DNA damage response that had already been activated. MTT analysis of single and double stressed LUHMES over 96 hours revealed a gradual recovery of metabolic function in single stressed cells, while a sustained reduction of cell metabolic activity was found in double stressed cells. In addition, a significant number of double stressed LUHMES had detectable γ H2AX foci 96 hours after treatment compared to single stressed LUHMES where no γ H2AX foci could be detected at the 96 hr timepoint. Chronic oxidative stress models have been developed and investigated previously using H₂O₂ in different cell types, including mouse myoblasts (Santa-Gonzalez et al., 2016) and cerebellar granule rat neurones (Hohnholt et al., 2015), but most of the studies use a single dose of H₂O₂ to study the effects of oxidative stress *in vitro*. Double stressed LUHMES show evidence of chronic oxidative DNA damage and metabolic dysfunction; these characteristics could stimulate DNA damage response and cell cycle changes that could lead to the development of a senescent-like state in neurones, similar to the one that has been described in mitotic cells.

It is important to establish that, even with the exposure to a second H₂O₂ challenge, the percentage of cells that showed persistent DNA damage 96 hours after was of only 18%, although significantly higher when compared to controls and single stressed LUHMES. The presence of γ H2AX foci in less than 20% of neurones in the DS-samples could have limited the detection of changes linked to senescence that will be described in Chapter 4, and could be related to the validation issues faced in the gene profiling analysis, which are described and discussed in Chapter 4. Even though exposure of LUHMES to a double dose of H₂O₂ seemed as a simple approach to cause persistent oxidative stress *in vitro*, based on work previously done (), the use of a different stressor such as tert-butyl

hydroperoxide (TBHP), could have also been an option, especially since TBHP is more stable in solution, compared to H₂O₂.

TBHP has been shown to cause lipid peroxidation and to promote ROS formation, leading to oxidative DNA damage (Park et al., 2003). This compound has also been used to induce senescence *in vitro* in human fibroblasts by exposing cells to a repeated sub-lethal stress of 30 μM TBHP or to a single acute stress of 450 μM TBHP (Dumont et al., 2000). Repeated stresses involved exposure of the cells to the TBHP sub-lethal concentration every day or every two days; this protocol resulted in an increase in the percentage of cells undergoing senescence, when compared to the single acute stress (Dumont et al., 2000). Knowing this, it would have been of interest to compare the oxidative effect of H₂O₂ and TBHP in the LUHMES model, especially in the kinetics of DSBs formation and repair. This comparison would have allowed the selection of the most appropriate oxidant and protocol, being this one that could cause DSBs formation and maintenance for 96 hours in at least half of the LUHMES population present in the experimental samples. Having a higher fraction of cells positive to γH2AX foci after 96 hours would have allowed a more reliable study of changes related to this oxidative DNA damage and the investigation of senescence induction.

2.6. Main conclusions

- Advanced DMEM/F12 media, enriched with N2-supplement and bFGF is the optimal culture media for the maintenance of proliferating LUHMES.
- The 2-step differentiation protocol developed by Scholz et al. (2011) successfully results in homogeneous cultures of post-mitotic neurones. Replacement of bFGF

with tetracycline is enough to promote full differentiation of LUHMES, however, the use of GDNF during differentiation promotes LUHMES health and survival

- Hydrogen peroxide has a detrimental impact on LUHMES cell metabolic activity and induces DNA damage, depending on its concentration. Sub-lethal concentrations of H₂O₂ range from 10 to 50 μM and induce repairable DNA damage.
- By challenging previously stressed LUHMES with a second dose of H₂O₂, a persistent DNA damage model can be achieved. A reduction in cell metabolic activity and the presence of DSBs 96 hours after the second stress confirmed this finding.

Chapter 3. Investigating induction of senescence in the LUHMES single and double stress models

3.1. Introduction

Work presented in Chapter 2 suggested that a second H₂O₂ challenge causes a persistent oxidative DNA damage in differentiated LUHMES, which can be detected 96 hours after stress. This type of damage has been linked to the induction of senescence in mitotic cells and results in cell cycle arrest, expression of SA- β -gal activity and the development of the senescence-associated secretory phenotype, or SASP (Brandl et al., 2011; Wang et al., 2013). To investigate if LUHMES activate senescence when undergoing a persistent DNA damage, SA- β -gal activity, changes in heterochromatin organisation and the development of a secretory phenotype were assessed.

To date, there is no single marker that can be used to identify senescent cells. The identification of senescent cells *in vitro* and *in vivo* relies on the use of different biomarkers to detect distinctive changes that senescent cells go through. These include the activity of a senescence-associated β -gal enzyme at a suboptimal pH, chromatin organisation alterations, and the activation of the p16 and p21 signalling pathways (Itahana et al., 2013; Narita et al., 2003; Stein et al., 1999). Senescence in mitotic cells is related as well to a secretory phenotype, which is characterised by the release of cytokines, chemokines, proteases and other molecules. This phenotype can act in an autocrine and paracrine manner to reinforce the senescent state and spread it to neighbouring cells (Rodier et al., 2009). Identification of senescent cells also involves the detection of some of the molecules that characterise the SASP, including interleukins IL-6 and IL-8, among others.

This chapter focused on the assessment of two of the main senescence biomarkers in stressed LUHMES: SA- β -gal activity and heterochromatin re-organisation in the form of senescence-associated heterochromatin foci (SAHF). Development of a secretory phenotype was also investigated in single and double stressed LUHMES by evaluating the toxic effects of conditioned media from stressed LUHMES on healthy LUHMES. For this, cell metabolic activity and neurite outgrowth impairment were used as indicators of toxicity. Detrimental effects of a secretory phenotype were also analysed in a co-culture system of stressed LUHMES/healthy GFP-LUHMES.

3.2. Aims and objectives

The aim of the experiments performed for this chapter was to determine if the double stress model induced activation of senescence in differentiated LUHMES by:

- Analysing the expression of common markers of senescence in the single and double stress models.
- Determining whether double stressed LUHMES develop a secretory phenotype in response to persistent DNA damage.

3.3. Materials and methods

All chemicals were obtained from Sigma-Aldrich (St Louis, MO, USA) unless stated. Solutions required for the experiments described in this chapter were prepared as specified in **Appendix A**.

3.3.1. Double –stress model in post-mitotic LUHMES

Proliferating LUHMES were differentiated as described in Chapter 2. Briefly, proliferating LUHMES were seeded on to pre-coated T75 flasks in Advanced DMEM/F12 + 1x N2-supplement + 2 mM L-glutamine + 40 ng/μl bFGF. LUHMES were left to settle overnight and proliferation media was replaced with Advanced (+/+) to start pre-differentiation. After 2 days, pre-differentiated LUHMES were replated on to pre-coated glass coverslips, in 24-well plates, for immunocytochemistry/neurite outgrowth analysis, or 12-well plates for protein and RNA extraction (cell densities are specified for each experiment). LUHMES were left in differentiation media for 3 more days.

To generate the single (SS) and double (DS) stressed models, post-mitotic LUHMES were stressed with a first dose of 50 μM H₂O₂; 6 hours after, a second challenge of the same H₂O₂ concentration was applied to the DS-LUHMES. SS, DS and untreated control LUHMES were kept in culture for further 96 hours.

3.3.2. Detection of common senescence markers in single/double stressed LUHMES

The identification of senescent cells *in vivo* and *in vitro* requires the use of a panel of markers, since currently there is no specific marker that indicates activation of senescence on its own. To investigate whether oxidative stress could induce senescence in the SS/DS models in differentiated LUHMES, expression of two established senescence markers was assessed.

3.3.2.1. Senescence associated – β – galactosidase (SA- β - gal) activity

SA- β -gal activity can be detected *in vivo* and in cultured cells by incubating fixed samples with the enzyme substrate, which results in either the precipitation of a coloured compound or in the emission of a fluorescent signal, both detectable by microscopy (Debacq-Chainiaux et al., 2009). For this work, a method based on the cleavage of the chromogenic substrate 5-bromo-4-chloro-3-indolyl β -D-galactopyranoside (X-gal) was used to assess SA- β -gal activity. Briefly, Senescence Cells Histochemical Staining Kit (Sigma-Aldrich, UK) components were thawed on ice; the X-gal solution was warmed up at 37 °C for 1 hour prior to the experiments. SS and DS-LUHMES were fixed with 1x Fixation Buffer 1, 6, 24 and 96 hours after stress. Fixed cells were incubated with the staining mixture (potassium ferricyanide (5 mM), potassium ferrocyanide (5 mM), X-gal solution (0.1mg/ml), 1x Staining Solution) at 37°C, overnight. Cells were washed with 1x PBS and mounted with Fluoromount Mounting media (Sigma-Aldrich, UK). Activity of the enzyme was identified as a blue, insoluble precipitate within cells and was assessed qualitatively in images captured at high magnification (40x objective).

3.3.2.2. Immunocytochemistry

3.3.2.2.1. Detection of senescence-associated heterochromatin foci (SAHF)

To investigate senescence-heterochromatin foci (SAHF) formation in DS-LUHMES, expression of H3K9Me3, a histone modification associated with heterochromatin and one of the main components of SAHF, was explored. The immunocytochemistry protocol was described in detail in **Chapter 1, section 2.3.2**. In summary, SS and DS-LUHMES plated on to glass coverslips were fixed with 4% PFA at different time-points (1, 6, 24, and 96 hours post-stress). After fixation, cells were washed with 1x PBS and permeabilised with 0.3% Triton-X100. Cells were washed with 1x PBS and blocked with 3% BSA blocking

solution. Cells were incubated with a primary rabbit polyclonal antibody against trimethyl-Histone H3 (Lys9) H3K9me3 (Merck Millipore, MA, USA) for 1hr at RT. For nuclear staining, cells were incubated with Hoechst 33342 (Sigma-Aldrich, MA, USA). Coverslips were mounted with Fluoromount Mounting Media.

3.3.3. Induction of a SASP

3.3.3.1. Effect of stressed cells conditioned media on viability of healthy LUHMES

To investigate whether DS-LUHMES developed a secretory phenotype, healthy LUHMES seeded at a density of 3.5×10^5 cells/well were incubated with conditioned media (CM) from 1, 6, 24, and 96 hours SS and DS-LUHMES. Cell health was assessed using the MTT assay as described in **Chapter 1, section 2.3.1.2**. Briefly, 24 hours after incubation with either SS-CM or DS-CM, 50 μ l of MTT solution were added to each well and cells were incubated for 3 hours at 37 °C. 550 μ l of 20% SDS/DMF solution were added to each well to solubilise the formazan crystals and the plates were incubated for 30 minutes at RT under darkness and constant agitation. The solubilised solution was homogenised by pipetting it up and down gently; three 200 μ l aliquots/well were transferred to a 96-well plate and their absorbance was read at 595 nm in a PHERAStar microplate reader (BMG Labtech, Ortenberg, Germany). The absorbance value from the medium-only control (background) was subtracted from the values of the control and treated samples for data analysis.

3.3.3.2. Effect of stressed cells conditioned media on neurite outgrowth of healthy

LUHMES

Neurite outgrowth impairment was also used to detect the release of SASP-soluble factors by DS-LUHMES. For this, CM from 1, 6, 24 and 96 hours SS and DS-LUHMES was transferred to 3-days differentiating LUHMES (1×10^4 cells/well). After 24 hours, cells were fixed with 4% PFA. Cells were immunostained for β -III-Tubulin following the immunocytochemistry protocol described in **Chapter 1, section 2.3.2**. LUHMES were incubated with a primary chicken anti- β -III-Tubulin (Merck Millipore, MA, USA, 1:1000) for 2 hours at RT. Nuclei were stained with Hoechst 33342. Five images/coverlip in a cross pattern were taken for each condition with the 20x objective of a Nikon Eclipse 80i microscope. Images were processed with the Image J Fiji plug-in “Simple Neurite Tracer”, which calculates the length of neurites in pixels. Data is presented as neurite length/soma (sum of neurite lengths/number of cell bodies per field).

3.3.3.3. Healthy GFP-LUHMES/stressed LUHMES co-culture

The toxic effects of the SASP are not limited to the soluble factors present in the surrounding cell environment. Cell-to-cell contact also plays a role in its detrimental consequences over surrounding cells. To study this in the DS-LUHMES model, a co-culture system was developed.

3.3.3.3.1. GFP-LUHMES production

Generation of GFP-LUHMES was achieved by transducing low passage (P3) proliferating LUHMES with GFP-expressing lentivirus (GFP-LV, MOI=8). LUHMES (P3) were seeded at a density of 3.5×10^5 cells/flask on to a pre-coated T25 flask and

transduced for 24 hours. Media was changed after this time and GFP expression was detected 72 hours after transduction.

3.3.3.3.2. GFP-LUHMES/non-transduced LUHMES co-culture optimisation

Non-transduced proliferating LUHMES (3.5×10^5 cells/well) were differentiated on to pre-coated glass coverlips following the 2-step differentiation protocol. Pre-differentiated GFP-LUHMES were replated on top of 5-day differentiated non-transduced LUHMES at 3 different densities: 7.5×10^3 , 1×10^4 and 5×10^4 cells/well. Once the GFP-LUHMES completed 5 days of differentiation, co-cultures were fixed with 4% PFA for 10 minutes at RT. Cells were washed 3 times with 1x PBS and incubated with Hoechst 33342 for 10min at RT. After washing 3 times with 1x PBS, coverslips were mounted with Fluoromount Mounting Media. Images were taken with a Nikon Eclipse 80i microscope with the 20x and 40x objectives.

3.3.3.3.3. Neurite outgrowth assays in GFP-LUHMES co-cultured with stressed

LUHMES

Non-transduced differentiated LUHMES (3.5×10^5 cells/well) were stressed with 50 μM H_2O_2 following the “single/double stress” protocol described before. Pre-differentiated GFP-LUHMES were plated on top of the SS and DS-LUHMES at different time-points, at a density of 1×10^4 cells/well. Co-cultures were fixed with 4% PFA (10 min, at RT) 24 hours after pre-differentiated GFP-LUHMES were re-plated on top. Nuclei were stained with Hoechst 33342 for 10 min, at RT. Coverslips were mounted with Fluoromount Mounting Media. Images from five fields/coverslip were taken with a Nikon Eclipse 80i microscope with the 20x and 40x objectives. Neurite outgrowth was analysed with the “Simple Neurite Tracer” plug-in from Image J Fiji as explained previously.

3.3.3.3.4. Detection of DSBs formation in GFP-LUHMES co-cultured with stressed

LUHMES

Induction of DNA damage was also assessed in the GFP-LUHMES/stressed LUHMES co-culture. Co-cultures were fixed with 4% PFA and immunodetection of γ H2AX was performed as described in **sections 2.3.2 and 2.3.3.2**. For this, co-cultures were incubated with an anti- γ H2AX mouse monoclonal antibody (1:1000; Merck Millipore, MA, USA) for 1 hour at RT and nuclei were stained with Hoechst 33342. Coverslips were mounted with Fluoromount Mounting media and analysed a Nikon Eclipse 80i microscope. The analysis focused on identifying γ H2AX⁺ GFP-LUHMES.

3.3.4. Statistical analysis

Data obtained from the conditioned media (MTT and neurite outgrowth) and co-culture experiments (neurite outgrowth) was analysed with Prism 7.0c (GraphPad Software, Inc., CA, USA). All data is presented as mean \pm standard error of the mean (SEM).

3.4. Results

3.4.1. SA- β -gal activity in differentiated LUHMES

SS and DS-LUHMES were assessed for SA- β -gal activity. Analysis of the staining revealed unexpected high activity in untreated LUHMES. The blue precipitate was localised to the axon hillock from untreated controls of every time-point under assessment (**Figure 3.1**). The staining pattern was similar across untreated LUHMES samples, with all the neurones presenting SA- β -gal activity. SS and DS-LUHMES were also positive for SA- β -gal activity and the intensity of the blue precipitate was similar to that seen in untreated LUHMES. No change in the intensity or localisation of the staining

was identified with increasing time of incubation for both untreated and SS/DS-neurones, when assessed for the first 24 hours post-stress. However, more intense staining was observed in the 96-hour samples; the staining localised to the axon hillock and throughout the length of the axon. These changes were seen in the untreated and SS/DS-LUHMES, with no obvious difference between conditions.

Further analysis revealed that SA- β -gal activity was highly variable in control differentiated LUHMES, and increased with passage number, as shown in **Figure 3.2**. Low passage (P4) differentiated LUHMES had a low level of enzyme activity, but a significant increase was noticeable in cells of medium passage (P9). In P9 LUHMES the activity was not localised just to the axon hillock but to most of the cytoplasm in the cell soma. Older passage cells (P14) were intensely stained and the activity of SA- β -gal was detected in the neurites.

The staining protocol uses a mix of reagents to maintain a pH of 6-6.5 during incubation with the enzyme substrate; however, it is possible for acidification of the media to occur as a result of normal cellular metabolism. To prevent acidification and determine whether this would increase SA- β -gal activity under normal conditions, neurones were incubated with Bafilomycin A1 (BafA1). Incubation with BafA1 did not have an effect on SA- β -gal activity, as pre-treated cells showed similar staining as non-treated LUHMES (**Figure 3.2**).

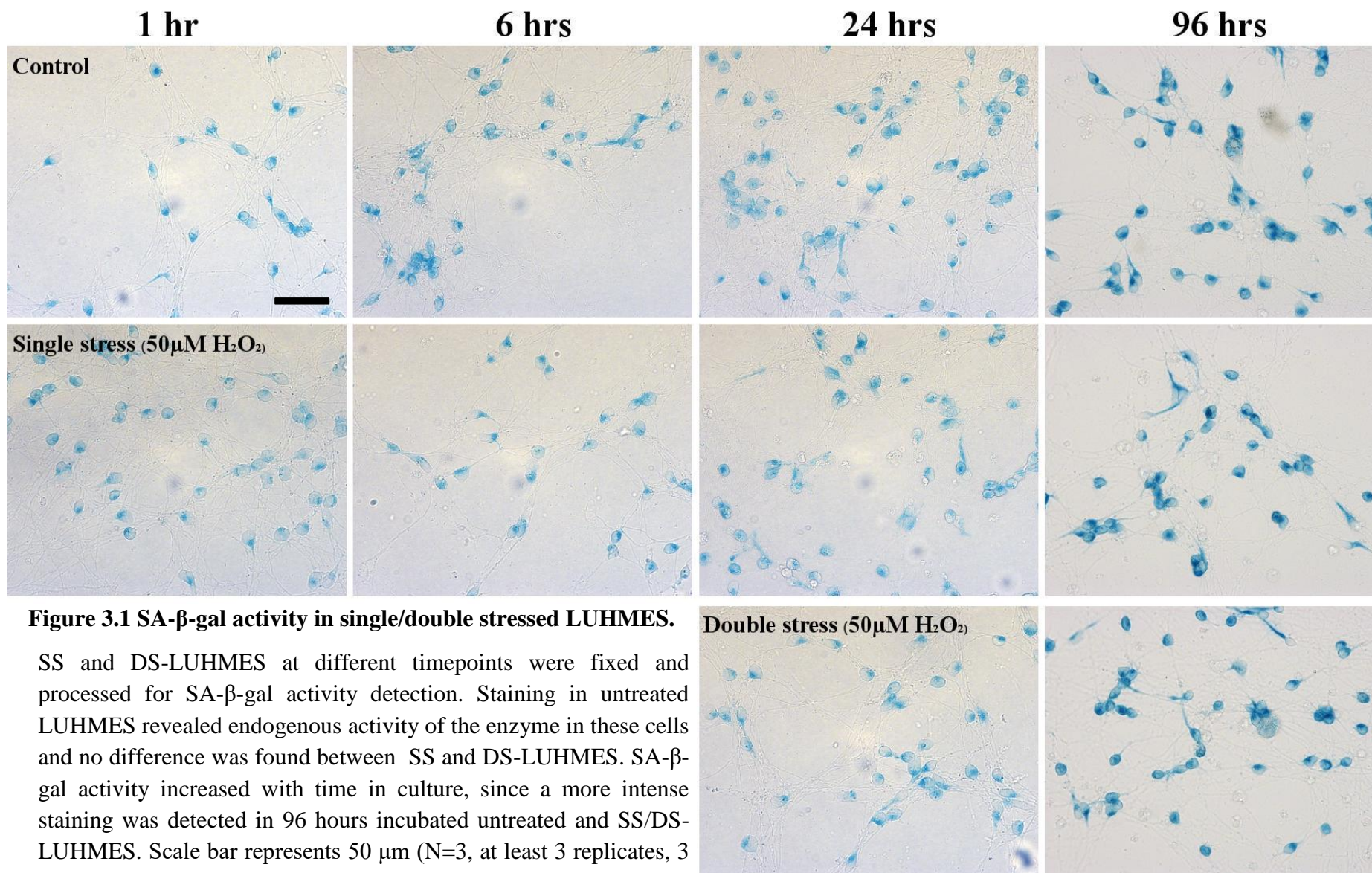


Figure 3.1 SA-β-gal activity in single/double stressed LUHMES.

SS and DS-LUHMES at different timepoints were fixed and processed for SA-β-gal activity detection. Staining in untreated LUHMES revealed endogenous activity of the enzyme in these cells and no difference was found between SS and DS-LUHMES. SA-β-gal activity increased with time in culture, since a more intense staining was detected in 96 hours incubated untreated and SS/DS-LUHMES. Scale bar represents 50 μm (N=3, at least 3 replicates, 3 experiments/replicate).

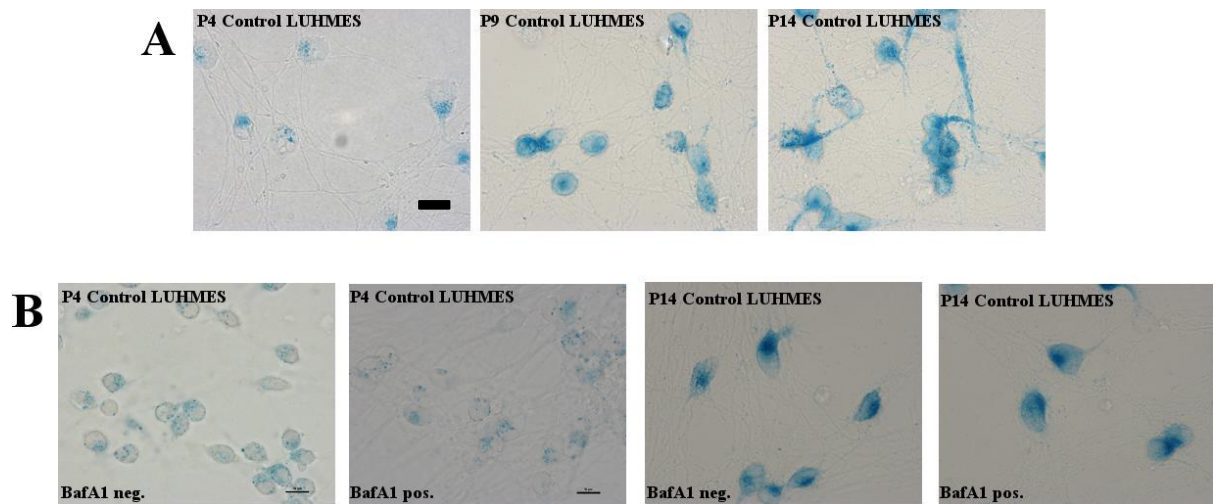


Figure 3.2 SA- β -gal activity increases with passage number in differentiated LUHMES. A.

SA- β -gal activity was investigated in low, medium and old passage differentiated LUHMES. The intensity and localisation of the enzyme activity varied with passage number. SA- β -gal activity in low passage LUHMES was restricted to the axon hillock, whereas medium and high passage neurones had widespread cytoplasmic activity that localised to the neurites as well. **B.** LUHMES were incubated with Bafilomycin A1 to prevent lysosomal acidification. The use of BafA1 did not affect SA- β -gal activity of low and old passage differentiated LUHMES. Scale bar represents 10 μ m (N=3, at least 3 replicates, 3 experiments/replicate).

3.4.2. Formation of heterochromatin foci (SAHFs) in single/double stressed LUHMES

SAHFs are DNA-stained dense foci present in senescent cells that silence expression of proliferation-promoting genes, such as E2F1 target genes, contributing in this way to the irreversible cell cycle arrest that characterises senescence (Narita et al., 2003; Zhang et al., 2007). Detection of SAHFs can be performed using immunocytochemistry against the SAHFs components macroH2A, HP1 proteins and H3K9me2/3, which are hallmarks of heterochromatin (Aird and Zhang, 2013). In the SS and DS-LUHMES model, formation of SAHFs was investigated through the detection of H3K9me3, an epigenetic marker associated with pericentric heterochromatin that has an important function in gene silencing and in the maintenance of genome stability (Peters et al., 2002; Muramatsu et al., 2016). In senescent cells, H3K9me3 is localised to the core of SAHFs (Chandra et al., 2012) and H3K9me3 enriched sites are known to provide a docking spot for HP1 proteins (Bannister et al., 2001).

Formation of SAHFs was not seen in stressed LUHMES (**Figure 3.3**). Expression of H3K9me3 was present in the nuclei of untreated post-mitotic LUHMES. The staining pattern was diffuse and specific chromatin structures were not visible. Chromatin organisation was not altered in SS and DS-LUHMES according to H3K9me3 staining at any of the time-points assessed. To make sure H3K9me3 would detect heterochromatin foci formation, old passage human fibroblasts (P12) were stained as well. Staining in these cells confirmed localisation of H3K9me3 in small round nuclear structures in the fibroblasts.

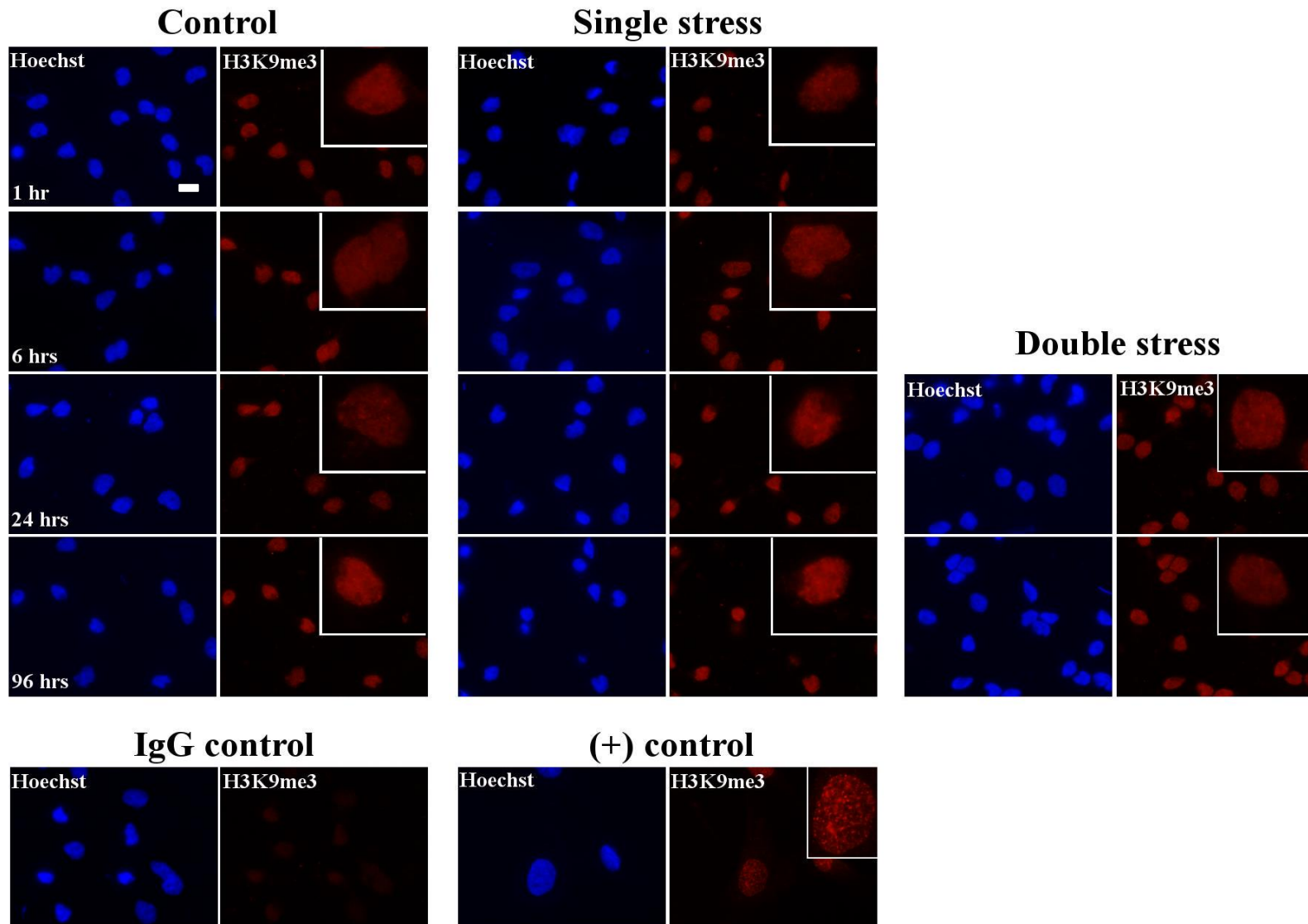


Figure 3.3 H3K9me3 expression in stressed LUHMES.

SS and DS-LUHMES were stained for H3K9me3 to detect formation of senescence-associated heterochromatin foci (SAHF) in response to oxidative DNA damage. SS and DS-LUHMES were fixed at different timepoints and stained for H3K9me3 by immunocytochemistry. H3K9me3 was present in the nucleus of control and stressed cells, but no specific chromatin structures were identified. Staining of old passage human fibroblasts was included as a positive control. H3K9me3 was localised to small foci within the nuclei of fibroblasts. Scale bar represents 10 μ m (N=3, at least 3 replicates, 3 experiments/replicate).

3.4.3. DS-LUHMES have a detrimental effect on healthy LUHMES suggesting

propagation of injury

The development of a SASP occurs in mitotic cells when senescent pathways are activated. To investigate if a similar mechanism was triggered in neurones exposed to a persistent oxidative stress, healthy differentiated LUHMES were incubated with conditioned media (CM) from 1, 6, 24 and 96 hours SS and DS-LUHMES. Cell health using the MTT assay was measured in CM exposed neurones 24 hours after. A small (less than 10%) significant reduction in cell metabolic activity of healthy LUHMES was seen after incubation with SS and DS-CM compared to cells incubated with untreated-CM (**Figure 3.4**). Toxicity was not dependent on the time point of CM collection. SS-CM collected 1 and 6 hours after adding the bolus of 50 μM H_2O_2 had an effect on cell metabolic activity of healthy LUHMES comparable to the effect of the CM collected 24 and 96 hours after. There was no difference in cell metabolic activity between cells incubated with SS and DS-CM.

The toxic effects of SS- and DS-CM were evaluated on neurite outgrowth of healthy LUHMES as well (**Figure 3.5**). Healthy LUHMES incubated with untreated CM had a mean neurite length of 80 pixels/soma, except for the cells incubated with 96 hours untreated CM, which had a neurite length of 54 pixels/soma, in both SS and DS-CM incubation conditions. When incubated with 1-hour SS-CM, neurite length of healthy LUHMES was significantly reduced to 63 pixels/soma ($p=0.0003$). Incubation with the 6 ($p=0.3788$) and 24 hours ($p=0.1473$) SS-CM did not have an effect on neurite outgrowth. The 96 hours SS-CM impaired neurite development significantly ($p<0.0001$). The mean neurite length for LUHMES under this condition was of 36 pixels/soma.

Incubation of healthy differentiating LUHMES in the DS-cells also caused significant neurite length reduction. Neurons incubated in untreated-CM for 24 hrs developed neurites with a mean length of 85 pixels/soma, whereas neurones in 24 hours DS-CM showed a reduction of almost 23 pixels/soma ($p=0.0003$). The 96 hours DS-CM also impaired neurite outgrowth of healthy LUHMES, causing a reduction in length from 54 to 39 pixels/soma ($p=0.0080$).

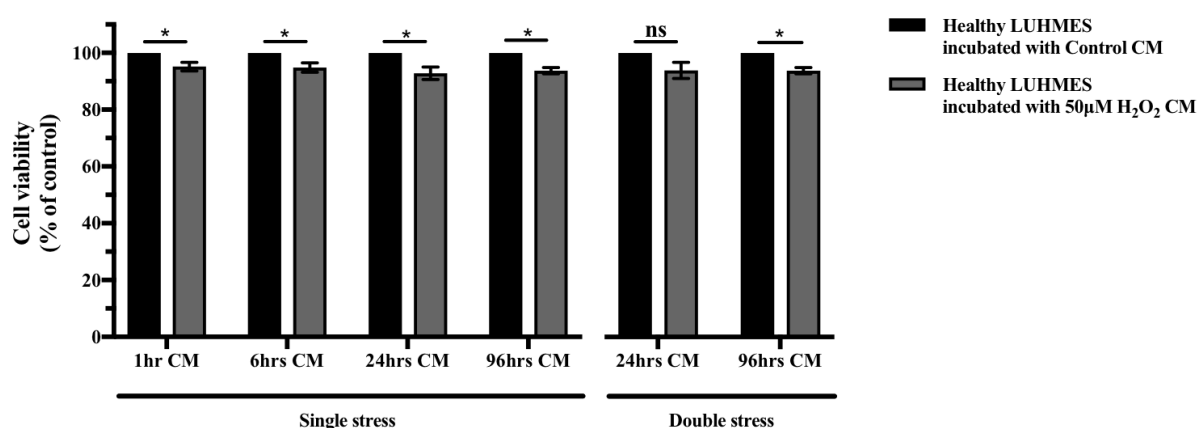


Figure 3.4 Incubation of healthy LUHMES with SS and DS-CM has a small significant effect on cell metabolism of healthy LUHMES.

CM from SS and DS-LUHMES was collected at different timepoints. Healthy LUHMES were incubated with SS and DS-CM for 24 hours and its effect on LUHMES metabolism was assessed using the MTT assay. SS and DS-CM caused an effect on LUHMES metabolism. This effect was similar in cells incubated with SS and with DS-CM and it was not related to the CM time of collection. (Data represent mean \pm SEM; Two-Way ANOVA with multiple comparisons (Tukey correction), $*p \leq 0.05$, N=3, 3 experiments/replicate).

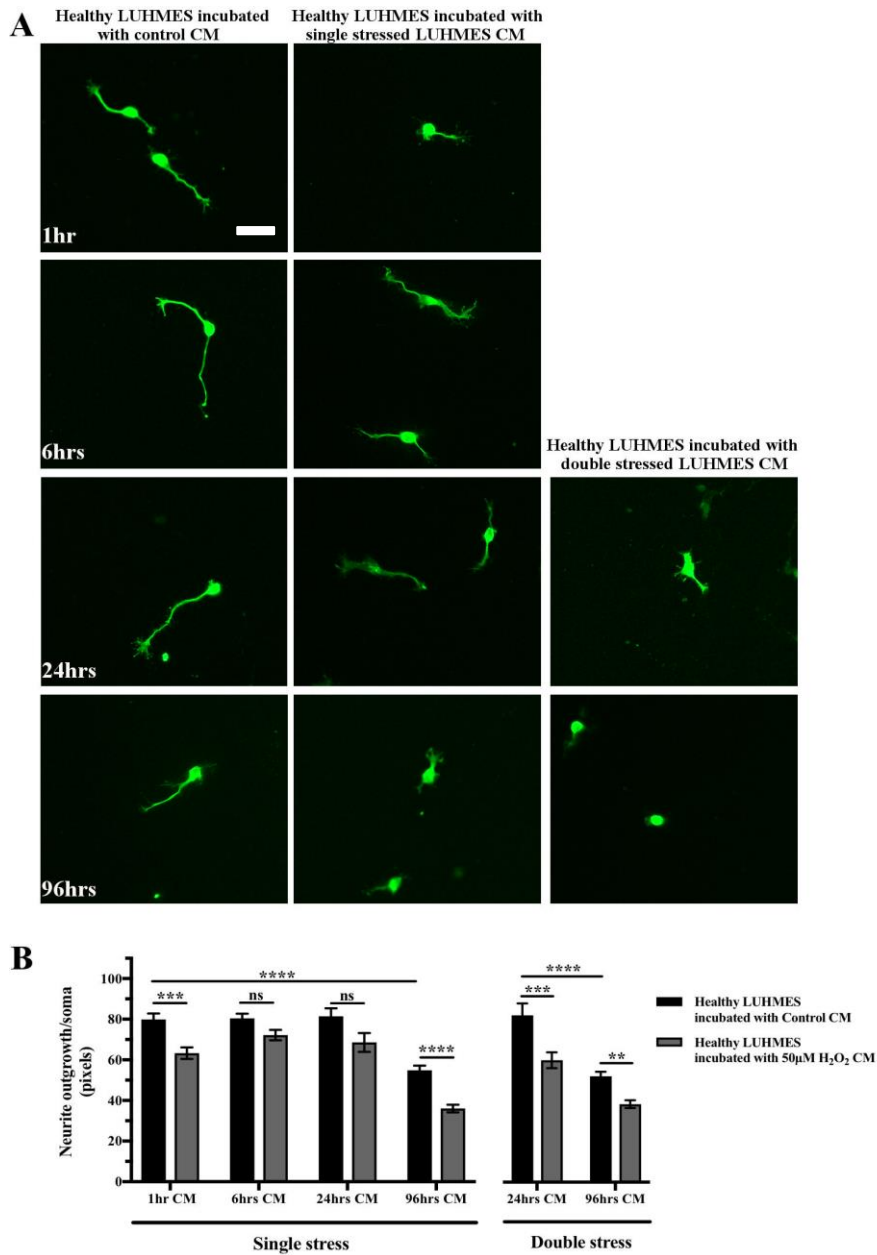


Figure 3.5 Incubation in SS and DS-CM impaired neurite outgrowth of healthy differentiating LUHMES.

Healthy differentiating LUHMES were incubated in SS and DS-CM collected at 1, 6, 24 and 96 hours post-H₂O₂ stress. To assess cell health under these conditions impairment of neurite outgrowth was assessed. A. Representative images of differentiating LUHMES exposed to SS and DS-CM. B. A significant reduction in neurite length was seen when differentiating LUHMES were cultured in 24 hours SS and DS-CM, and in 96 hours DS-CM. Scale bar represents 20 μm (Data represent mean ± SEM; Two-Way ANOVA with multiple comparisons (Tukey correction), **p≤0.01, ***p≤0.001, ****p≤0.0001, N=3, 3 experiments/replicate).

3.4.4. GFP-LUHMES/non-transduced LUHMES co-culture optimisation

To investigate the effects of cell-to-cell contact by measuring neurite outgrowth, a co-culture of healthy GFP-LUHMES/stressed LUHMES was designed and optimised. GFP-LUHMES were obtained by transducing low passage proliferating LUHMES with a GFP-expressing lentivirus, as described in **section 3.3.3.3.1**. The optimal seeding density of GFP-LUHMES for the neurite length measurement was found by assessing three different cell densities (**Figure 3.6**). 10,000 cells/well was the optimal plating density. Under this condition, single cell analysis was feasible, as cells were sparse enough to measure neurite outgrowth and the development of neurites appeared as expected. With a lower cell density (7,500 cells/well), GFP-LUHMES viability was compromised, as evidenced by very short, almost non-perceivable neurites, as well as by cell death in some of the samples assessed. Even though a higher cell density allowed the growth of longer neurites, the fact that the GFP-LUHMES were more confluent facilitated the formation of GFP colonies, which precluded the measurement of single neurites.

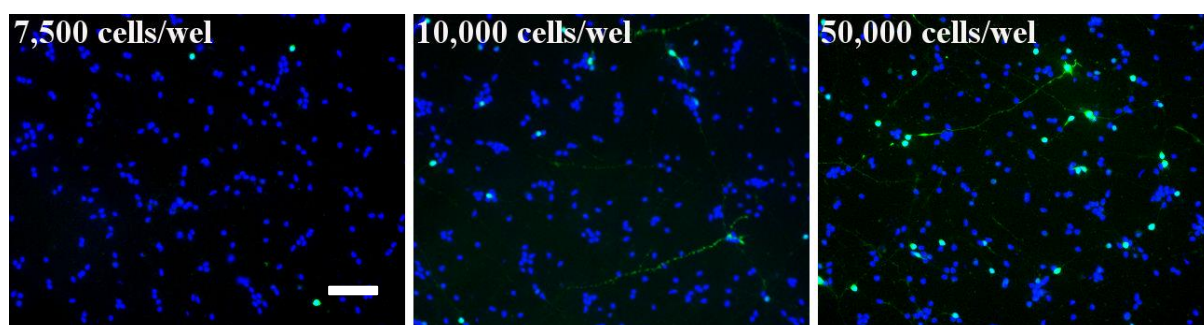


Figure 3.6 Optimisation of healthy GFP-LUHMES/stressed LUHMES co-culture.

Representative images of differentiating GFP-LUHMES/post-mitotic LUHMES co-culture. Differentiating (d2) GFP-LUHMES were replated on d6 differentiated LUHMES at 3 different densities: 7.5×10^4 , 1.0×10^4 and 5.0×10^4 cells/well. The best cell density was chosen based on the presence of single cells, which would allow measurement of single neurites. Scale bar represents 100 μm .

3.4.5. Neurite outgrowth assays in GFP-LUHMES co-cultured with stressed LUHMES

Neurite outgrowth from healthy GFP-LUHMES was assessed in a co-culture system with SS and DS-stressed LUHMES (

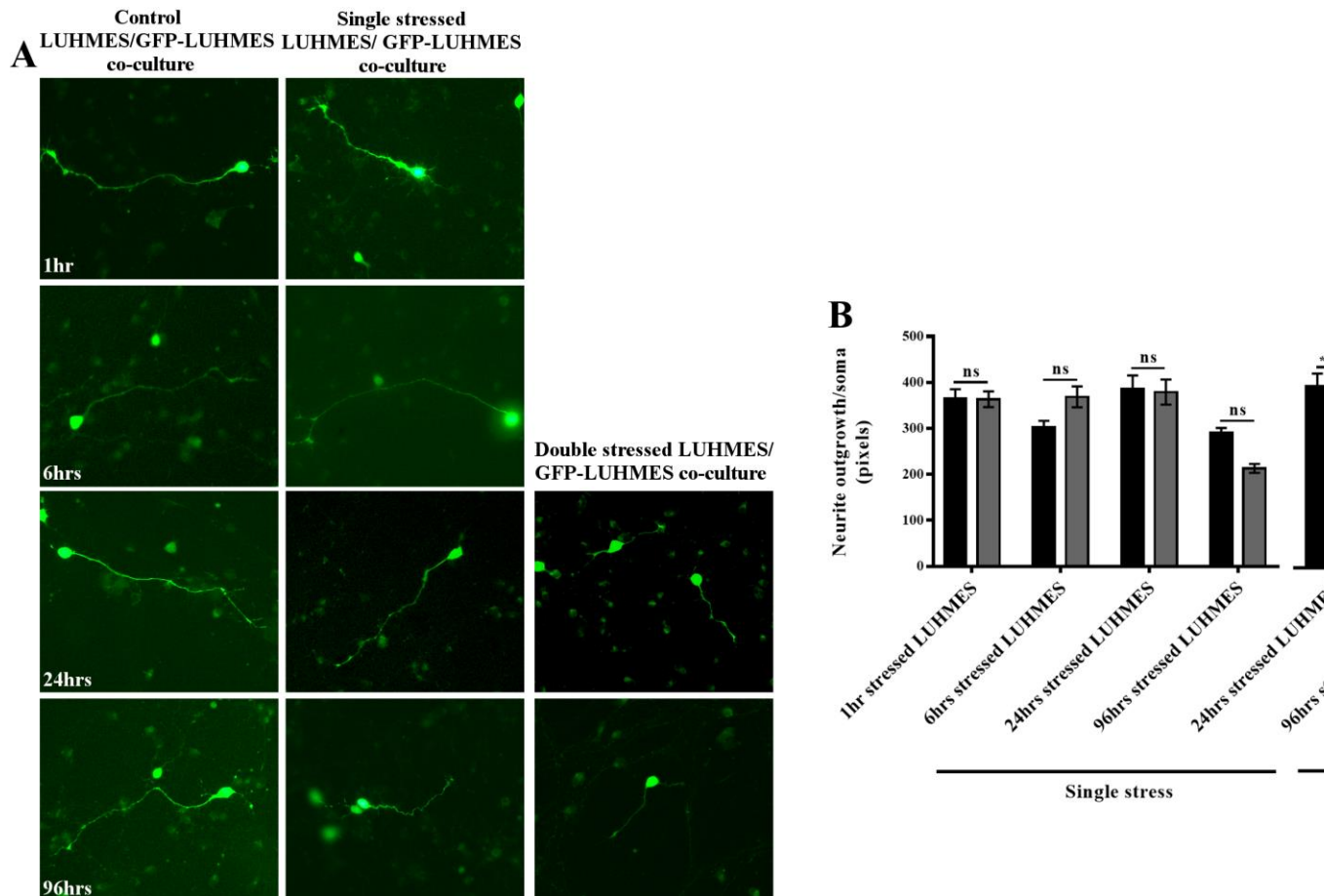


Figure 3.7). It was evident that neurite outgrowth in the control co-culture system was enhanced. Data presented in the previous section showed that the neurite length of LUHMES in monoculture under normal conditions was of 80 pixels/soma, while in co-culture, neurites reached lengths of more than 300 pixels/soma. When healthy LUHMES were co-cultured with 96 hours SS and DS-LUHMES, their neurite length was of 290 pixels/soma and 269 pixels/soma, respectively.

SS-LUHMES incubated with H₂O₂ for 1,6 and 24 hours did not impair neurite outgrowth of healthy LUHMES. Even though a reduction in neurite length was seen in neurones co-cultured with 96 hours SS-LUHMES, the effect was not significant ($p=0.0956$). DS-LUHMES had a greater effect on neurite outgrowth of GFP-LUHMES. 24 hours DS-LUHMES inhibited neurite outgrowth significantly, causing a reduction of almost half (222 pixels/soma, $p<0.0001$) the length of cells in control co-cultures. 96 hours DS-LUHMES also caused a significant reduction in neurite length (162 pixels/soma, $p=0.0029$).

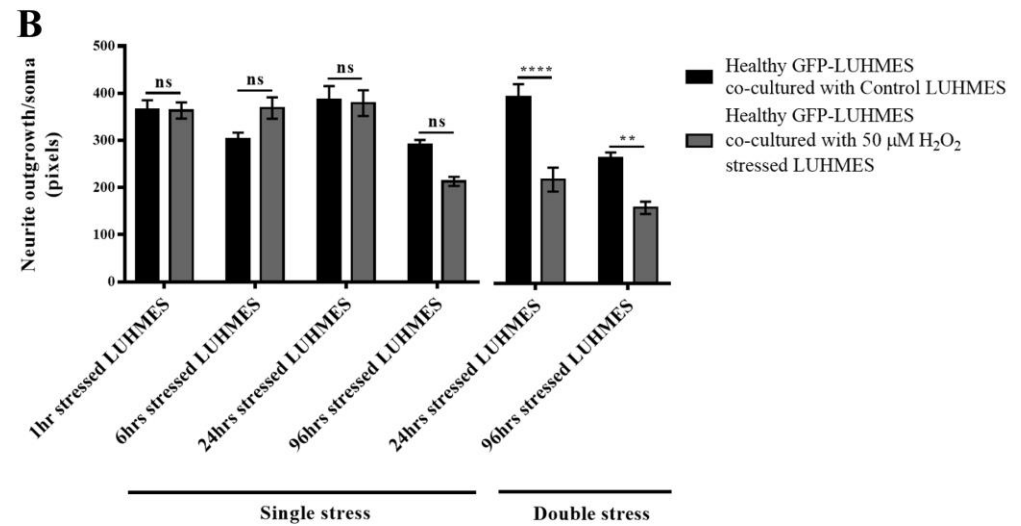
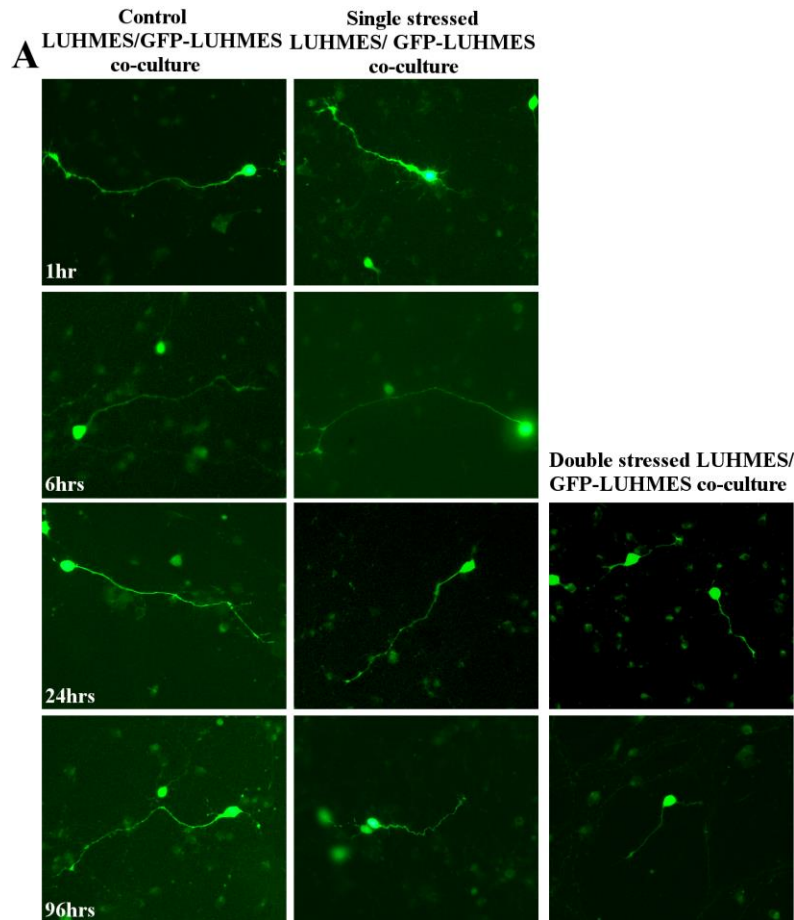


Figure 3.7 DS-LUHMES impair neurite outgrowth significantly of differentiating GFP-LUHMES in a co-culture system.

To assess the development of a SASP in DS-LUHMES, a co-culture system with healthy GFP-LUHMES was developed. Neurite length was used as a marker of cell health in this system. A. Representative images of GFP-LUHMES in a co-culture system with SS and DS-LUHMES. B. A significant impairment in neurite outgrowth was seen in GFP-LUHMES when co-cultured with 24 and 96 hours DS-LUHMES. Scale bar represents 20 μ m (Data represent mean \pm SEM; Two-Way ANOVA with multiple comparisons (Tukey correction), ** p < 0.01, **** p < 0.001, N=3, 3 experiments/replicate).

3.4.6. DNA damage under co-culture conditions

SASP in mitotic cells promotes inflammation and oxidative stress, which reinforces the senescent state by causing chronic DNA damage in neighbouring cells (Acosta et al., 2013). To investigate if stressed LUHMES could promote DNA damage in GFP-LUHMES in the co-culture system, detection of γ H2AX foci in these cells was conducted using immunocytochemistry. γ H2AX⁺ GFP-LUHMES were not present in any of the conditions assessed (**Figure 3.8**).

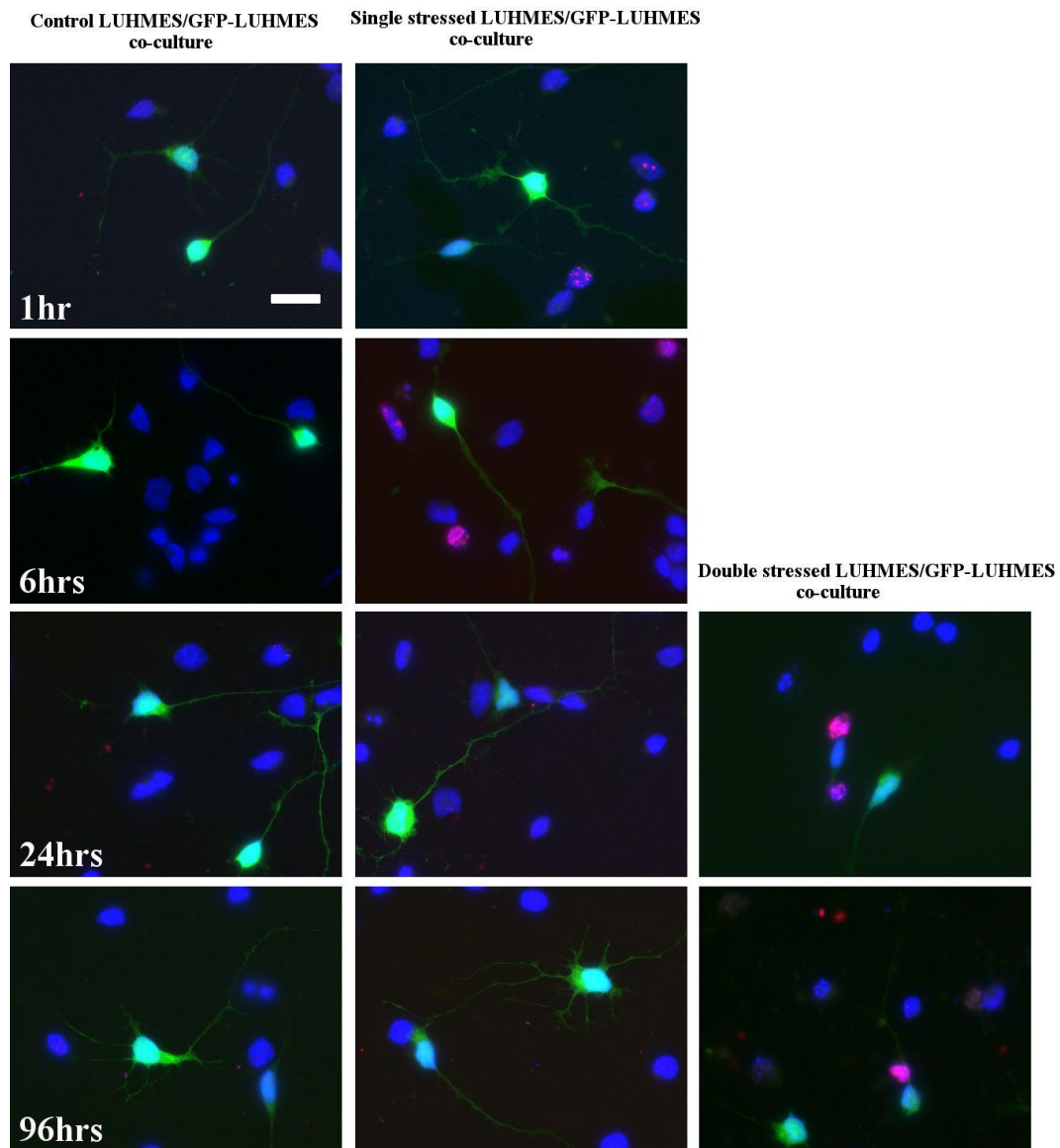


Figure 3.8 96 hours DS-LUHMES did not cause DNA damage on healthy LUHMES.

The ability of DS-LUHMES to induce DNA damage in surrounding cells as a result of a secretory phenotype was studied. GFP-LUHMES co-cultured with SS and DS-LUHMES were single labelled for γ H2AX. Formation of γ H2AX foci was not evident in GFP-LUHMES under any of the conditions assessed. Scale bar represents 20 μ m (N=3, at least 3 replicates, 3 experiments/replicate).

3.5. Discussion

After establishing a model of persistent oxidative DNA damage in differentiated LUHMES, the expression of common senescence markers was investigated. Irreversible cell cycle arrest is one of the main characteristics of cellular senescence, but *in vivo* and *in vitro* evidence suggests that neurones express some of the senescence markers that are found in mitotic cells despite their post-mitotic nature. The data presented here suggests that, despite achieving a state of persistent DNA damage, senescence markers, such as increased SA- β -gal activity and changes in chromatin organisation are not a feature of the neuronal model under study. At the same time, even though alteration in neurite development was detected in the healthy GFP-LUHMES that were co-cultured with DS-LUHMES, results did not suggest propagation of injury, since DNA damage in the form of γ H2AX was not seen in GFP-LUHMES.

3.5.1. SA- β -gal activity is present in untreated and stressed LUHMES

From its discovery, cytochemical detection of SA- β -gal has been used to identify senescent cells in culture and in tissue (Berkenkamp et al., 2014; Cohen et al., 2017; Debacq-Chainiaux et al., 2009; Itahana et al., 2013). The work of Dimri et al. (1995) on human fibroblasts and keratinocytes demonstrated activity of a β -gal at pH6 in late but not in early passage cultures (Dimri et al., 1995). Additionally, they reported an age dependent increase in SA- β -gal staining in skin biopsies but not in cultured skin fibroblasts, which only correlated with reduced cell replicative capacity (Dimri et al., 1995). Despite this, Dimri et al. suggested the use of SA- β -gal activity at pH6 as a marker of ageing and senescence both *in vivo* and *in vitro*. Later studies confirmed the origin of SA- β -gal as a lysosomal enzyme (Kurz et al., 2000). Its activity at a suboptimal pH was

shown to be, in part, product of increased mRNA and protein levels, but it was established that other conditions could also contribute to it (Lee et al., 2006).

More recently and related to brain ageing and neurodegeneration, SA- β -gal activity was studied in murine neuronal primary cultures. Geng et al. published a paper in 2010 where they demonstrated a time-dependant increase in the number of SA- β -gal⁺ cells in cultures of rat hippocampal neurones (Geng et al., 2010). Another study conducted in primary cortical neurones from Balb/c mice also showed increased SA- β -gal staining after 20 days *in vitro*, and even reported morphological changes in neurones, such as increased size, a characteristic of senescence in mitotic cells; however, no clear evidence is presented for this last claim (Chernova et al., 2006). These findings correlate with what has been published on senescence in human mitotic cells, but not with what was seen in differentiated LUHMES. Other studies have also challenged the use of SA- β -gal staining as a marker of senescence both in proliferative and post-mitotic cells.

Differentiated LUHMES showed endogenous SA- β -gal activity. Staining was localised in the axon hillock of the majority of cells and varied in intensity and localisation, depending on passage number and days in culture. Treatment with Bafilomycin A1 did not reveal any change in the intensity of the staining or in the number of stained cells and incubation with H₂O₂ did not seem to cause changes either, which indicated that SA- β -gal activity in LUHMES was not affected by lysosomal acidification. These results are similar to those reported by Piechota et al. (2016). Their study found SA- β -gal activity to be variable in 8-days cultured rat cortical neurones; this activity significantly increased after 30 days *in vitro*, but did not correlate with markers of DNA damage or DNA damage response (Piechota et al., 2016), suggesting that SA- β -gal in neurones in culture

could be linked to mechanisms other than senescence. SA- β -gal activity was also seen in differentiated HL60 and U937 cells and in Swiss 3T3 quiescent cultures (Yegorov et al., 1998). This evidence and the findings shown in the LUHMES suggest that increased SA- β -gal activity *in vitro* is not limited to senescent cells but can also be found in non-proliferative cells. The exact role of this enzyme in differentiated cells is yet to be determined.

The *in vitro* production of differentiated LUHMES involves the activation and silencing of cellular mechanisms that are necessary for neuronal development. Cell cycle exit, neurite growth and synapse formation are just some of the events that occur in neuronal maturation (Budnik and Salinas, 2011; Buttitta and Edgar, 2007; Sainath and Gallo, 2014), and degradation and synthesis of macromolecules accompany these processes. In 2000, Kurtz et al. confirmed that SA- β -gal activity resulted from an increase in lysosomal mass (Kurtz et al., 2000). Even though the exact role of SA- β -gal in replicative senescence has not been described, its lysosomal origin suggests it may be related to autophagy (Gerland et al., 2003). It has been shown that autophagy plays an important role in neuronal differentiation *in vitro* (Vázquez et al., 2012; Zeng and Zhou, 2008). It is possible that differentiated LUHMES presented some residual lysosomal activity from the 5-days differentiation process and that this could be reflected in SA- β -gal activity. The 2-step differentiation protocol of Scholz et al. (2011) results in a stable post-mitotic phenotype in LUHMES in terms of cell cycle exit and expression of neuronal markers. However, after day 5, differentiated LUHMES still go through differentiation-related changes, including electrophysiological maturation, axodendritic polarisation, expression of dopaminergic markers and synapse development (Scholz et al., 2011). This could mean that differentiation-related autophagy could still be active after day 5, contributing to an

increase in lysosomal mass and SA- β -gal activity. Mitochondrial biogenesis and metabolic changes are also implicated in neuronal maturation (Agostini et al., 2016). These changes have not been described yet in the LUHMES model, but they could contribute to a potential differentiation stress and influence SA- β -gal activity.

Finally, cell culture stress could also enhance SA- β -gal activity in differentiated LUHMES. pH changes and the use of tetracycline could increase ROS accumulation under normal conditions and stimulate lysosomal activity (Moullan et al., 2015).

3.5.2. Heterochromatin foci (SAHFs) are not present in SS or DS-LUHMES

Formation of senescence associated heterochromatin foci (SAHFs) appears in certain senescent cell types (Narita et al., 2003). These nuclear domains are constituted by a type of facultative heterochromatin enriched in macroH2A, a transcription-silencing histone variant, and heterochromatin proteins, such as HP1 and di- or tri-methylated lysine 9 histone H3 (H3K9me_{2/3}) (Narita et al., 2003; Zhang et al., 2005, 2007). SAHFs have an important role in cell cycle arrest in senescent cells as well as in the maintenance of this state through the repression of proliferation-related E2F target genes (Narita et al., 2003). SAHF formation can be detected with DAPI/Hoechst staining, to localise the heterochromatin structures, complemented with the immunocytochemical detection of any of the heterochromatin related proteins, including H3K9me_{2/3} (Aird and Zhang, 2013).

Immunocytochemistry for H3K9me₃ in differentiated LUHMES did not reveal changes of its localisation within the nucleus of SS or DS-LUHMES. Staining was diffuse and foci formation was not detectable at any of the time-points assessed. This pattern for H3K9me₃ is similar to the one presented for day-6 differentiated LUHMES maintained

under normal culture conditions (Weng, 2014). It is known that epigenetic modifications occur in post-mitotic neurones in response to DNA damage. Cell cycle re-entry is necessary for the activation of repair mechanisms in neurones (Tomashevski et al., 2010). This involves chromatin modifications that promote expression of E2F-regulated cell cycle related genes (Lui et al., 2005). It is interesting that the oxidative DNA damage model in LUHMES does not reflect chromatin changes at the level of H3K9 methylation. This had already been seen in day-4 differentiated LUHMES incubated with proliferation media up to day-6 to promote cell cycle re-entry (Weng, 2014). Weng (2014) showed that gene repression in differentiated LUHMES was supported by the formation of a specific chromatin structure enriched with the heterochromatin-specific histone modifications H3K27me3 and to a lesser level, H3K9me3. This structure was localised to the periphery of the nucleus and was not altered when LUHMES were induced to re-activate their cell cycle (Weng, 2014). Weng suggests that this chromatin structure functions act as a barrier in neurones to prevent cell division in response to replicative stress. This would explain why there were no changes in H3K9me3 staining in SS or DS-LUHMES.

The fact that H3K9 methylation could participate in a post-mitotic neuron-specific chromatin structure suggests that SAHF conformation could be different in these cells, if possible to form at all. For instance, macroH2A expression in neurones from young (4 months) and old (32 months) mice varied between Purkinje cells and cortical and hippocampal neurones. While macroH2A foci were more prevalent in old mice cortical neurones than young mice, no difference was detected in Purkinje cells and the hippocampus (Jurk et al., 2012). macroH2A was also investigated in rat cortical neurones kept in culture for 30 days and no change on its expression or localisation was seen during this time (Piechota et al., 2016). This evidence corroborates how different the

organisation of chromatin is in post-mitotic cells, such as neurones, compared to proliferating cells. Even though Jurk et al. confirmed SAHF formation based on macroH2A expression in cortical neurones from old mice, it is important to clarify the role of SAHF proteins in neurones and evaluate the feasibility of SAHF formation in these brain cells, before any conclusions can be drawn.

3.5.3. Do LUHMES develop a secretory phenotype in response to persistent DNA damage?

The SASP has been extensively studied *in vitro* and *in vivo* in different cell types and under different conditions. In 2008 Coppé et al. investigated the components of the SASP in 5 different strains of pre-senescent and senescent fibroblasts. Senescent fibroblasts secreted significantly higher levels of different proteins compared to pre-senescent cells; among these proteins, growth and survival factors, cell surface molecules and inflammatory chemokines and cytokines were present (Coppé et al., 2008). Later studies have also characterised the SASP in endothelial cells, muscle cells, mesenchymal stromal cells, keratinocytes and astrocytes (Hsu et al., 1999; Mombach et al., 2015; Muck et al., 2008; Özcan et al., 2016)

The analysis of conditioned media from senescent cells has been an important tool to examine the composition of the SASP, its regulation in senescence and the effects it exerts over the cellular microenvironment (Coppé et al., 2008, 2011; Freund et al., 2011; Kang et al., 2015; Maciel-Barón et al., 2016; Rodier et al., 2009). These studies have shown that the development of a SASP is independent of p16 and p21 activation; furthermore, the SASP results from a persistent DNA damage, and does not relate to cell cycle arrest and expression of other senescence markers, such as SA- β -gal (Coppé et al., 2011; Rodier et al., 2009). This evidence suggests that despite the post-mitotic nature and

the variable SA- β -gal activity found in the LUHMES it could be possible for these cells to develop a SASP in the DS model.

Before trying to characterise the components of a secretory phenotype, it was important to determine if soluble toxic factors were being released by LUHMES in response to oxidative DNA damage. For this, conditioned media (CM) from SS and DS-LUHMES was collected at different time-points. Healthy differentiated LUHMES were incubated with the CM for 24 hours and their viability was assessed. A small, but significant decrease in cell metabolic activity was seen, except for the 24 hours CM from DS-LUHMES. These results did not confirm if a secretory phenotype was being activated in the model. The percentage reduction of viability did not differ significantly between SS and DS conditions, suggesting that the effect was not enhanced by a persistent DNA damage. MTT cell metabolic activity assays presented in Chapter 2 showed that incubation of differentiated LUHMES with 50 μ M H₂O₂ caused mitochondrial dysfunction. This altered metabolic state could promote ROS accumulation in the culture medium and affect healthy LUHMES. Metabolic dysfunction in SS and DS-LUHMES, detectable even after 96 hours of being stressed could be an interesting condition to study; however, it does not suggest relation with a SASP.

A different approach to assess neuronal health was used to further investigate the presence of SASP-related toxic molecules in DS-CM from LUHMES. Neurite outgrowth has been previously used to assess neuronal function and health under different conditions (Harrill et al., 2010; Radio et al., 2008). For these experiments, 2-day-pre-differentiated LUHMES were replated and incubated for 24 hours in CM from SS and DS-LUHMES, collected at different time-points. Results showed a marked reduction in

neurite length in the LUHMES incubated with 50 μ M H₂O₂ CM, from both SS and DS-LUHMES. The 1hr SS-CM had a significant effect on neurite length, which could be related to the presence of a residual concentration of H₂O₂ and not to a secretory phenotype.

The study of the SASP in mitotic cells has revealed that its induction requires several days to occur (Acosta et al., 2013). This suggested that if a secretory phenotype were activated in DS-LUHMES, its effects would be detectable on the 96 hours-CM incubated neurones. Neurite length was impaired by the 24 hours DS-CM but not by the SS-CM collected at the same time-point. However, a significant decrease in neurite outgrowth was seen in differentiating LUHMES incubated with 96 hours SS and DS-CM. It is also important to consider that even the 96 hours-control-CM compromised neurite outgrowth. This evidenced the substantial influence that accumulation of products from the normal metabolism of LUHMES in the 96 hours-CM had on neurite outgrowth. Added to this, treatment with H₂O₂ could have enhanced accumulation of ROS and acidification of the culture media. Taking this into account, it is not possible to determine if the effects seen on the 24 and 96 hours DS-LUHMES were caused by SASP-related soluble factors, by the incubation in acidic cell culture media, or both.

To address this issue, a co-culture system of healthy GFP-LUHMES with SS and DS-LUHMES was designed. It has been shown that the SASP effects depend to a certain extent on cell-to-cell contact. Acosta et al. (2013) investigated this in oncogene-induced (OIS) senescent IMR90 human lung fibroblasts. Co-cultures in a transwell format confirmed the release of soluble factors by senescent cells that could propagate the senescent state to normal fibroblasts (Acosta et al., 2013). Direct co-cultures also showed

cell-to-cell contact contributed to this observed paracrine senescence and more importantly, it depended on the proximity of normal cells to senescent ones (Acosta et al., 2013). To investigate if this was also the case in the LUHMES model of persistent oxidative DNA damage, pre-differentiated GFP-LUHMES were co-cultured on top of SS and DS-LUHMES, at different time-points. Cell health was investigated indirectly through neurite outgrowth of GFP-LUHMES after 24 hours of incubation.

Neurite outgrowth of GFP-LUHMES was significantly impaired when co-cultured with 24 and 96 hours DS-LUHMES. A reduction in neurite length was also seen in the GFP-LUHMES/24 hours-SS-LUHMES co-culture, but this did not reach significance. This reduction in neurite length indicated that stressed LUHMES had a detrimental effect over normal LUHMES. The fact that this reduction was significant only in the DS-LUHMES co-culture suggested a higher toxicity exerted under these conditions, which could be related to the persistent DNA damage state. As described before, expression of common senescence markers, including SA- β -gal activity and growth arrest, does not relate to the development of a SASP in mitotic cells (Coppé et al., 2011). Persistent oxidative DNA damage in LUHMES could induce a secretory phenotype, despite being a non-proliferative cell type and having a variable pattern of SA- β -gal activity.

Acosta et al. (2013) also found that propagation of senescence by OIS-fibroblasts caused cell cycle arrest, expression of the SASP-associated cytokine IL-8, p16 and p21 activation and DNA damage in normal cells. To investigate if this happened in the co-culture LUHMES model, formation of DSBs was assessed in GFP-LUHMES using immunocytochemistry for γ H2AX. DSBs were expected to be present in the 96 hours-DS LUHMES co-culture, but no evidence of DNA damage was found in the GFP-LUHMES.

Earlier time-points were assessed as well, for both the SS and DS models, but all GFP-LUHMES were negative for γ H2AX under these conditions.

Not seeing an effect on the DNA of neighbouring cells in the DS-LUHMES co-culture does not exclude the possibility of DS-LUHMES being capable of secreting toxic factors and affecting their microenvironment. There is only one report of a SASP-like mechanism in neurones *in vitro*. The study showed a time-dependent increase in IL-6 mRNA levels, a SASP-associated cytokine, in rat neuronal cultures; a significant up-regulation was first detected after almost 20 days in culture, and reached a 5-fold increase at day 30 (Piechota et al., 2016). Analysis of LUHMES co-cultures was restricted to 24 hours after plating. A longer time in culture may be necessary for stressed LUHMES to cause detectable DNA damage in surrounding healthy LUHMES. Also, it is not possible to know whether the release of soluble factors by DS-LUHMES would be similar in composition, quantity and time with respect to fibroblasts, the model of senescence. In this section, the effects of paracrine senescence were only evaluated in terms of the propagation of DNA damage in DS-LUHMES co-cultures. To investigate if other common SASP factors were also being released and participated in the neurite length impairment presented previously, changes in the transcriptome of 96 hours DS-LUHMES vs SS-LUHMES and controls were analysed. This part of the project is presented and discussed in Chapter 4.

Analysis of senescence markers and propagation of DNA damage to healthy neurones did not suggest activation of a senescence program in DS-LUHMES. This could be linked to the embryonic nature of this cell line, which does not reproduce the ageing conditions that cells are exposed to *in vivo* and that could contribute to the development of a senescent

phenotype in mitotic cells. The direct conversion of fibroblasts into induced neurones (iNs) could be an alternative to LUHMES that would better represent the changes that neurones go through as we age. A recent report has shown that transcription factor-based conversion of fibroblasts from donors of different ages successfully results in iNs that express common neuronal markers and that are electrically active. Contrary to induced pluripotent stem cells (iPSCs), conversion of fibroblasts into iNs does not involve reprogramming of the cells into an embryonic-like state, and so iNs maintain age-related features that are list in iPSCs (Mertens et al., 2015). These characteristics would make iNs ideal for the study of ageing and senescence related changes in neurones *in vitro*.

3.6. Main conclusions

- Differentiated LUHMES express endogenous SA- β -gal activity under normal conditions. This could result from lysosomal accumulation related to the differentiation process, as well as from a high vulnerability of the cells to standard cell culture conditions.
- Changes in chromatin structure of DS-LUHMES in the form of SAHF formation were not detected. Chromatin organisation in response to a persistent DNA damage in LUHMES and neurones in general, could be regulated differently in comparison to mitotic cells.
- CM and co-cultured experiments suggested a toxic effect based on neurite length impairment. This effect was contact dependent, since incubation in conditioned media did not alter healthy LUHMES viability. Based on these findings, neurones with persistent DNA damage can affect healthy neurones. The mechanism of this and whether it is due to a secretory phenotype similar to the SASP is unclear from this chapter.

Chapter 4. Transcriptome analysis of single and double stressed LUHMES

4.1. Introduction

In Chapter 3, induction of senescence in 96 hours DS-LUHMES was first investigated through the detection of two widely used senescence markers: SA- β -gal activity and SAHF formation. SA- β -gal activity in LUHMES under normal conditions was variable and H₂O₂ stress did not cause changes on its activity. SAHF formation was not present in DS-LUHMES. However, assessment of a SASP in DS-LUHMES in a co-culture system of GFP-LUHMES/stressed LUHMES suggested that DS-LUHMES could affect the viability of healthy LUHMES through a secretory phenotype that could resemble the SASP. To address this hypothesis, microarray analysis was used to assess changes in the transcriptome of control, SS and DS-LUHMES.

Transcription profiling has been used for the study of senescence and the SASP in different cell types. Microarray analysis provides valuable information on changes in the expression of RNA transcripts both *in vivo* and *in vitro*. This information can be used to determine if there are specific pathways, functional groups or individual genes affected by specific experimental conditions, such as exposure to genotoxic agents. Investigating the transcriptome of senescent cells has revealed the involvement of several genes and pathways in senescence activation and the SASP, that were previously not known to be related to this mechanism. For instance, Nagano et al. identified *PRODH* and *DAO*, which encode for proline dehydrogenase 1 and D-amino acid oxidase respectively, to be up-regulated in senescent cells and to promote ROS-induced senescence when overexpressed (Nagano et al., 2016). Moreover, this experimental tool has provided

evidence of the heterogeneity of senescence by identifying expression of senescence and SASP components that are exclusive to specific cell types or senescence-induction mechanisms; at the same time, identification of common genes involved in senescence regardless of cell type or induction have been found (Hernandez-Segura et al., 2017; Nelson et al., 2014; Shelton et al., 1999).

Despite the evidence available on expression of senescence markers in ageing neurones, the exact inductors and mechanisms by which senescent pathways are activated are not well understood. The expression and composition of a secretory phenotype by damaged neurones have also not been described. It is possible that the same pathways that activate senescence in cycling cells are present in neurones; however, their function and involvement in mechanisms such as DNA damage and cell cycle regulation could differ as a result of the post-mitotic nature of neurones. Taking this into account, we decided that a microarray profiling approach would be ideal to detect changes in LUHMES in response to H₂O₂. Analysis of the array data would focus on identifying genes and pathways linked to senescence and the SASP in mitotic cells.

4.2. Aims and objectives

The aim of the work presented in this chapter was to perform a detailed characterisation of the transcriptomic profile of DS-LUHMES and identify specific gene expression changes in response to persistent DNA damage. This was done by:

- Characterising the gene expression profile of control, SS and DS-LUHMES using a microarray approach.
- Performing pathway enrichment and functional grouping analysis of the microarray data to identify dysregulation of candidate genes and specific pathways linked to senescence and the SASP.
- Validating expression of a panel of candidate, biologically relevant genes by qRT-PCR (quantitative polymerase chain reaction) and interrogating their expression changes at a functional level.

4.3. Materials and methods

4.3.1. Transcriptome analysis of stressed LUHMES

To investigate if “classical” markers of senescence are expressed by neurones in response to a persistent DNA damage, a microarray analysis was performed in the 96 hours single/double stress LUHMES model; deregulation of “classical” senescence and SASP related pathways were studied, as well as pathways suggesting changes in the DNA damage response, cell cycle regulation and immune response.

4.3.2. Trizol RNA extraction

SS and DS-LUHMES (4.5×10^5 cells/well, in 12-well plates) were harvested 96 hours after stress. For this, cells were collected in 200 μ l of TRIzol Reagent (ThermoFisher Scientific, MA, USA) per well; each condition was composed by extracts from 4 wells, giving a final volume of 800 μ l/condition TRIzol extract. RNA was purified using the Direct-zol RNA MiniPrep extraction protocol (Zymo Research, Irvine, CA, USA), following the manufacturer’s instructions. In summary, 800 μ l of 100% ethanol were added to the 800 μ l TRIzol extracts. After mixing thoroughly, the mixture was transferred into a Zymo-Spin IIC Column in a collection tube and centrifuged at 16,000xg for 30 seconds. Since the total sample volume was >700 μ l, the sample was transferred and centrifuged in the column in two steps of 800 μ l/step. The column was then washed with 400 μ l of Direct-zol RNA PreWash and centrifuged at 16,000xg for 30 seconds. The flow-through was discarded and the pre-washing step repeated. 700 μ l of RNA Wash Buffer were added to the column and it was centrifuged at 16,000xg for 2 minutes. The column was transferred into a 1.5 ml RNase free tube. RNA samples were eluted in 30 μ l of RNase free water by centrifuging at 16,000xg for 30 seconds. The RNA concentration was determined by

analysing 1 µl of sample in the NanoDrop Spectrophotometer (ThermoFisher Scientific, MA, USA) and RNA integrity assessed using the Agilent RNA 6000 Nano Chip (Agilent Technologies INC, CA, USA).

4.3.2.1. RNA amplification and microarray hybridisation

The RNA extracted from the 96 hours untreated control, SS and DS-LUHMES was used to investigate changes in their transcriptome. For this, RNA samples were amplified with the 3' IVT Pico Reagent kit (ThermoFisher Scientific, MA, USA). Even though the quantity of TRIzol extracted RNA was sufficient and did not require amplification, LUHMES RNA samples were treated following the same protocol as the one described in **Chapter 5** for the enriched neuronal samples obtained from frozen post-mortem tissue. This would allow for both sets of data to be discussed in conjunction without technical limitations in terms of pre-microarray sample treatments. In summary, LUHMES RNA samples were diluted 1:20 (**Table 4.1**) and the poly-A RNA control mix (5 µl/sample) was added to each sample. This control mix was added to monitor the entire process and consisted of polyadenylated transcripts from *B. subtilis* that are not expected to be present in eukaryotic samples. RNA amplification started with the synthesis of first-strand cDNA from the RNA samples by reverse transcription, which resulted in single-stranded (ss)-cDNA with a T7 promoter sequence at the 5' end (primers containing a T7 promoter sequence were used). In a second reaction, a 3'-Adaptor was added to the ss-cDNA; this 3'-Adaptor functioned as template in a third reaction and stimulated the synthesis of the double-stranded (ds)-cDNA. Following this, *In Vitro* Transcription (IVT) of the ds-cDNA was done, resulting in the synthesis of antisense RNA (complimentary RNA, cRNA), which was purified and quantitated in a NanoDrop Spectrophotometer (ThermoFisher

Scientific, MA, USA). The cRNA quality and concentration were also assessed with the Agilent 6000 Nano Chip (Agilent Technologies INC, CA, USA).

Purified cRNA was used for sense-strand cDNA synthesis by reverse transcription; antisense-strand cDNA was then obtained from a second round of ds-cDNA synthesis, which contained dUTP at a specific ratio relative to dTTP. The cRNA template was removed from the samples by hydrolysis and the ds-cDNA was purified and then quantified by spectrophotometry, before preparing the sample for fragmentation and labelling.

The ds-cDNA was fragmented at the dUTP residues by the enzymes uracil-DNA glycosylase (UDG) and apurinic/ apyrimidinic endonuclease 1 (APE 1); these fragments were labelled with the DNA Labeling Reagent (Affymetrix), which is linked to biotin, by a terminal deoxynucleotidyl transferase (TdT).

GeneChip Human Genome U133 Plus 2 Arrays (ThermoFisher Scientific, MA, USA) (containing >54,000 probe sets for approximately 39,000 well-characterised human genes) were prepared for hybridization by pre-hybridizing the cartridges with Pre-hybridization mix for 30 minutes, at 45 °C and 60rpm. This mix contained the Hybridization controls (bioB, bioC, bioD and cre) as well as the control Oligo B2. At the same time, the Hybridization cocktail was prepared by mixing 160 µl of Hybridization Master Mix and 60 µl of the sample ds-cDNA. This mix was incubated for 5min at 99°C and then for 5 minutes at 45 °C, followed by a brief centrifugation to collect tube contents. The Pre-Hybridization mix was removed from the cartridge and 200 µl of Hybridization Mix were pipetted in, followed by a 16 hours incubation, at 45 °C and 60rpm. Arrays were then

washed with Wash Buffer A and placed in the Affymetrix GeneChip Command Console Fluidics Control (ThermoFisher Scientific, MA, USA) for staining. Arrays were stained using the Fluidics Protocol FS450_0001.

4.3.2.2. Microarray data quality control

Data was analysed in the Affymetrix Expression Console 1.4.1.46 and normalised using the Robust Multi-Array Average (RMA).

4.3.2.3. Microarray data analysis

The Qlucore Omics Explorer software (Qlucore, Lund, Sweden) was used for analysis of the normalised data. Two-group comparisons, setting $p \leq 0.05$ and a fold change ≥ 1.2 , were performed (Single stressed LUHMES vs Controls; Double stressed LUHMES vs Controls; SS and DS-LUHMES). DAVID Functional Annotation Tool Version 6.7 (NIAID, NIH, USA) (Huang et al., 2009a, 2009b) and IMPaLA (Integrated Molecular Pathway Level Analysis) (Cavill et al., 2011; Kamburov et al., 2011) were used to perform the pathway analysis on the lists of significantly, differentially expressed genes.

4.3.2.4. qRT-PCR validation of microarray genes of interest

Validation of candidate dysregulated transcripts in DS-LUHMES was assessed by qRT-PCR (quantitative real time polymerase chain reaction). For this, differentiated LUHMES were stressed following the SS/DS protocol, as previously described. TRIzol extracts from control, SS and DS-LUHMES were collected 96 hours after stress and RNA was purified using the Direct-zol RNA MiniPrep and the Zymo-Spin IIC Columns as described in **section 4.3.2**. cDNA was synthesized using the qScript cDNA Supermix (Quanta

Biosciences, MA, USA). The PrimeTime qPCR assays (Integrated DNA Technologies®) listed in **Table 4.1** were used for the qRT-PCR. Each sample mix contained 60 ng of cDNA, 500 nM forward and reverse primer, and 250 nM probe, 2 x Brilliant III qPCR Master mix (Agilent Technologies, Sta Clara, CA, USA) and nuclease free distilled H₂O. qRT-PCR was performed on a 2 step thermal profile on a Stratagene MX3000P™ Real Time Thermal Cycler (Agilent Technologies Ltd). The incubation was performed as follows: 10 minutes at 95°C then 40 cycles of 30 seconds at 95°C, 60 seconds at 60°C and 60 seconds at 72°C. LMNB1 was used as housekeeping gene (HK) and was amplified on each plate. Expression levels were normalised to LMNB1 using the $\Delta\Delta C_t$ calculation.

Gene	PrimeTime [®] Assay ID	Ref Seq	Exon location	Probe and Primer Sequence
<i>ATR</i>	Hs.PT.56a.399 57055	NM_001184	18-19	Probe: 5'-/56-FAM/AGCGAACAA/ZEN/AGCAGTCCCAAGC 3IABkFQ/-3' Primer 1: 5'-CCCAGACAAGCATGATCCAG-3' Primer 2: 5'-GAAGATGATGACCACACTGAGA-3'
<i>RPA1</i>	Hs.PT.58.2293 974	NM_002945	1-3	Probe: 5'-/56-FAM/TCCTCCAAG/ZEN/TCATCAACATCCGTCC 3IABkFQ/-3' Primer 1: 5'-TCATGAGCAGTCGATAACGC-3' Primer 2: 5'-GCGGCCATCATGCAGAA-3'
<i>CLSPN</i>	Hs.PT.58.7651 77	NM_0011904 81	1-2	Probe: 5'-/56-FAM/TCATGACTT/ZEN/CTGCCTCCCTGC/3IABkFQ/-3' Primer 1: 5'-GACTATCTGCTTCTCTTGTGA-3' Primer 2: 5'-ACAGCTCCGTCCTTAGTG-3'
<i>CDH1</i>	Hs.PT.58.3324 071	NM_004360	6-7	Probe: 5'-/56-FAM/TCTTCCCG/ZEN/CCCTGCCAAT/3IABkFQ/-3' Primer 1: 5'-GCTGTGGGGTCAGTATCAG-3' Primer 2: 5'-GCCTGAAGTGACTCGTAACG-3'
<i>CDC27</i>	Hs.PT.58.2053 47	NM_001256	18-19	Probe: 5'-/56-FAM/CCAGGAGA/ZEN/GCAGCATGACAGATG/3IABkFQ/-3' Primer 1: 5'-GCTGCATGAAGTTGTGTGTC-3' Primer 2: 5'-GCCAATAACCAAGAAGAACAG-3'
<i>CCNB1</i>	Hs.PT.56a.395 64933	NM_031966	4-5	Probe: 5'-/56-FAM/ATGTTTCCA/ZEN/GTGACTTCCCGACCC/3IABkFQ/-3' Primer 1: 5'-TGAACCTGTACTAGCCAGTCA-3' Primer 2: 5'-TGTAGTGAATATGTGAAAGATATTTATGCT-3'
<i>NDUFS8</i>	Hs.PT.58.2284 3831	NM_002496	5-6	Probe: 5'-/56-FAM/AGATGGCCT/ZEN/CGCAGAGCTTGC/3IABkFQ/-3' Primer 1: 5'-TGCACTTGGTCATGTCGAT-3' Primer 2: 5'-GGGAGGAGCGTTGCATT-3'
<i>NDUFV3</i>	Hs.PT.58.2476 9161	NM_0010015 03	1-2	Probe: 5'-/56-FAM/AGCATAGTC/ZEN/TTCAGCGCCCG/3IABkFQ/-3' Primer 1: 5'-GATTCCGCAGACAAAGAAACC-3' Primer 2: 5'-CTGTGGCCCTGCTTGGT-3'
<i>DDX58</i>	Hs.PT.58.4273 674	NM_014314	15-16	Probe: 5'-/56-FAM/AGAGGCAGA/ZEN/GGAAGAGCAAGAGGTA/3IABkFQ/-3' Primer 1: 5'-CCAGCATTACTAGTCAGAAGGAA-3' Primer 2: 5'-CCACAGTGCAATCTTGTCATCC-3'
<i>LMNB1</i>	Hs.PT.58.4013 3522	NM_0011985 57	6-7	Probe: 5'-/56-FAM/AGGCGAAGA/ZEN/AGAGAGGTTGAAGCTG/3IABkFQ/-3' Primer 1: 5'-CTTGAGGATGCTCGGGATAC-3' Primer 2: 5'-GGAAATCAGTGCTTACAGGAAAC-3'

Table 4.1 PrimeTime[®] qPCR assays used for validation of the candidate gene expression changes in control, SS and DS-LUHMES.

PrimeTime[®] qPCR assays were resuspended in TE buffer to a 20x concentration. The final 1x concentration contained 500 nM primer (forward or reverse) and 250 nM probe.

4.3.2.5. Functional validation of microarray genes of interest

4.3.2.5.1. Detection of Ki67 and MCM2 expression in DS-LUHMES

To further investigate if transcriptional changes related to DDR and cell cycle regulation were indicative of cell cycle re-entry in 96 hours DS-LUHMES, expression of proliferation markers Ki67 and Mcm2 were assessed by immunocytochemistry. For this, control, SS and DS-LUHMES were fixed with 4% PFA 96 hours after H₂O₂ incubation. Double labelling for Ki67/ β -III-tubulin and Mcm2/ β -III-tubulin was conducted as described previously, in **Chapter 2, section 2.3.3. Table 4.2** and **Table 4.3** contain information for primary and secondary antibodies used for this experiments. Fixed proliferating LUHMES were included as positive controls, as due to their proliferative state, expression of Ki67 and Mcm2 was expected.

Antibody	Species	Clone	Dilution and incubation conditions	Source	Catalog Number
Ki67	Mouse monoclonal	MM1	1:50 (overnight at 4 °C)	Leica Microsystems, Wetzlar, Germany.	NCL-L-Ki67-MM1
MCM2	Rabbit polyclonal	-	1:50 (1 hour, RT)	Proteintech, Rosemont, IL, USA	10513-1-AP
β -III-tubulin	Chicken polyclonal	-	1:1000 (2 hours, RT)	Merck Millipore, Darmstadt, Germany.	AB9354

Table 4.2 Primary antibodies used for immunocytochemistry.

Primary antibodies, dilutions and incubation conditions used for single and double labelling of SS/DS-LUHMES.

Antibody	Species	Dilution and incubation conditions	Source	Catalog Number
488 Alexa Fluor [®] anti-chicken	Goat	1:1000 (1 hour, RT)	Thermo Fisher Scientific, Waltham, MA, USA	A-11039
568 Alexa Fluor [®] anti-rabbit	Donkey	1:1000 (1 hour, RT)		A10042
568 Alexa Fluor [®] anti-mouse	Goat	1:1000 (1 hour, RT)		A-11004

Table 4.3 Primary antibodies used for immunocytochemistry.

Secondary antibodies, dilutions and incubation conditions used for single and double labelling of SS/DS-LUHMES.

4.3.2.5.2. Investigating Complex I activity in DS-LUHMES

Complex I altered function in response to persistent oxidative DNA damage in DS-LUHMES was assessed with the Complex I Enzyme Activity Microplate Assay Kit (Abcam, Cambridge, UK). Microplate wells are coated with antibodies specific for Complex I. These antibodies capture Complex I from cell lysates allowing for its activity to be determined by measuring oxidation of NADH to NAD⁺. Measurement of this reaction is possible thanks to the simultaneous reduction of a dye, which can be detected as an increase in absorbance at 450 nm.

Pre-differentiated LUHMES were seeded onto T75 flasks at a density of 9.5×10^6 cells/flask and treated with $50 \mu\text{M}$ H_2O_2 following the SS/DS-LUHMES protocol. Protein lysates from control, SS and DS-LUHMES were collected 96 hours after incubation with H_2O_2 . In order to get enough protein for the assay, 2 T75 flasks per condition were harvested with $500 \mu\text{l}$ of PBS per flask. Samples were centrifuged at $500 \times g$ for 5 minutes and the cell pellet was resuspended in $50 \mu\text{l}$ PBS. $5 \mu\text{l}$ of 10x detergent was added to each sample, which was followed by 30 minutes incubation in ice. Samples were centrifuged for 20 minutes at $16000 \times g$ and 4°C . The supernatant was collected in a clean tube and $5 \mu\text{l}$ of sample were saved for protein determination. $50 \mu\text{l}$ of sample were combined with $150 \mu\text{l}$ of incubation buffer and the final $200 \mu\text{l}$ were added to the multiplate wells; $200 \mu\text{l}$ of incubation buffer were added to one of the wells to be used as blank. The plate was incubated for 3 hours at RT. Wells were then washed twice with washing buffer and the assay solution was prepared as follows: 0.835 ml of 1x Buffer, $42 \mu\text{l}$ of 20x NADH and $8.5 \mu\text{l}$ of dye. The assay solution was added to each well ($200 \mu\text{l}/\text{well}$) and absorbance was read immediately after addition. For this, a PHERAStar microplate reader (BMG Labtech, Ortenberg, Germany) was used to measure absorbance at 450 nm , every 30 seconds, for 30 minutes. For data analysis, the MARS Data Analysis Software (BMG Labtech, Ortenberg, Germany) calculated the slope based on 64 readings. This value was divided by the extinction coefficient (ϵ) of the dye ($\epsilon=25.9$), which allowed for conversion of the data from mOD to mM oxidised NADH per minute. The values obtained were divided by the amount of protein in μg present in each sample. Data was normalised to controls.

4.4. Results

4.4.1. Integrity of purified RNA from control and stressed LUHMES

The RNA yield obtained from control and SS/DS-LUHMES was on average 217.17 ± 12.93 ng/ μ l in a total volume of 30 μ l nuclease free water. RNA quality was determined by the A260/280 ratio, which was on average 2.01 ± 0.02 . The RIN (RNA integrity number) value for the samples was of 8.18 ± 0.16 and electropherograms from all samples showed two distinct 28S and 10S rRNA (ribosomal RNA) peaks (**Table 4.4, Figure 4.1**).

Condition	RNA concentration (ng/ μ l)	260/280 ratio
Control-1	216.41	2.03
SingleS-1	200.89	2.00
DoubleS-1	217.08	2.00
Control-2	215.49	1.98
SingleS-2	224.95	2.03
DoubleS-2	193.92	2.01
Control-3	235.65	2.02
SingleS-3	225.70	2.00
DoubleS-3	224.43	2.00
Mean \pm SD	212.17 ± 12.93	2.01 ± 0.02

Table 4.4 Initial concentrations of RNA in untreated control, SS and DS-LUHMES samples.

After TRIzol extraction, RNA concentration was measured in the Nanodrop and an initial assessment of RNA quality was done using the 260/280 ratio.

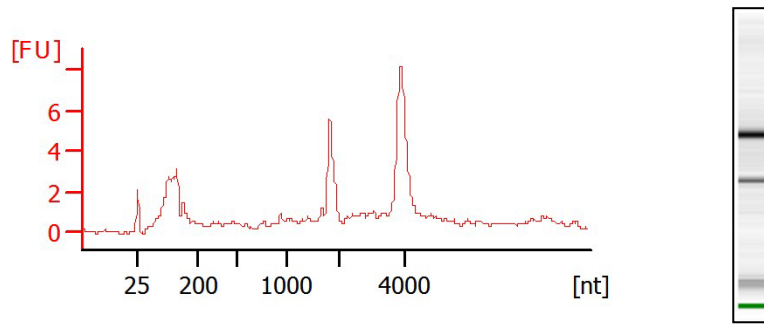


Figure 4.1 RNA integrity of control and SS/DS-LUHMES.

Example of an electropherogram and electrophoresis gel obtained with the Agilent 2100 Bioanalyzer from a DS-LUHMES RNA sample. Electropherograms were used to assess the RNA integrity of RNA samples extracted from control, SS and DS-LUHMES. Peaks represent the 18S and 28S rRNA and indicate good quality RNA (FU: fluorescence unit).

4.4.2. RNA preparation for microarray analysis

RNA extracts from control, SS and DS-LUHMES were diluted 1:20 (**Table 4.5**) to be processed using the 3' IVT Pico Reagent kit. Diluted samples contained 10.88 ± 0.64 ng/ μ l RNA on average.

Condition	RNA concentration (ng/ μ l)	Dilution 1:20 (ng/ μ l)
Control-1	216.41	10.82
SingleS-1	200.89	10.04
DoubleS-1	217.08	10.85
Control-2	215.49	10.77
SingleS-2	224.95	11.24
DoubleS-2	193.92	9.69
Control-3	235.65	11.78
SingleS-3	225.70	11.28
DoubleS-3	224.43	11.22
Mean \pm SD	212.17 ± 12.93	10.88 ± 0.64

Table 4.5 Initial concentrations of RNA in untreated control, single and double stressed LUHMES samples.

A 1:20 dilution of all samples was used for the RNA amplification protocol, prior to sample preparation for microarray hybridisation.

Approximately 10 ng RNA per sample were used for the single-strand cDNA (ss-cDNA) synthesis. After purification, the yield of cRNA was measured by spectrophotometry with a NanoDrop 1000. **Table 4.6** shows the concentration of cRNA obtained per sample. The mean concentration of cRNA was 3309.51 ± 302.37 ng/ μ l and the mean 260/280 ratio was 1.84 ± 0.08 .

Condition	cRNA concentration (ng/μl)	260/280 ratio
Control-1	3112.69	1.89
SingleS-1	3627.35	1.70
DoubleS-1	3498.12	1.77
Control-2	2949.45	1.94
SingleS-2	2769.25	1.87
DoubleS-2	3617.18	1.80
Control-3	3439.61	1.87
SingleS-3	3461.16	1.82
DoubleS-3	3310.81	1.93
Mean ± SD	3309.51± 302.37	1.84±0.08

Table 4.6 Initial concentrations of cRNA in untreated control, single and double stressed LUHMES samples.

The cRNA yield was measured in the Nanodrop and an initial assessment of its quality was done using the 260/280 ratio.

For the 2nd – cycle double stranded cDNA (ds-cDNA) synthesis, 20 µg of cRNA were used for sense-strand and anti-sense strand DNA synthesis. The ds-cDNA was purified and measured by spectrophotometry. The mean ds-cDNA concentration was 630.87±37.7 ng/µl (**Table 4.7**)

Condition	ds-cDNA concentration (ng/µl)	260/280 ratio
Control-1	608.8	1.89
SingleS-1	671.2	1.70
DoubleS-1	633.3	1.77
Control-2	690.0	1.94
SingleS-2	660.3	1.87
DoubleS-2	625.3	1.80
Control-3	619.2	1.87
SingleS-3	600.4	1.82
DoubleS-3	569.3	1.93
Mean ± SD	630.87 ± 37.7	1.84±0.08

Table 4.7 Initial concentrations of ds-cDNA in untreated control, single and double stressed LUHMES samples.

The ds-cDNA yield was measured in the Nanodrop and an initial assessment of its quality was done using the 260/280 ratio.

For the fragmentation step, 6.6 µg of ds-cDNA were used. Fragmentation of the ds-cDNA was done by UDG and APE 1 enzymes at the dUTP residues. To ensure that fragmentation was successful, this was assessed with the Agilent 2100 Bioanalyser (**Figure 4.2**). Labelling of the fragmented cDNA was done by a TdT using the Affymetrix proprietary DNA labelling reagent, which contains biotin. After labelling, samples were processed for cartridge array hybridisation, as explained in **section 4.3.2.1**.

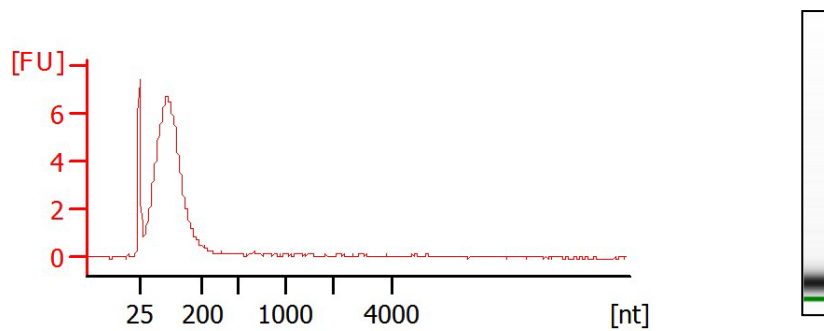


Figure 4.2 Assessing fragmentation of ss-cDNA.

Representative electropherogram and electrophoresis gel showing ss-cDNA fragmentation. (FU=fluorescence unit).

4.4.3. Microarray data quality control (QC) overview

Standard quality control parameters for the MAS 5.0 algorithm data were assessed prior to the microarray data analysis. Affymetrix Expression Console™ Software was used for the QC analysis and included parameters for the assessment of sample quality, hybridisation and signal quality and signal comparability.

Overall, the QC analysis did not show evidence of an outlier. Some samples (Control 1, Control 3, DS 1, 2 and 3) had metric values that were outside of the trend, but no single sample differed consistently from the others. This reflected in the clustering analysis, which segregated the 9 samples in 3 well-differentiated groups and did not reveal samples that did not aligned consistently to these groups (**section 4.4.4, Figure 4.9**). Based on these results, no samples were deemed as being outliers that would skew the data and mask biologically relevant gene expression changes and so, all 9 samples were included in the pathway analysis.

4.4.3.1. Sample quality

The quality of the RNA samples as well as of the amplification and labelling processes were monitored by assessing the signals obtained from labelling controls and internal controls (housekeeping genes) as described in the following sections.

4.4.3.1.1. Labelling controls

Labelling controls consisted of bacterial poly-A RNA controls that were added to each sample before the synthesis of the ss-cDNA and that allowed the monitoring of the entire process. The GeneChip Human Genome U133 Plus 2 contained probe sets from the *B. subtilis* genes *lys*, *phe*, *thr* and *dap* at different concentrations each (1:100,000, 1:50,000, 1:25,000 and 1:6,667, respectively). The hybridisation intensity of these controls were used to evaluate the efficiency of the labelling process. All poly-A controls should be present in the samples and their signal values should increase in the order previously described. Results from the poly-A controls showed that all samples, except for Control 1, labelled efficiently (**Figure 4.3**). The labelling efficiency for Control 1 was lower in the *dap* poly-A control when compared to the rest of the samples; however, signals from the rest of the controls were consistent with the other 8 samples.

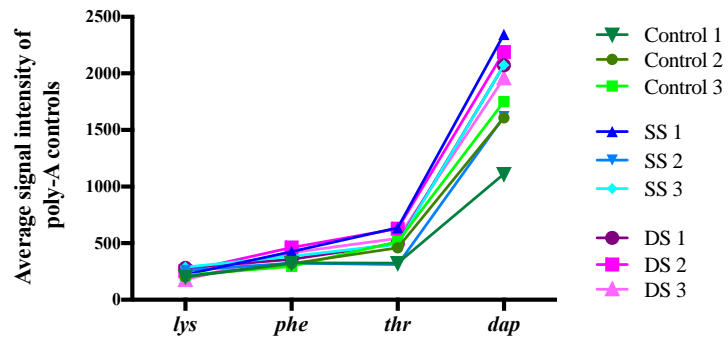


Figure 4.3 Poly-RNA controls for 96 hours control and SS/DS LUHMES.

Plot depicting the average signal intensity of poly-A controls *lys*, *phe*, *thr* and *dap* for each of the 9 samples (SS, single stressed LUHMES; DS, double-stressed LUHMES).

4.4.3.1.2. 3'/5' ratio for β -actin and GAPDH

GAPDH and β -actin probes function as internal controls to monitor the 2-cycle amplification and labelling process. The GAPDH and β -actin 3' probe to 5' probe ratios for the 96 hours control and SS/DS LUHMES arrays are shown in **Figure 4.4**. Affymetrix indicates that ratio values should be below 3 for 1-cycle assays, but 2-cycle assays can give higher values as a result of the additional amplification cycle. GAPDH and β -actin ratio values for the 96 hours control and SS/DS arrays were similar between replicates; β -actin values were higher than 3, as expected for a 2-cycle assay.

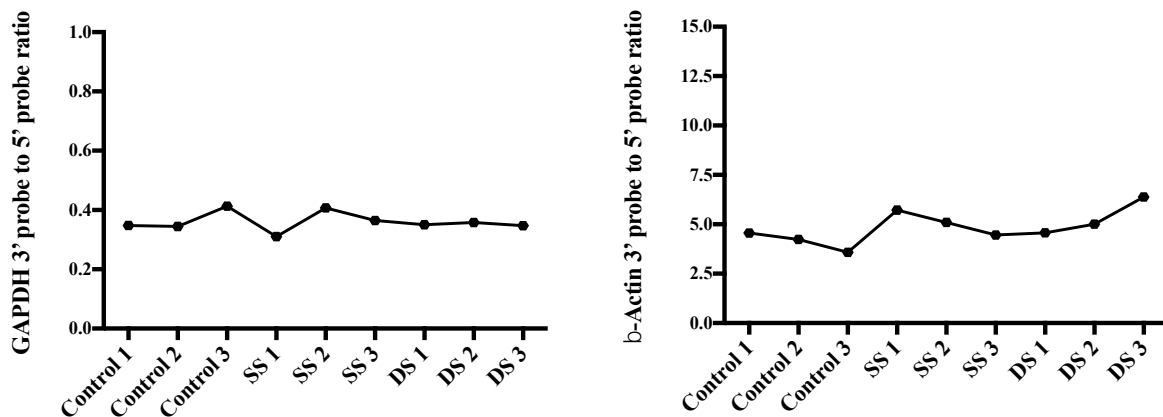


Figure 4.4 Housekeeping (HK) genes GAPDH and β -actin signal ratios for 96 hours control and SS/DS LUHMES arrays.

HK genes GAPDH and β -actin were used as internal controls to assess the quality of the samples and the amplification and labelling process. The 3' probe to 5' probe ratio should be consistent between arrays. (SS, single-stressed LUHMES; DS, double-stressed LUHMES).

4.4.3.2. Hybridisation and signal quality

Signal from the hybridisation controls and the percentage of probes present in the arrays are useful parameters to evaluate overall signal quality.

4.4.3.2.1. Spike-in eukaryotic hybridisation controls

Hybridisation controls are included into the hybridisation cocktail and are composed by a mixture of biotin-labelled cRNA transcripts from *E.coli* and the P1 bacteriophage. These controls include *BioB*, *bioC*, *bioD* (*E. Coli*) and *Cre* (P1) transcripts in a concentration of 1.5 pM, 5 pM, 25 pM and 100 pM, respectively. The concentration of *BioB* is at the level of array sensitivity and should be present at least 70% of the time. *bioC*, *bioD* and *Cre* should be present and show increasing signal values. **Figure 4.5** shows signal for *BioB* in all 9 samples. Overall, hybridisation controls suggest a good hybridisation efficiency for all samples, although Control 3 had a lower signal for *Cre*.

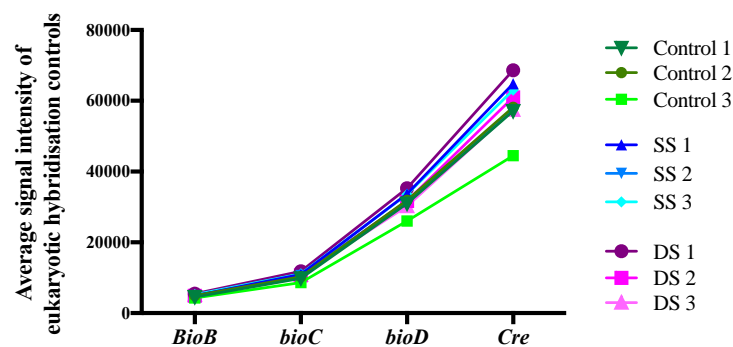


Figure 4.5 Eukaryotic hybridisation controls for 96 hours control and SS/DS LUHMES.

Plot depicting the average signal intensities of hybridisation controls *BioB*, *bioC*, *bioD* and *Cre* at increasing concentrations for each of the 9 samples (SS, single-stressed LUHMES; DS, double-stressed LUHMES).

4.4.3.2.2. Percent present (% P)

The % P indicates the percentage of probes that are present in the arrays, relative to the total number of probes. This value depends on several variables, including array type, cell type, biological stimuli and RNA quality. Replicates should have similar % P values. In **Figure 4.6**, a plot for the % P in the 9 arrays is consistent between replicates and GeneChip arrays.

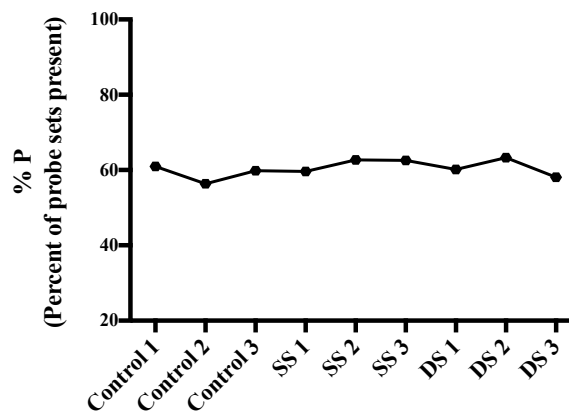


Figure 4.6 Percentage of probes present in the 96 hours control and SS/DS LUHMES array.

% P is the percentage of probes that are detected relative to the total number of probe sets that the array contains, which are 54,675 probes for the GeneChip Human Genome U133 Plus 2.0 Array.

4.4.3.3. Signal comparability

Quality control metrics given by Affymetrix Expression Console™ also produce a signal histogram that shows the intensity of the signals from the probes in each array. This histogram allows comparison of the signals between GeneChip arrays. In **Figure 4.7**, signals from the 9 arrays (3 controls, 3 SS, 3 DS) are compared. The signal profile should be the same across samples, however there are some discrepancies between arrays. DS 1 and DS 2 signal intensities are higher for some of the probes; the other 7 samples show comparable signal intensities.

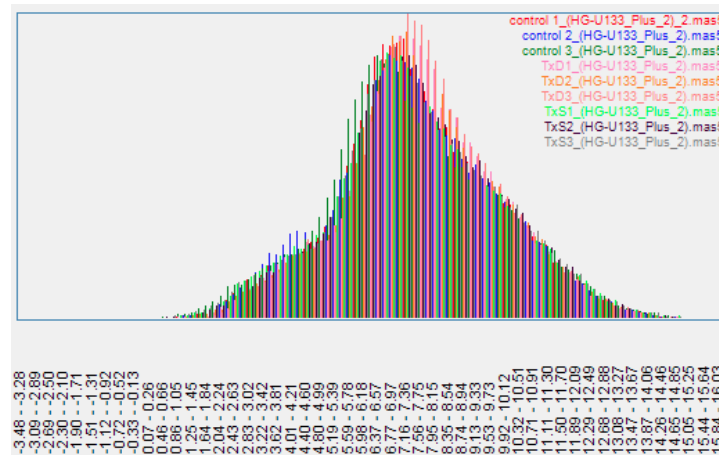


Figure 4.7 Signal histogram for the 96 hours control and SS/DS LUHMES arrays.

The signal histogram was used to compare the signal intensities of the probe sets across the 9 arrays under analysis (TxS, single-stressed LUHMES; TxD, double-stressed LUHMES; number indicates replicate).

The signal detected by each of the probe-sets present in the array can be compared to the median signal value of this same probe-set across all arrays in the experiment. This calculation is represented by the Relative Log Expression (RLE) values, which can be plotted as shown in **Figure 4.8**. The array quality can be assessed by looking at the spread of the data across samples: RLE values should be 0 or close to 0 on a log scale, otherwise, the array could have a poor quality and could be considered as an outlier. RLE values for

the 96 hours control and SS/DS arrays show a similar spread; the 9 arrays have RLE values of 0 or close to 0.

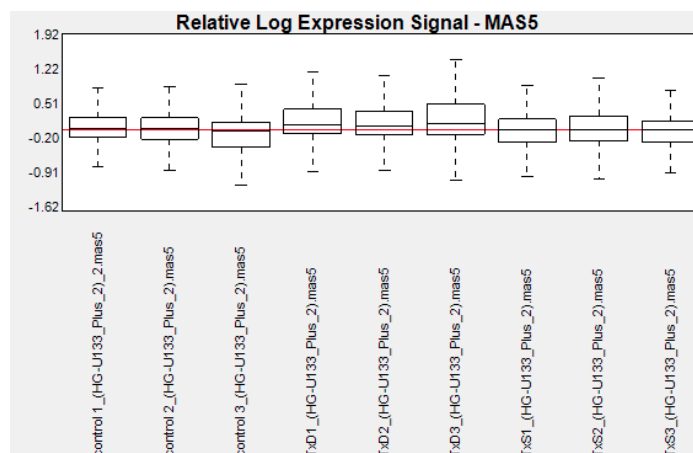


Figure 4.8 Relative log expression (RLE) box plots for the 96 hours control and SS/DS LUHMES arrays.

The RLE values of the 9 arrays are close to 0, except for the 3 DS replicates, which have higher RLE values (TxS, single-stressed LUHMES; TxD, double-stressed LUHMES).

4.4.4. Microarray data analysis

4.4.4.1. Clustering Analysis

To identify differences in the transcriptome of 96 hours control, single stressed and double stressed LUHMES the array data was analysed with the Qlucore Omics Explorer (version 3.0) software. The 9 data sets (3 controls, 3 SS-LUHMES and 3 DS LUHMES) were imported to Qlucore Omics Explorer and normalised using the RMA method. For the analysis, a fold change (FC) ≤ 1.2 and a significant value of $p < 0.05$ were set. Data was first analysed using a Multi Group comparison between control, SS and DS-LUHMES. The PCA (principal component analysis) plot for this analysis is shown in **Figure 4.9A**, where a clear separation of the 3 conditions can be seen: Control – blue, SS – yellow and

DS – pink. The difference in the signal between these 3 groups is also visible in the heatmap for the differentially expressed genes (**Figure 4.9B**). The Multi Group analysis resulted in 4042 differentially expressed transcripts among the 3 groups.

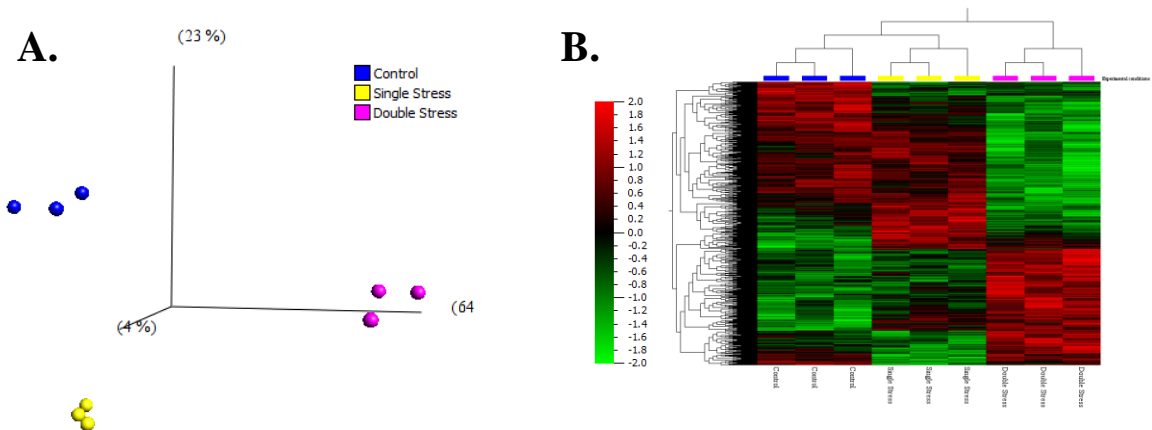


Figure 4.9 Clustering analysis of 96 hours control LUHMES compared to 96 hours SS and DS-LUHMES – Multi Group Comparison.

A. The PCA plot of 96 hours control (blue) LUHMES and 96 hours SS (yellow)/DS (pink) LUHMES shows the separation of differentially expressed genes between the 3 groups. **B.** Hierarchical clustering heat map of 96 hours control, SS and DS-LUHMES (red – up-regulated transcripts; green – down-regulated transcripts).

A Two Group comparison was also performed to identify significantly, differentially expressed genes in SS and DS-LUHMES when compared to controls, as well as in DS-LUHMES when compared to SS-LUHMES. The PCA plots and heat maps for these 3 analyses are shown in **Figure 4.10**. Heat maps help visualise how different the gene expression is between control and stressed LUHMES. Challenging stressed LUHMES with a second dose of H₂O₂ caused an important change in the transcriptome of these cells, as shown in **Figure 4.10B** and **Figure 4.10F**. 450 differentially expressed genes, 276 up and 174 down-regulated, were identified in SS-LUHMES compared to controls (**Figure 4.10A-B**), while a larger number of genes were differentially expressed in DS-LUHMES (1285 genes; 695 up and 590 down-regulated), compared to controls (**Figure 4.10C-D**). 1607 genes were differentially expressed in DS-LUHMES compared to SS-LUHMES (649 up and 958 down-regulated) (**Table 4.8**). The complete lists of differentially expressed genes can be found in the electronic version of this work, as described in **Appendix C**.

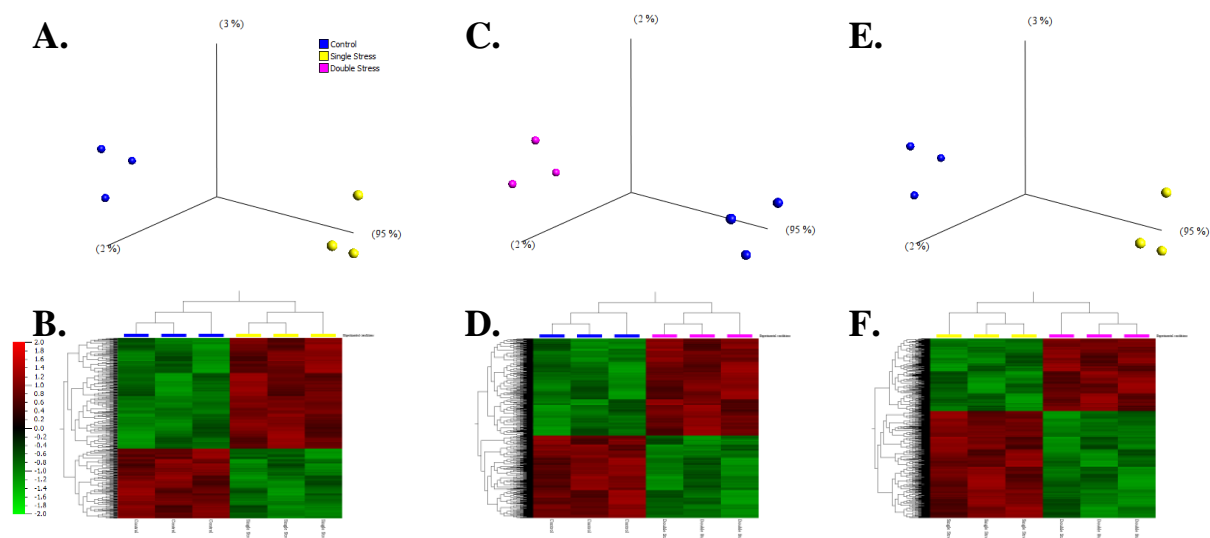


Figure 4.10 Clustering analysis of 96 hours control LUHMES compared to 96 hours SS and DS-LUHMES – Two Group Comparison.

A-B. PCA plot and heat map for 96 hours control vs SS-LUHMES analysis. **C-D.** PCA plot and heat map for 96 hours control vs DS-LUHMES analysis. **E-F.** PCA plot and heat map for 96 hours DS-LUHMES vs SS-LUHMES analysis. Control – blue; SS – yellow; DS – pink.

Two Group Comparison	Total number of differentially expressed transcripts	Number of up-regulated transcripts	Number of down-regulated transcript
SS vs Control	450	276	174
DS vs Control	1285	695	590
DS vs SS	1607	649	958

Table 4.8 Number of differentially expressed transcripts for each of the 3 comparisons computed by Qlucore Omics Explorer and used for the pathway enrichment analysis.

4.4.5. Candidate analysis

Before conducting the enrichment analysis, the lists of differentially expressed transcripts were examined for the presence of dysregulated transcripts from common senescence and SASP markers, which were p21 (*CDKN1A*), p16 (*CDKN2A*), SA- β -galactosidase (*GLB1*), IL-6 (*IL6*) and/or IL-8 (*CXCL8*), but none of these genes were altered in the SS or DS-LUHMES. A functional annotation analysis was then performed to identify dysregulated pathways in the SS and DS-LUHMES that could be related to the development of a senescence-like state.

4.4.5.1. Functional Enrichment Analysis using DAVID Bioinformatics Tool

The lists of probe IDs from the total number of differentially expressed transcripts for the 3 comparisons computed by Qlucore Omics Explorer (SS vs Control/DS vs Control/SS vs DS) were entered into DAVID (Database for annotation, Visualization and Integrated Discovery) Bioinformatics Tool (version 6.7). To identify dysregulated pathways changing in the same direction, the lists of up and down-regulated transcripts were inputted independently as well (**Table 4.8**). Results from the DAVID Functional Enrichment Analysis are summarised in **Table 4.9**, **Table 4.10**, and **Table 4.11**. The analysis focused on pathways (highlighted in green) that are known to be affected in senescence and that have been linked to DNA damage, a DDR and the SASP in mitotic cells.

The dysregulated pathways identified by DAVID in the **SS vs Control** group included focal adhesion, type II diabetes mellitus and purine metabolism. A higher number of pathways were dysregulated in the **DS vs Control** group, which included adherens junctions, axon guidance, calcium signalling and TGF- β signalling. Pathways related to ubiquitin

mediated proteolysis, autophagy, regulation of actin cytoskeleton and JAK-STAT signalling were the most enriched when comparing **DS vs SS** conditions (**Table 4.9**).

Analysis of the UP-REGULATED transcripts (**Table 4.10**) resulted in the identification of enrichment of axon guidance and MAPK signalling pathways in the **SS vs Control** group; whereas calcium signalling, adherens junctions, homologous recombination and TGF- β signalling were the most enriched pathways in the **DS vs Control** group. Comparison of the **DS vs SS** UP-REGULATED transcripts indicated RNA degradation, ubiquitin mediated proteolysis, autophagy and JAK-STAT signalling as the most enriched pathways.

Analysis of the DOWN-REGULATED transcripts (**Table 4.11**) showed enrichment of genes linked to lysosome and focal adhesion pathways in the **SS vs Control** group; while in the **DS vs Control** group, the most enriched pathways were related to p53, homologous recombination and axon guidance signalling. Comparison of the DS vs SS conditions revealed enrichment of genes associated with ubiquitin mediated proteolysis, RNA degradation, cell cycle and Wnt signalling.

Two group comparison	Pathway name	Pathway source	Differentially expressed genes	p value	FDR value
SS vs Control (372 David IDs)	Focal adhesion	KEGG	9	5.7E-2	4.9E1
	Type II Diabetes Mellitus	KEGG	4	7.4E-2	5.8E1
	Purine metabolism	KEGG	7	9.9E-2	6.9E1
DS vs Control (1052 David IDs)	Adherens junction	KEGG	12	1.7E-3	2.0E0
	Axon guidance	KEGG	14	1.4E-2	1.6E1
	Calcium signalling pathway	KEGG	16	3.5E-2	3.5E1
	Homologous recombination	KEGG	5	5.2E-2	4.7E1
	Thyroid cancer	KEGG	5	5.8E-2	5.1E1
	Drug metabolism	KEGG	6	6.6E-2	5.6E1
	Acute myeloid leukemia	KEGG	7	7.4E-2	6.0E1
	TGF- β signalling pathway	KEGG	9	7.5E-2	6.1E1
	DS vs SS (1322 David IDs)	RNA degradation	KEGG	10	1.3 E-2
Ubiquitin mediated proteolysis		KEGG	17	2.1E-2	2.3E1
Endometrial cancer		KEGG	8	5.8E-2	5.2E1
T cell receptor signalling pathway		KEGG	13	5.8E-2	5.2E1
B cell receptor signalling pathway		KEGG	10	6.4E-2	5.5E1
Endocytosis		KEGG	19	6.9E-2	5.8E1
Butanoate metabolism		KEGG	6	7.5E-2	6.2E1
Pathways in cancer		KEGG	30	7.8E-2	6.3E1
Regulation of autophagy		KEGG	6	8.3E-2	6.5E1
Regulation of actin cytoskeleton		KEGG	21	8.7E-2	6.7E1
JAK-STAT signalling pathway	KEGG	16	9.8E-2	7.2E1	

Table 4.9 DAVID Functional Enrichment analysis of the total number of differentially expressed transcripts in stressed LUHMES.

DAVID analysis was conducted in the SS vs Control, DS vs Control and DS vs SS groups. Pathways that could be linked to oxidative DNA damage, a DDR, and to senescence and the SASP in mitotic cells, are highlighted in green (KEGG - Kyoto encyclopedia of genes and genomes).

Two group comparison	Pathway name	Pathway source	Differentially expressed genes	P value	FDR value
SS vs Control (214 David IDs)	Axon guidance	KEGG	5	6.8E-2	5.4E1
	MAPK signalling pathway	KEGG	7	9.9E-2	6.8E1
DS vs Control (527 David IDs)	Calcium signalling pathway	KEGG	13	1.2E-3	1.4E0
	Vascular smooth muscle contraction	KEGG	9	6.0E-3	6.8E0
	Adherens junction	KEGG	7	1.1E-2	1.2E1
	Cell adhesion molecules (CAMs)	KEGG	9	1.5E-2	1.7E1
	Melanoma	KEGG	6	3.0E-2	3.0E1
	Thyroid cancer	KEGG	4	3.3E-2	3.3E1
	Endometrial cancer	KEGG	5	3.8E-2	3.6E1
	Retinol metabolism	KEGG	5	4.3E-2	4.0E1
	Acute myeloid leukemia	KEGG	5	5.3E-2	4.7E1
	Colorectal cancer	KEGG	6	5.5E-2	4.8E1
	Hematopoietic cell lineage	KEGG	6	6.0E-2	5.1E1
	Prostate cancer	KEGG	6	6.7E-2	5.5E1
	Melanogenesis	KEGG	6	9.6E-2	6.9E1
DS vs SS (491 David IDs)	Autoimmune thyroid disease	KEGG	6	1.4E-2	1.5E1
	Neuroactive ligand-receptor interaction	KEGG	14	2.8E-2	2.9E1
	Retinol metabolism	KEGG	5	6.6E-2	5.5E1
	Cytosolic DNA-sensing pathway	KEGG	5	6.9E-2	5.7E1
	Butanoate metabolism	KEGG	4	7.0E-2	5.8E1
	Antigen processing and presentation	KEGG	6	8.5E-2	6.5E1
	Metabolism of xenobiotics by cytochrome P450	KEGG	5	8.9E-2	6.7E1
	Hematopoietic cell lineage	KEGG	6	9.6E-2	6.9E1
Drug metabolism	KEGG	5	9.8E-2	7.0E1	

Table 4.10 DAVID Functional Enrichment analysis of the UP-REGULATED transcripts in stressed LUHMES.

DAVID analysis was conducted in the SS vs Control, DS vs Control and DS vs SS groups. Pathways that could be related to oxidative DNA damage, a DDR, and to senescence and the SASP in mitotic cells, are highlighted in green.

Two group comparison	Pathway name	Pathway source	Differentially expressed genes	P value	FDR value
SS vs Control (157 David IDs)	Lysosome	KEGG	4	8.0E-2	5.8E1
	Focal adhesion	KEGG	5	9.4E-2	6.4E1
DS vs Control (533 David IDs)	P53 signalling pathway	KEGG	6	3.5E-2	3.4E1
	Homologous recombination	KEGG	4	3.8E-2	3.6E1
	Axon guidance	KEGG	8	5.8E-2	5.0E1
	Progesterone-mediated oocyte maturation	KEGG	6	8.1E-2	6.2E1
DS vs SS (831 David IDs)	Ubiquitin mediated proteolysis	KEGG	16	2.6E-4	3.1E1
	RNA degradation	KEGG	10	3.2E-4	3.7E1
	Cell cycle	KEGG	11	2.4E-2	2.5E1
	Spliceosome	KEGG	11	2.5E-2	2.6E1
	Progesterone-mediated oocyte maturation	KEGG	8	5.0E-2	4.6E1
	T cell receptor signalling pathway	KEGG	9	6.0E-2	5.2E1
	Oocyte meiosis	KEGG	9	6.5E-2	5.5E1
	Wnt signalling pathway	KEGG	11	7.1E-2	5.8E1
	Chronic myeloid leukemia	KEGG	7	7.2E-2	5.9E1
Lysine degradation	KEGG	5	9.2E-2	6.8E1	

Table 4.11 DAVID Functional Enrichment analysis of the DOWN-REGULATED transcripts in stressed LUHMES.

DAVID analysis was conducted in the SS vs Control, DS vs Control and DS vs SS groups. Pathways that could be related to oxidative DNA damage, a DDR, and to senescence and the SASP in mitotic cells, are highlighted in green.

4.4.5.2. Pathway enrichment analysis using IMPaLA

The lists of gene symbols of the differentially expressed genes from the 3 comparisons processed in Qlucore Omics Explorer (SS vs Control; DS vs Control; DS vs SS) were also entered into IMPaLA (Integrated Molecular Pathway Level Analysis, version 9). As with the DAVID analysis, the total number of differentially expressed genes, as well as the separate lists of UP and DOWN-REGULATED transcripts were analysed and are presented in **Table 4.12**, **Table 4.13** and **Table 4.14**. The pathways highlighted in yellow are related to oxidative DNA damage, a DDR and/or have been shown to be altered in mitotic cells, as part of the senescent program.

Analysis of the total number of dysregulated transcripts (**Table 4.12**) revealed enrichment of cellular response to stress and IL-6 pathways in the **SS vs Control** group. Enriched pathways in the **DS vs Control** group related to gene expression, homology directed repair, DSB repair and cell cycle. Comparison of the **DS vs SS** conditions showed enrichment of inflammation and immune system related pathways, as well as cell cycle regulation.

Analysis of the UP-REGULATED genes (**Table 4.13**) showed enrichment of pathways linked to TGF- β signalling and E3 ubiquitin ligases ubiquitinate target proteins **SS vs Control** group; of VEGF and VEGFR signalling, calcium signalling and ATR signalling in the **DS vs Control** group; and of T-cell antigen receptor signalling, cytokine-cytokine receptor interaction and INF- α signalling in the **DS vs S** group.

Analysis of the DOWN-REGULATED transcripts (**Table 4.14**) showed enrichment of vesicle mediated transport, cellular responses to stress, membrane trafficking and electron

transport chain pathways in the **SS vs Control** group; of gene expression, transcriptional regulation by TP53 and cell cycle pathways in the **DS vs Control** group; and of TGF- β , autophagy and cell cycle pathways in the **DS vs SS** group.

Two group comparison	Pathway name	Pathway source	Differentially expressed genes	p value	FDR value
SS vs Control	TGF-B Signalling pathway	Wikipathways	7	0.00261	1
	Cellular responses to stress	Reactome	10	0.00594	1
	IL-6 mediated signalling events	PID	3	0.028	1
	Oxygen-dependent proline hydroxylation of HIF alpha	Reactome	2	0.028	1
DS vs Control	Gene expression	Reactome	103	3.81E-05	0.0834
	Generic transcription pathway	Reactome	59	3.86E-05	0.0834
	HDR through homologous recombination (HR) or single strand annealing (SSA)	Reactome	15	0.000343	0.494
	Homology Directed Repair	Reactome	15	0.00055	0.523
	Transcriptional regulation by TP53	Reactome	29	0.000606	0.523
	DNA double –strand break repair	Wikipathways	8	0.00123	0.756
	Cell cycle checkpoints	Reactome	14	0.00469	1
	APC/:Cdc20 mediated degradation of mitotic proteins	Reactome	5	0.00762	1
DS vs SS	Antigen processing: Ubiquitination and proteasome degradation	Reactome	35	1.98E-06	0.00855
	T-Cell antigen receptor (TCR) signalling pathway	Wikipathways	17	1.2E-05	0.0196
	Class I MHC mediated antigen processing and presentation	Reactome	38	1.36E-05	0.0196
	Adaptitve immune system	Reactome	71	7.53E-05	0.0813
	Generic transcription pathway	Reactome	74	0.000113	0.0976
	B cell receptor signalling pathway	Wikipathways	15	0.000349	0.215
	TGF-beta signalling pathway	Wikipathways	17	0.00112	0.285
	Autophagy	KEGG	8	0.00146	0.333
Cell cycle	Wikipathways	24	0.00349	0.555	

Table 4.12 IMPaLA Pathway Analysis of the total number of differentially expressed transcripts in stressed LUHMES.

IMPaLA analysis was conducted in the SS vs Control, DS vs Control and DS vs SS groups. Pathways linked to oxidative DNA damage, a DDR, and to senescence and the SASP in mitotic cells, are highlighted in yellow. Some of the pathways have very high FDR values. This suggests that a high percentage of the genes may be incorrectly identified as differentially expressed and subsequent validation experiments could be significantly affected.

Two group comparison	Pathway name	Pathway source	Differentially expressed genes	p value	FDR value
SS vs Control	Atypical NF-kappaB pathway	Wikipathways	3	0.00126	1
	TGF-B signalling in thyroid cells for epithelial-mesenchymal transition	Wikipathways	2	0.00385	1
	DCC mediated attractive signalling	Reactome	2	0.00442	1
	E3 ubiquitin ligases ubiquitinate target proteins	Reactome	2	0.00503	1
	Glycosphingolipid biosynthesis-neolactoseries	Reactome	2	0.00503	1
	Activation of NF-kappaB in B cells	Reactome	2	0.00503	1
	Protein-protein interactions at synapses	Reactome	3	0.013	1
DS vs Control	VEGF and VEGFR signalling networks	PID	3	0.000417	1
	Signalling by activin	Reactome	3	0.000961	1
	Neural crest differentiation	Wikipathways	7	0.00103	1
	Calcium signalling pathway	KEGG	9	0.00218	1
	Immune system	Reactome	43	0.00969	1
	ATR signalling pathway	PID	3	0.0198	1
DS vs SS	T-cell antigen receptor signalling pathway	Wikipathways	8	0.000201	0.397
	FGFR1c ligand binding and activation	Reactome	3	0.000782	0.675
	VEGFA-VEGFR2 signalling pathway	Wikipathways	11	0.00291	0.838
	Cytokine-cytokine receptor interaction	KEGG	12	0.00242	0.838
	Cytosolic DNA-sensing pathway	KEGG	5	0.0048	1
	IFN alpha signalling	INOH	3	0.00554	1

Table 4.13 IMPaLA Pathway Analysis of the UP-REGULATED transcripts in stressed LUHMES.

IMPaLA analysis was conducted in the SS vs Control, DS vs Control and DS vs SS groups. Pathways linked to oxidative DNA damage, a DDR, and to senescence and the SASP in mitotic cells, are highlighted in yellow. Some of the pathways have very high FDR values. This suggests that a high percentage of the genes may be incorrectly identified as differentially expressed and subsequent validation experiments could be significantly affected.

Two group comparison	Pathway name	Pathway source	Differentially expressed genes	p value	FDR value
SS vs Control	Vesicle-mediated transport	Reactome	14	0.000158	0.534
	Binding and uptake of ligands by scavenger receptors	Reactome	3	0.000247	0.534
	Membrane trafficking	Reactome	11	0.00339	1
	Apoptosis induced DNA fragmentation	Reactome	2	0.00358	1
	Extracellular matrix organisation	Reactome	7	0.00587	1
	Electron transport chain	Wikipathways	4	0.00695	1
DS vs Control	Gene expression	Reactome	86	1.29E-10	5.56E-07
	Transcriptional regulation by TP53	Reactome	14	5.28E-05	0.076
	Cell cycle	Reactome	26	0.00127	0.486
	HDR through homologous recombination (HR) or single strand annealing (SSA)	Reactome	10	0.0019	0.486
	Mitotic G1-G1/S phases	Reactome	8	0.00205	0.486
	APC/C:Cdc20 mediated degradation of cyclin B	Reactome	4	0.0027	0.486
DS vs SS	Gene expression	Reactome	114	6.14E-09	2.65E-05
	Generic transcription pathway	Reactome	64	2.58E-07	0.000556
	Antigen processing: Ubiquitination and proteasome degradation	Reactome	29	4.55E-07	0.000655
	RNA polymerase II transcription	Reactome	18	5.7E-05	0.0493
	TGF-beta signalling pathway	Wikipathways	15	0.000182	0.0654
	Cell cycle	Wikipathways	12	0.000628	0.172

Table 4.14 IMPaLA Pathway Analysis of the DOWN-REGULATED transcripts in stressed LUHMES.

IMPaLA analysis was conducted in the SS vs Control, DS vs Control and DS vs SS groups. Pathways linked to oxidative DNA damage, a DDR, and to senescence and the SASP in mitotic cells, are highlighted in yellow. Some of the pathways have very high FDR values. This suggests that a high percentage of the genes may be incorrectly identified as differentially expressed and subsequent validation experiments could be significantly affected.

4.4.6. Pathways of interest

Several pathways were identified as dysregulated by the analysis performed using DAVID and IMPaLA in the SS and DS-LUHMES. Both DAVID and IMPaLA suggested changes in cell cycle signalling, but IMPaLA also detected alteration in other pathways directly related to DNA damage and cellular stress, including chromatin modification signalling pathways, inflammation and metabolism. A more detailed examination of the genes involved in these pathways is described in the following sections.

4.4.6.1. Cell cycle

DAVID and IMPaLA identified dysregulation in cell cycle pathways in DS-LUHMES. The differentially expressed genes in the 3 different comparison groups are presented in **Table 4.15**. Dysregulation of cell cycle related transcripts was only identified in DS-LUHMES and not in SS-LUHMES. The majority of the transcripts were linked to the anaphase promoting (APC/C:Cdh1) complex (*ANAPC10*, *CDC27*, *CCNB1*, *CDH1*, *ANAPC4*, *MAD2L1*). Downregulation of genes implicated in the minichromosome maintenance (MCM) protein complex was also detected (*MCM3* and *MCM8*) only in DS-LUHMES.

Group	Gene symbol	Gene name	FC	<i>p</i> value
SS vs control				
DS vs control	CDH1	Cadherin 1, type 1	1.222	0.0051
	MAD2LI	MAD2 mitotic arrest deficient-like 1	1.350	0.0314
	ANAPC10	Anaphase promoting complex subunit 10	0.709	0.0282
	CDC27	Cell division cycle 27	0.828	0.0419
	CCNB1	Cyclin B1	0.827	0.0403
	RPS27A	Ribosomal protein S27a	0.791	0.0087
DS vs SS	ANAPC10	Anaphase promoting complex subunit 10	0.742	0.0381
	ANAPC4	Anaphase promoting complex subunit 4	0.732	0.0064
	CDC27	Cell division cycle 27	0.811	0.0025
	PTTG1	Pituitary tumor-transforming 1	1.291	0.0360
	SMC1A	Structural maintenance of chromosomes 1A	0.827	0.0458
	UBE2F	ubiquitin-conjugating enzyme E2F (putative)	0.687	0.0135
	APC	Adenomatous polyposis coli	0.732	0.0488
	RBL1	Retinoblastoma-like 1	0.829	0.0352
	SKP2	S-phase kinase-associated protein 2, E3 ubiquitin protein ligase	0.701	0.0327
	MCM3	Minichromosome maintenance complex component 3	0.829	0.0259
	MCM8	Minichromosome maintenance 8 homologous recombination repair factor	0.803	0.0113
	SMAD4	SMAD family member 4	0.752	0.0121
	HDAC8	Histone deacetylase 8	0.768	0.0083

Table 4.15 Genes involved in cell cycle regulation in SS and DS-LUHMES.

Transcripts linked to the APC/C:Cdh1 complex and replication licencing factors were identified as being differentially expressed in SS and DS-LUHMES compared to controls. (Red: up-regulated; Green: down-regulated, FC: fold change).

4.4.6.2. DNA damage response

DAVID and IMPaLa pathway analysis indicated dysregulation in DNA damage signalling transcripts that are known to participate in DSBs repair through the ATR-dependent DNA damage response (*ATR*, *PP2R2B*, *CLSPN*, *RPA1*, *TIPIN*), and homologous recombination (HR) (*RAD52*, *TOP3A*, *SPIDR*) in both SS and DS-LUHMES; however, a higher number of dysregulated transcripts linked to DNA damage response was identified in DS-LUHMES (Table 4.16).

Group	Gene symbol	Gene name	FC	<i>p</i> value
SS vs control	ATR	ATR serine/threonine kinase	1.32	0.0224
DS vs control	ATR	ATR serine/threonine kinase	1.207	0.0168
	PPP2R2B	Protein phosphatase 2, regulatory subunit B, beta	1.404	0.0156
	CLSPN	Claspin	1.235	0.0055
	RPA1	Replication protein A1	0.753	0.0209
	TIPIN	TIMELESS interaction protein	0.782	0.0072
	RIFI	Replication timing regulatory factor 1	1.239	0.0346
	RAD52	RAD52 homolog, DNA repair protein	0.816	0.0247
	ERCC1	Excision repair cross-complementation group 1	0.745	0.0151
	TOP3A	Topoisomerase (DNA) III alpha	0.725	0.0379
	SPIDR	Scaffolding protein involved in DNA repair	1.326	0.0455
DS vs SS				

Table 4.16 Genes involved in DNA damage response pathways in SS and DS-LUHMES.

Transcripts linked to ATR signalling and HR DNA repair were differentially expressed in SS and DS-LUHMES compared to controls. (Red: up-regulated; Green: down-regulated, FC: fold change).

4.4.6.3. Metabolism

IMPALA analysis suggested dysregulation in the mitochondrial electron transport chain in SS and DS-LUHMES. The differentially expressed transcripts codify for Complex I (*NDUFA2*, *NDUFA3*, *NDUFS8*, *NDUFV3*, *NDUFS1*, *NDUFA10*), Complex III (*UCP2*, *UQCRI1*) and Complex V (*PPA2*, *ATP6VIG3*) genes. These pathways were down-regulated in SS-LUHMES, but some of the Complex I and III genes were also up-regulated in DS-LUHMES (Table 4.17).

Group	Gene symbol	Gene name	FC	p value
SS vs Control	<i>NDUFA2</i>	NADH dehydrogenase (ubiquinone) 1 alpha subcomplex, 2, 8kDa	0.815	0.0082
	<i>NDUFA3</i>	NADH dehydrogenase (ubiquinone) 1 alpha subcomplex, 3, 9kDa	0.772	0.0142
	<i>UCP2</i>	Uncoupling protein 2 (mitochondrial, proton carrier)	0.817	0.0275
	<i>UQCRI1</i>	Ubiquinol-cytochrome c reductase, complex III subunit XI	0.807	0.0498
	<i>ACO2</i>	Aconitase 2, mitochondrial	0.794	0.0421
DS vs Control	<i>NDUFS8</i>	NADH dehydrogenase (ubiquinone) Fe-S protein 8, 23kDa (NADH-coenzyme Q reductase)	1.309	0.0173
	<i>PPA2</i>	Pyrophosphatase (inorganic) 2	1.218	0.0403
	<i>NDUFV3</i>	NADH dehydrogenase (ubiquinone) flavoprotein 3, 10kDa	0.753	0.0053
	<i>IDH3G</i>	isocitrate dehydrogenase 3 (NAD+) gamma	0.812	0.0485
DS vs SS	<i>NDUFS8</i>	NADH dehydrogenase (ubiquinone) Fe-S protein 8, 23kDa (NADH-coenzyme Q reductase)	1.334	0.0055
	<i>ATP6VIG3</i>	ATPase, H+ transporting, lysosomal 13kDa, V1 subunit G3	1.339	0.0315
	<i>NDUFS1</i>	NADH dehydrogenase (ubiquinone) Fe-S protein 1, 75kDa (NADH-coenzyme Q reductase)	0.830	0.0338
	<i>NDUFA10</i>	NADH dehydrogenase (ubiquinone) 1 alpha subcomplex, 10, 42kDa	0.811	0.0248

Table 4.17 Genes involved in senescence and cellular responses to stress in SS and DS-LUHMES.

Transcripts linked to Histone cluster 1 and the APC/C:Cdh1 complex were down-regulated in SS and DS-LUHMES compared to controls. (Green: down-regulated, FC: fold change).

4.4.6.4. Inflammation and immune response

There were several transcripts annotated to immune-like response pathways (**Table 4.18**). Only 3 transcripts were dysregulated in SS-LUHMES (*SMAD2*, *IL5R*, *RNF125*), but 24 genes were differentially expressed in DS-LUHMES, from which 22 were up-regulated. From this group of transcripts, *DDX3X*, *DDX58*, *TRAF6*, *IFNA16*, *IFNA4*, *SMURF1* have a role in the innate immune response that is related to the production of type 1 interferons and proinflammatory cytokines. Several cytokine and cytokine receptor transcripts were also up-regulated in the DS-LUHMES, including *IL5RA*, *IL23A*, *IL2RA*, *IL20*, *IL25*, *IL1A*, *CCR3* and *CRLF2*. Transcripts that are known to participate in TGF- β signalling (*ACVR1C*, *FST*, *INHBA*) as well as VEGF signalling (*VEGFA*) were also up-regulated in DS-LUHMES.

Group	Gene symbol	Gene name	FC	p value
SS vs Control	SMAD2	SMAD family member 2	1.221	0.0180
	IL5R	Interleukin 5	1.289	0.0374
	RNF125	Ring finger protein 125, E3 ubiquitin protein ligase	0.831	0.0297
DS vs Control	DDX3X	DEAD (Asp-Glu-Ala-Asp) box helicase 3, X-linked	1.206	0.0276
	SMURF1	SMAD specific E3 ubiquitin protein ligase 1	1.216	0.0077
	ACVR1C	Activin A receptor type IC	1.376	0.0023
	FST	Follistatin	1.382	0.0493
	INHBA	Inhibin beta A	1.312	0.0125
	IL5RA	Interleukin 5 receptor, alpha	1.399	0.0271
	IL23R	Interleukin 23 receptor	1.255	0.0357
	CRLF2	Cytokine receptor-like factor 2	1.294	0.0263
	PDGFRA	platelet-derived growth factor receptor, alpha polypeptide	1.208	0.00208
	TNFSF15	tumor necrosis factor (ligand) superfamily, member 15	1.339	0.01844
	SMAD5	SMAD family member 5	0.622	0.0326
DS vs SS	DDX58	DEAD (Asp-Glu-Ala-Asp) box polypeptide 58	1.293	0.0137
	IFNA16	Interferon, alpha 16	1.501	0.0406
	IFNA21	Interferon, alpha 21	1.228	0.0401
	IFNA4	Interferon, alpha 4	1.430	0.0334
	CCR3	chemokine (C-C motif) receptor 3	1.261	0.0453
	ITK	IL2-inducible T-cell kinase	1.460	0.0189
	ACVR1C	activin A receptor type IC	1.233	0.0365
	IL2RA	Interleukin 2 receptor, alpha	1.231	0.0042
	VEGFA	Vascular endothelial growth factor	1.267	0.0096
	IL20	Interleukin 20	1.222	0.0475
	TNFSF8	tumor necrosis factor (ligand) superfamily, member 8	1.540	0.0094
	IL25	Interleukin 25	1.225	0.0018
	IL1A	Interleukin 1, alpha	1.216	0.0353
	TRAF6	TNF receptor-associated factor 6, E3 ubiquitin protein ligase	0.755	0.0219

Table 4.18 Genes involved in immune response in SS and DS-LUHMES.

Transcripts related to cytokine production, interferon and TGF- β signalling were up-regulated in DS-LUHMES. (Red: up-regulated; Green: down-regulated, FC: fold change).

4.4.6.5. Cellular responses to stress

Down-regulation of pathways involved in stress responses was detected in SS and DS-LUHMES. The majority of the transcripts linked to these pathways were histone cluster 1 family members (*HIST1H1E*, *HIST1H2BH*, *HIST1H4j*, *HIST1H3J*, *HIST1H2BM*). Cell cycle and DNA damage response transcripts were also annotated to the cellular responses pathways, including some of the APC/C-Cdh1 related genes (*CDC27*, *ANAPC10*) (Table 4.19).

Group	Gene symbol	Gene name	FC	p value
SS vs Control	<i>HIST1H1E</i>	Histone cluster 1, H1e	0.802	0.0233
	<i>HIST1H2BH</i>	Histone cluster 1, H2bn	0.725	0.0014
	<i>HIST1H1C</i>	Histone cluster 1, H1c	0.823	0.0117
	<i>HIST1H4J</i>	Histone cluster 1, H4j	0.820	0.00059
	<i>TCEB2</i>	Transcription elongation factor B (SIII)	0.823	0.0431
	<i>CBX2</i>	Chromobox homolog 2	0.813	0.0464
	<i>MAP2K7</i>	Mitogen-activated protein kinase kinase 7	0.790	0.0383
DS vs Control	<i>HIST1H3J</i>	Histone cluster 1, H3j	0.810	0.0207
	<i>HIST1H4C</i>	Histone cluster 1, H4c	0.820	0.0315
	<i>HIST1H2BM</i>	Histone cluster 1, H2bm	0.593	0.0406
	<i>CDC27</i>	Cell division cycle 27	0.828	0.0419
	<i>RPA1</i>	Replication protein A1	0.753	0.0209
	<i>HDAC6</i>	Histone deacetylase 6	0.821	0.0165
	<i>RPS27A</i>	Ribosomal protein S27a	0.791	0.0087
	<i>ANAPC10</i>	Anaphase promoting complex subunit 10	0.709	0.0282
	<i>DNAJB1</i>	DnaJ (Hsp40) homolog, subfamily B, member 1	0.740	0.0380
	<i>CBX2</i>	Chromobox homolog 2	0.765	0.0317
DS vs SS	<i>CDC27</i>	Cell division cycle 27	0.811	0.0025
	<i>HDAC8</i>	Histone deacetylase 8	0.768	0.0083
	<i>ANAPC10</i>	Anaphase promoting complex subunit 10	0.742	0.0381

Table 4.19 Genes involved in senescence and cellular responses to stress in SS and DS-LUHMES.

Transcripts linked to Histone cluster 1 and the APC/C:Cdh1 complex were down-regulated in SS and DS-LUHMES compared to controls. (Green: down-regulated, FC: fold change).

4.4.7. Validation of candidate genes by qRT-PCR

Overall, the enrichment analysis detected dysregulation of genes involved in cell cycle regulation, DNA damage response, chromatin organisation, immune response and oxidative phosphorylation pathways in DS-LUHMES. Even though these changes do not specifically indicate induction of senescence and a SASP, they all result as a response to an oxidative environment and have been linked to the activation of senescence pathways in mitotic cells. Based on these pathways, it is possible that oxidative stress in DS-LUHMES could be causing an ATR-dependent DNA damage response in order to repair the oxidative DNA damage caused by H₂O₂; at the same time, cell cycle dysregulation in DS-LUHMES could be linked to the activation of the DDR but also to replicative stress. H₂O₂ exposure could also have an effect on mitochondrial activity, which is reflected in the dysregulation of Complex I genes in DS-LUHMES. Finally, an obviously complex immune response was triggered by H₂O₂ in DS-LUHMES, however, *DDX58* was the only transcript that had been previously linked to the SASP in mitotic cells. The genes that were selected for validation as a result of this analysis are listed in **Table 4.20**.

Pathway	Gene
DNA damage response	<i>ATR</i>
	<i>CLSPN</i>
Cell cycle	<i>CDH1</i>
	<i>CCNB1</i>
	<i>CDC27</i>
Oxidative phosphorylation	<i>NDUFS8</i>
	<i>NDUFV3</i>
Immune response	<i>DDX58</i>

Table 4.20 Genes selected for qRT-PCR validation.

Genes in red were up-regulated while genes in green were down-regulated according to the microarray data.

Validation of the chosen genes was conducted on RNA extracts obtained from control, SS and DS-LUHMES following the same stress protocols as with the RNA extracts obtained for the microarray analysis. All conditions, including passage number and time of collection of trizol extracts were matched to the microarray sample conditions. Results are presented on **Figures 4.11, 4.12, 4.13 and 4.14**.

4.4.7.1. Validation of DNA damage response genes

qRT-PCR for *ATR* and *CLSPN* did not validate the up-regulation of these genes in DS-LUHMES (**Figure 4.11**). A non-significant directional change for assessment of *ATR* in DS-LUHMES by qRT-PCR correlated with the up-regulation of *ATR* detected in the microarray. Eventhough significant changes in *CLSPN* expression were detected in both SS ($p < 0.01$) and DS-LUHMES ($p < 0.001$), the direction of change did not validate the microarray data.

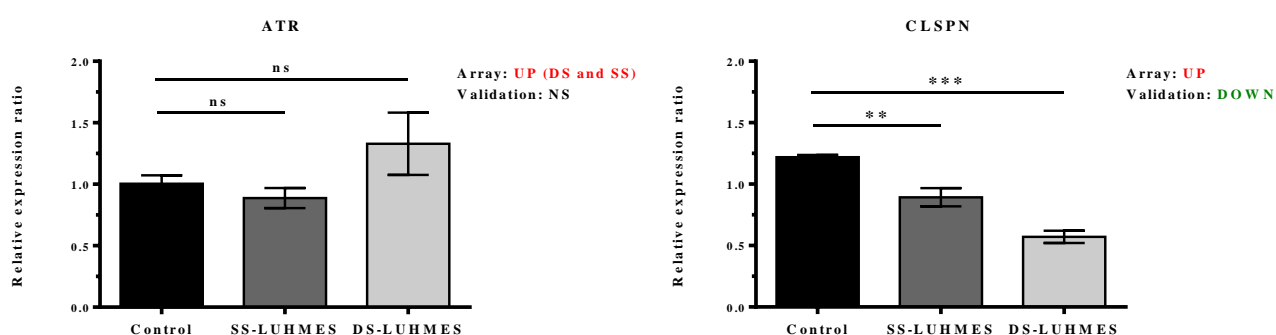


Figure 4.11. Validation of DNA damage response genes by qRT-PCR.

Differentiated LUHMES were stressed with H₂O₂ following the SS/DS protocol. Changes in DNA damage response genes *ATR* and *CLSPN* were validated by qRT-PCR. (One-Way ANOVA with multiple comparisons; data are means \pm SEM; n=3 in duplicate).

4.4.7.2. Validation of APC/C:Cdh1 complex genes

The genes *CDH1*, *CCNB1* and *CDC27* from the APC/C:Cdh1 complex were selected for validation of dysregulation in cell cycle control in DS-LUHMES (**Figure 4.12**). qRT-PCR results showed a significant down-regulation of *CDC27* ($p < 0.05$) and *CCNB1* ($p < 0.01$) in DS-LUHMES, which validated the findings of the microarray. *CCNB1* expression showed a trend towards a decrease in SS-LUHMES, but this did not reach significance. Amplification of *CDH1* was not successful, as no Ct value was observed for any of the samples. Due to this, its validation was not pursued further.

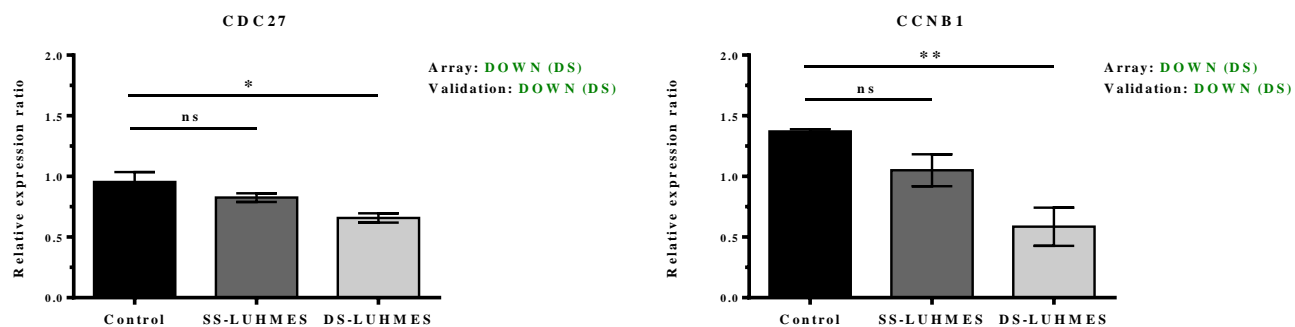


Figure 4.12 Validation of APC/C:Cdh1 complex genes by qRT-PCR.

Differentiated LUHMES were stressed with H_2O_2 following the SS/DS protocol. Changes in cell cycle genes *CDC27* and *CCNB1* were validated by qRT-PCR. (One-Way ANOVA with multiple comparisons; data are means \pm SEM; $n=3$ in duplicate).

4.4.7.3. Validation of oxidative phosphorylation genes

NDUFV3 and *NDUFS8* were selected to validate the findings of the array in terms of mitochondrial dysfunction (**Figure 4.13**). *NDUFV3* expression was down-regulated in DS-LUHMES according to microarray analysis; qRT-PCR findings showed the same

directional change in *NDUFV3*, but these results were not significant when compared to controls. On the other hand, a significant decrease in *NDUFS8* was identified by qRT-PCR in both SS ($p<0.01$) and DS-LUHMES ($p<0.01$). These findings correlate with the array results in DS-LUHMES, which also showed a decrease in mRNA expression; however, down-regulation of *NDUFS8* in SS-LUHMES was only detected by qRT-PCR analysis, but was not detected in the microarray.

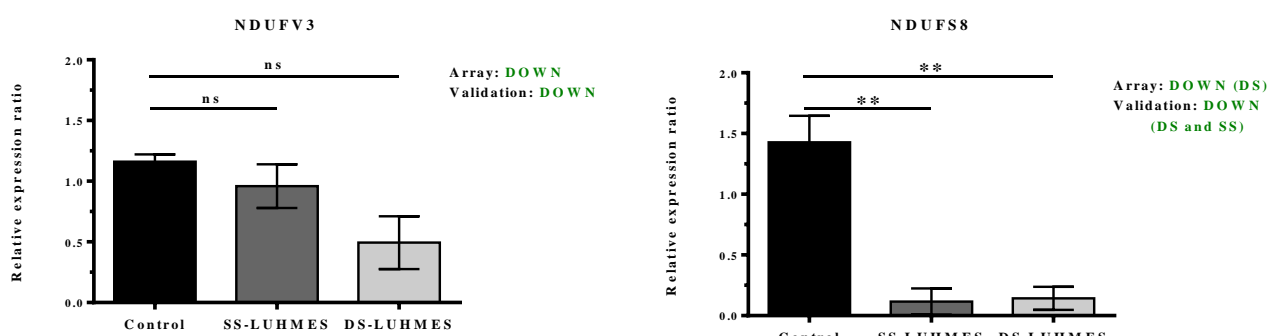


Figure 4.13 Validation of oxidative phosphorylation genes by qRT-PCR.

Differentiated LUHMES were stressed with H_2O_2 following the SS/DS protocol. Changes in the mitochondrial Complex I genes *NDUFV3* and *NDUFS8* were validated by qRT-PCR. (One-Way ANOVA with multiple comparisons; data are means \pm SEM; $n=3$ in duplicate).

4.4.7.4. Validation of RIG-I-like signalling pathway genes

qRT-PCR results indicated a significant decrease in the expression of *DDX58*, which codes for a RIG-I-like receptor that participated in the innate immune response. This down-regulation was detected in SS ($p<0.05$) and DS-LUHMES ($p<0.01$). qRT-PCR results are opposite to what was found in the microarray analysis, which suggested that *DDX58* expression was up-regulated in DS-LUHMES (**Figure 4.14**).

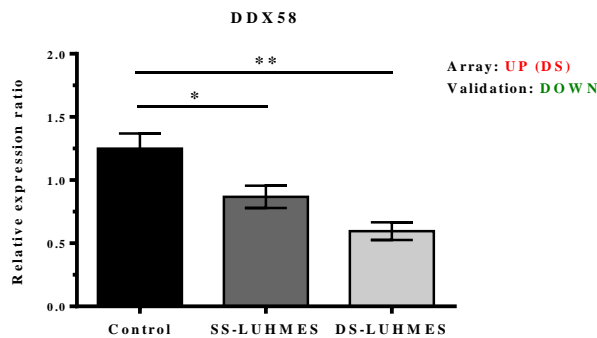


Figure 4.14 Validation of RIG-I-like signalling pathway genes by qRT-PCR.

Differentiated LUHMES were stressed with H₂O₂ following the SS/DS protocol. Changes in the *DDX58* gene, which codes for a RIG-1-like receptor, were validated by qRT-PCR. (One-Way ANOVA with multiple comparisons; data are means ± SEM; n=3 in duplicate).

4.4.8. Functional validation of dysregulated pathways

Microarray findings were validated by qRT-PCR only for the cell cycle and oxidative phosphorylation genes. Down-regulation of APC/C:Cdh1 genes suggested re-activation of the cell cycle in response to DNA damage in DS-LUHMEs; while down-regulation of mitochondrial Complex I genes in SS and DS-LUHMEs indicated mitochondrial dysfunction as a result of an oxidative environment. To further investigate these changes in cell cycle and mitochondrial alteration, a functional validation was performed on SS and DS-LUHMEs.

4.4.8.1. Assessing cell cycle re-activation in DS-LUHMEs

To investigate cell cycle re-entry in DS-LUHMEs, 96 hours control, SS and DS-LUHMEs were processed for Ki67 and MCM2 detection by immunocytochemistry. Both

antigens are commonly used as cell proliferation markers. Ki67 is known to participate in chromatin organisation during cell proliferation (Sobecki et al., 2016). MCM2 is a licencing factor, part of the MCM complex, which promotes DNA replication during S-phase (Bochman and Schwacha, 2008). Ki67 and MCM2 expression were absent in stressed LUHMES (SS and DS), as shown in **Figure 4.15**. To ensure that the absence of the antigens in stressed LUHMES was not a result of a technical issue, a positive control was included. Proliferating LUHMES were used as a positive control and so expression of Ki67 and MCM2 was expected in these cells. **Figure 4.15** also shows staining of proliferating LUHMES, confirming that the antibodies detected Ki67 and MCM2 successfully and the negative results seen in stressed LUHMES were genuine.

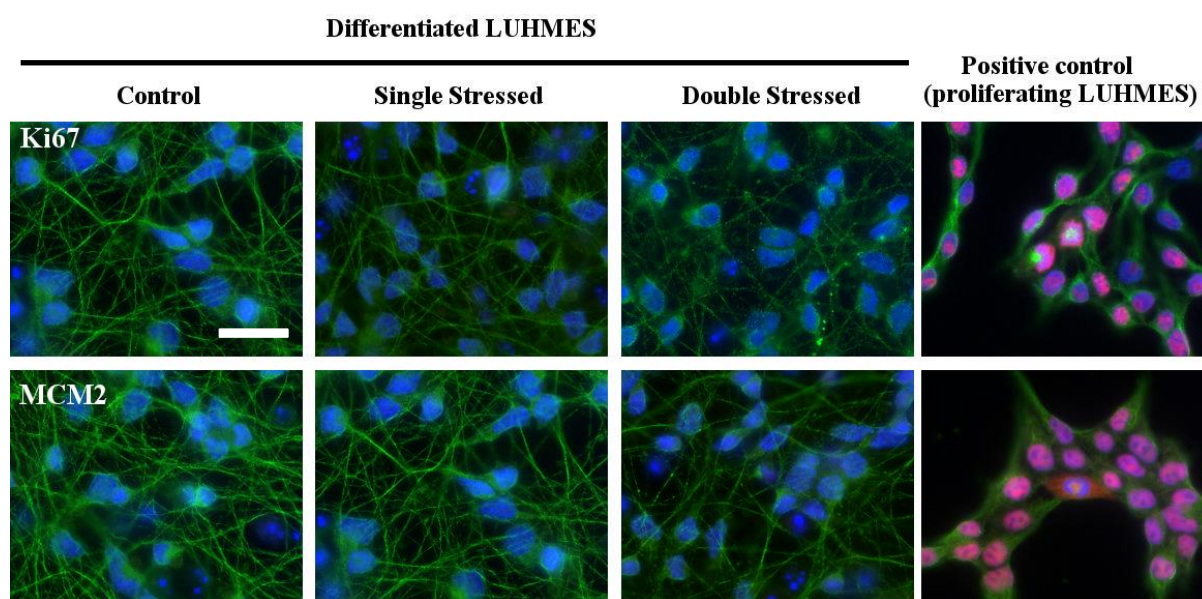


Figure 4.15 Assessing expression of Ki67 and MCM2 in SS and DS-LUHMES.

Functional validation of cell cycle re-entry in 96 hours SS and DS-LUHMES was done by investigating the expression of Ki67 and MCM2 cell cycle activation marker by immunocytochemistry. Ki67 and MCM2 nuclear expression is seen in red in the positive control panel, which consisted of proliferating LUHMES. There was no expression of either marker in SS or DS-LUHMES. Scale bar represents 20 μ m.

4.4.8.2. Assessing complex I dysfunction in DS-LUHMES

Complex I mitochondrial dysfunction was investigated by assessing NADH-activity dependent on Complex I. The down-regulation of *NDUFV3* and *NDUFS8* genes suggested that Complex I activity would be decreased in DS-LUHMES, and probably in SS-LUHMES as well. Results for the analysis of Complex I activity in stressed LUHMES is shown in **Figure 4.16**. Despite Complex I genes being down-regulated in the array study and qRT-PCR validation, assessment of its activity suggested otherwise. A significant increase in the activity of Complex I was detected in DS-LUHMES ($p < 0.01$) compared to controls, while SS-LUHMES did not show any change in Complex I activity.

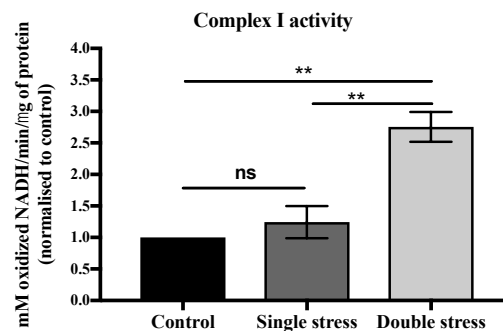


Figure 4.16 Assessing mitochondrial Complex I activity in stressed LUHMES.

96 hours SS and DS-LUHMES were processed for NADH-dependent complex I activity (One-way ANOVA with multiple comparisons; $n=3$; data represent means \pm SEM).

4.5. Discussion

Microarray analysis identified significant changes in the transcriptome of LUHMES as a result of exposure to H₂O₂. Changes in both SS and DS-LUHMES were investigated in order to determine whether a persistent oxidative stress (DS) would increase the expression of senescence genes. Overall, pathway analysis of microarray results did not indicate up-regulation of senescence or SASP-related pathways in DS-LUHMES. However, changes in signalling pathways linked to DNA damage response, cell cycle, metabolism and immune response were detected in DS-LUHMES when compared to controls. qRT-PCR and functional validation was conducted on a range of candidate genes from each of these pathways. Results confirmed dysregulation in the ATR-dependent DDR response, as well as in cell cycle regulation and oxidative phosphorylation. These pathways have been involved in the development of a senescent state, but its relation to senescence in the DS-LUHMES model is still not clear.

4.5.1. H₂O₂ induces changes in the transcriptome of DS-LUHMES

Transcriptomic changes in stressed LUHMES (SS and DS) were identified using a microarray gene expression profiling approach. As demonstrated in **Chapter 2** challenging stressed LUHMES with a second H₂O₂ dose (DS-LUHMES) causes oxidative DNA damage in the form of γ H2AX foci; this damage persisting for up to 96 hours after stress when compared to SS-LUHMES and controls. Therefore, the research in the current chapter aimed to determine whether this persistent DNA damage promotes the activation of senescence mechanisms or alteration of related pathways in DS-LUHMES. Microarray data analysis identified dysregulation of almost 3 times the number of transcripts in DS-LUHMES compared to SS-LUHMES confirming that a second H₂O₂ challenge has a more pronounced effect on differentiated LUHMES, in

terms of gene expression. Initially, before proceeding to the pathway analysis, a detailed search for senescence related genes in the lists of differentially expressed transcripts was conducted. Specifically, analyses to determine expression of senescence-associated *CDKN1A* (p21), *CDKN2A* (p16) and *GLB1* (SA- β -galactosidase) were conducted. SASP-related genes were also interrogated in these lists, including the most common cytokines known to be part of the SASP in mitotic cells, *IL6* (IL-6) and *CXCL8* (IL-8), but none of these transcripts were differentially expressed in either DS-LUHMES or SS-LUHMES.

Functional annotation analysis was conducted with DAVID and IMPaLA bioinformatics tools. DAVID annotated 24.8% of the significant, differential expression of genes associated with dysregulation of axon guidance, Ca⁺² signalling, DNA damage repair by homologous recombination and cell cycle in DS-LUHMES; while 28.8% of the differentially expressed transcripts in SS-LUHMES were annotated to a fewer number of KEGG pathways, including focal adhesion and axon guidance signalling. On the other hand, IMPaLA annotated a higher percentage of differentially expressed transcripts from both SS (57.9%) and DS-LUHMES (52.5%) to biological pathways of relevance to this study, which could result from IMPaLA annotation analysis being based on a greater number of databases, including Reactome, Wikipathways and KEGG. In contrast, DAVID annotation analysis was performed using the KEGG pathway database alone. Hence IMPaLA provided a more comprehensive and detailed pathway analysis, but it should be noted that some pathways were common to both DAVID and IMPaLA, including DNA damage repair and cell cycle regulation.

The pathways of interest identified in the IMPaLA analysis were not directly related to senescence, but they were pathways that suggested activation and alteration of key

cellular functions as a result of the DNA damage exerted by H₂O₂ exposure, especially in the DS-LUHMEs. These pathways included DNA damage repair signalling, cell cycle and chromatin regulation, oxidative phosphorylation and immune response. These findings and their relation of oxidative DNA damage and senescence are discussed in detail in the following sections.

4.5.1.1. DNA damage response and cell cycle regulation

4.5.1.1.1. ATR-signalling pathway

DNA oxidation can result in DNA lesions such as single-strand (SSBs), double-strand breaks (DSBs), base modifications, DNA cross-links and deoxyribose modification. In mitotic cells, the main function of the DNA damage response (DDR) is to maintain genome integrity through the detection and repair of these lesions. At the same time, the DDR also controls the cell cycle through the activation of cell cycle checkpoints, which prevents damaged cells from proliferating and activates apoptosis in case the damage cannot be reversed. The main transducers of the DDR are ATM (ataxia-telangiectasia-mutated), ATR (ataxia-telangiectasia-mutated and Rad3 related) and DNA-PK (DNA dependent kinase), all members of the phosphoinositide-3-kinase-related protein kinase (PIKK) family. ATM and DNA-PK recognise DSBs formation and activate downstream cascades to promote their repair, including the BER (base excision repair) and NHEJ (non-homologous end-joining) pathways. ATR, on the other hand, is not only activated by DSBs but also by lesions that generate single-strand DNA (ssDNA) (Zou, 2003).

The DDR in neurones is involved in the maintenance of genome integrity; however, due to the post-mitotic nature of neurones, its function is executed differently. Differentiated neurones rest in a G₀ phase under normal conditions, but exposure to genotoxic stress

induces re-activation of the cell cycle by the DDR, which is required for DNA repair or to induce apoptosis (Kruman et al., 2004; Schwartz et al., 2007; Tomashevski et al., 2010). Several studies have shown that ATM signalling is the main DDR pathway activated in neurones in response to DSBs caused by genotoxic stress, including oxidative stress (Alvira et al., 2007; Kruman et al., 2004; Otsuka et al., 2004). The ATM signalling cascade promotes transition from G0 to G1 phase and recruitment of the non-homologous end-joining (NHEJ) machinery to the site of the lesion (Schwartz et al., 2007). Although it has been shown that neurones do not undergo mitosis, they can progress through DNA synthesis (S-phase) and G2, in which case, activation of G2/M checkpoint could be caused by replication stress and prevent entry into mitosis (Schwartz et al., 2007).

Previously discussed detection of γ H2AX foci in SS and DS-LUHMES (**Chapter 2**) suggests activation of a DDR in response to H₂O₂, most probably related to ATM activation. H2AX phosphorylation is one of the first reactions to DSBs. Phosphorylation of H2AX is mainly executed by ATM (Burma et al., 2001), although ATR phosphorylates H2AX in response to replicational stress (Ward and Chen, 2001). In LUHMES, detection of γ H2AX foci 1 hour after incubation with H₂O₂ suggests induction of ATM-dependent DDR within the first hour of exposure to H₂O₂. It should be noted that the current study was conducted on DS-LUHMES following stress for 96h and it is highly likely that significant changes in the expression of ATM-related transcripts in SS and DS-LUHMES would have been detected in the first hours after H₂O₂ incubation.

ATR-dependent signalling is not well described in neurones, but dysregulation in ATR-signalling in DS-LUHMES could be related to cell cycle reactivation, S-phase progression and aberrant DNA synthesis. IMPaLA analysis identified up-regulation of the

ATR and *CLSPN* transcripts, whereas *RPA1* and *TIPIN* mRNA levels were down-regulated. *ATR* transcript encodes for the signal transducer ATR and *CLSPN* encodes for claspin, an adaptor protein that binds to ssDNA and facilitates interaction between ATR and Chk1 to induce cell cycle checkpoint signalling (Lee et al., 2003; Liu et al., 2007). *RPA1* gene encodes for replication protein A1 (RPA1), which is part of the RPA complex that binds to ssDNA and activates ATR-dependent DDR (Zou, 2003). Finally, *TIPIN* encodes for TIMELESS Interacting protein (Tipin), which together with Timeless protein, participate in DNA synthesis and cell cycle checkpoint in S-phase (Smith et al., 2009). In cycling cells, ATR-dependent DDR signalling is triggered by lesions that cause ssDNA, specifically in response to replication stress during S-phase (Petermann and Caldecott, 2006). In these cases, ATR initiates DNA damage repair through homologous recombination (HR) and activates G2/M cell cycle checkpoints by phosphorylation of Chk1; this last step requires the assistance of claspin (Liu et al., 2006). Work done by Schwartz et al. (2007) in cortical rat neuronal cultures exposed to 5 and 100 μM H_2O_2 confirmed that cell cycle re-entry in neurones is necessary for DDR activation. They showed that neurones incubated in 5 μM H_2O_2 for 24 hours, which caused repairable DSBs, would progress from G0 phase to G1; however, when exposed to non-repairable DSBs induced by 100 μM H_2O_2 , neurones would transition from G1 to S-phase and eventually induce apoptosis (Schwartz et al., 2007). This suggests that the intensity of the oxidative DNA damage will determine whether neurones transition up to G1 or S phases during cell cycle re-entry. S-phase activation would mean aberrant DNA synthesis and subsequent apoptosis.

Taking into account that ATR has a specific role in DNA damage caused during S-phase in mitotic cells, up-regulation of *ATR* and *CLSPN* mRNA in DS-LUHMES suggests

progression into S-phase and an attempt to induce DNA synthesis. The latter would cause replication stress in DS-LUHMES and subsequent activation of ATR-dependent DDR. qRT-PCR validation of *ATR* expression in DS-LUHMES was not significant but had the same directional change as seen in the microarray analysis; however, *CLSPN* levels assessed by qRT-PCR did not correlate with the array data. Moreover, down-regulation of *RPA1* and *TIPIN* are also not in accordance with what would be expected if ATR signalling was active in DS-LUHMES, since these two proteins participate in ATR signalling; however, validation was not conducted for these two transcripts and so further investigation on mRNA and protein levels needs to be done to be able to confirm these findings.

Overall, the results of this study suggest a second H₂O₂ challenge in DS-LUHMES likely causes cell cycle re-entry and progression to S-phase. DNA synthesis under these circumstances would be abnormal, cause replication stress and probably end in apoptotic cell death; however, microarray data did not suggest activation of apoptotic pathways in DS-LUHMES. An exact mechanism of S-phase progression and replication stress in DS-LUHMES cannot be determined with the information available, but would be of interest, since ATR-signalling and its specific circumstances in neurones are not well described. It is possible that a second H₂O₂ challenge caused cumulative DNA damage on already stressed LUHMES, inducing G1/S transition, inducing activation of ATR-dependent cell cycle checkpoint pathways to prevent DS-LUHMES from entering mitosis.

It is not possible to say whether ATR signalling induces a senescent-like state in DS-LUHMES either. In mitotic cells, an ATR-dependent DDR activates senescence pathways in response to replicative stress induced by oncogene expression. DNA damage

associated to oncogene-induced replicative stress in human fibroblasts activates ATR, causes cell cycle arrest and promotes formation of SAHF (Di Micco et al., 2011).

4.5.1.1.2. Cell cycle regulation: APC/C-Cdh1 complex

The APC/C-Cdh1 complex is a multimeric E3 ubiquitin ligase, member of the ring/cullin subfamily of ubiquitin ligases, and it is formed by 19 subunits (APC1-13, APC15-16) (Chang et al., 2015; Zhang et al., 2013). This complex targets cell-cycle regulatory proteins for ubiquitin mediated degradation under normal conditions, which requires binding to its co-activators Cdc20 or Cdh1. Interaction with Cdc20 occurs upon mitotic entry and remains until the metaphase-to-anaphase transition; at this point, Cdh1, which remains associated with APC/C until the initiation of G1, replaces Cdc20. (Kramer et al., 2000).

Recent evidence indicates that the APC/C-Cdh1 complex also participates in the DDR in mitotic cells. Its ubiquitin activity is determined by the cell cycle stage at which the DDR activation is needed. Specifically, activation of APC/C-Cdh1 is important for G2-DNA damage cell cycle arrest (Bassermann et al., 2008; Sudo et al., 2001). In DS-LUHMES, several genes associated with the APC/C complex including *CDC27* and *CCNB1*, were down-regulated; *CDHI* mRNA levels, on the other hand, were up-regulated. *CDC27* encodes for the Cdc27 subunit of the APC/C complex, while *CCNB1* codes for cyclin B1, one of the complex' degradation targets. *CDHI* gene corresponds to the Cdh1 protein, a co-activator of APC/C. Cdh1 is part of the substrate recognition region of the APC/C complex, while Cdc27 is essential for Cdh1 interaction with APC (Kraft et al., 2005; Thornton et al., 2006; Vodermaier et al., 2003). It has been shown that Cdh1 is essential for neuronal survival (Almeida et al., 2005; Fuchsberger et al., 2016). Almeida et al.

(2005) showed expression of APC and Cdh1 in rat cortical neurones under normal conditions, as well as down-regulation of cyclin B1 protein levels; shRNA inhibition of Cdh1 led to apoptosis through accumulation of nuclear cyclin B1 (Almeida et al., 2005).

Based on this evidence, up-regulation of *CDH1* mRNA levels in DS-LUHMES suggests activation of the APC/C-Cdh1 as part of cell cycle re-activation, characterised by S/G2 progression. This would correlate with dysregulation of the ATR signalling pathway linked to replication stress that has been discussed in the previous section and with downregulation of *CCNB1* transcripts. However, qRT-PCR amplification of *CDH1* was not successful and so it was not possible to confirm increased expression of this transcript in DS-LUHMES. Moreover, down-regulation of *CDC27*, which was also seen by qRT-PCR, does not correlate with the APC/C-Cdh1 activation hypothesis.

In addition to qPCR analysis, the current study examined the expression of cell cycle proliferation marker Ki67 and of replication licencing factor MCM2 in DS-LUHMES to determine whether re-activation of the cell cycle was occurring under these conditions. Ki67 is a nuclear protein that controls gene expression through a role in heterochromatin reorganisation (Sobecki et al., 2016). Ki67 protein levels peak during G2 and M phases, but decline from M to G1 (Sobecki et al., 2017). Mcm2 is a component of the replication licencing MCM (minichromosome maintenance) complex, a DNA helicase that is essential for DNA replication and that ensures regulation of replication origins as cell cycle progresses in order to avoid incomplete DNA replication or re-duplication during S-phase (Bochman and Schwacha, 2008). Assembly of the MCM complex occurs in late mitosis and early G1 and its components (Mcm2-7) are present throughout the cell cycle, which make them good proliferation markers (Wharton et al., 2001). Expression of Ki67

and Mcm2 was not detected in DS-LUHMES and therefore, no cell cycle re-activation in these cells. The DDR and cell cycle regulation are very dynamic processes. Dysregulation of ATR and APC/C-Cdh1-related transcripts in DS-LUHMES may reflect an earlier response to oxidative DNA damage that involves these pathways. Changes in ATR and APC/C-Cdh1 mRNA levels in 96 hours DS-LUHMES could be residual effects from this early activation, which would also explain why proliferation markers were not present in DS-LUHMES at this time-point.

The role of APC/C-Cdh1 complex in neurones is not restricted to cell cycle control and DNA damage. Recent evidence revealed the involvement of this complex in regulation of neuronal metabolism and oxidative status (Herrero-Mendez et al., 2009) and axonal growth (Konishi, 2004). Dysregulation of the APC/C-Cdh1-related genes in DS-LUHMES could be linked to these mechanisms, but a more detailed investigation would be required to confirm this.

4.5.1.2. Mitochondrial dysfunction

Pathway analysis in IMPaLA suggested dysregulation of mitochondrial transcripts in SS and DS-LUHMES. Transcripts encoding for mitochondrial Complex I subunits were down-regulated in both SS and DS-LUHMES, although these subunits differed between conditions. Other transcripts related to Complex III, Complex V, mitochondrial transport and the tricarboxylic acid (TCA) cycle were also dysregulated in SS and DS-LUHMES. To further investigate mitochondrial dysfunction in DS-LUHMES, the qRT-PCR and functional validation focused on Complex I activity under these conditions.

NDUFS8 and *NDUFV3* mRNA levels were significantly reduced in DS-LUHMES compared to controls and SS-LUHMES. *NDUFS8* (NADH:Ubiquinone oxidoreductase core subunit S8) and *NDUFV3* (NADH:Ubiquinone Oxidoreductase Subunit V3) encode for mitochondrial Complex I subunits. Complex I (NADH:ubiquinone oxidoreductase), is part of the mitochondrial electron transport chain (ETC), which produces ATP from electrons collected from catabolic processes (glycolysis, fatty acid oxidation and TCA) (Sazanov, 2015) in a process known as oxidative phosphorylation. The mitochondrial electron transport chain is composed of proton-pumping multi-subunit protein assemblies, known as complexes (I-IV), that are embedded in the mitochondrial inner membrane. Complex I consist of 45 subunits and it catalyzes the first step of the ETC, where electrons are used to create a proton gradient across the mitochondrial membrane. Complex I structure is quite intricate and is composed by 7 core subunits, *NDUFV1*, *NDUFV2*, *NDUFS1*, *NDUFS2*, *NDUFS3*, *NDUFS7* and *NDUFS8*, and 31 supernumerary subunits, which activity is not yet fully described. Complex I dysfunction is associated with increased ROS in different cell types, including neurones (Gueguen et al., 2015; Taddei et al., 2012; Ward et al., 2017) and has been linked to PD (Parker et al., 1989; Schapira et al., 1990) and AD (Fukuyama et al., 1996; Manczak et al., 2004).

In DS-LUHMES, qRT-PCR confirmed down-regulation of *NDUFS8* not only in DS-LUHMES but also in SS-LUHMES, and suggested the same for *NDUFV3*, although this last was not significant for either condition. This data suggested impaired function of Complex I in LUHMES exposed to H₂O₂, regardless of the number of H₂O₂ treatments. However, functional assessment of Complex I activity revealed hyperactivity of Complex I in DS-LUHMES, which was not consistent with down-regulation of *NDUFS8* and *NDUFV3* transcript levels. As mentioned before, *NDUFS8* is one of the core Complex I

subunits and is part of the hydrogenase module that directs electrons to ubiquinone (Bourges et al., 2004). Mutations in *NDUFS8* lead to severe Complex I deficiency and are linked to development of Leigh Syndrome, a severe neurodegenerative disease that causes cognitive and motor decline (Loeffen et al., 1998; M€ et al., 2012; Procaccio and Wallace, 2004). *NUDFV3* is one of the supernumerary subunits and its role has not been fully established, although it is thought that *NDUFV3* and the other supernumerary subunits are involved in Complex I biogenesis and stability (Schulte et al., 1999). Incubation of LUHMES in H_2O_2 might cause mitochondrial dysfunction at different levels, as seen in SS and DS-LUHMES, which could explain dysregulation of mRNA levels of different subunits from complex I, III and V detected in the microarray analysis. It is possible that Complex I is more susceptible to oxidative stress than the other complexes; this susceptibility could be related to the role of Complex I as the major site of ROS generation and to the low levels of Complex I present in the inner mitochondrial membrane compared to other complexes. A study on bovine heart mitochondria suggested that the ratios of Complexes I:II:III:IV:V were of 1:1.5:3:6, indicating that dysfunction of Complex I would have a greater impact on the ETC compared to altered function of Complexes II, III, IV and V (Schägger and Pfeiffer, 2001). Mitochondrial hyperactivity has previously been described in mouse dopaminergic neuronal cultures (Pacelli et al., 2015) and more recently, in pancreatic cells, in diabetes (Wu et al., 2017). This hyperactivity promotes ROS accumulation and contributes to oxidative stress. In pancreatic β -cells obtained from diabetic mice, Complex I hyperactivity caused an increase in ROS production, but a decrease in ATP, suggesting a dysfunctional ETC (Wu et al., 2017). It is evident that a second dose of H_2O_2 had a greater impact on mitochondrial function in DS-LUHMES compared to SS-LUHMES. A second H_2O_2 exposure could have caused Complex I hyperactivity, probably as a result of

redox imbalance, in DS-LUHMES. In an attempt to compensate for Complex I abnormal hyperactivity and prevent ROS formation and oxidative damage, DS-LUHMES could be reducing expression of Complex I genes *NDUFS8* and *NDUFV3*. Compensatory mechanisms like this one have an impact on transcriptome analysis and demonstrate the importance of validation of microarray results at the protein and functional levels, since they do not always correlate with gene expression.

Mitochondrial dysfunction is a feature of senescent cells. Increase in mitochondrial mass and accumulation of mitochondria with reduced membrane potential were seen in stress-induced premature senescent (SIPS) human fibroblasts (Passos et al., 2010). Passos et al. proposed that mitochondrial dysfunction leading to increase ROS levels in senescent cells occurs through TGF β via p21 (*CDKN1*) signalling; this pathway promotes ROS formation, oxidative DNA damage and persistent DDR activation that results in a stable senescent state (Passos et al., 2010). It is not possible to determine whether mitochondrial dysfunction in DS-LUHMES is related to a senescent-like state. Further investigation on mitochondrial accumulation and morphology in DS-LUHMES, as well as expression of senescent mitochondrial proteins, including the ones participating in the p21- TGF β signalling would need to be done.

4.5.1.3. Immune response

IMPALA pathway analysis detected dysregulation of 23 immune response-related transcripts in DS-LUHMES when compared to control and SS-LUHMES. A more detailed investigation of this data revealed up-regulation of ***DDX58*** in DS-LUHMES, which encodes for an immune response receptor known as retinoic acid-inducible gene I (RIG-1) receptor.

RIG-I is a member of the RIG-I-like receptors family, DExD/H RNA helicases characterised by a conserved Asp-Glu-Ala-Asp (DEAD) motif. As part of the innate immune response, RIG-I-like receptors act as cytoplasmic detectors of viral RNA (Yoneyama et al., 2004). This action triggers type I interferon (IFN) production and expression of an antiviral response through a pathway independent to Toll-like receptor 3 (TLR3) (Kato et al., 2005). RIG-I has been also linked to inflammation and secretion of pro-inflammatory cytokines (Bogefors et al., 2011; Zhang et al., 2014a).

More recently, RIG-I receptor was associated to senescence and the SASP in senescent HUVECs (Human umbilical vein endothelial cells) and WI-38 fibroblasts. This study showed increased RIG-I mRNA and protein levels when measured in these cells; increased RIG-1 receptor correlated with increased expression of IL-6 and IL-8 genes, cytokines that are known to be part of the SASP, but not with IFN- β . Knockdown of ATM in senescent HUVECs caused a reduction in RIG-1 and IL-6 mRNA levels, which confirmed an ATM-dependent expression of this two proteins (Liu et al., 2011). *In vivo* experiments in 60-week-old mice also revealed increased expression of RIG-1 and IL-6 interleukin in brain extracts; these findings correlated with increased p16 (Liu et al., 2011). Transcriptomic analysis suggested up-regulation of RIG-1 gene *DDX58* in DS-LUHMEs, however qRT-PCR results were the opposite to what was detected by the microarray analysis. RIG-1 receptor has been reported in primary mice cortical neurones infected with Japanese encephalitis virus (JEV). Viral infection caused up-regulation of RIG-1 protein expression 12 and 24 hours post-infection, along with downstream targets IL-6, IL-2, TNF- α and MCP-1 (Nazmi et al., 2011). This confirms that neurones can induce a pro-inflammatory response through the RIG-1 pathway, with IL-6 as one of the

cytokines that are released as a result of viral infection. Detection of DDX58 up-regulation in DS-LUHMES could be indicative of activation of this pathway in response to oxidative stress, but its relation with senescence is not clear from these experiments.

4.6. Main conclusions

Overall, transcriptome analysis of DS-LUHMES did not reveal dysregulation of “classical” senescence genes or pathways; however, a persistent oxidative DNA damage affected several neuronal functions, including DNA damage response, cell cycle regulation, oxidative phosphorylation and immune response, which could be linked to a senescent-like phenotype. Our data correlates with numerous reports indicating the involvement of cell cycle regulatory proteins, DDR and mitochondrial alterations in the pathology of neurodegenerative diseases (Höglinger et al., 2007; Silva et al., 2014) and provides further evidence on the involvement of oxidative stress and accumulation of DNA damage in neuronal dysfunction. To expand this work and to investigate whether these changes are linked to a neuronal senescent-like state it would be interesting to assess the neuronal response to oxidative DNA damage at different timepoints, since it is possible that important changes were missed by focusing on just the 96-hour timepoint. Changes in the immune response were not directly linked to known SASP-components, however, the SASP signature in post-mitotic neurones could differ from the one described for mitotic cells. Thus, investigating the involvement of some of the dysregulated immune response genes at the protein level could provide information on whether neurones also develop a secretory phenotype, specially taking into account that we also report a cell-to-cell contact mediated dysfunction in healthy LUHMES when co-cultured with DS-LUHMES.

Chapter 5. Relevance of neuronal senescence *in vivo*: DNA damage and senescence in the brain of ALS/MND patients

5.1. Introduction

The role of senescence in ageing and its contribution to degenerative diseases has been of increasing interest in recent years. The fact that senescent cells accumulate with age and that they can develop a toxic phenotype could contribute to the development of age-related diseases, such as type 2 diabetes, osteoarthritis, atherosclerosis, cancer and neurodegeneration. Senescence in the brain has been mainly studied in non-neuronal cells, including astrocytes, microglia, oligodendrocytes, endothelial cells and neural stem cells (NSCs), but investigation of senescence in neurones has not been fully explored, mainly due to the idea that post-mitotic cells are not capable of activating senescence.

Recent evidence obtained from a mouse model of ageing suggest that neurones can undergo a p21 dependent senescent-like state, which is linked to the release of IL-6, one of the main SASP cytokines (Jurk et al., 2012). SA- β -gal⁺ neurones were also found in the frontal cortex of cases with low levels of AD pathology (Simpson et al., 2014). These studies suggest that a mechanism similar to mitotic senescence could be developed by neurones in response to persistent DNA damage *in vivo*. Based on this evidence, this project focused on the detection of senescent neurones in ALS/MND, since it is known that oxidative stress and DNA damage are deeply involved in its pathology, which could potentially activate senescent pathways in neurones (Bogdanov et al., 2000; Lopez-Gonzalez et al., 2016; Martin et al., 2007).

5.2. Aims and objectives

The aim of the work presented in this chapter was to investigate expression of senescence markers in ALS/MND and control brains and to assess association of these markers with oxidative DNA damage and DNA damage response mechanisms activated in the disease.

This was done by:

- Identifying the expression of p16 and p21 cell cycle regulatory proteins and increased activity of SA- β -gal in neurones and glia of ALS/MND brains and controls. Differences between groups were assessed quantitatively.
- Relating expression of senescence markers to oxidative DNA damage and DNA damage response mechanisms through the assessment of 8-OHdG and γ H2AX expression
- Investigating changes at the transcriptomic level of neurones expressing senescence markers in order to identify gene expression patterns indicative of a senescent-like state and the development of a SASP.

5.3. Materials and methods

All chemicals were obtained from Sigma-Aldrich (St Louis, MO, USA) unless stated. Solutions required for the experiments described in this chapter were prepared as specified in **Appendix A**.

5.3.1.1. Human Brain Tissue

Post-mortem formalin-fixed paraffin-embedded (FFPE) and frozen brain tissue samples from ALS/MND and control donors were obtained from the Sheffield Brain Tissue Bank (SBTB; Ethical Committee Approval REC Ref. 08/MRE00/103) (**Appendix B**). FFPE samples from motor cortex (MCx), cervical spinal cord (Sc), frontal association cortex (FACx, Brodmann area 8/9) and occipital cortex (OCx) were used for immunohistochemistry experiments. Frozen sections were used for detection of SA- β -galactosidase activity and for laser capture microdissection (LCM). **Table 5.1** summarises the number of cases available for each brain area under study.

The cohort consisted of 17 male and 4 female control donors (mean age of 61.4 years, range 26-84) and 6 male and 4 female ALS/MND donors (mean age of 64.33 years, range 48-80). Three cases were diagnosed with the familial form of the disease, while the rest were sporadic. Four cases, 1 sporadic and 3 familial, were positive for the C9orf72 mutation. The mean post mortem delay (PMD) for controls was 28.92 hours (range 5-75 hours) and for the ALS/MND group was 35.62 hours (range 9-96 hours). Detailed information about the disease and control donors is shown in **Table 5.2**.

Brain region	Cases available for the FFPE samples		Cases available for the frozen samples	
	ALS/MND	Control	ALS/MND	Control
MCx	10	9	8	9
FACx	10	10	8	6
Sc	10	11	9	5
OCx	10	10		

Table 5.1 Number of cases available for each brain region studied from controls and ALS/MND donors.

Group	Case	Sex	Age (y)	PMD (hours)	Clinical diagnosis ([+]: C9orf72 expansion)
ALS/MND	1	M	79	13	Familial ALS/MND [+]
	2	M	64	Not recorded	Sporadic ALS/MND [+]
	3	M	48	23	Familial ALS/MND-PD [+]
	4	F	59	28	Familial FTD-ALS/MND [+]
	5	M	Not recorded	9	Sporadic ALS/MND
	6	M	51	40	Sporadic ALS/MND
	7	F	69	40	Sporadic ALS/MND
	8	M	66	96	Sporadic ALS/MND
	9	F	80	Not recorded	Sporadic ALS/MND
	10	F	63	36	Sporadic ALS/MND
Control	1	F	59	5	Myocardial infarction
	2	M	63	Not recorded	Control
	3	F	63	Not recorded	Control
	4	M	63	20	CVD
	5	M	67	63	HCC
	6	M	51	25	Mesothelioma
	7	M	55	24	Carcinoid tumour
	8	M	82	36	Carcinomatosis
	9	F	29	20	IHD
	10	M	54	8	IHD
	11	M	65	34	Bronchopneumonia
	12	M	72	31	IHD
	13	M	26	Not recorded	Control
	14	M	69	Not recorded	Control
	15	M	78	75	Basal ganglia calcification
	16	Not recorded	Not recorded	Not recorded	Control
	17	M	84	Not recorded	Age related atrophy
	18	M	54	8	Ischaemic heart disease
	19	M	75	27	Lewy body dysphagia
	20	M	53	Not recorded	MS
	21	M	78	60	Pneumonia
	22	F	66	Not recorded	Sensory motor neuropathy

Table 5.2 Clinical and demographic data for the control and ALS/MND donors.

For the current study, data from donors was anonymised but a list of the cases linked to the anonymised IDs is available.

5.3.1.1.1. Classification of ALS/MND cases based on p62 pathology in the FACx

ALS/MND cases were classified based on their p62 staining in the FACx to investigate any correlation between p62 pathology and the expression of senescence and DNA damage markers. For this, p62 stained sections from the ALS/MND cases in our cohort were provided by the Sheffield Brain Tissue Bank. The FTLD pattern was established according to the new consensus criteria, which classifies patterns into FTLD-TDP A, B or C based on the presence of specific p62 structures, including neuronal cytoplasmic inclusions (NCI), dystrophic neurites (DN), neuronal intranuclear inclusions (NII) and glial cytoplasmic inclusions (GCI) (Mackenzie et al., 2011). ALS/MND cases were classified as FTD-0 when no pathology was found and FTLD-MC (minimal change) when occasional p62 structures were seen. The distribution of the p62 structures as well as any atypical features were indicated as well.

5.3.1.1.2. Detection of senescence associated- β -galactosidase (SA- β -gal) activity in post-mortem tissue

The histochemical protocol used for this study was adapted from a previously published report, which investigated SA- β -gal activity in skin biopsies (Dimri et al., 1995). Briefly, histochemical detection of SA- β -gal activity in frozen tissue was performed using the Senescence Cells Histochemical Staining Kit (Sigma-Aldrich, UK), according to the manufacturer's instructions. Briefly, all kit components were thawed on ice and the X-gal solution was warmed to 37 °C for 1hr, prior to use. Frozen sections were warmed to RT for 3 min, fixed with 1x Fixation Buffer for 7 minutes and rinsed with 1x Phosphate Buffered Saline (PBS) 3 times prior to the addition of the staining mixture. The staining mixture consisted of potassium ferricyanide (5 mM), potassium ferrocyanide (5 mM), X-gal solution (0.1mg/ml) and 1x Staining Solution. The staining mix was added to the

tissue sections and these were covered with Parafilm (Sigma-Aldrich, St Louis, MO, USA), to prevent evaporation of the mixture and to ensure the tissue was in contact with an even layer of substrate. Sections were incubated overnight at 37 °C, then rinsed with 1x PBS, and counterstained with Nuclear Fast Red for 5 min. Sections were rinsed with deionized water before they were dehydrated, cleared and mounted in DPX mountant (Sigma-Aldrich, St Louis, MO, USA). SA- β -gal activity was identified as a blue, insoluble precipitate within cells and was assessed qualitatively in images captured at medium (20x objective) and high magnification (40x objective).

5.3.1.3. Immunohistochemistry

5.3.1.3.1. Senescence markers p16 and p21

As mentioned previously, the detection of senescent cells requires the use of several markers. In addition to SA- β -gal activity, the identification of the proteins that are involved in the two pathways that activate senescence is also useful. The p16/pRb and p21/p53 pathways induce senescence in response to a persistent DDR and their study complements the information given by SA- β -gal activity.

For the immunohistochemical detection of p16 and p21 in FFPE tissue sections, a standard biotin horseradish peroxidase enzyme complex method (ABC-HRP) was used. Primary antibodies and antigen retrieval methods used for each marker are described in **Table 5.3**. After antigen retrieval and incubation in 3% H₂O₂ in methanol for 5 minutes, sections were blocked in 1.5% normal serum for 30 min before incubation with the primary antibody. Sections were washed with 1x Tris-buffered saline (TBS) and incubated in 0.5% of the suitable biotinylated secondary antibody for 30 min. At the same time, the avidin-biotin complex solution (Vector Laboratories, CA, USA) was prepared,

as specified by the supplier, to be used in the next step. Sections were washed again with 1x TBS and incubated with the avidin-biotinylated complex-horse radish peroxidase solution (ABC-HRP solution) for 30 minutes. Following this incubation, excess of the ABC-HRP solution was removed by washing 1x TBS and the sections were incubated with the enzyme substrate DAB (Vector Laboratories, UK). The DAB solution was left for 5 minutes and peroxidase activity was quenched by washing with deionised water. Sections were counterstained with haematoxylin for 30 seconds – 1 min, dehydrated through a graded series of 70%, 95% and 100% ethanol and cleared in xylene. Finally, sections were mounted with DPX mountant and left to dry overnight. Negative controls consisted of sections incubated with omission of the primary antibody and relevant isotype controls.

5.3.1.3.1.1. Double labelling to identify the cell type expressing p16 and p21

To determine glial expression of p16 and p21, dual immunolabelling was performed. Following immunostaining for p16 or p21, sections were washed with 1x TBS, blocked with 1.5% normal serum for 30 minutes at RT and incubated with avidin/biotin blocking solution (Vector Laboratories, UK). To determine the association with astrocytes, sections were incubated with primary antibodies raised against glial fibrillary acidic protein (GFAP) (**Table 5.3**). Sections were washed with TBS and incubated with 0.5% relevant biotinylated secondary antibody for 1 hr at RT, followed by a TBS wash and incubation with 2% avidin biotinylated alkaline phosphatase enzyme complex (ABC-AP) (Vector Laboratories, UK). The signal was visualized using an alkaline phosphatase substrate, which produces a red precipitate.

Dual immunostaining to determine neuronal expression of p21 was performed using a fluorescence approach on frozen sections. Briefly, acetone-fixed sections were incubated with 0.2% glycine and blocked with normal serum (1.5%), followed by incubation with the anti-p21 primary antibody for 1 hr at RT. Sections were washed and incubated with a biotinylated secondary antibody (0.5%) for 30 min at RT, followed by incubation with streptavidin-TRITC complex (0.2%) for 1 hour. Sections were blocked with normal serum (1.5%) for 30 minutes at RT, followed by avidin/biotin blocking solution (Vector Labs) and overnight incubation with an anti-NeuN primary antibody, at 4 °C (Table 5.3). Sections were washed and incubated with a biotinylated secondary (1%) antibody for 45 min, followed by incubation with a streptavidin-FITC complex (0.2%) for 1 hour at RT. Sections were counterstained with Hoechst solution before mounting with Fluoromount Mounting Media (Sigma-Aldrich, St Louis, MO, USA).

	Antibody	Species	Dilution and conditions	Antigen retrieval	Supplier
Senescence markers	p16	Mouse monoclonal	Prediluted O/N, 4 °C	Pressure cooker, Access Revelation Buffer pH 9.5	BioGenex, UK
	p21	Mouse monoclonal	1:100 O/N, 4 °C	MW 10 min TSC buffer pH 6	Millipore UK Limited, UK
DNA damage markers	γ H2AX	Rabbit polyclonal	1:500 O/N, 4 °C	Pressure cooker, EDTA pH 8	R&D Systems, UK
	8-OHdG	Mouse monoclonal	1:400 1hr, RT	Pressure cooker, Access Revelation Buffer pH6	Abcam, Cambridge UK
Microglial markers	MHC class II α -chain	Mouse monoclonal	1:20, 1 hour, RT	MW 15 min TSC buffer, pH 6	DakoCytomation, Ely UK
	CD68 clone PG-M1	Mouse monoclonal	1:100, 1 hour RT	MW 10 min TSC buffer, pH 6.5	DakoCytomation, Ely UK
Neuronal marker	NeuN	Mouse monoclonal	1:100 1 hr, RT	NA (used for double labelling on frozen tissue)	Chemicon-Millipore UK Limited, UK
Astrocytic marker	GFAP	Rabbit polyclonal	1:500 1h, RT	NA (used for double labelling)	DakoCytomation, Ely UK

Table 5.3 Antibodies used for immunohistochemistry experiments.

Antibodies, antigen retrieval and incubation conditions used for the detection of senescence, DNA damage and cell specific markers in ALS/MND and control brains by immunohistochemistry.

5.3.1.3.2. Oxidative DNA damage markers 8-OHdG and γ H2AX

Immunohistochemistry for 8-OHdG and γ H2AX was conducted in the MCx and FCx of ALS and control donors. The primary antibodies, antigen retrieval and incubation conditions for 8-OHdG and γ H2AX staining are listed in **Table 5.3**. The staining protocol was identical to the one described in **section 5.3.1.3.1**.

5.3.1.3.3. MHC class II and CD68 staining

SA- β -gal activity and a significantly higher proportion of p21⁺ neurones in the FACx of ALS/MND donors could be related to a senescent-like state in this cell type, which would involve the development of a SASP. To investigate this further, we decided to determine if a pro-inflammatory environment was present in this brain area of ALS/MND patients through the detection of activated microglia. For this, immunocytochemistry for MHC class II and CD68 microglial markers was performed following the same ABC-HRP method described in **section 5.3.1.3.1**. The antibodies used, as well as the antigen retrieval and incubation conditions are presented in **Table 5.3**.

5.3.1.4. Quantitative analysis

5.3.1.4.1. p21⁺, p16⁺ and 8-OHdG⁺ cells

Glial and neuronal nuclear staining was assessed quantitatively for p21, p16 and 8-OHdG in the grey matter of the FACx and MCx sections of ALS/MND and control donors. Using the Nikon ECLIPSE Ni microscope (Nikon Instruments, Amsterdam, Netherlands), the region with the most intense staining was selected for each case. Images were taken from one cortical ribbon of grey matter, starting from the outer cortex up to the white matter border and excluding cortical layer 1. Images taken with a 40x objective were imported into a Power Point file and a previously designed grid was overlaid on to each image to help with the quantification (**Figure 5.1**). Two independent observers (Irina Vázquez-Villaseñor and Julie Simpson) quantified the number of p16⁺, p21⁺ and 8-OHdG⁺ glial and neuronal nuclei and total number of glial and neuronal nuclei in each image. The proportion of positive nuclei was determined by dividing the number of positive cells (neurones or glia) by the number of total cells (neurones or glia) per field. A percentage was obtained by multiplying the proportion by 100.

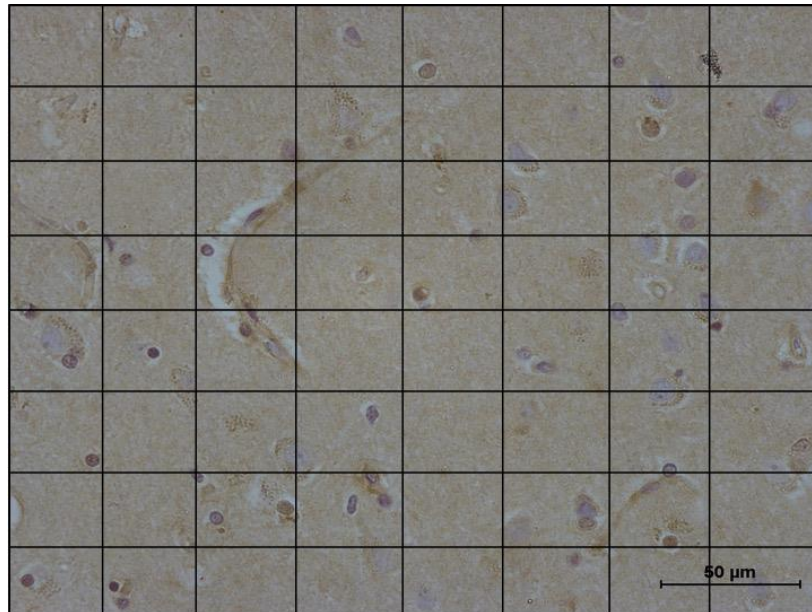


Figure 5.1 Grid used for quantitative analysis of p21, p16 and 8-OHdG staining.

5.3.1.4.2. Quantification of γ H2AX⁺ cells

Quantification of the total number of γ H2AX⁺ nuclei was performed in FACx and MCx sections of ALS/MND and control donors, using the Cell[^]R software (Olympus Biosystems, Watford, UK). Images were taken from one cortical ribbon of the grey matter, starting from the outer cortex up to the white matter border, using a 20x objective and uploaded into Cell[^]R. Detection of γ H2AX⁺ neuronal nuclei was done using size exclusion (>500 pixels) and the number of positive small nuclei (glia) was determined by subtracting the number of pyramidal neuronal nuclei from the total number of positive nuclei. To assess the total number of cells (neurones and glia), the same detection protocol was applied to haematoxylin-only stained sections, which allowed the determination of the percentage of immunopositive cells (total number of positive neurones/total number of neurones; total number of positive glia/total number of glia) per case.

5.3.1.4.3. Quantification of MHC class II and CD68 staining

Percentage (%) area of immunoreactivity was calculated for MHC class II and CD68 staining in FACx sections of ALS/MND and control donors with the Olympus Cell[^]R software. As with the other markers, images were taken from one cortical ribbon of grey matter, starting from the outer cortex up to the white matter border, using a 20x objective. Images were transferred to Cell[^]R software, which calculated the % area of immunoreactivity per image. For the data analysis, the mean % area of immunoreactivity was calculated based on the total number of images per case.

5.3.1.5. Statistical analysis of immunohistochemical staining

Statistical analyses were performed in IBM SPSS Statistics v22 (IBM, NY, USA). Comparisons between ALS/MND and control groups were done using the Mann U-Whitney nonparametric analysis for independent samples. The effect size was calculated using the formula

$$r = Z/\sqrt{N}$$

where r represents the effect size, as proposed by Cohen (Cohen, 1988); Z represents the Mann U-Whitney Z-score; and N represents the sample size. Cohen's guidelines were used for the interpretation of the data (**Table 5.4**).

Value for r	Effect size
0.1	Small
0.3	Medium
0.5	Large

Table 5.4 Effect size Cohen's guidelines.

Cohen's guide lines to determine the effect size of the Mann U-Whitney nonparametric analysis based on r (Fritz et al., 2012).

The relation between senescence markers expression and oxidative DNA damage and a DDR were assessed using Spearman's correlation coefficient. Mann U-Whitney nonparametric analysis was also used when comparing expression of senescence and DNA damage markers in ALS/MND cases based on the FTLD-TDP type and the presence of the C9orf72 expansion.

5.3.2. Transcriptome analysis of FACx neurones from ALS/MND and control donors

5.3.2.1. Checking for RNA quality from tissue for microarray

Before isolation of neurones by laser capture microdissection (LCM), the quality of the RNA obtained from frozen samples was assessed. RNA isolation was performed using the PicoPure RNA Isolation Kit (ThermoFisher Scientific, MA, USA). Briefly, two 5 µm sections from ALS/MND cases 1,2 and 3, and controls 1, 2, 4 and 5 were placed in a 0.5 ml eppendorf and were incubated in Extraction Buffer, from the PicoPure RNA Isolation Kit, for 30 minutes at 42 °C. Samples were centrifuged at 3000 xg for 2 minutes and the supernatant was collected in a sterile 0.5 ml eppendorf. The RNA Purification Column was pre-conditioned by incubating it with 250 µl of Conditioning Buffer for 5 minutes at RT. The column was centrifuged at 16000 xg for 1 minute. To prepare the sample, the supernatant was mixed with 50 µl of 70% Ethanol and added on to the column, which was centrifuged for 2 minutes at 100xg followed by a centrifugation at 16000 xg for 30 seconds. The column was washed with 100µl of Wash Buffer (W1) and centrifugation for 1 minute at 8000xg. 100 µl of Wash Buffer 2 (W2) were pipetted into the column and it was again centrifuged at 8000 xg for 1 minute. A last wash was performed by adding 100 µl of W2, followed by centrifugation at 16000xg for 2 minute. To collect the extract, the column was transferred to a sterile 0.5 eppendorf. The RNA was eluted with 11 µl of Elution Buffer and centrifuged at 1000 xg, for 1 minute, followed by a final

centrifugation at 16000xg for 1 minute. The RNA concentration was measured in a NanoDrop Spectrophotometer (ThermoFisher Scientific, MA, USA) and the RNA quality was assessed with an Agilent RNA 6000 Pico Chip (ThermoFisher Scientific, CA, USA) in an Agilent 2100 Bioanalyzer (Agilent, CA, USA).

5.3.2.2. Laser capture microdissection (LCM) of neurones from the FACx

LCM was used to isolate neurones from the FACx of ALS/MND and control donors. For this, freshly cut sections of 3 ALS/MND cases and 3 controls placed on to non-charged slides (**Table 5.5**) were warmed up at RT for 5 minutes and fixed in acetone at 4 °C for 5 minutes. Sections were stained with toluidine blue for 1 minute, washed in DEPC (diethyl pyrocarbonate) water for 5 seconds and dehydrated in a series of alcohols of increasing concentrations (70%, 95%, 100%). After clearing in xylene, sections were air-dried for at least 1 hour.

Group	Case	ID
Control	1	Control 1
	2	Control 2
	3	Control 3
ALS/MND	1	ALS/MND 1
	2	ALS/MND 1
	3	ALS/MND 3

Table 5.5 Control and ALS/MND cases that were selected for LCM isolation of neurones from the FACx.

LCM was performed in the PixCell Iie Laser Capture Microdissection System (ThermoFisher Scientific, MA, USA) and using the Arcturus® CapSure® Macro LCM Caps (ThermoFisher Scientific, MA, USA). An approximate number of 2,000 neurones per case were isolated. After picking, the film was removed carefully using sterile

tweezers and incubated for 30 minutes at 42 °C in Extraction Buffer, from the PicoPure RNA Isolation kit. Samples were stored at -80 °C.

5.3.2.3. RNA isolation from LCM samples

RNA isolation was performed according to the PicoPure RNA Isolation kit instructions as explained in **section 5.3.2.1**. To confirm the success of the RNA extraction, a preliminary determination of the RNA concentration in the samples was performed in the NanoDrop Spectrophotometer, using 1 µl of the sample for the reading. RNA quality was determined with an Agilent RNA 6000 Pico Chip.

5.3.2.3.1. Confirmation of neuronal enrichment

To confirm that RNA samples represented an enriched neuronal population, amplification of neuronal and glial specific transcripts was assessed in all samples by standard PCR. For this, 5 µl of RNA template extracted from the samples obtained by LCM were mixed with 2 µl of 5x qScript™ cDNA SuperMIX (Quanta Biosciences, Inc, MA, USA) and 3 µl of nuclease free water. The reaction protocol consisted of 5 minutes' incubation at 25 °C, followed by a 30 minutes' incubation at 42 °C and finally, 5 minutes' incubation at 85 °C. After cDNA was synthesised, samples were prepared for PCR amplification of neuronal and glial markers. The primers used for NEUN, GFAP, OLIG2, CD68 and ACTNB amplification are listed in Table 5.6. Samples consisted of 1 µl of cDNA template, 10 µl of 2x DreamTaq Green PCR Master Mix, 1 µl of forward (F) primer, 1 µl (R) of reverse primer and 7 µl of nuclease free water. The amplification protocol is described in **Table 5.7**. 10 µl of each amplification product were loaded in a 3% agarose gel containing ethidium bromide (100 ng/ml) and ran at 80 V for 45 minutes. The gel was imaged in a GENI UV light imaging system (Syngene).

Gene	Product size	Primer Sequence
NeuN	84	F: 5'-ACG ATG GTA GAG GGA CGG AA R: 5'-AAT TCA GGC CCG TAG ACT GC
GFAP	213	F: 5'-GCA GAA GCT CCA GGA TGA AAC R: 5' TCC ACA TGG ACC TGC TGT C
CD68	135	F: 5'- CGA GCA TCA TTC TTT CAC CAG CT R: 5'- ATG AGA GGC AGC AAG ATG GAC C
OLIG2	474	F: 5'-CCC TGA GGC TTT TCG GAG CG R: 5'-GCG GCT GTT GAT CTT AGA CGG
ACTNB	100	F: 5'- TCC CCC AAC TTG AGA TGT AAG R: 5'- AAC TGG TCT CAA GTC AGT GTA CAG G

Table 5.6. Gene specific primers used to confirm neuronal enrichment of LCM samples.

Step	Temperature (°C)	Time	Cycles
Initial denaturation	94	1-3 min	1
Denaturation	94	30 seconds	25-40
Annealing	67	1 minute	
Extension	72	30 seconds	

Table 5.7 Amplification reaction protocol.

Protocol used for amplification of neuronal and glial specific genes to confirm enrichment of LCM samples with a neuronal population.

5.3.2.4. RNA amplification and microarray hybridisation

Changes in the transcriptome of FACx neurones from ALS/MND donors were investigated using the enriched neuronal samples obtained by LCM. 3 control and 3 ALS/MND cases were included in this analysis (**Table 5.5**). For this, RNA samples were amplified with the 3' IVT Pico Reagent kit (ThermoFisher Scientific, MA, USA). The RNA amplification and microarray hybridisation protocol was described in detail in **Chapter 4, section 4.3.2.1**. In summary, 10 ng of RNA per sample were mixed with 5 µl of poly-A RNA control mix. Complimentary RNA (cRNA) was synthesized by *In Vitro*

Transcription (IVT) of the ds-cDNA that was obtained from RNA. cRNA was purified and quantified in a NanoDrop Spectrophotometer. The cRNA quality and concentration was also assessed with an Agilent 6000 Nano Chip. Purified cRNA was used for sense-strand cDNA synthesis by reverse transcription; antisense-strand cDNA was then obtained from a second round of ds-cDNA synthesis, which contained dUTP at a specific ratio relative to dTTP. ds-cDNA was purified and quantified by spectrophotometry, before being fragmented at the dUTP residues. Fragments were labelled with the DNA Labeling Reagent (Affymetrix), which is linked to biotin.

GeneChip Human Genome U133 Plus 2 Arrays (ThermoFisher Scientific, MA, USA) cartridges were pre-hybridised with Pre-hybridisation mix for 30 minutes at 45 °C and 60 rpm. The Hybridization cocktail was prepared by mixing 160 µl of Hybridization Master Mix and 60 µl of the sample labelled ds-cDNA. The mix was incubated for 5 min at 99 °C and then for 5 min at 45°C, followed by a brief centrifugation to collect tube contents. The Pre-Hybridization mix was removed from the cartridge and 200 µl of Hybridization Mix were pipetted in. Cartridges were incubated for 16 hours at 45°C and 60 rpm. Arrays were then washed with Wash Buffer A and placed in the Affymetrix GeneChip Command Console Fluidics Control (ThermoFisher Scientific, MA, USA) for staining. Arrays were stained using the Fluidics Protocol FS450_0001.

5.3.2.5. *Microarray data quality control*

Data was analysed in the Affymetrix Expression Console 1.4.1.46 and normalised using the Robust Multi-Array Average (RMA).

5.3.2.6. Microarray data analysis

The Qlucore Omics Explorer software (Qlucore, Lund, Sweden) was used for analysis of the normalised data. Two-group comparisons, setting $p=0.05$ and a fold change of 1.2, were performed (ALS/MND vs Controls) . DAVID Functional Annotation Tool Version 6.7 (NIAID, NIH, USA) and IMPaLA (Integrated Molecular Pathway Level Analysis) were used to perform the functional group and pathway analysis on the lists of differentially expressed genes.

5.3.2.7. qRT-PCR validation of microarray genes of interest

Validation of dysregulated transcripts in ALS/MND FACx neurones was done by qRT-pCR. Validation was conducted in the 6 cases included in the microarray analysis, plus 2 additional control and 3 additional ALS/MND cases (**Table 5.8**). Enriched neuronal RNA samples for the validation experiments were obtained by LCM of FACx frozen sections. This protocol was described previously, in **section 5.3.2.2.** and **section 5.3.2.3.** cDNA was synthesized using the qScript cDNA Supermix (Quanta Biosciences, MA, USA). The PrimeTime qPCR assays (Integrated DNA Technologies®) listed in **Table 5.9** were used for the qRT-PCR. Each sample mix contained 50 ng of cDNA, 500 nM forward and reverse primer, and 250 nM probe, 2 x Brilliant III qPCR Master mix and nuclease free distilled H₂O. qRT-PCR was performed on a 2 step thermal profile on a Stratagene MX3000P™ Real Time Thermal Cycler (Agilent Technologies Ltd). The incubation was performed as follows: 10 minutes at 95°C then 40 cycles of 30 seconds at 95°C, 60 seconds at 60°C and 60 seconds at 72°C. LMNB1 was used as housekeeping gene (HK) and was amplified on each plate. Expression levels were normalised to LMNB1 using the $\Delta\Delta C_t$ calculation.

Group	Case	ID
Control	1	Control 1
	2	Control 2
	3	Control 3
	4	Control 4
	5	Control 5
ALS/MND	1	ALS/MND 1
	2	ALS/MND 2
	3	ALS/MND 3
	4	ALS/MND 4
	5	ALS/MND 5
	6	ALS/MND 6

Table 5.8 Control and ALS/MND selected qRT-PCR validation.

Control and ALS/MND cases selected for LCM isolation of neurones from the FACx. Samples were then processed for qRT-PCR validation of microarray results.

Gene	PrimeTime® Assay ID	Ref Seq	Exon location	Primer Sequence
<i>COX20</i>	COX20 Set 1	NM_198076	1	Probe: 5'-/56-FAM/TGGTGACTT/ZEN/TGGGATGCTGGTTTCA/3IABkFQ/-3' Primer 1: 5'-GATGTTGGAGTAGGAGGGTTTAT-3' Primer 2: 5'-CTGGCAATTCTTTCCTGGATTC-3'
<i>GADD45A</i>	Hs.PT.58.765177	NM_001190481(2)	2-4	Probe: 5'-/56-FAM/ATCCATGTA/ZEN/GCGACTTTCCTCCGGC/3IABkFQ/-3' Primer 1: 5'-GGAGATTAATCACTGGAACCCA -3' Primer 2: 5'-TGTACGAAGCGGCCAAG-3'
<i>SLC25A37</i>	Hs.PT.58.3324071	NM_004360(1)	6-7	Probe: 5'-/56-FAM/TGCTTCACC/ZEN/ACTTCTGCTGGATT/3IABkFQ/-3' Primer 1: 5'-GTGCTGCGAGTTGTACATC-3' Primer 2: 5'-GAAACAGCCACCTAGCCAA-3'

Table 5.9 PrimeTime® qPCR assays used for validation of the transcripts of interest in control, SS and DS-LUHMEs.

PrimeTime® qPCR assays were resuspended in TE buffer to a 20x concentration. The final 1x concentration contained 500 nM primer (forward or reverse) and 250 nM probe.

5.4. Results

5.4.1. Classification of ALS/MND cases according to the p62 pathology is not linked to expression of senescence and DNA damage markers in ALS/MND cases

First, ALS/MND cases were classified according to the p62 pathology present in the FACx, MCx and Sc. **Table 5.10** shows the classification for each case according to the guidelines described in **section 5.3.1.1.1**. **Figure 5.2** shows the different p62 structures identified in the FACx and MCx of ALS/MND cases. Four cases were identified as FTLD-TDP type B; these cases had moderate neuronal cytoplasmic inclusions (NCI) and few dystrophic neurites (DN) in all cortical layers. Two cases had minimal p62 pathology and were identified as FTLD-MC (minimal change). The remaining two cases did not show cortical p62 pathology and were identified as FTLD-0. For the statistical analysis, FTLD-MC and FTLD-0 cases were analysed as a single group (FTLD-MC/0).

Case	FTLD pattern
LP8310	B (<i>C9orf72</i> ⁺)
LP5909	MC
LP2408	0
LP1411	MC
LP6909	B (<i>C9orf72</i> ⁺)
LP6608	B (<i>C9orf72</i> ⁺)
LP9608	0
LP4104	B (<i>C9orf72</i> ⁺)

Table 5.10 Classification of ALS/MND cases according to their p62 pathology.

Following the guidelines proposed by McKenzie et al. (2011), 4 ALS/MND cases were classified as FTLD-TDP type B. The other four cases were either classified as having minimal changes (MC) or no p62 pathology (0).

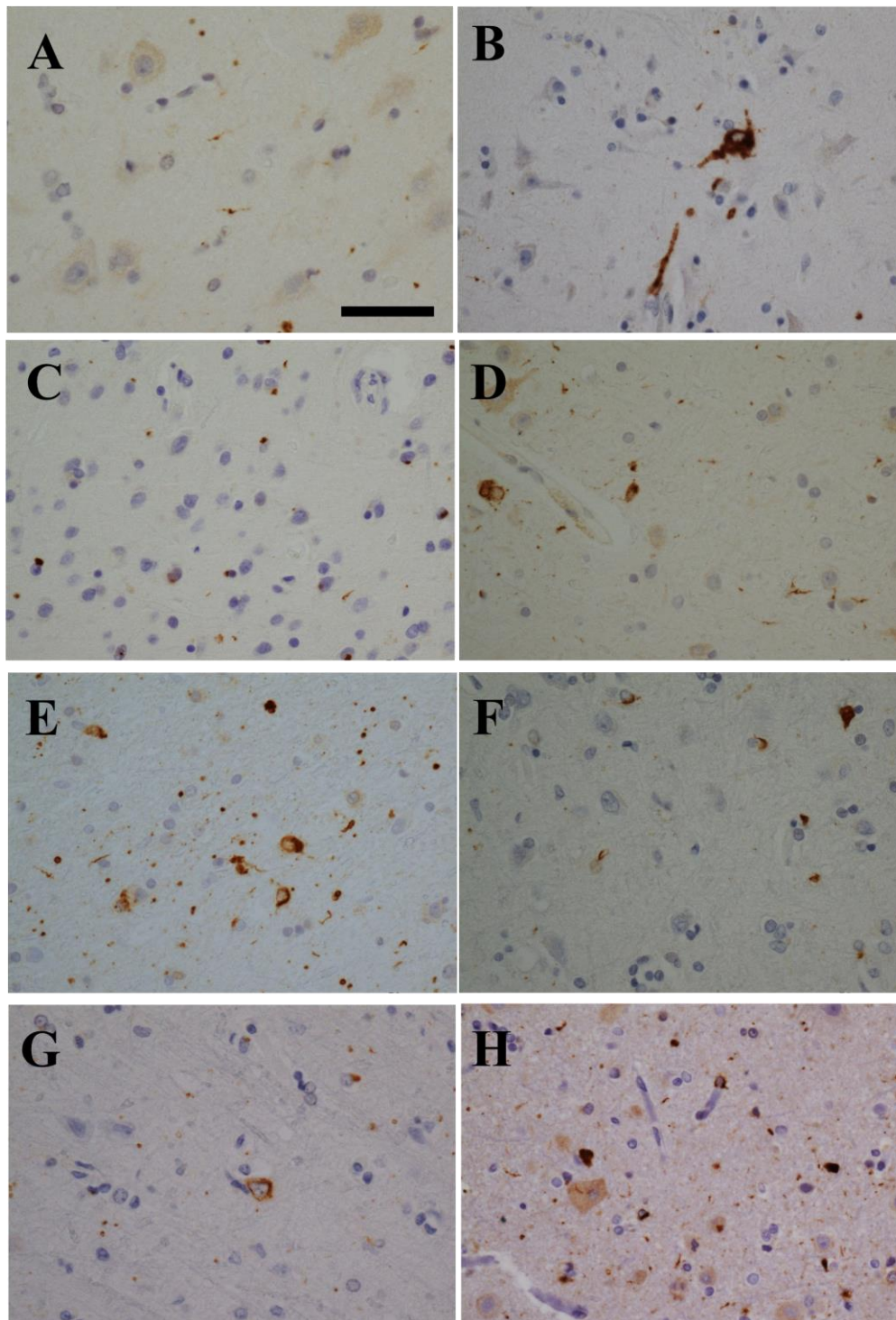


Figure 5.2. Classification of ALS/MND cases according to p62 pathology.

Representative images of specific p62 structures in ALS/MND cases. **A.** Threads observed in the FACx. **B.** Diffuse neuronal reactivity in the FACx, **C.** NCI with occasional DN in the FACx. **D.** GCI and DN in the MCx. **E.** NCI, GCI and DN in the MCx. **F.** GCI in the MCx. **G.** NCI in the MCx. **H.** NCI, GCI and DN in the MCx. Scale bar represents 50 μm .

5.4.2. SA- β -gal activity is a feature of brains from ALS/MND and control donors

Histochemical detection of increased activity of SA- β -gal in ALS/MND and control donors revealed glial and neuronal activity in the FACx, MCx and Sc, which was identified as a blue cytoplasmic precipitate. The intensity and pattern of the blue precipitate that indicates enzyme activity was variable between brain regions and groups. Due to this variability, quantification of SA- β -gal positive cells was not pursued, but a thorough descriptive analysis was performed instead. Two of the 9 available control MCx cases had intense cytoplasmic staining in neurones as well as in glial cells from the grey and white matter (**Figure 5.3B**); however, the FCx sections from these same cases showed only weak granular cytoplasmic staining in both cell types (**Figure 5.3D**), or no staining at all. The remaining control cases (7 MCx and 4 FCx) had either weak or no detectable staining in neurones and glia (**Figure 5.3A** and **Figure 5.3C**). Sc sections from control donors showed various staining patterns as well: 1 case had intense neuronal cytoplasmic blue staining and widespread cytoplasmic glial staining; the remaining 4 controls had a less intense, granular cytoplasmic staining in some neurones (**Figure 5.3C** and **Figure 5.3F**), while glial staining was very intense in some cases (2) and weak and localised (2) in others.

A similar result was obtained from SA- β -gal staining in ALS/MND brains (**Figure 5.4**). Neurones with intense staining were detected in 3 cases in the MCx (**Figure 5.4A** and **Figure 5.4D**); the remaining 5 cases showed either weak or no neuronal staining at all. Analysis of the staining in the FACx revealed 3 cases with strong neuronal staining (**Figure 5.4E**), which were not necessarily the same cases with SA- β -gal⁺ neurones in the MCx. The remaining cases (5) showed weak and granular neuronal staining in the FACx (**Figure 5.4B**). SA- β -gal⁺ neurones were found in Sc sections from 3 ALS/MND donors;

these cases also showed intense glial staining (**Figure 5.4C** and **Figure 5.4F**). In the remaining 6 ALS/MND Sc sections neurones showed a weak granular staining or no staining at all.

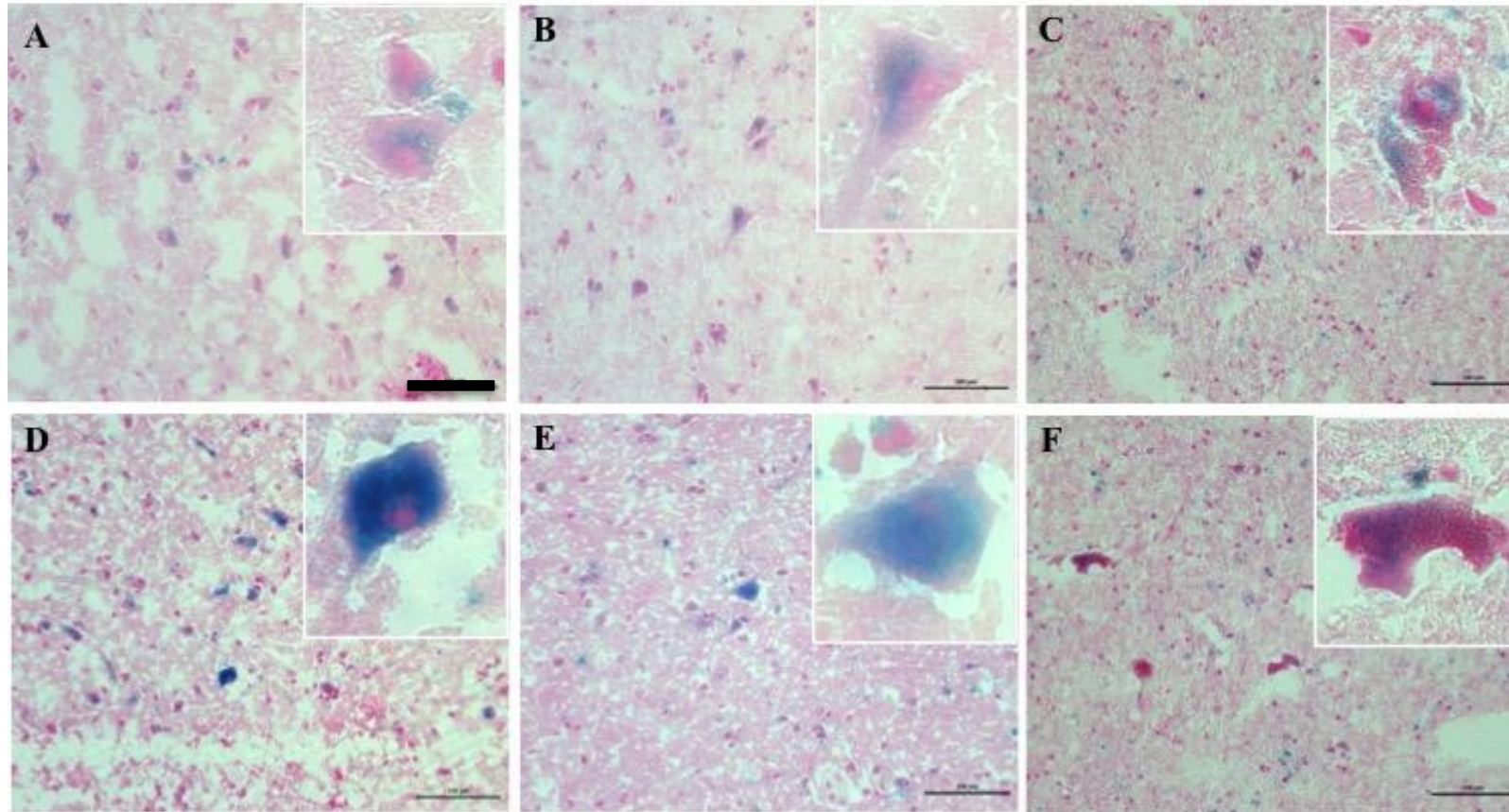


Figure 5.3 Representative images of SA- β -gal activity in brains of two control donors.

SA- β -gal activity was detected in the MCx (**A-D**), FACx (**B-E**) and Sc (**C-F**) of controls and ALS/MND donors following a histochemical protocol based on the cleavage of the SA- β -gal substrate X-gal. SA- β -gal activity was visualised as a blue precipitate and was localised to neurones and glia in the grey matter. Intense neuronal staining was seen in some control sections (**D-E**), however, it was also possible to detect neurones with faint granular staining (**A, B, C** and **F**). Scale bar represents 100 μ m.

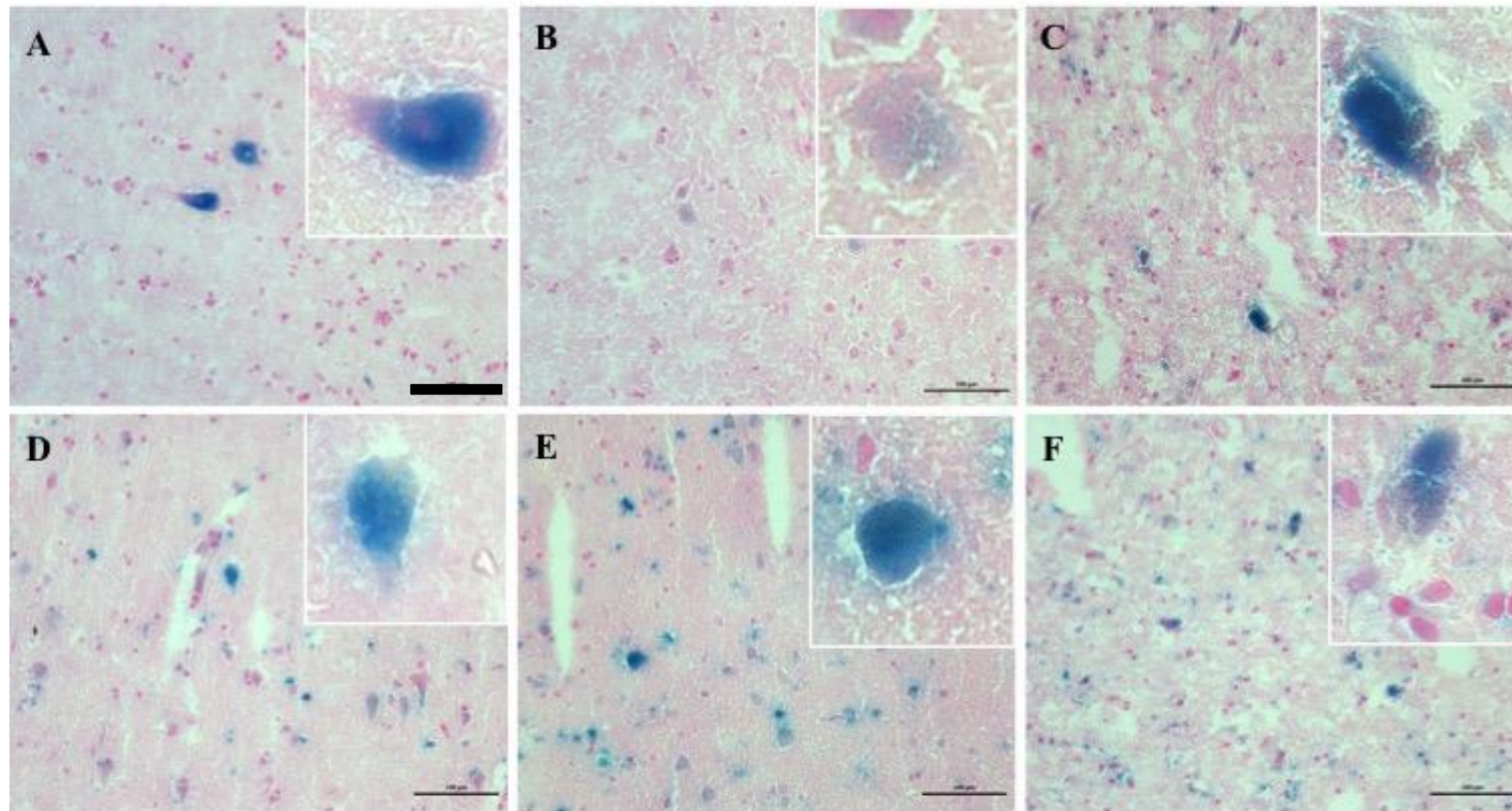


Figure 5.4 Representative images of SA- β -gal activity in brains of two ALS/MND donors.

SA- β -gal activity was detected in the MCx (A-D), FACx (B-E) and Sc (C-F) of ALS/MND donors. SA- β -gal activity was present in neurones and glia in the grey matter, however the staining intensity and pattern differed between cases and brain regions. In the FACx of these two cases (B and E) it is possible to see very faint granular neuronal staining (B) against an intense neuronal staining. Scale bar represents 100 μ m.

Even though this study focused on detection of SA- β -gal⁺ neurones, a descriptive analysis of glial staining in the white matter of controls and ALS/MND donors was also conducted, since white matter staining exemplified perfectly the variability in the SA- β -gal activity that could be seen within groups. Images of the white matter from 4 controls and 4 ALS/MND donors are shown in **Figure 5.5**. The intensity of SA- β -gal staining was very variable, from non-existing (**Figure 5.5A** and **Figure 5.5E**) to a strong blue (**Figure 5.5D** and **Figure 5.5H**). The spread of the staining also varied. Some cases had sporadic SA- β -gal⁺ glial staining (**Figure 5.5B-D** and **Figure 5.5F**), while others showed a higher number of SA- β -gal⁺ glial cells throughout the white matter (**Figure 5.5G-H**).

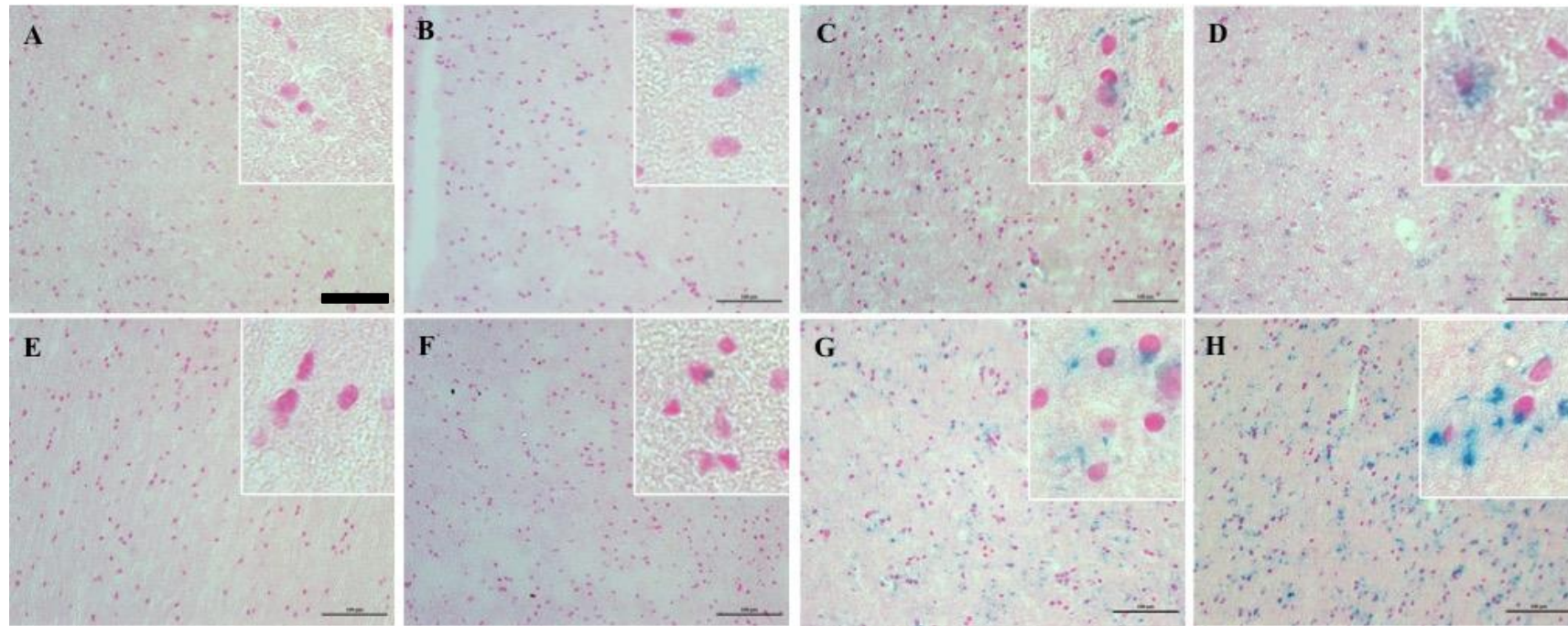


Figure 5.5 Representative images of SA-β-gal activity in the white matter of control and ALS/MND donors.

SA-β-gal activity was detected in the white matter of controls and ALS/MND donors. Blue staining was localised to the cytoplasm of glial cells of control (A-D) and ALS/MND donors (E-H). The intensity as well as the quantity of SA-β-gal⁺ cells was highly variable between cases and groups. Scale bar represents 100 μm.

5.4.3. Expression of p16 is exclusive to glial cells

Immunohistochemistry for p16 resulted in nuclear and cytoplasmic staining of glial cells. The cytoplasmic staining was localised to the processes of cells resembling reactive astrocytes (**Figure 5.6A-B** and **Figure 5.6D-E**). The majority of controls and ALS/MND cases showed some level of p16⁺ glial staining in the grey matter of MCx and FACx sections (**Figure 5.6A-B** and **Figure 5.6D-E**). In the Sc, p16 was also localised to the nuclei of glial cells present in the anterior horn; however, cytoplasmic staining of motor neurones was detected in 6 of 11 controls and 4 of 10 ALS/MND cases. Cytoplasmic staining of motor neurones differed in intensity between cases. (**Figure 5.6C** and **Figure 5.6F**). Double staining for p16 and GFAP confirmed the expression of p16 in the nuclei of astrocytes and in some cases, in the cytoplasm of GFAP⁺ astrocytes. However, not all GFAP⁺ astrocytes were positive for p16 (**Figure 5.7**).

The percentage of p16⁺ glial cells in the FACx sections was significantly higher in ALS/MND ($p=0.015$) donors compared to controls (**Figure 5.8B**). No difference was detected in the MCx ($p=0.965$) (**Figure 5.8A**). Calculation of Cohen's r suggested a large effect size ($r=0.541$) of the difference in the percentage of p16⁺ glia in the FACx between groups.

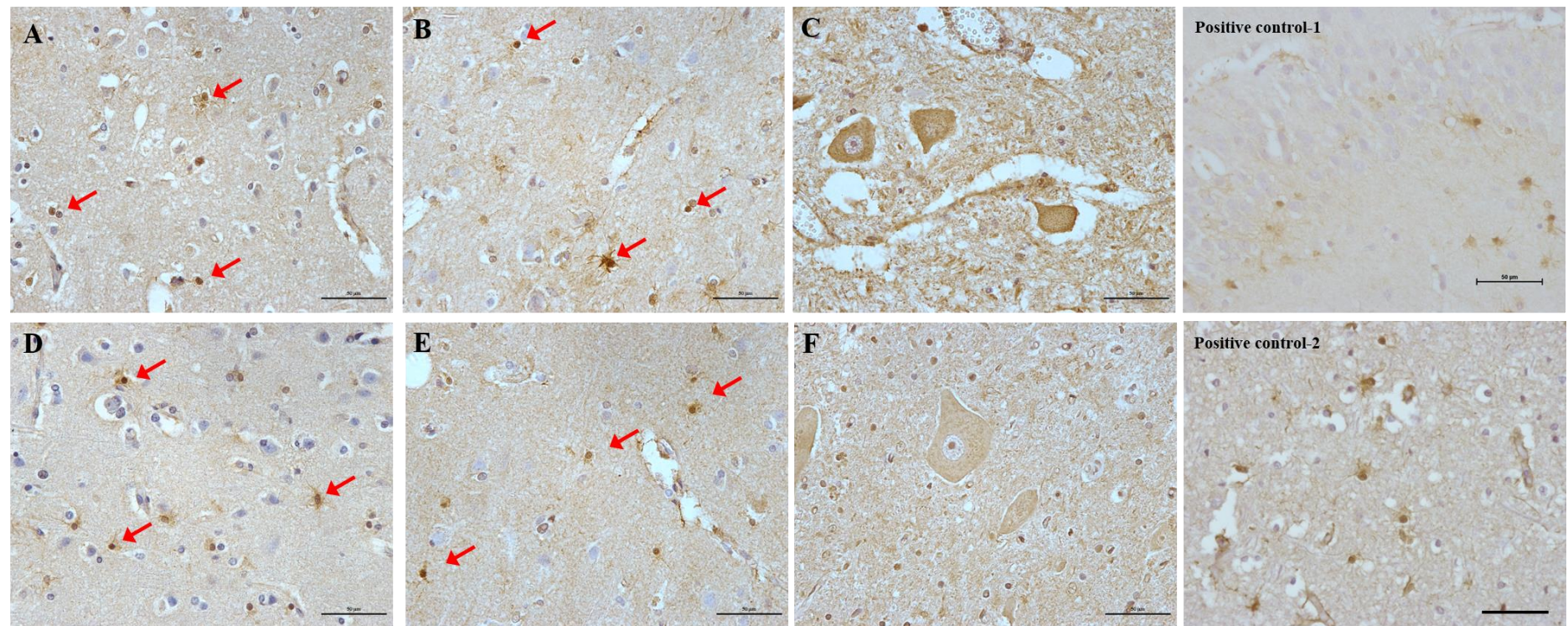


Figure 5.6 Representative images of p16 staining in control and ALS/MND brains.

Expression of p16 in MCx, FACx and Sc of control (**A, B, C**) and ALS/MND donors (**D, E, F**) was assessed by immunohistochemistry. Staining was predominantly localised to the nuclei of glial cells however, cytoplasmic staining was also present in some of these cells and in Sc motor neurones. Previously studied sections from the hippocampus and frontal cortex of AD patients were included as positive controls. Scale bar represents 50 µm.

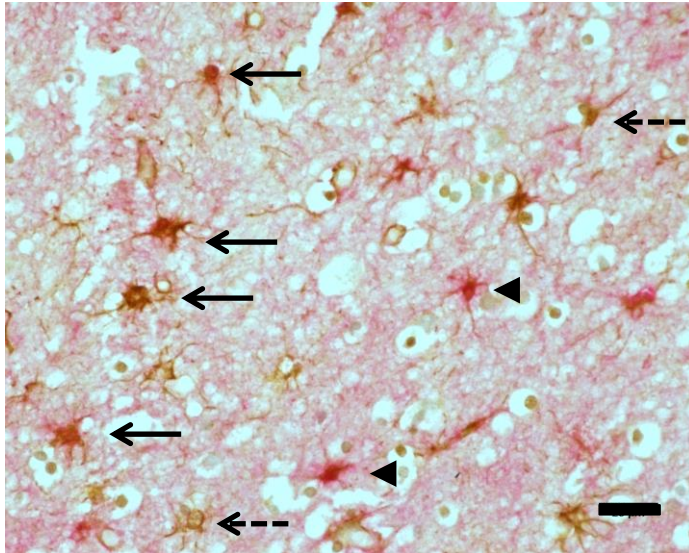


Figure 5.7 Representative images of dual immunostaining for p16/GFAP.

FACx and MCx FFPE sections were stained for p16 using an ABC-HRP method, which can be seen as a brown precipitate. GFAP staining was visualised using an ABC-alkaline phosphatase method, which results in a red precipitate. Arrows show colocalisation of p16 and GFAP, confirming expression of p16 in astrocytes. p16⁺/GFAP⁻ glial cells (dotted arrows), as well as p16⁻/GFAP⁺ (arrowheads) cells were also detected. Scale bar represents 25 μ m.

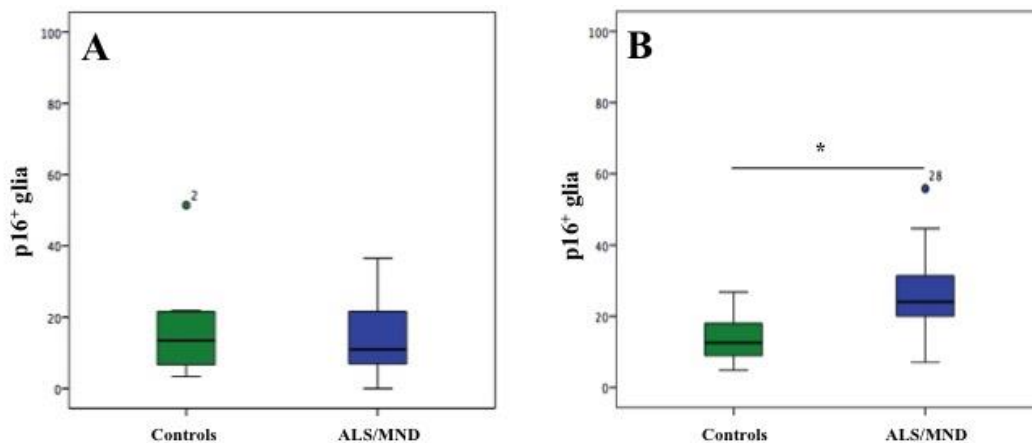


Figure 5.8 Quantitative analysis of p16⁺ glial cells in control and ALS/MND brains.

Box plots showing the percentage of p16⁺ glial cells in the MCx (A) and FACx (B) of ALS/MND and control donors. Quantitation of p16 staining revealed a significantly higher percentage of p16⁺ glial cells in the FACx of ALS/MND donors but not in the MCx (Mann Whitney-U Test; * $p < 0.05$).

5.4.4. Expression of p21 is detected in glial and neuronal nuclei

Immunohistochemistry for p21 revealed expression of this marker in both neurones and glia in the MCx, FACx and Sc of ALS/MND and control donors (**Figure 5.9**). The staining was mainly nuclear, although there were a few ALS/MND and control cases with neuronal and glial cytoplasmic staining, as seen in **Figure 5.9A-B** (MCx and FACx – control), and **Figure 5.9D-E** (MCx and FACx – ALS/MND). Glial cytoplasmic staining localised to the processes of what looked like reactive astrocytes. To confirm this, a double staining for GFAP and p21 was performed, resulting in co-localisation of both markers. Double immunohistochemistry also showed that not all GFAP⁺ astrocytes were positive for p21 and viceversa (**Figure 5.10**). Double labelling for p21/NeuN was also conducted and results confirmed expression of p21 in pyramidal neurones of the MCx and FACx of control and ALS/MND donors (**Figure 5.11**). p21⁺ motor neurones were detected in Sc sections of ALS/MND and control cases; nuclear staining in neurones was seen in 2 ALS/MND cases and 8 controls (**Figure 5.9C**), but cytoplasmic staining was seen in 3 ALS/MND donors and 9 controls as well. (**Figure 5.9F**).

Quantitative analysis of p21⁺ glia and neurones focused on nuclear staining only. The percentage of p21⁺ glial cells was not significantly different in the MCx of ALS/MND donors when compared to controls ($p=0.515$), but a significantly higher percentage of p21⁺ glia was detected in the FACx ($p=0.019$) (**Figure 5.12A** and **Figure 5.12C**). Calculation of Cohen's r suggested a medium to large effect size ($r=0.477$) of the difference in the percentage of p21⁺ glia in the FACx between groups.

Quantification of p21⁺ neuronal nuclei resulted in a significantly higher percentage in the FACx ($p=0.035$) as well, but not in the MCx of ALS/MND donors ($p=0.360$) (**Figure**

5.12B and **Figure 5.12D**). Calculation of Cohen's r suggested a large effect size ($r=0.524$) of the difference in the percentage of p21⁺ neurones in the FAcx between ALS/MND and control donors.

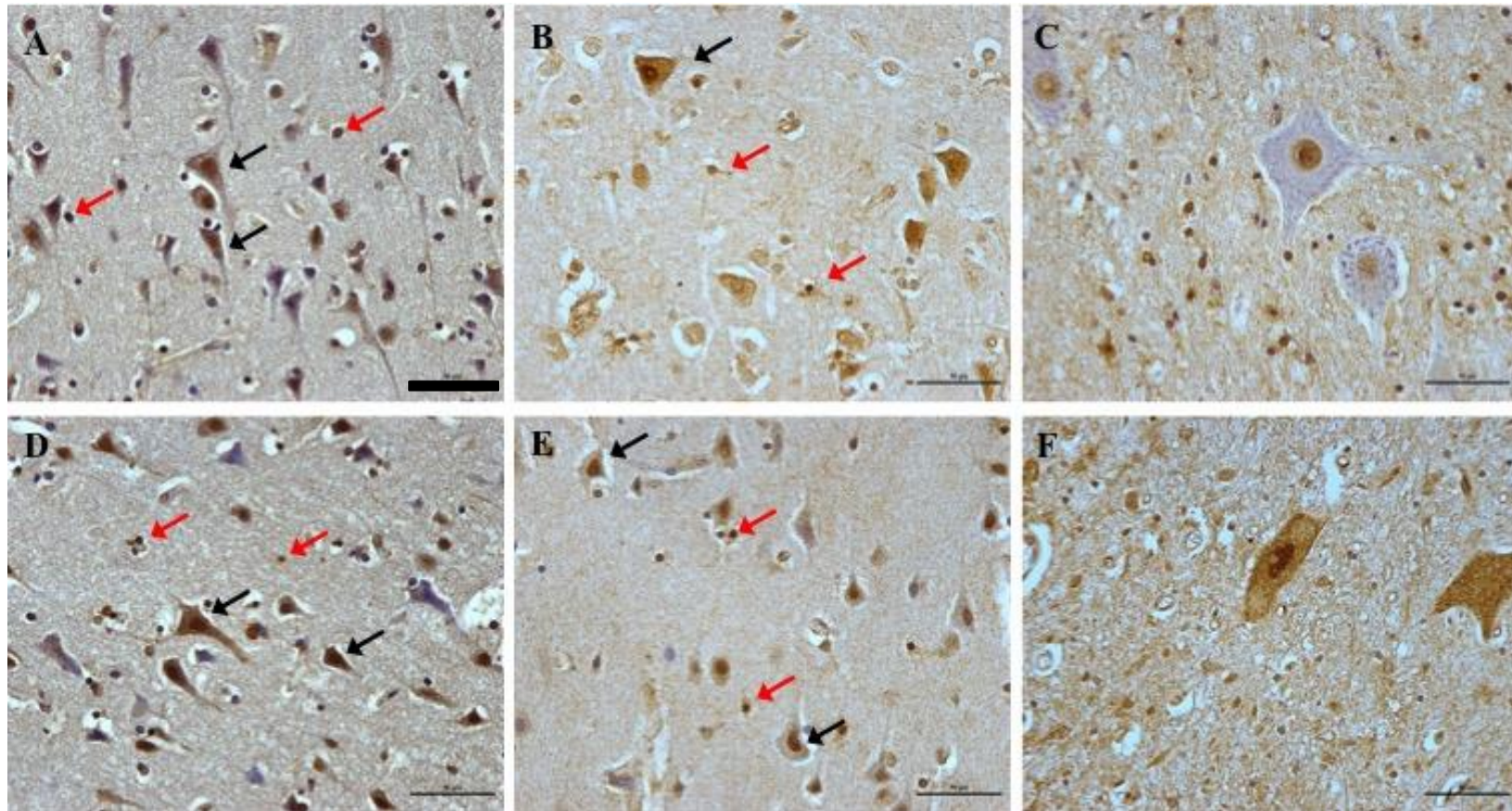


Figure 5.9 p21 staining on controls and ALS/MND brains (Mcx, Fcx, Sc).

Expression of p21 in MCx, FACx and Sc of control (A, B, C) and ALS/MND donors (D, E, F) was assessed by immunohistochemistry. Staining was localised to the nuclei of glial (red arrows) and neuronal cells (black arrows). Cytoplasmic staining was also detected in some neurones and glia (most probably reactive astrocytes). Expression of p21 was seen in motor neurones; some cases exhibited nuclear staining (C) while others also had cytoplasmic staining (F). Scale bar represents 50 μm.

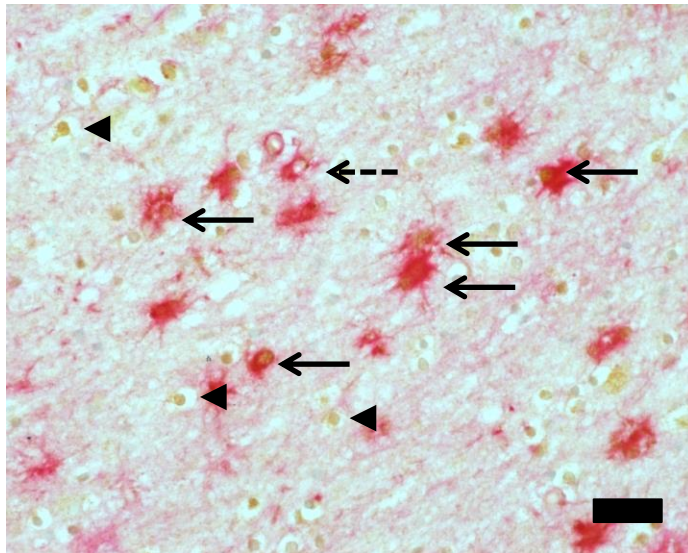


Figure 5.10 Representative images of dual immunostaining for p21/GFAP.

FACx and MCx FFPE sections were stained for p21 using an ABC-HRP method, which can be seen as a brown precipitate. GFAP staining was visualised using an ABC-alkaline phosphatase method, which results in a red precipitate. Arrows show colocalisation of p21 and GFAP, confirming expression of p21 in astrocytes. p21⁺/GFAP⁻ glial cells (arrowheads), as well as p21⁻/GFAP⁺ (dotted arrows) cells were also detected. Scale bar represents 25 μ m.

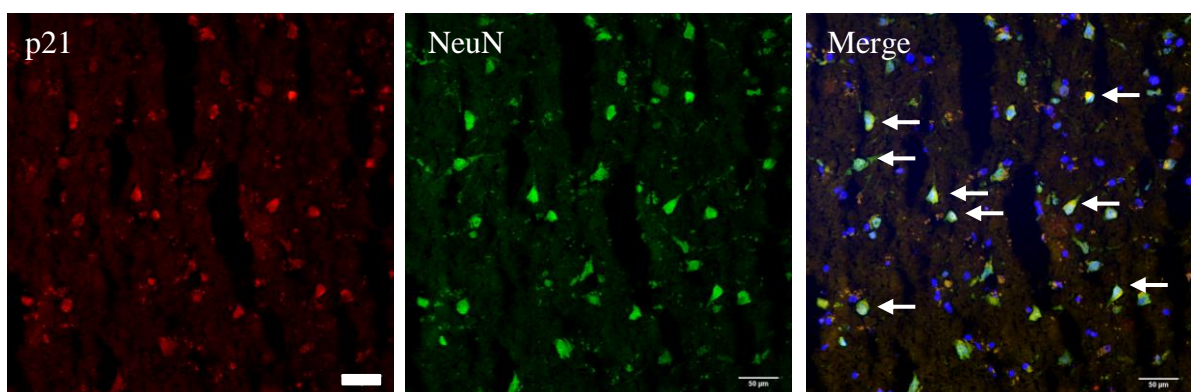


Figure 5.11 Representative images of double fluorescence immunostaining for p21/NeuN.

FACx and MCx frozen sections were stained for p21 and NeuN using double fluorescence approach. p21 expression (red) colocalised with NeuN⁺ neurones (green) (arrows in Merge). Nuclei were stained with Hoechst. Scale bar represents 50 μ m.

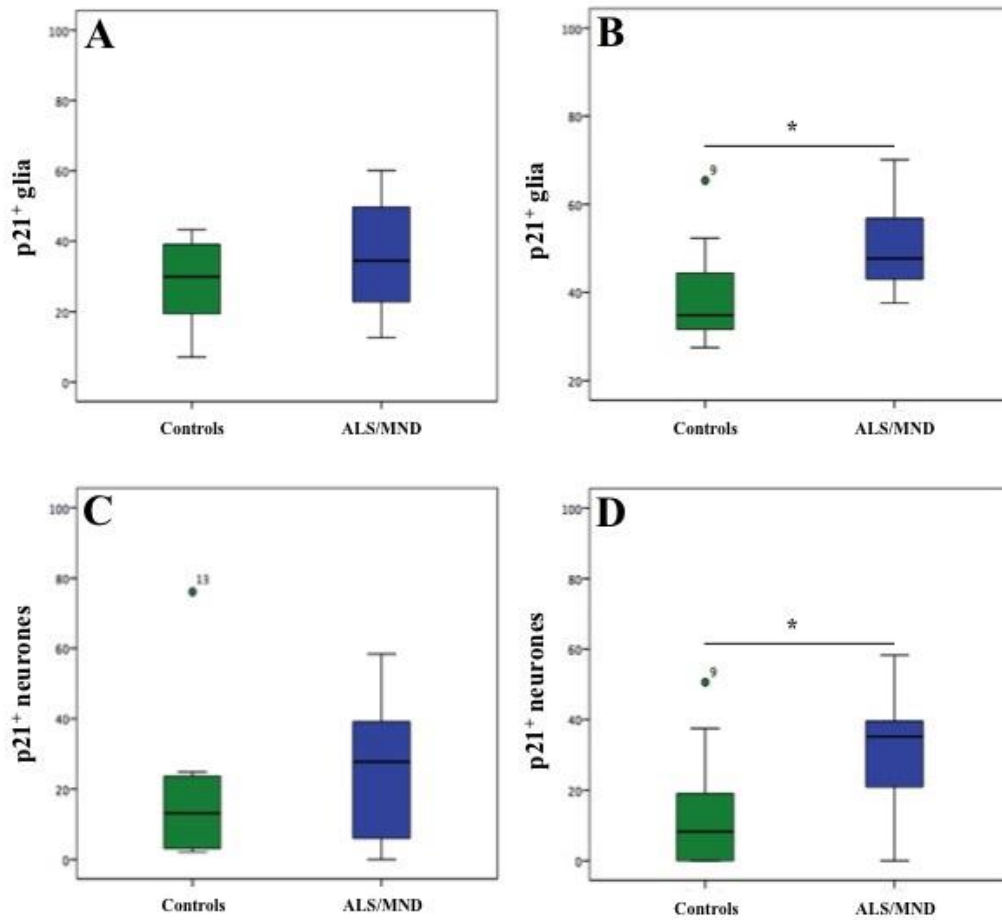


Figure 5.12 Quantitative analysis of p21+ glial and neuronal cells in control and ALS/MND brains.

A-B. Box plots showing the percentage of p21+ glial cells in the MCx (**A**) and FACx (**B**) of ALS/MND and control donors. Quantitation of p21 staining revealed a significantly higher percentage of p21+ glial cells in the FACx of ALS/MND donors but not in the MCx. **C-D.** Box plots showing the percentage of p21+ neurones in the MCx (**A**) and FACx (**B**) of ALS/MND and control donors. Quantitation of p21+ neurones indicated a significantly higher percentage of p21+ neurones in the FACx of ALS/MND donors but not in the MCx (Mann Whitney-U Test; * $p < 0.05$).

5.4.5. Expression of p16 and p21 in the occipital cortex of ALS/MND and control donors

Detection of p16 and p21 senescence markers was also conducted in the occipital cortex (OCx). This brain region was included in the study as a comparison region not pathologically involved in ALS/MND, even in late stage disease. Results revealed expression of p16 in glial cells (**Figure 5.13A**) and expression of p21 in glia and neurones (**Figure 5.13B**) in both control and ALS/MND cases. These results correlated with what was seen in the MCx and FACx. Quantitation of p16⁺ glial cells and p21⁺ glia/neurones did not reveal a significant difference in the percentage of immunoreactive glia to p16 and glia/neurones to p21 in ALS/MND cases when compared to controls (**Figure 5.14**).

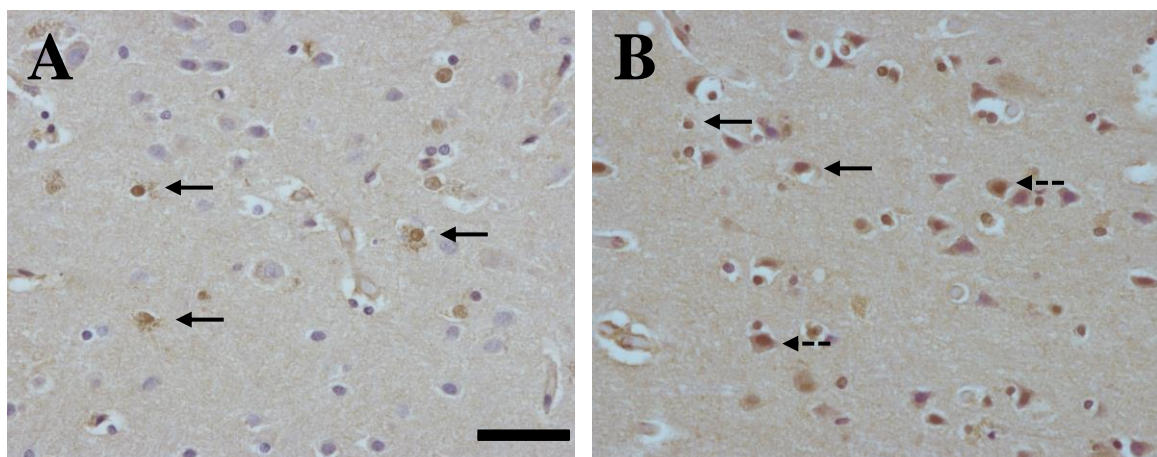


Figure 5.13 Representative images of p16 and p21 staining in the OCx of ALS/MND and control donors.

Expression of glial (arrows) p16 (**A**) and glial (arrows) and neuronal (dotted arrows) p21 (**B**) in the OCx of ALS/MND and control cases was detected by immunohistochemistry. Scale bar represents 50 μ m.

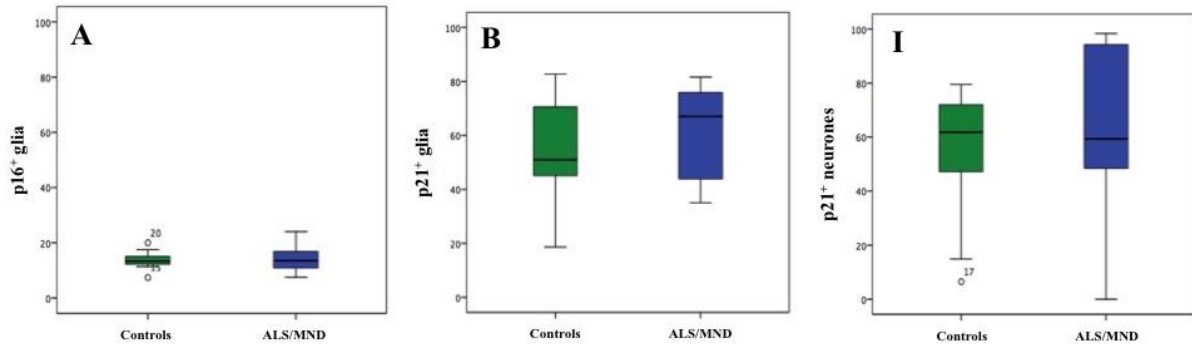


Figure 5.14 Quantitative analysis of p16 and p21 immunohistochemistry in the OCx.

Box plots indicating the percentage of p16⁺ glia (A), p21⁺ glia (B) and p21⁺ neurones (C) in the OCx of ALS/MND and control donors. Even though expression of both markers was present in this brain area, there was no significant difference in the percentage of positive p16 glia and p21 glia/neurones in ALS/MND donors (Mann Whitney-U Test).

5.4.6. Detection of DNA damage and DNA damage response markers

5.4.6.1. γ H2AX expression in ALS/MND and control brains

After identifying the expression of p16 and p21 cell cycle checkpoint proteins in the brain of ALS/MND and control donors, markers of oxidative DNA damage and of a DDR were assessed in the same brain areas. γ H2AX immunohistochemical detection showed expression of this marker in the nuclei of neurones and glia. The presence of γ H2AX⁺ cells was localised in both ALS/MND and control donors, in the MCx (**Figure 5.15A**) and FACx (**Figure 5.15B**). Quantification of γ H2AX⁺ glia in the MCx and FACx did not show a significant difference in the percentage of positive glia between ALS/MND and control cases (**Figure 5.16A-B**). Moreover, quantification of γ H2AX⁺ showed no difference in the percentage of positive neurones in ALS/MND cases either (**Figure 5.16C-D**).

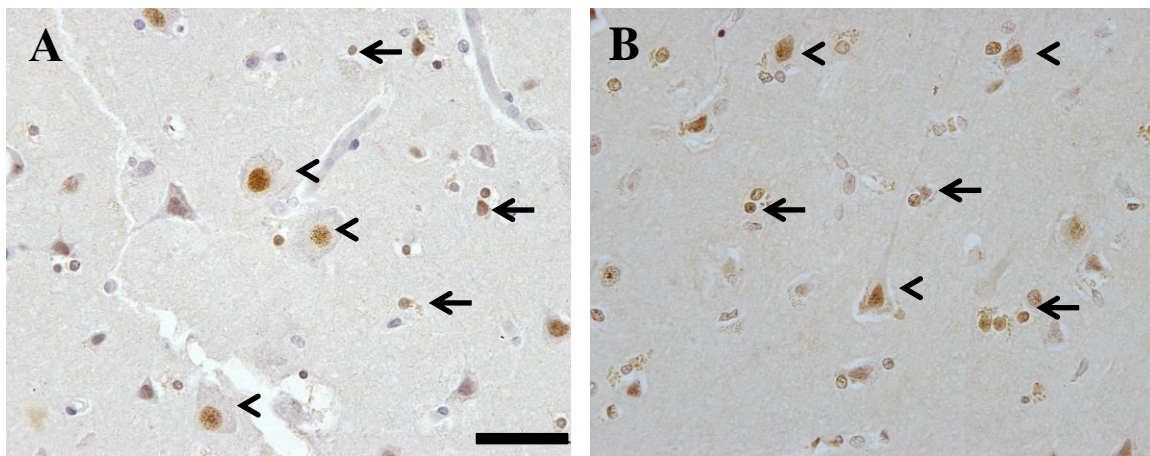


Figure 5.15 Representative images γ H2AX staining in the MCx and FACx of ALS/MND donors.

Phosphorylation of H2AX was detected in neurones and glial cells of ALS/MND cases and controls in both the MCx (**A**) and FACx (**B**) brain areas. Arrows indicate γ H2AX⁺ glia and arrowheads indicate γ H2AX⁺ neurones. Scale bar represents 50 μ m.

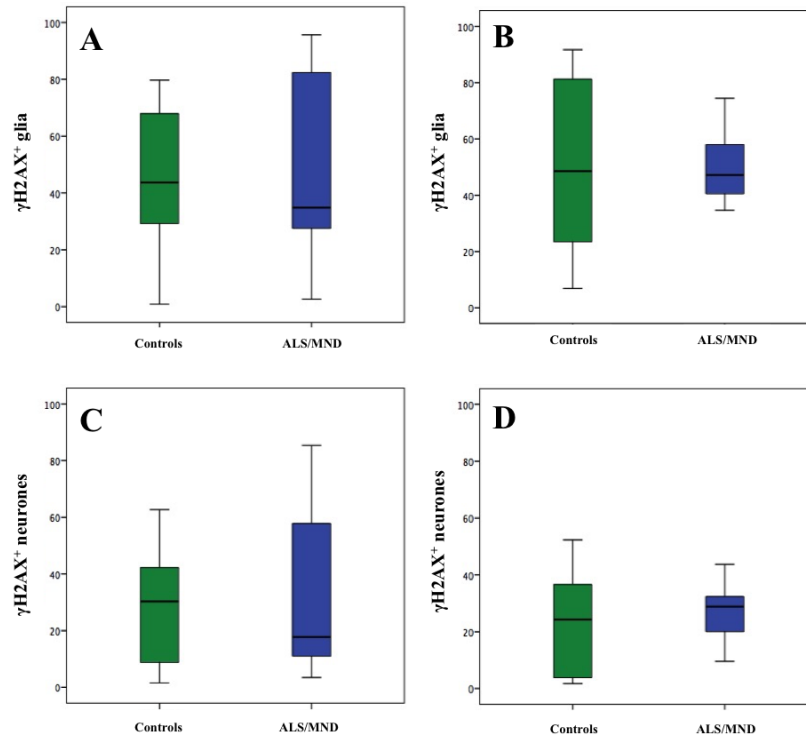


Figure 5.16 Quantitative analysis of γ H2AX+ cells.

The percentage of γ H2AX+ glia and neurones in the MCx and FACx was assessed using the image analysis software Cell[^]R. Box plots **A** and **C** show no difference in the percentage of γ H2AX+ glia and neurones in the MCx between ALS/MND and control donors. Box plots **B** and **D** indicate no significant difference in the percentage of γ H2AX+ glia and neurones in the FACx of ALS/MND cases when compared to controls (Mann Whitney-U test).

5.4.6.2. 8-OHdG expression in ALS/MND and control brains

Immunohistochemical detection of oxidative DNA damage was done using an antibody against 8-OHdG, one of the main products of nucleic acids oxidation. 8-OHdG was present in the cytoplasmic and nuclear compartments of glia and neurones, which would account for both RNA and DNA oxidation (Figure 5.17). The percentage of 8-OHdG⁺ nuclei of pyramidal neurones in ALS/MND and control donors did not differ significantly in the MCx ($p=0.968$) (Figure 5.17A) and in the FACx ($p=0.165$) (Figure 5.17B).

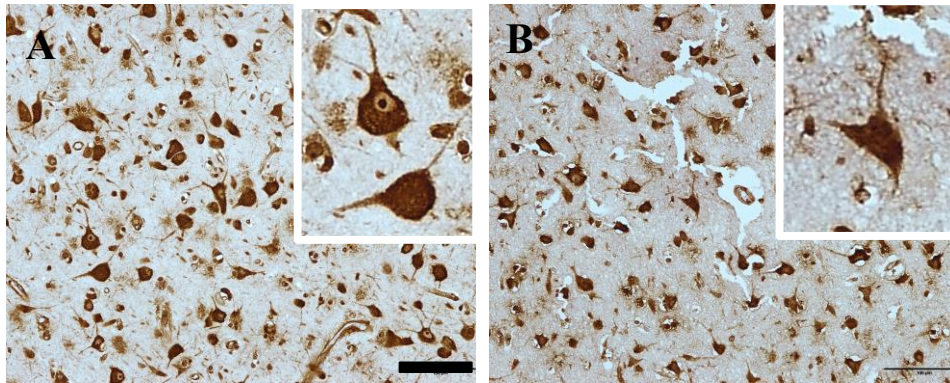


Figure 5.17 Representative images of 8-OHdG in ALS/MND and controls.

Immunohistochemistry for 8-OHdG was performed on MCx (A) and FACx (B) sections from ALS/MND and control donors. Cytoplasmic and nuclear staining was detected in glia and neurones in both brain areas; also, some neurones exhibited only cytoplasmic staining (A) but the quantitative analysis focused on neuronal nuclear staining. Scale bar represents 100 μm .

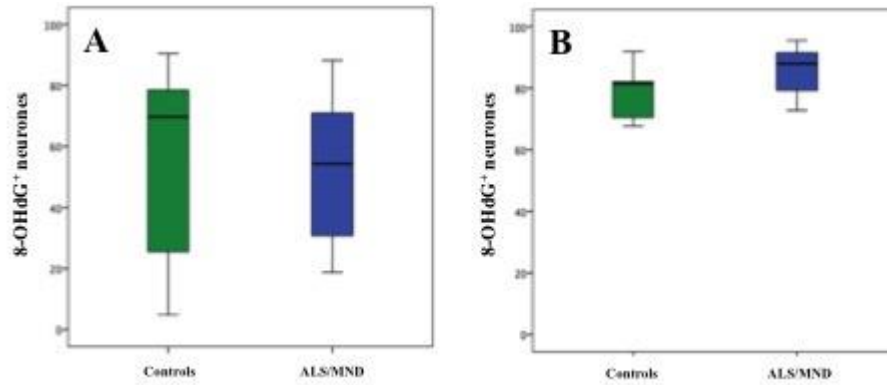


Figure 5.18 Quantitative analyses of 8-OHdG⁺ neurones.

The percentage of 8-OHdG⁺ nuclei of pyramidal neurones in the MCx and FACx was assessed using the image analysis software Cell[^]R. Box plots show no difference in the percentage of 8-OHdG⁺ neurones in the MCx (A) and FACx (B) between ALS/MND and control donors (Mann Whitney-U Test).

5.4.6.3. Association between DNA damage and senescence markers in neurones

To determine the relationship between the expression of p21 and the DNA damage markers 8-OHdG and γ H2AX in neurones, a statistical dependence analysis between these variables was conducted. **Figure 5.19** shows scatterplots displaying the relationship between 8-OHdG⁺ and γ H2AX⁺ neurones in the MCx (**Figure 5.19A**) and FACx (**Figure 5.19B**) of ALS/MND donors. No significant correlation was found between 8-OHdG and γ H2AX markers in neurones in the MCx ($\rho=-0.115$, $p=0.751$) or the FACx, ($\rho=-0.297$, $p=0.405$) of ALS/MND donors. The association analysis between the percentages of p21⁺ and γ H2AX⁺ did not show a significant correlation in the MCx ($\rho=-0.067$, $p=0.855$) (**Figure 5.20A**) or the FACx ($\rho=-0.176$, $p=0.627$) (**Figure 5.20B**) brain regions either. Finally, determination of the relationship between p21⁺ and 8-OHdG⁺ neurones did not indicate a significant correlation between these two markers in MCx neurones ($\rho=0.224$, $p=0.533$) (**Figure 5.21A**) or in the FACx neurones ($\rho=0.479$, $p=0.162$) of ALS/MND donors (**Figure 5.21B**).

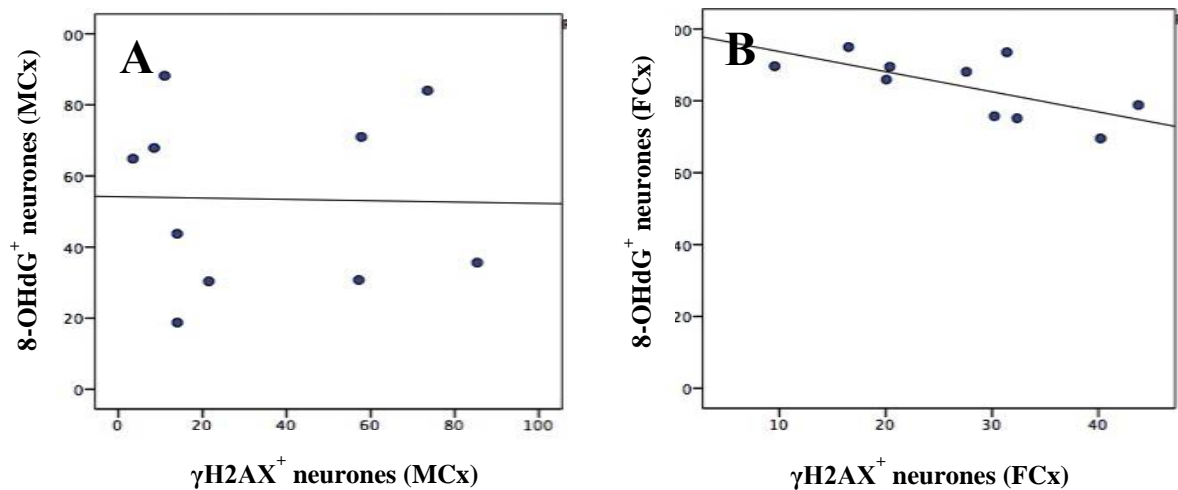


Figure 5.19 Association between 8-OHdG⁺ and γH2AX⁺ neurones in ALS/MND brains.

Scatterplots showing no significant correlation between the percentages of 8-OHdG⁺ and γH2AX⁺ neurones in the MCx (A) and FACx (B) of ALS/MND cases. Correlation was determined using Spearman's rank correlation coefficient (rho).

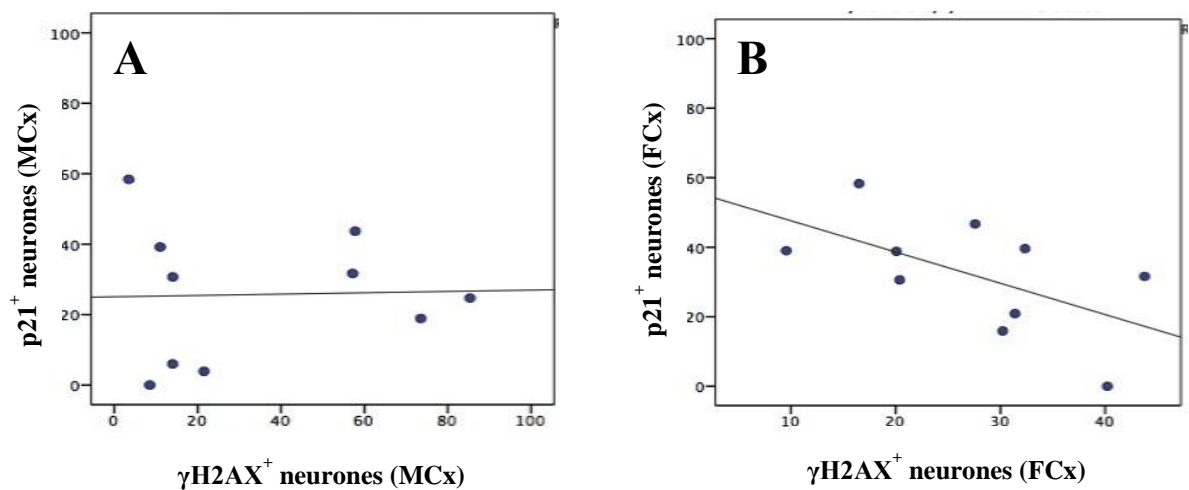


Figure 5.20 Association between p21⁺ and γH2AX⁺ neurones in ALS/MND brains.

Scatterplots showing no significant correlation correlations between the percentages of p21⁺ and γH2AX⁺ neurones in the MCx (A) and FACx (B) of ALS/MND cases. Correlation was determined using Spearman's rank correlation coefficient (rho).

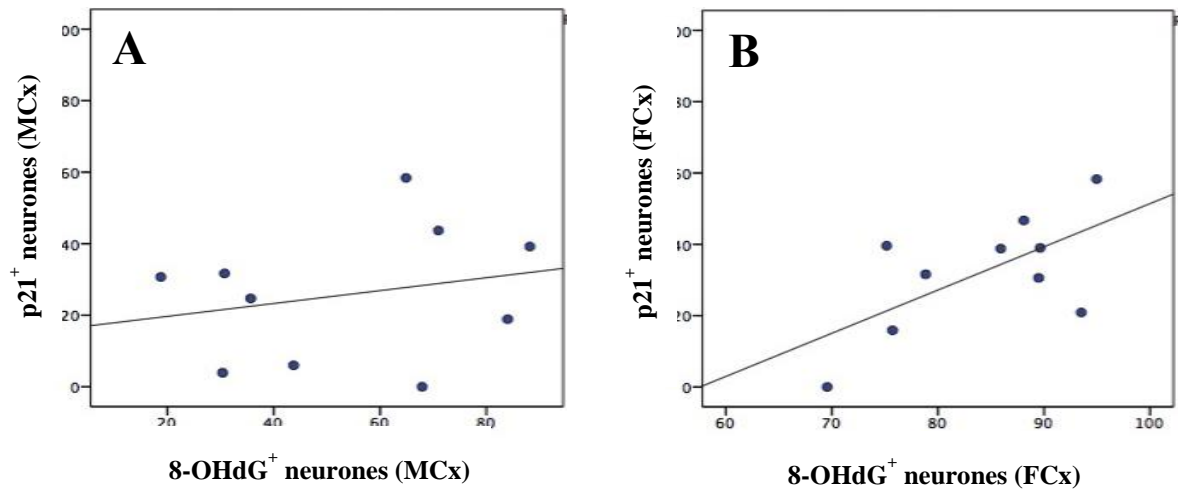


Figure 5.21 Association between p21⁺ and 8-OHdG⁺ neurones in ALS/MND brains.

Scatterplots showing no significant correlation between the percentages of p21⁺ and 8-OHdG⁺ neurones in the MCx (**A**) and FACx (**B**) of ALS/MND donors. Correlation was determined using Spearman's rank correlation coefficient (ρ).

5.4.7. Microglial activation in the FACx of ALS/MND cases

To investigate whether the significantly higher expression of p21 in neurones and glia and p16 in glia in the FACx were related to a SASP-like phenotype in the brain of ALS/MND donors, microglial activation was assessed by looking at the expression of MHC class II and CD68 in this brain region. CD68 immunoreactive microglia was present in the FACx of both controls and ALS/MND cases. The morphology of CD68⁺ microglia was mainly ramified in both control and ALS/MND cases (**Figure 5.22A-B**), and no amoeboid microglia were detected. Quantification of the % immunoreactive area for CD68 expression confirmed no significant difference between ALS/MND cases and controls (**Figure 5.24A**). MHC class II staining was also present in controls and ALS/MND cases and it was not evident if there was up-regulation of MHC class II expression in ALS/MND donors (**Figure 5.23**). The quantitative analysis showed no difference in the % area of immunoreactivity to MHC class II in the FACx of ALS/MND cases when compared to controls (**Figure 5.24B**).

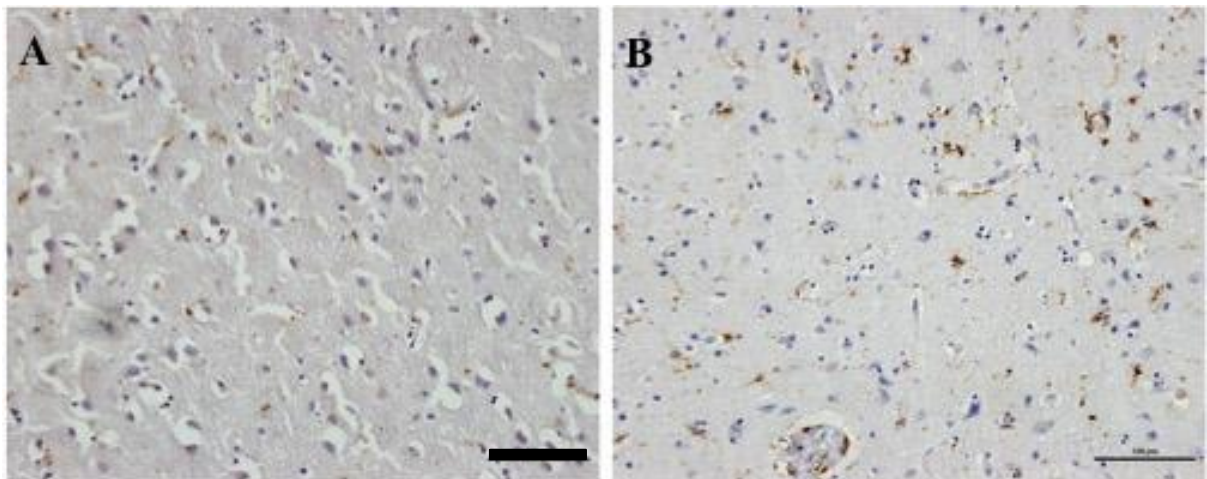


Figure 5.22 Representative images of CD68⁺ microglia in the FACx of ALS/MND and control donors.

Immunohistochemistry for CD68 revealed the presence of immunopositive microglia with a ramified phenotype in the FACx of controls (**A**) and ALS/MND (**B**) cases. Scale bar represents 100 μ m.

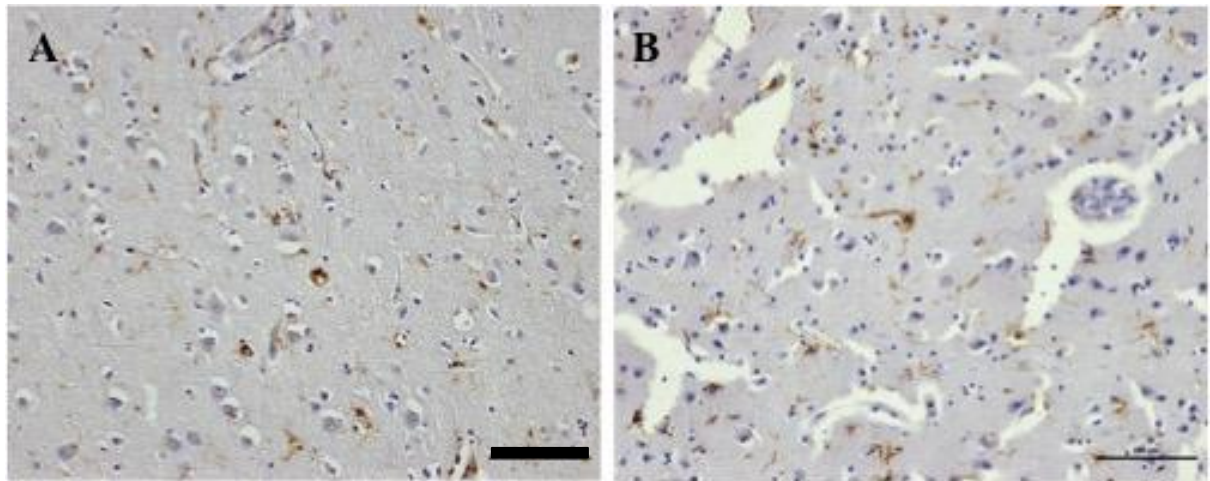


Figure 5.23 Representative images of MHC II+ microglia in the FACx of ALS/MND and control donors.

Immunohistochemistry for MHC class II revealed the presence of immunopositive microglia in the FACx of controls (A) and ALS/MND (B) cases. Scale bar represents 100 μm .

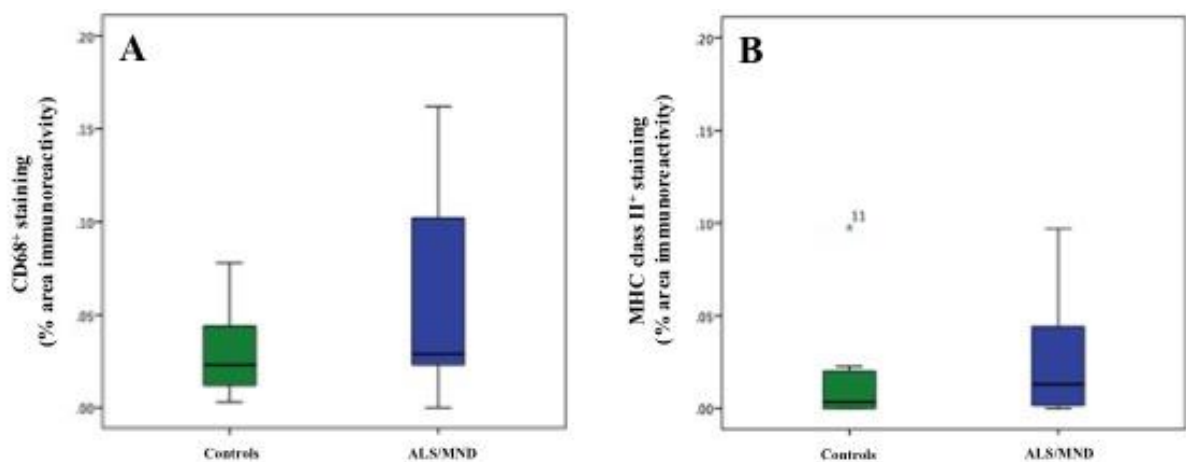


Figure 5.24 Quantitative analysis of CD68 and MHC class II expression in the FACx of controls and ALS/MND donors.

Box plots showing no significant difference in the % area of immunoreactivity for CD68 (A) and MHC class II (B) in the FACx of ALS/MND cases when compared to control donors (Mann Whitney-U Test).

5.4.8. p62 pathology is not linked to the of senescence and DNA damage markers in

ALS/MND cases

Differences in the percentage of p16/p21⁺ glia and p21⁺ neurones between FTLD-TDP type B and FTLD-MC/0 cases were assessed for both the MCx and FACx brain areas. There was no significant difference in the percentage of p16⁺ glia in the MCx ($p=0.686$) or FACx ($p=0.886$) (**Figure 5.25A-B**) and in the percentage of p21⁺ glia in the MCx ($p=0.686$) or FACx ($p=0.886$) between FTLD-TDP B and FTLD-MC/0 cases (**Figure 5.25C-E**). Analysis of the percentage of p21⁺ neurones in the MCx ($p=0.114$) and FACx ($p=1.00$) of FTLD-TDP B cases compared to FLD-MC/0 cases was not statistically significant either (**Figure 5.26A-B**).

Differences in the percentage of γ H2AX⁺ and 8-OHdG⁺ neurones between FTLD-TDP type B and FTLD-MC/0 cases were also investigated. There was no significant difference in the percentage of γ H2AX⁺ neurones in the MCx of FTLD-TDP B cases when compared to the FTLD-MC/0 group ($p=0.486$) (**Figure 5.27A**), but the percentage of γ H2AX⁺ neurones in the FACx was significantly higher in the FTLD-MC/0 group ($p=0.029$) (**Figure 5.27B**). Differences in the percentage of 8-OHdG⁺ neurones between FTLD-TDP B and FTLD-MC/0 cases were not statistically significant (MCx, $p=0.343$; FACx, $p=0.686$) (**Figure 5.27C-D**).

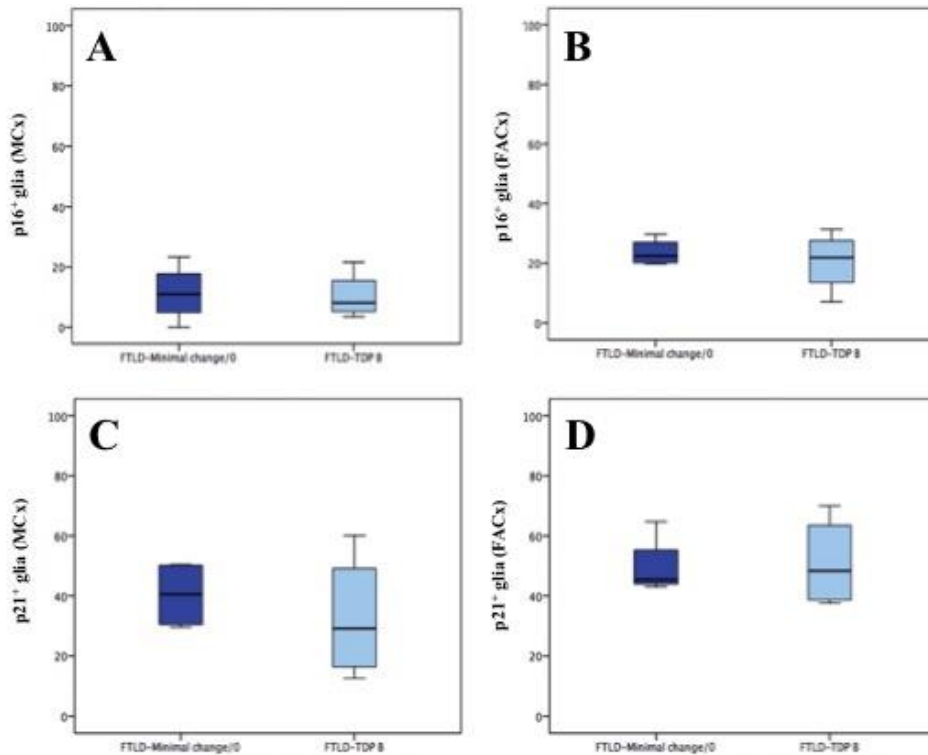


Figure 5.25 Analysis of p16 and p21 expression in glial cells of FTLD-TDP B cases. Box plots showing the percentage of p16⁺ and p21⁺ glial cells in the MCx (A and C) and FACx (B and D) of FTLD-TDP B and FTLD-Minor changes/0 cases. No significant difference was found between groups for either one of the senescence markers (Mann Whitney-U Test).

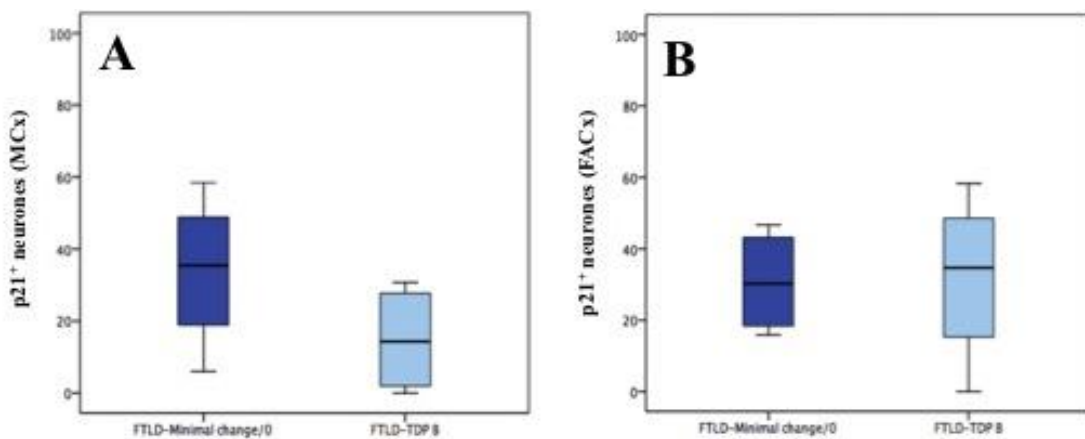


Figure 5.26 Analysis of p21 expression in neurons of FTLD-TDP B cases. Box plots showing the percentage of p21⁺ neurons in the MCx (A) and FACx (B) of FTLD-TDP B and FTLD-Minor changes/0 cases. There was no significant difference in the percentage of p21⁺ neurons between groups (Mann Whitney-U Test).

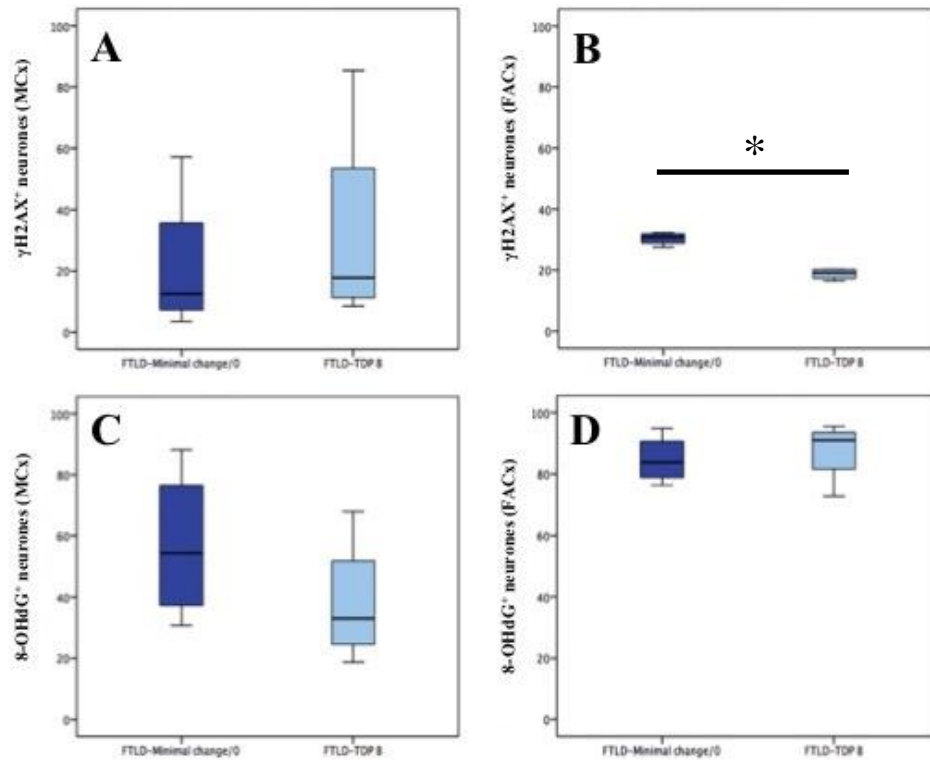


Figure 5.27 Analysis of γ H2AX and 8-OHdG expression in neurones of FTLD-TDP B cases.

Box plots showing the percentage of γ H2AX⁺ and 8-OHdG⁺ neurones in the MCx (A and C) and FACx (B and D) of FTLD-TDP B and FTLD-Minor changes/0 cases. The percentage of γ H2AX⁺ neurones in the FACx of FTLD-TDP B cases was significantly lower when compared to the FTLD-Minor changes/0 group; no significant difference was found in the MCx. No significant difference in the percentage of 8-OHdG⁺ neurones was found between groups (Mann Whitney-U Test).

5.4.9. Microarray analysis of the neuronal transcriptome in the frontal cortex of MND patients.

5.4.9.1. Integrity of purified RNA from frozen tissue

Previous to the LCM isolation of neuronal cells from the FACx of ALS/MND and control donors, an assessment of the RNA quality from the available frozen sections was performed. Results from the Nanodrop readings are presented in **Table 5.11**. The yield and RNA quality of the samples extracted from control and ALS/MND FACx frozen sections had an RNA yield of 35.22 ± 22.72 ng/ μ l on average. RNA determined by the A260/280 ratio, was on average 2.46 ± 0.5 . The RIN value for the samples was of 5.68 ± 2.7 . and electropherograms from all samples showed two distinct 28S and 10S rRNA peaks (**Figure 5.28**).

Condition	RNA concentration (ng/μl)	260/280 ratio	RIN value
Control 1	8.79	3.47	2.5
Control 2	25.26	2.30	5.4
Control 3	27.18	2.26	7.7
ALS/MND 1	59.06	2.21	8.2
ALS/MND 2	67.16	2.22	7.8
ALS/MND 3	23.85	2.29	2.5
Mean \pm SD	35.22 ± 22.72	2.46 ± 0.5	5.68 ± 2.7

Table 5.11 Initial concentrations of RNA in FACx frozen tissue samples.

Before proceeding to the isolation of neurones by LCM, the overall quality of the RNA obtained from frozen FACx sections was assessed. 260/280 and RIN values suggested RNA was of an acceptable quality.

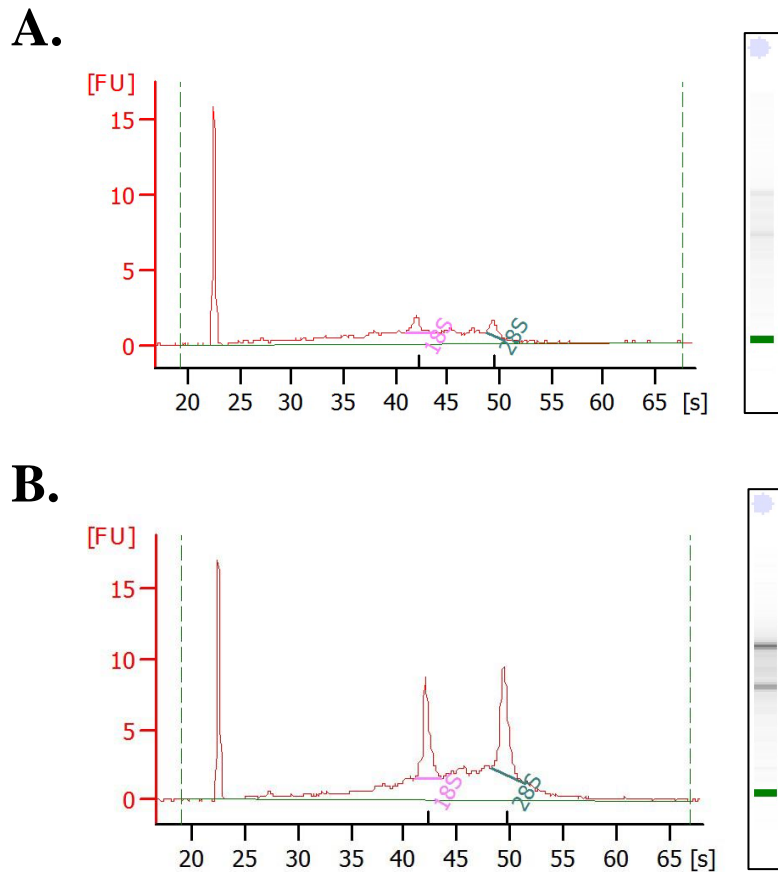


Figure 5.28 RNA integrity from FACx frozen tissue.

Example of two electropherograms and electrophoresis gels obtained with the Agilent 2100 Bioanalyzer from two RNA samples from FACx frozen human tissue with low (A) (RIN=5.4) and high (B) (RIN=7.8) RIN values. Electropherograms were used to assess the RNA integrity. Peaks represent the 18S and 28S rRNA and confirm the presence of non-degraded RNA in the samples (FU: fluorescence unit).

5.4.9.2. RNA integrity from LCM neurone enriched RNA samples

After confirming that RNA could be successfully extracted from FACx frozen samples and that its quality was acceptable for the subsequent experiments, FACx neurones from 3 control donors and 3 ALS/MND donors were isolated using LCM. RNA was eluted in 15 µl of RNase free water and the RNA yield and quality were assessed. Nanodrop results are presented in **Table 5.12** and an example of an electropherogram is presented in **Figure 5.29**. The yield of RNA extracted from the 6 FACx neurone enriched samples was of 13.85 ± 15.62 ng/µl on average. The average A260/280 ratio was of 1.51 ± 0.19 and the average RIN value was of 3.62 ± 0.71 . All samples showed 28S and 10S RNA peaks in the electropherograms (**Figure 5.29**).

Condition	RNA concentration (ng/µl)	260/280 ratio	RIN value
Control 1	45.30	1.52	2.8
Control 2	5.05	1.52	3.4
Control 3	6.47	1.52	3.7
ALS/MND 1	5.19	1.53	4.9
ALS/MND 2	9.51	1.19	3.2
ALS/MND 3	11.60	1.8	3.7
Mean ± SD	13.85±15.62	1.51±0.19	3.62±0.71

Table 5.12 RNA concentration and quality in neurone enriched samples.

RNA obtained from FACx neurones isolated by LCM from control and ALS/MND donors was assessed. 260/280 ratios and RIN values confirmed RNA samples were of an acceptable quality to use for microarray experiments.

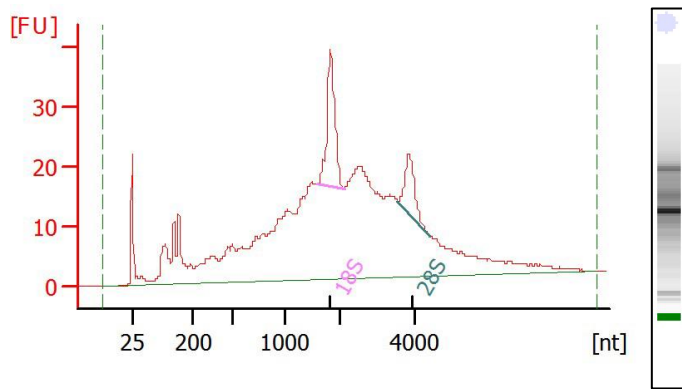


Figure 5.29 RNA integrity from FACx frozen tissue.

Example of an electropherogram and electrophoresis gel obtained with the Agilent 2100 Bioanalyzer for an RNA sample from FACx neurones isolated by LCM. Electropherograms were used to assess the RNA integrity. Peaks represent the 18S and 28S rRNA and indicate intact RNA (FU: fluorescence unit).

5.4.9.3. Confirmation of neuronal enrichment in LCM samples

The expression of the neuronal marker *NEUN* was used to assess enrichment of LCM samples with a neuronal population. Expression of *GFAP*, *OLIG2* and *CD68* was also investigated to identify contamination of astrocyte, oligodendrocyte and microglial populations, respectively. Expression of *NEUN* was detected in the 6 samples obtained from LCM isolated neurones from the FACx (**Figure 5.30**). *GFAP* expression was detected in Control 1, Control 3 and ALS/MND 1 indicating astrocytic contamination in these samples; however, *OLIG2* and *CD68* expression was not found in any of the samples. Amplification of *ACTNB* was included as control. Expression of *ACTNB* was present in all samples, as expected. These results confirmed that isolation of neurones from the FACx by LCM indeed produced samples enriched with a neuronal population.

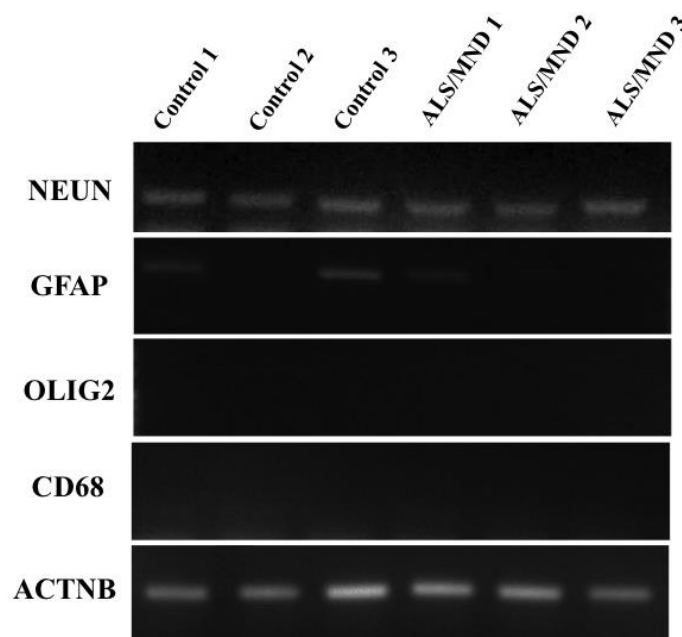


Figure 5.30 Enrichment of LCM samples with a population of neuronal cells.

DNA gel showing expression of *NEUN* and confirming enrichment of neuronal population following RNA extraction from LCM isolated FACx neurones. *GFAP* expression was present in 3 of the 6 samples (Control 1, Control 3 and ALS/MND 1), but *OLIG2* and *CD68* products were not detected.

5.4.9.4. RNA preparation for microarray analysis

RNA extracts obtained from neurone enriched samples were processed with the 3' IVT Pico Reagent kit, which prepares low concentrated RNA samples for gene expression profiling. Approximately 10 ng RNA per sample were used for the single-strand cDNA (ss-cDNA) synthesis. After purification, the yield of cRNA was measured by spectrophotometry with a NanoDrop 1000. **Table 5.13** shows the concentration of cRNA obtained per sample. The mean concentration of cRNA was 3132.80 ± 681.05 ng/ μ l and the mean 260/280 ratio was 1.92 ± 0.18 .

Condition	cRNA concentration (ng/μl)	260/280 ratio
Control 1	3520.82	1.87
Control 2	3614.78	1.74
Control 3	3403.06	1.95
ALS/MND 1	1985.56	2.10
ALS/MND 2	3659.31	1.70
ALS/MND 3	2613.29	2.15
Mean \pm SD	3132.80 ± 681.05	1.92 ± 0.18

Table 5.13 Concentrations of cRNA obtained after ss-cDNA synthesis.

Next, 20 µg of cRNA were used for the synthesis of sense-strand and anti-sense strand DNA in a 2nd – cycle. The ds-cDNA was purified and measured by spectrophotometry. The mean ds-cDNA concentration was 630.87±37.7 ng/µl (**Table 5.13**)

Condition	ds-cDNA concentration (ng/µl)	260/280 ratio
Control 1	743.98	1.98
Control 2	580.90	1.99
Control 3	708.28	1.96
ALS/MND 1	497.05	1.94
ALS/MND 2	672.59	1.97
ALS/MND 3	564.28	2.30
Mean ± SD	627.85 ± 95.2	2.02±0.14

Table 5.14. Concentration of ds-cDNA obtained after the 2nd amplification cycle.

For the fragmentation step, 6.6 µg of ds-cDNA were used. Fragmentation of the ds-cDNA was done by UDG and APE 1 enzymes at the dUTP residues. To ensure that fragmentation was successful, this was assessed with the Agilent 2100 Bioanalyser (**Figure 5.31**). Labelling of the fragmented cDNA was done by a TdT using the Affymetrix proprietary DNA labelling reagent, which contains biotin. After labelling, samples were processed for cartridge array hybridisation. To ensure accurate comparison between microarrays, spike-in controls *bioB*, *bioC*, *bioD* (E. Coli) and *Cre* (P1) were used to normalise hybridisation measurements. Biotin labelled cRNA transcripts of *bioB*, *bioC*, *bioD* and *cre* were spiked in the Hybridisation Cocktail in different concentrations (1.5 pM, 5 pM, 25 pM, and 100 pM final concentrations for *bioB*, *bioC*, *bioD*, and *cre*, respectively).

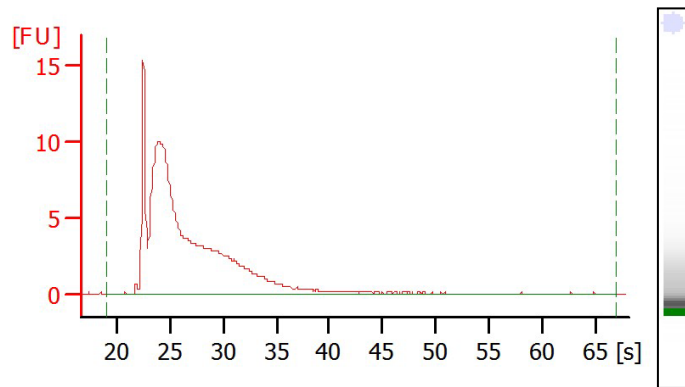


Figure 5.31 Assessing fragmentation of ss-cDNA.

Representative electropherogram and electrophoresis gel showing ss-cDNA fragmentation. (FU=fluorescence unit).

5.4.9.5. Microarray data quality control (QC) overview

Standard quality control parameters for the MAS 5.0 algorithm data were assessed prior to the microarray data analysis, as done with the LUHMES microarray data (**Chapter 4, section 4.3.2.2**). The QC analysis was done using the Affymetrix Expression Console™ Software and sample quality, hybridisation, signal quality and signal comparability were the parameters assessed.

In summary, the QC analysis identified Control 3 as an outlier. This sample consistently showed values for the standard quality control parameters that were outside of the trend. The clustering analysis segregated the ALS/MND and control groups in two well defined groups, however, Control 3 did not conform (**section 5.4.9.6.1**). Based on these results, Control 3 was excluded from the functional and pathway enrichment analysis.

5.4.9.5.1. Sample quality

5.4.9.5.1.1. Labelling controls

Bacterial poly-A RNA controls from the *B. subtilis* genes *lys*, *phe*, *thr* and *dap* were present at different concentrations each (1:100,000, 1:50,000, 1:25,000 and 1:6,667, respectively) in all samples. Samples Control 1 and Control 3 showed a higher signal intensity compared to the rest of the samples, which had a similar labelling efficiency for all poly-A RNA controls (**Figure 5.32**). In summary, all poly-A RNA controls were called as present in increasing concentrations in the 6 arrays.

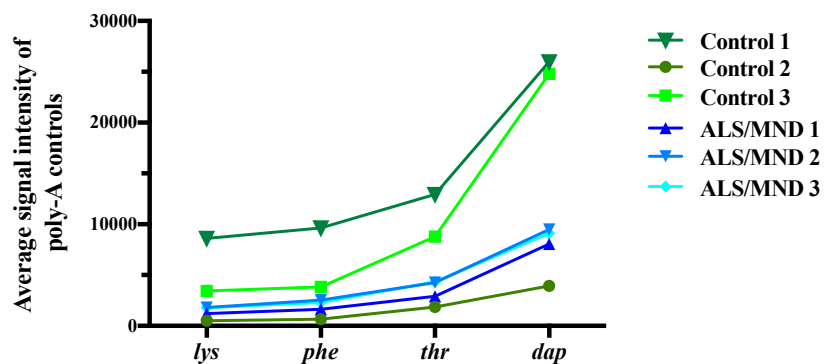


Figure 5.32 Poly-RNA controls for neurone RNA enriched samples from controls and ALS/MND cases.

Plot depicting the average signal intensity of poly-A controls *lys*, *phe*, *thr* and *dap* for each of the 6 samples.

5.4.9.5.1.2. 3'/5' ratio for β -actin and GAPDH

The GAPDH and β -actin 3' probe to 5' probe ratios for the FACx neurone arrays are shown in **Figure 5.33**. Affymetrix indicates that ratio values should be below 3 for 1-cycle assays, but 2-cycle assays can give higher values as a result of the additional amplification cycle. GAPDH and β -actin ratio values for the FACx neurones arrays were similar between replicates, except for Control 3, which differed from the other samples. β -actin values were higher than 3, as expected for a 2-cycle assay.

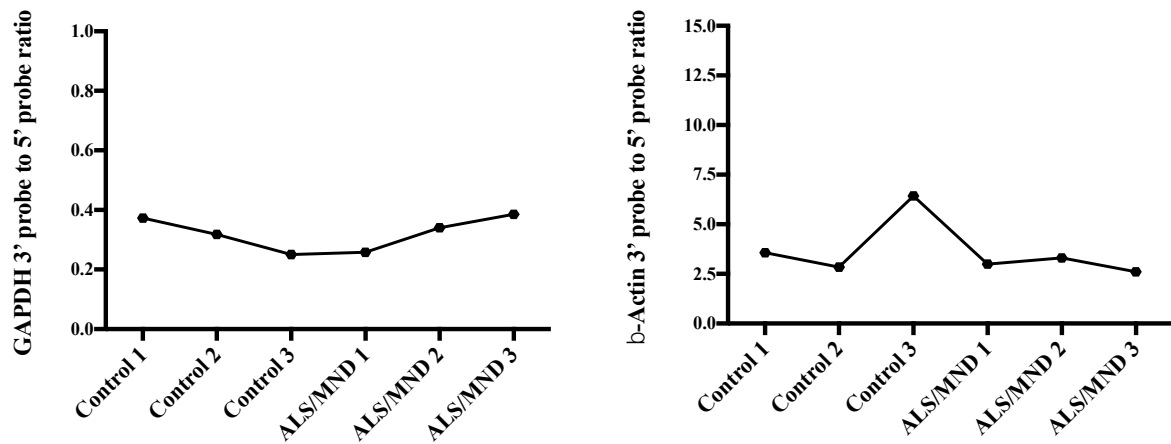


Figure 5.33 Housekeeping (HK) genes GAPDH and β -actin signal ratios.

HK genes GAPDH and β -actin were used as internal controls to assess the quality of the samples and the amplification and labelling process. The 3' probe to 5' probe ratio should be consistent between arrays.

5.4.9.5.2. Hybridisation and signal quality

5.4.9.5.2.1. Spike-in eukaryotic hybridisation controls

Average signals for the hybridisation controls *BioB*, *bioC*, *bioD* (E. Coli) and *Cre* (P1) transcripts are shown in **Figure 5.34**. The concentration of *BioB* is at the level of array sensitivity and should be present at least 70% of the time. *bioC*, *bioD* and *Cre* should be present and show increasing signal values. Signals for all hybridisation controls show increasing values in all samples, as expected. Signal for Control 3 was higher, compared to the rest of the samples that had similar signal values between them. Overall, all eukaryotic hybridisation controls were called as present in increasing concentrations in the 6 arrays, which suggests a good hybridisation efficiency for all samples.

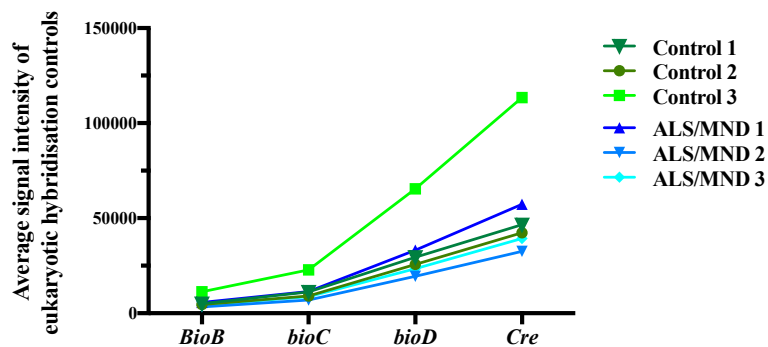


Figure 5.34 Eukaryotic hybridisation controls for FACx neurone arrays.

Plot depicting the average signal intensities of hybridisation controls *BioB*, *bioC*, *bioD* and *Cre* at increasing concentrations for each of the 6 FACx neurones arrays.

5.4.9.5.2.2. Percent present (% P)

In **Figure 5.35**, the % P indicates the percentage of probes that are present in the arrays, relative to the total number of probes. Replicates should have similar % P values. The values for the % P in the 6 FACx neurones arrays is consistent between replicates and GeneChip arrays.

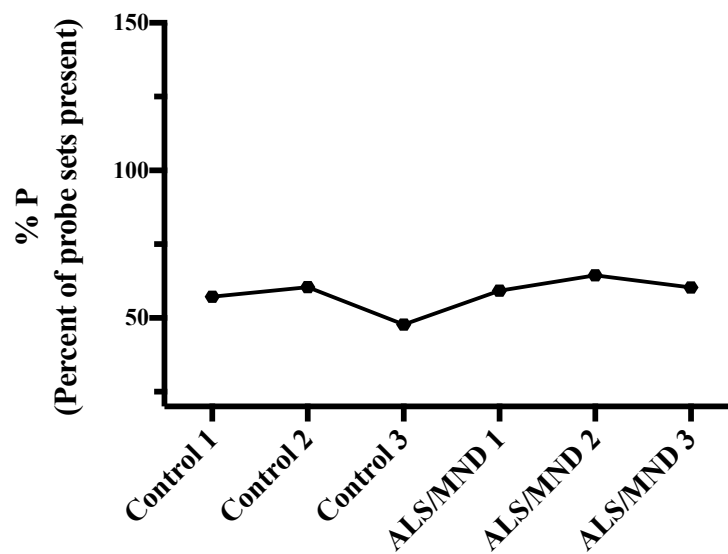


Figure 5.35 Percentage of probes present in the 96 hours control and SS/DS LUHMES array.

% P is the percentage of probes that are detected relative to the total number of probe sets that the array contains, which are 54,675 probes for the GeneChip Human Genome U133 Plus 2.0 Array.

5.4.9.5.3. Signal comparability

The signal histogram shown in **Figure 5.36** shows the signal intensities from the probes in each array, which allows comparison of the signals between GeneChip arrays. The signal profile should be the same across samples, however the profile for Control 3 (Irina 6) indicates higher signal intensities for some of the probes; the other 5 samples show comparable signal intensities.

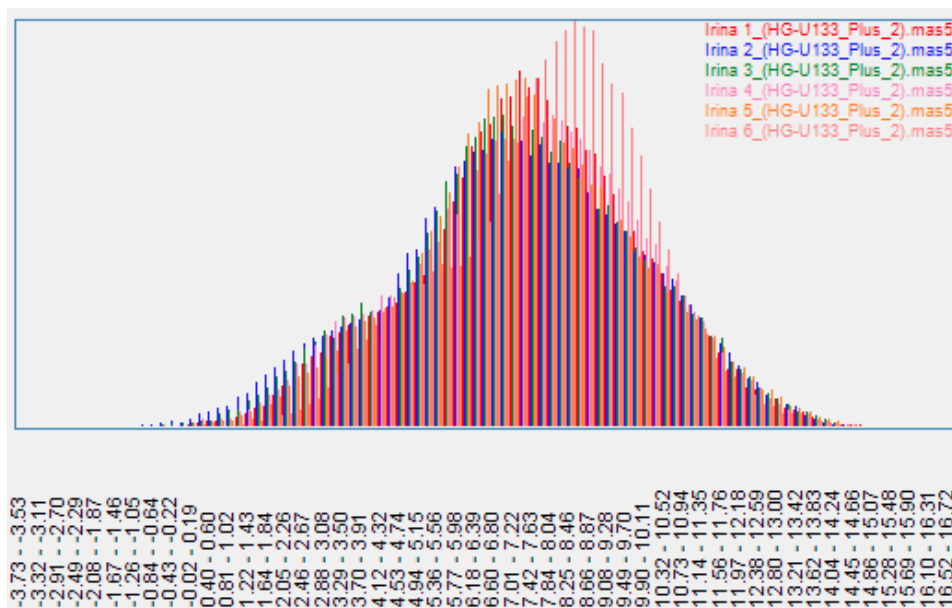


Figure 5.36 Signal histogram for ALS/MND and control FACx neurones arrays.

The signal histogram was used to compare the signal intensities of the probe sets across the 6 FACx neurones arrays under analysis (Irina 1=ALS/MND 1; Irina 2=ALS/MND 2, Irina 3=ALS/MND 3; Irina 4=control 1; Irina 5=control 2; Irina 6=control 3).

The Relative Log Expression (RLE) values compares the signal detected for each of the probe sets present in the array to the median signal value for each probe set across all arrays. RLE values should be 0 or close to 0 on a log scale. RLE values for the FACx neurones arrays show a similar spread between them, except for array Control 3 (Irina 6) (Figure 5.37).

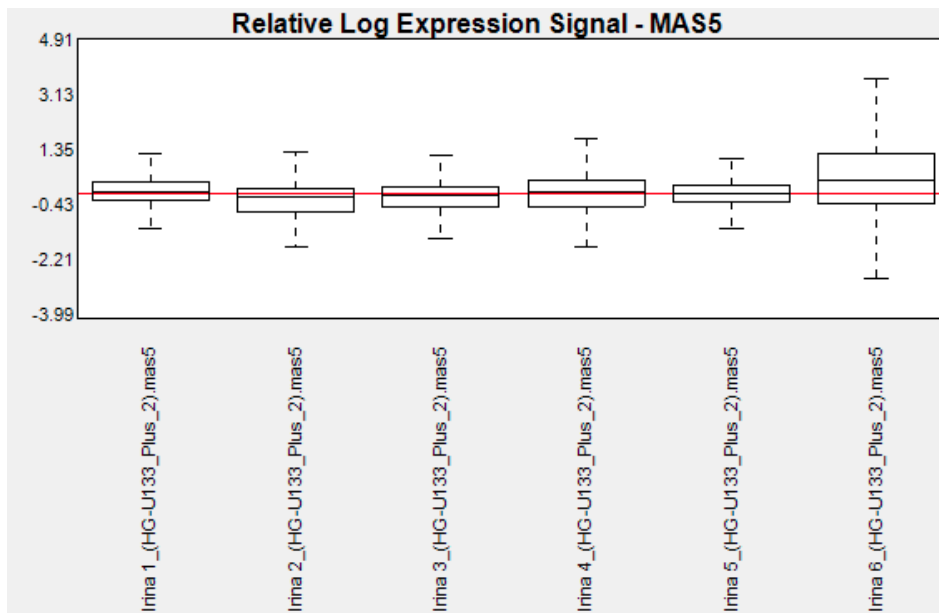


Figure 5.37 Relative log expression (RLE) box plots for the ALS/MND and control FACx neurones arrays.

The RLE values of the 6 arrays are close to 0, except for the Control 3 (Irina 6) array, which has a higher RLE value (Irina 1=ALS/MND 1; Irina 2=ALS/MND 2, Irina 3=ALS/MND 3; Irina 4=control 1; Irina 5=control 2; Irina 6=control 3).

5.4.9.6. Microarray data analysis

5.4.9.6.1. Clustering Analysis

Differences in the transcriptome of control and ALS/MND FACx neurones were analysed with the Qlucore Omics Explorer (version 3.0) software. Initially, the 6 data sets (3 controls and 3 ALS/MND FACx neurones) were imported to Qlucore Omics Explorer and normalised using the RMA method. For the analysis, a fold change (FC) ≤ 1.2 and a significant value of $p < 0.05$ were set. Data was analysed using a Two-group comparison between Control FACx neurones and ALS/MND FACx neurones. The PCA plot for this analysis is shown in

Figure 5.38A. A clear separation of the 2 conditions can be seen: Control FACx neurones– blue, ALS/MND FACx neurones - yellow. However, Control 3 (indicated in red, in

Figure 5.38A) was not as well aligned with the other 2 control arrays. These results are consistent with the quality control parameters obtained for this sample and presented in **section 5.3.9.5**. Due to these results a second PCA analysis was performed excluding Control 3 (

Figure 5.38B), which resulted in a better differentiation of the ALS/MND and control groups.

The two-group comparison identified 820 differentially expressed genes, 358 up and 462 down-regulated, in ALS/MND FACx neurones (**Table 5.15**). Exclusion of Control 3 from the analysis reduced the number of differentially expressed genes from 1371 to 820 (40% reduction). The complete list of differentially expressed genes can be found in the electronic version of this work, as specified in **Appendix C**.

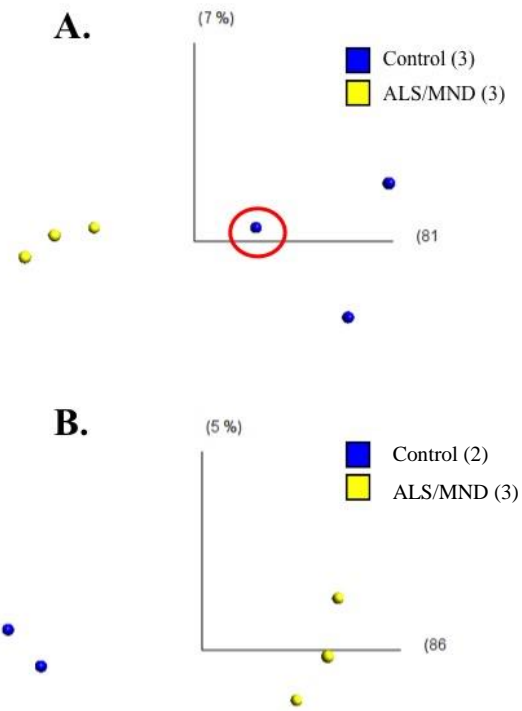


Figure 5.38 Clustering analysis of ALS/MND FACx neurones compared to Control FACx neurones – Two groups analysis.

A. PCA plot of ALS/MND FACx neurones (yellow) and Control neurones (blue) shows the separation of differentially expressed genes between the 2 groups. **B.** PCA plot of ALS/MND FACx neurones (yellow) and Control neurones (blue) excluding Control 3 (identified with the red circle in Panel A).

Two Group Comparison	Total number of differentially expressed transcripts	Number of up-regulated transcripts	Number of down-regulated transcript
ALS/MND vs Control FACx neurones (excluding Control 3)	820	358	462
ALS/MND vs Control FACx neurones (including all 6 array data sets)	1371	500	871

Table 5.15 Number of differentially expressed transcripts in ALS/MND FACx neurones.

Contrary to what was expected, exclusion of Control 3 from the analysis resulted in the reduction in the number of differentially expressed genes, which could correlate with Control 3 gene expression profiling being similar to the profile of ALS/MND neurones.

5.4.9.6.2. Functional annotation and pathway enrichment analysis

A functional annotation analysis was conducted to group genes according to their function and to identify dysregulated pathways in ALS/MND FACx neurones that could be linked to a DDR and the development of a senescence like-state. Previous to this analysis, a manual examination of the list of differentially expressed genes was done to identify dysregulated transcripts from common senescence and SASP markers: p21 (*CDKN1A*), p16 (*CDKN2A*), SA- β -galactosidase (*GLB1*), IL-6 (*IL6*) and/or IL-8 (*CXCL8*). This examination did not identify alteration in any of these genes in the ALS/MND FACx neurones.

5.4.9.6.2.1. Functional Enrichment Analysis using DAVID Bioinformatics Tool

The list of probe IDs from the total number of differentially expressed transcripts computed by Qlucore Omics Explorer were entered into DAVID Bioinformatics Tool

(version 6.7). To identify functional groups and altered pathways changing in the same direction, the lists of up and down-regulated transcripts were inputted independently as well. Results from the DAVID Functional Enrichment Analysis are summarised in **Table 5.16**, **Table 5.17** and **Table 5.18**.

Differentially expressed transcripts in ALS/MND FACx neurones were categorised in alternative splicing, phosphoprotein, calcium, ATP and cell adhesion functional groups. The dysregulated pathways identified by DAVID included calcium signalling pathway and p53 signalling pathway (**Table 5.16**).

Analysis of the UP-REGULATED transcripts (**Table 5.17**) resulted in enrichment of alternative splicing, phosphoprotein, calcium and synapse functional groups. Pathway analysis suggested dysregulation of dilated cardiomyopathy, calcium signalling, GAP junction regulation of actin cytoskeleton and p53 signalling pathways in the **ALS/MND FACx neurones**.

Functional grouping of DOWN-REGULATED transcripts (**Table 5.18**) resulted in enrichment of immunoglobulin domain, DNA binding, alternative splicing, ATP, calcium and cell adhesion functions. DAVID identified enrichment of the KEGG pathway linked to metabolism of lipids in the ALS/MND FACx neurones.

Two group comparison	Functional group		Differentially expressed genes	<i>p</i> value	FDR value
ALS/MND vs Control (FACx neurones) (318 David IDs)	Alternative splicing		317	3.2E-8	4.5E-5
	Phosphoprotein		294	3.6E-3	2.2E-2
	Calcium		45	1.3E-1	1.2E0
	Immunoglobulin domain		29	2.4E-1	3.2E0
	SH2 domain		10	6.8E-1	1.6E1
	DNA binding		20	7.9E-1	2.5E1
	Metal-binding		119	7.6E-1	2.6E1
	Cell adhesion		23	7.9E-1	3.1E1
	ATP		15	7.7E-1	3.2E1
	Lipid-binding		8	7.9E-1	3.7E1
	Pathway name	Pathway source	Differentially expressed genes	<i>p</i> value	FDR value
	Calcium signalling pathway	KEGG	12	5.3E-2	4.7E1
	p53 signalling pathway	KEGG	6	9.9E-2	7.0E1

Table 5.16 DAVID Functional and Pathway Enrichment analysis of the total number of differentially expressed transcripts in the ALS/MND FACx neurones

Two group comparison	Functional group		Differentially expressed genes	<i>p</i> value	FDR value
ALS/MND vs Control (FACx neurones) (318 David IDs)	Alternative splicing		159	2.1E-7	2.8E-4
	Phosphoprotein		152	1.6E-6	2.1E-3
	Calcium		22	1.2E-2	1.6E1
	Zinc-finger		39	1.4E-2	1.7E1
	Synapse		9	1.7E-2	2.1E1
	Nucleus		82	2.0E-2	2.4E1
	Metal-binding		60	2.1E-2	2.4E1
	Duplication		9	2.5E-2	2.9E1
	Citruiline		2	3.0E-2	3.4E1
	Zinc		45	3.7E-2	4.0E1
	Pathway name	Pathway source	Differentially expressed genes	<i>p</i> value	FDR value
	Dilated cardiomyopathy	KEGG	6	1.7E-2	1.7E1
	Calcium signalling pathway	KEGG	8	2.4E-2	2.4E1
	GAP junction	KEGG	5	5.7E-2	4.8E1
	Regulation of actin cytoskeleton	KEGG	8	6.0E-2	5.1E1
	GnRH signalling pathway	KEGG	5	7.5E-2	5.9E1
	p53 signalling pathway	KEGG	4	9.9E-2	6.9E1

Table 5.17 DAVID Functional and Pathway Enrichment analysis of the UP-REGULATED transcripts in the ALS/MND FACx neurones.

Two group comparison	Functional group		Differentially expressed genes	<i>p</i> value	FDR value
ALS/MND vs Control (FACx neurones) (402 David IDs)	Immunoglobulin domain		20	9.2E-4	1.3E0
	DNA binding		16	1.3E-3	1.8E0
	Alternative splicing		160	4.3E-3	5.8E0
	ATP		10	2.7E-2	3.2E1
	Calcium		23	3.4E-2	3.8E1
	Pyroglutamic acid		4	5.0E-2	5.1E1
	SH2 domain		6	5.0E-2	5.1E1
	Acetyllysine		2	5.3E-2	5.3E1
	Thyroid gland		2	7.0E-2	6.3E1
	Cell adhesion		13	8.2E-2	6.9E1
		Pathway name	Pathway source	Differentially expressed genes	<i>p</i> value
	Metabolism of lipids	KEGG	7	3.3E-2	2.6E1

Table 5.18 DAVID Functional and Pathway Enrichment analysis of the DOWN-REGULATED transcripts in the ALS/MND FACx neurones.

5.4.9.6.2.2. Pathway enrichment analysis using IMPaLA

IMPaLA (version 9) was also used to investigate dysregulated pathways in ALS/MND FAcx neurones. As with the DAVID analysis, the total number of differentially expressed genes, as well as the separate lists of UP and DOWN-REGULATED transcripts were analysed.

IMPaLA output for the total number of dysregulated transcripts (**Table 5.19**) indicated enrichment of Beta-agonist/Beta-blocker pathway, proteoglycans in cancer, integrin and leptin signalling pathways. Analysis of the UP-REGULATED genes (**Table 5.20**) showed enrichment of pathways linked to regulation of CDC42 activity, integrin and glutamatergic synapse, among others. Analysis of the DOWN-REGULATED transcripts (**Table 5.21**) showed enrichment of aromatase inhibitor pathway, Arf6 signalling events, nuclear receptors and retinoic acid biosynthesis pathways.

Two group comparison	Pathway name	Pathway source	Differentially expressed genes	<i>p</i> value	FDR value
ALS/MND vs Control (FACx neurones)	Beta-agonist/Beta-blocker Pathway, Pharmacodynamics	PharmaGKB	8	0.000465	0.969
	Proteoglycans in cancer – Homo sapiens	KEGG	15	0.000616	0.969
	Integrin	INOH	11	0.000675	0.969
	Hemostasis	Reactome	34	0.000897	1
	Regulation of nuclear SMAD2/3 signaling	PID	8	0.00142	1
	Leptin	NetPath	7	0.0016	1
	BMAL1:CLOCK, NPAS2 activates circadian gene expression	Reactome	4	0.00164	1
	Signaling of Hepatocyte Growth factor Receptor	Wikipathways	5	0.00232	1
	Arf6 signaling events	PID	5	0.00264	1
	NCAM1 interactions	Reactome	5	0.00339	1

Table 5.19 IMPaLA Pathway Analysis of the total number of differentially expressed transcripts in ALS/MND FACx neurones.

Two group comparison	Pathway name	Pathway source	Differentially expressed genes	<i>p</i> value	FDR value
ALS/MND vs Control (FACx neurones)	Regulation of CDC42 activity	PID	4	0.000586	1
	Integrin	INOH	7	0.00118	1
	Circadian entrainment	KEGG	6	0.00158	1
	Beta-agonist/Beta-blocker pathway, Pharmacodynamics	PharmGKB	5	0.00167	1
	Hemostasis	Reactome	19	0.00169	1
	BMAL1:CLOCK, NPAS2 activates circadian gene expression	Reactome	3	0.00503	1
	Glutamatergic synapse	KEGG	6	0.00376	1
	Transcriptional regulation of white adipocyte differentiation	Reactome	4	0.00403	
	Regulation of nuclear beta catenin signaling and target gene transcription	PID	5	0.00409	1
	Cross-presentation of particulate exogenous antigens (phagosomes)	Reactome	2	0.00449	1

Table 5.20 IMPaLA Pathway Analysis of the UP-REGULATED transcripts in ALS/MND FACx neurones.

Two group comparison	Pathway name	Pathway source	Differentially expressed genes	<i>p</i> value	FDR value
ALS/MND vs Control (FACx neurones)	Aromatase inhibitor pathway, Pharmacodynamics	PharmaGKB	2	0.00129	1
	Signaling of hepatocyte growth factor receptor	Wikipathways	4	0.00154	1
	Arf6 signaling events	PID	4	0.00172	1
	MET activates PTPN11	Reactome	2	0.00213	1
	Nuclear receptors	Wikipathways	4	0.00235	1
	MET activates PI3K/AKT signaling	Reactome	2	0.00317	1
	Pelp1 modulation of estrogen receptor toxicity	BioCarta	2	0.00317	1
	Thyroxine production	Wikipathways	2	0.00317	1
	POU5F1 (OCT4), SOX2, NANOG repress genes related to differentiation	Wikipathways	2	0.00439	1
	RA biosynthesis pathway	Reactome	3	0.00459	1

Table 5.21 IMPaLA Pathway Analysis of the DOWN-REGULATED transcripts in ALS/MND FACx neurones.

5.4.9.6.2.3. Summary of DAVID and IMPaLA results

Functional and pathway analysis of the differentially expressed genes in ALS/MND FACx neurones did not reveal dysregulation of pathways directly linked to senescence or the SASP; however, DAVID analysis identified dysregulation of p53 pathway, which is related to DNA damage, stress response and apoptosis. **Table 5.22** contains the dysregulated transcripts that were located to this pathway. A representation of the pathway is shown in **Figure 5.39**.

Gene symbol	Gene name	FC	<i>P</i> value
GADD45	growth arrest and DNA-damage-inducible, alpha	2.63	0.042
FAS	Fas cell surface death receptor	2.49	0.033
RCHY1	ring finger and CHY zinc finger domain containing 1, E3 ubiquitin protein ligase	1.41	0.033
PMAIP1	phorbol-12-myristate-13-acetate-induced protein 1	1.34	0.026

Table 5.22 Genes involved in p53 pathway in ALS/MND FACx neurones.

Transcripts linked to p53 signalling pathway were differentially expressed in FACx neurones from ALS/MND cases when compared to controls. (Red: up-regulated; Green: down-regulated, FC: fold change).

P53 SIGNALING PATHWAY

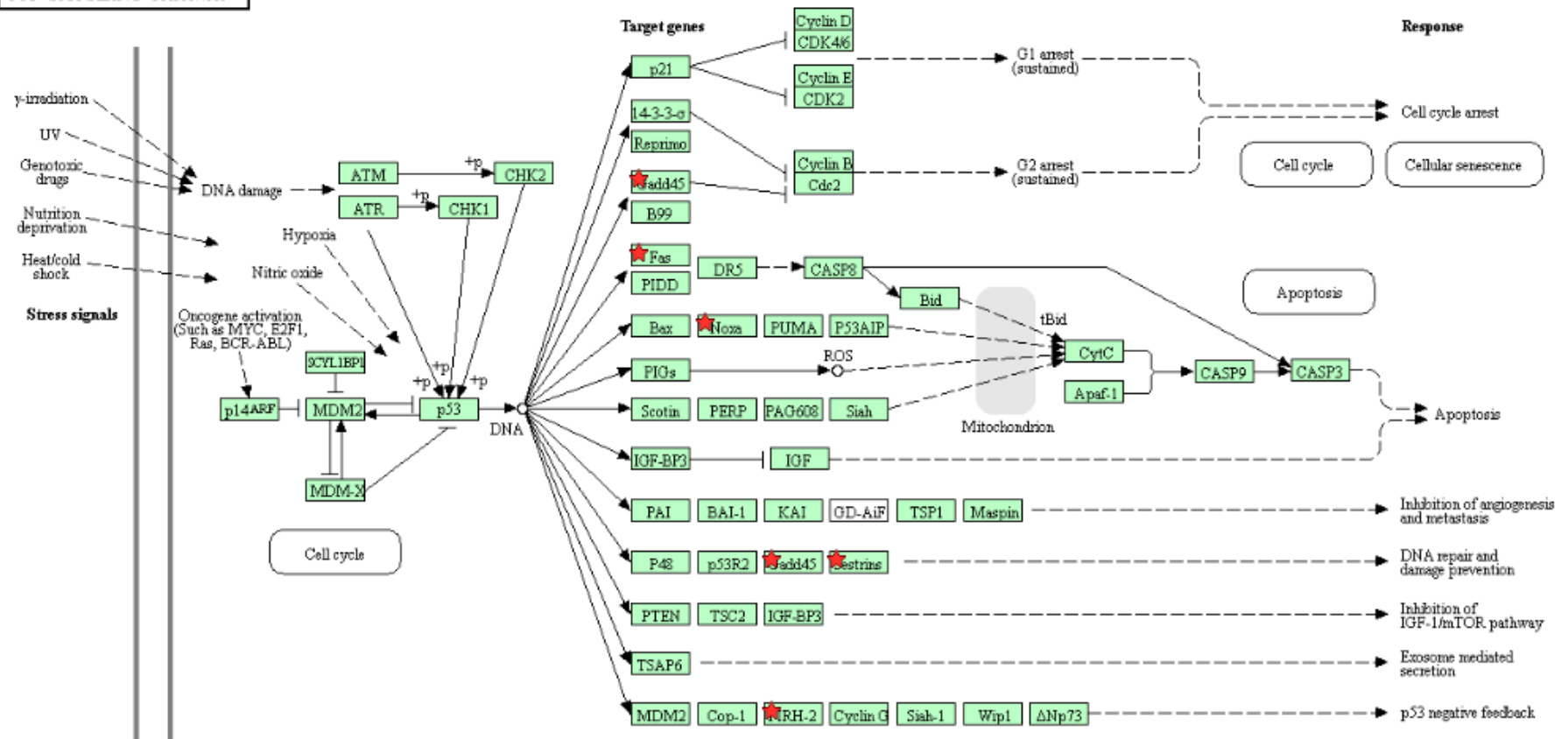


Figure 5.39 p53 signalling pathway (KEGG pathways).

Dysregulation of p53 signalling pathway was identified by DAVID analysis in the FACx neurones of ALS/MND cases. Differentially expressed genes are indicated with a red star.

5.4.9.6.3. Analysis of single dysregulated transcripts with fold change $FC \geq 2.0$

Manual assessment of the list of dysregulated transcripts in ALS/MND FACx neurones was conducted in order to identify candidates linked to neurodegeneration, DNA damage oxidative stress and cell cycle dysregulation. Only the genes with a $FC \geq 2.0$ were investigated. The dysregulated transcripts with $FC \geq 2.0$ are listed in **Table 5.23** and **Table 5.24**. For this part of the study, the GeneCards ® Human Genome Database and the Gene Ontology Consortium Database were used.

This analysis identified up-regulation of several genes involved in stress response, including the DNA damage response linked transcripts *GADD45* and *FAS*, which were detected by DAVID pathway analysis as part of the p53 signalling pathway. *GASL2L3*, *SMG1* and *XRCC5* transcripts were also identified. *GASL2L3* is involved in the maintenance of the cytoskeleton integrity and plays a role in neuronal survival; *SMG1* codes for a serine/threonine protein kinase involved in mRNA surveillance and genotoxic stress response pathways; and *XRCC5* is a single-stranded DNA-dependent ATP-dependent helicase involved in DSBs repair through DNA non-homologous end joining (NHEJ).

A second group of transcripts involved in mitochondrial function, autophagy and ubiquitination were dysregulated in the ALS/MND FACx neurones. Up-regulation of *NDUFAF7*, *COX20*, *ENOSF1* and *AK2*, and down-regulation of *SLC25A37* and *SLC9B1* were associated to mitochondrial function. *NDUFAF7* codes for an assembly factor of mitochondrial Complex I; *COX20* is also an assembly factor of cytochrome C oxidase and participates in the stabilisation of mitochondrial complex IV; *ENOSF1* codes for a mitochondrial enzyme that participates in the catabolism of L-fucose; and *AK2* codes for

adenylate kinase 2, which plays a role in adenine nucleotide metabolism and cellular energy homeostasis. *CISD2* codes for a zinc finger protein localised to the endoplasmic reticulum and mitochondria, where it plays a role in the regulation of autophagy. Finally, down-regulated transcripts *SLC25A37* and *SLC9B1* code for mitochondrial solute carrier proteins. *UBE2G2* codes for a ubiquitin conjugating enzyme from the E2 family that is mainly present in the endoplasmic reticulum; it catalyses ubiquitin covalent attachment to other proteins.

Gene symbol	Gene name	P value	FC
<i>PPP2R5C</i>	protein phosphatase 2, regulatory subunit B', gamma	0.029	4.03
<i>TSHZ2</i>	teashirt zinc finger homeobox 2	0.011	3.87
<i>WNT2B</i>	wingless-type MMTV integration site family, member 2B	0.032	3.79
<i>RHOQ</i>	ras homolog family member Q	0.041	3.36
<i>TUBA1B</i>	tubulin, alpha 1b	0.015	3.30
<i>PAX8-AS1</i>	PAX8 antisense RNA 1	0.037	3.21
<i>PCDH11X</i> /// <i>PCDH11Y</i>	protocadherin 11 X-linked /// protocadherin 11 Y-linked	0.046	3.15
<i>SH3BP2</i>	SH3-domain binding protein 2	0.011	3.14
<i>FAM126A</i>	family with sequence similarity 126, member A	0.010	3.13
<i>COL12A1</i>	collagen, type XII, alpha 1	0.030	3.00
<i>RAB3B</i>	RAB3B, member RAS oncogene family	0.011	2.98
<i>AHR</i>	aryl hydrocarbon receptor	0.008	2.97
<i>HTR2C</i>	5-hydroxytryptamine (serotonin) receptor 2C, G protein-coupled	0.032	2.95
<i>LLPH</i>	LLP homolog, long-term synaptic facilitation (Aplysia)	0.038	2.95
<i>ALG13</i>	ALG13, UDP-N-acetylglucosaminyltransferase subunit	0.047	2.86
<i>TBL1X</i>	transducin (beta)-like 1X-linked	0.031	2.75
<i>MAP3K3</i>	mitogen-activated protein kinase kinase kinase 3	0.028	2.68
<i>DUXAP8</i> /// <i>LINC01296</i>	double homeobox A pseudogene 8 /// long intergenic non-protein coding RNA 1296	0.030	2.66
GAS2L3	growth arrest-specific 2 like 3	0.038	2.63
GADD45A	growth arrest and DNA-damage-inducible, alpha	0.042	2.63
<i>GBP1</i>	guanylate binding protein 1, interferon-inducible	0.032	2.60
<i>ERV3-2</i>	endogenous retrovirus group 3, member 2	0.021	2.59
<i>ST8SIA4</i>	ST8 alpha-N-acetyl-neuraminide alpha-2,8-sialyltransferase 4	0.007	2.58
<i>CLIC4</i>	chloride intracellular channel 4	0.038	2.58
CISD2	CDGSH iron sulfur domain 2	0.010	2.57
<i>RDX</i>	radixin	0.044	2.56
<i>NME9</i>	NME/NM23 family member 9	0.012	2.54
<i>THAP1</i>	THAP domain containing, apoptosis associated protein 1	0.030	2.52
<i>DGKG</i>	diacylglycerol kinase gamma	0.030	2.51
<i>WRAP73</i>	WD repeat containing, antisense to TP73	0.038	2.51
<i>GCH1</i>	GTP cyclohydrolase 1	0.029	2.51
FAS	Fas cell surface death receptor	0.034	2.49
<i>DNHD1</i>	dynein heavy chain domain 1	0.031	2.45
<i>TAF1A-AS1</i>	TAF1A antisense RNA 1	0.048	2.44
<i>INHBA-AS1</i>	INHBA antisense RNA 1	0.033	2.42
<i>INTU</i>	inturned planar cell polarity protein	0.044	2.39
<i>RNF180</i>	ring finger protein 180	0.048	2.37

<i>CNOT7</i>	CCR4-NOT transcription complex subunit 7	0.035	2.36
<i>HTR2C</i>	5-hydroxytryptamine (serotonin) receptor 2C, G protein-coupled	0.004	2.31
<i>RORA</i>	RAR-related orphan receptor A	0.035	2.29
<i>SMG1</i>	SMG1 phosphatidylinositol 3-kinase-related kinase	0.010	2.27
<i>C18orf54</i>	chromosome 18 open reading frame 54	0.026	2.26
<i>MED7</i>	mediator complex subunit 7	0.012	2.25
<i>XRCC5</i>	X-ray repair complementing defective repair in Chinese hamster cells 5 (double-strand-break rejoining)	0.030	2.24
<i>NCF2</i>	neutrophil cytosolic factor 2	0.034	2.23
<i>DOPEY1</i>	dopey family member 1	0.023	2.17
<i>LINC00551</i>	long intergenic non-protein coding RNA 551	0.044	2.17
<i>EXT1</i>	exostosin glycosyltransferase 1	0.023	2.17
<i>AP5M1</i>	adaptor-related protein complex 5, mu 1 subunit	0.029	2.13
<i>SCAF11</i>	SR-related CTD-associated factor 11	0.030	2.11
<i>LARGE</i>	like-glycosyltransferase	0.031	2.10
<i>TWISTNB</i>	TWIST neighbor	0.012	2.08
<i>ERCC6L2</i>	excision repair cross-complementation group 6-like 2	0.029	2.08
<i>NDUFAF7</i>	NADH dehydrogenase (ubiquinone) complex I, assembly factor 7	0.046	2.08
<i>COX20</i>	COX20 cytochrome c oxidase assembly factor	0.031	2.07
<i>ZNF717</i>	zinc finger protein 717	0.013	2.04
<i>PRKCQ-AS1</i>	PRKCQ antisense RNA 1	0.039	2.03
<i>ENOSF1</i>	enolase superfamily member 1	0.043	2.02
<i>WDYHV1</i>	WDYHV motif containing 1	0.026	2.01
<i>AK2</i>	adenylate kinase 2	0.018	2.01
<i>BOK</i>	BCL2-related ovarian killer	0.014	2.00
<i>ANKRD13A</i>	ankyrin repeat domain 13A	0.023	2.00

Table 5.23 UP-REGULATED transcripts with FC \geq 2.0 in the ALS/MND FACx neurones.

Transcripts in pink are related to stress responses and DNA damage. Transcripts in light blue are linked to mitochondrial function and autophagy.

Gene symbol	Gene name	<i>P</i> value	FC
<i>LINC01619</i>	long intergenic non-protein coding RNA 1619	0.02	0.50
<i>BICD1</i>	bicaudal D homolog 1 (Drosophila)	0.03	0.48
<i>FERMT1</i>	fermitin family member 1	0.02	0.48
<i>KANK4</i>	KN motif and ankyrin repeat domains 4	0.02	0.48
<i>SLC25A37</i>	solute carrier family 25 (mitochondrial iron transporter), member 37	0.02	0.45
<i>SLC51A</i>	solute carrier family 51, alpha subunit	0.05	0.45
<i>WARS2</i>	tryptophanyl tRNA synthetase 2, mitochondrial	0.03	0.44
<i>UBE2G2</i>	ubiquitin conjugating enzyme E2G 2	0.04	0.42
<i>RBM43</i>	RNA binding motif protein 43	0.01	0.41
<i>IPO11 /// LRRC70</i>	importin 11 /// leucine rich repeat containing 70	0.05	0.41
<i>FERMT1</i>	fermitin family member 1	0.00	0.40
<i>WDR78</i>	WD repeat domain 78	0.00	0.36
<i>SLC9B1</i>	solute carrier family 9, subfamily B (NHA1, cation proton antiporter 1), member 1	0.03	0.30
<i>RNF144A-AS1</i>	RNF144A antisense RNA 1	0.04	0.22
<i>LOC101930105</i>	zinc finger protein 839-like	0.04	0.17

Table 5.24 DOWN-REGULATED transcripts with FC \geq 2.0 in the ALS/MND FACx neurones.

Transcripts in light blue are linked to mitochondrial function and autophagy.

Overall, manual assessment of the genes with a FC ≥ 2.0 did not reveal dysregulation of genes directly linked to senescence or the SASP; however, there were several dysregulated transcripts that are known to participate in mitochondrial function and cell stress responses, including DNA damage, autophagy and ubiquitination. From these, 3 transcripts were chosen to validate the microarray findings. These are listed in **Table 5.25**.

	Gene
DNA damage response	<i>GADD45A</i>
Mitochondrial function	<i>COX20</i>
	<i>SLC25A37</i>

Table 5.25 Genes selected for qRT-PCR validation.

Genes in red were up-regulated while genes in green were down-regulated according to the microarray data.

Validation of the chosen genes was conducted on RNA extracts obtained from ALS/MND and control FACx neurones by LCM. Results are presented on **Figure 5.40**. Due to the low RNA yield obtained from the LCM neurones samples, only one repeat of the qRT-PCR validation was performed. This limitation is examined in the **Discussion** section of this chapter. For *GADD45*, Ct values were only detected for 2 control and 4 ALS/MND cases; no difference was found in the expression of *GADD45A* between ALS/MND and control FACx neurones ($p > 0.9999$), which did not validate the microarray data. Ct values for *COX20* were detected for all control (5) and ALS/MND (6) samples but qRT-PCR did not validate the microarray findings ($p = 0.2273$), which suggested up-regulation of *COX20* in ALS/MND FACx neurones. Ct values for *SLC25A37* were detected for 4 control and for all (6) ALS/MND cases; qRT-PCR detection of this gene did not validate the microarray findings ($p = 0.7619$) that suggested downregulation of *SLC25A37* in ALS/MND FACx neurones.

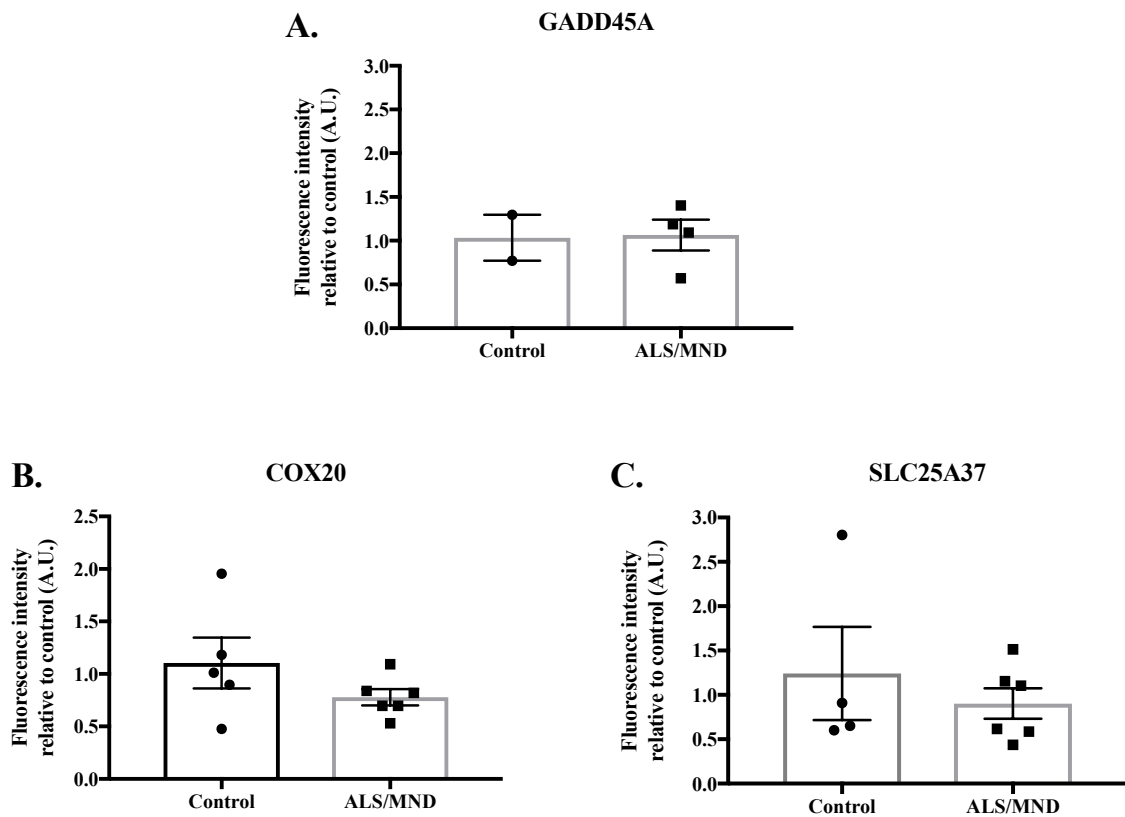


Figure 5.40 Validation of candidate genes by qRT-PCR.

Changes in *GADD45*, *COX20* and *SLC25A37* were validated by qRT-PCR. **A.** Ct values for *GADD45* were only detected for 2 controls and 4 ALS/MND cases. This gene was not validated. **B.** Ct values for *COX20* were detected for 5 control and 6 ALS/MND cases. This gene was not validated. **C.** Ct values for *SLC25A37* were only detected for 4 control and 6 ALS/MND cases. This gene was not validated. (Mann U-Whitney analysis, data are means \pm SEM; n=1).

5.5. Discussion

This chapter focused on the detection of senescence markers in neurones in a paradigm of neurodegeneration. Increased SA- β -gal activity, as well as expression of p16 and p21 was assessed in the brain of ALS/MND and control donors. SA- β -gal activity was identified in glial cells and neurones in the MCx, FACx and in the anterior horn of the Sc. p16 was exclusively expressed by glial cells and was significantly higher in the FACx of ALS/MND donors. Expression of p21 was found in both neurones and glia and was significantly higher for both cell types in the FACx of ALS/MND cases. Based on these results, microarray analysis was used to identify changes in the transcriptome of FACx neurones from ALS/MND donors that could be linked to senescence. Overall, pathway analysis of microarray results did not find dysregulation of senescence or SASP-related pathways in FACx neurones of ALS/MND donors. A more in depth discussion of these results is presented in the following sections.

5.5.1. *Oxidative DNA damage, DDR and senescence in ALS/MND*

Neurones are especially vulnerable to DNA insults as a result of their limited capacity for cell replacement and high metabolic rate. These conditions promote the formation of ROS and the induction of oxidative DNA damage, which accumulate with age. Oxidative stress and DNA damage are important players in the development of neurodegenerative diseases, including ALS/MND. Increased levels of oxidative stress have been shown in ALS/MND patients, although it is still not clear if this stress is a cause or a consequence of the pathological process. Mitochondrial oxidative damage, as measured by oxidised CoQ10, and oxidative DNA damage, as measured by 8-OHdG, is higher in the cerebrospinal fluid of fALS patients compared to controls; oxidised CoQ10 inversely correlates with illness duration, suggesting an early involvement of oxidative stress in the

disease (Murata et al., 2008). A more recent study found that the binding of Poly (GR) to mitochondrial ribosomal proteins results in mitochondrial dysfunction in iPSC-derived *C9ORF72* motor neurones, which promotes oxidative stress and DNA damage (Lopez-Gonzalez et al., 2016). Together, this data evidences the contribution that oxidative stress and DNA damage make to the initial stages of ALS/MND. Taking this into account, it is possible that a senescent-like state could develop in neurones in ALS/MND patients in response to early oxidative stress and DNA damage. To investigate this, the expression of a panel of senescence markers was assessed in ALS/MND and control brains and their relation to DNA damage and DNA damage response markers was analysed. The brain areas that were investigated included the anterior horn of the Sc and the grey matter of the MCx, which are directly affected by the pathogenesis of the disease. This study also included the FACx, which is known can develop neuroglial inclusions, but are less prevalent compared to the motor areas. In addition, the OCx was included as a comparison region not involved in the disease.

5.5.1.1. SA- β -gal activity is present in neurones and glia of ALS/MND and control brains

To study the activation of senescence in ALS/MND neurones, a panel of markers, including SA- β -gal activity at pH 6, was used. The detection of SA- β -gal *in vivo* has been widely used to identify the accumulation of senescent cells in different tissues. Early characterisation studies of SA- β -gal in skin biopsies resulted in the identification of an age-dependent increase in the enzyme activity (Dimri et al., 1995). Following this initial report, several studies have investigated the activation of senescence in relation to cancer, ageing and genotoxic stress. Increased SA- β -gal activity has been demonstrated in diverse human tissues and organs, including articular cartilage (Gao et al., 2016), upper intestinal tract (Going et al., 2002), coronary arteries of patients with atherosclerosis (Minamino et

al., 2002) and tumorigenic tissue. SA- β -gal activity has also been found in the human brain. In a recent study, increased SA- β -gal activity in oligodendrocytes and GFAP positive astrocytes has been reported in the brain of donors with and without age-associated white matter lesions (Al-Mashhadi et al., 2015). Moreover, SA- β -gal activity has also been detected in human and murine neurones *in vivo*. SA- β -gal⁺ neurones have been demonstrated in the FACx of an ageing cohort with low levels of Alzheimer's type pathology; in this cohort, SA- β -gal staining in neurones correlated weakly with the expression of DNA-PKcs, a marker of DDR (Simpson et al., 2014). Staining for SA- β -gal activity in the hippocampus of ageing rats (Geng et al., 2010) and Purkinje neurones of ageing mice (Jurk et al., 2012) has also been shown, suggesting the increase in SA- β -gal activity in neurones *in vivo* could also be linked to the activation of a senescent-like state as a response to a persistent DNA damage.

The current study demonstrates SA- β -gal activity in glia and neurones in both ALS/MND and control brain donors, which suggest activation of senescence in both cell types. SA- β -gal⁺ neurones and glia were not exclusively detected in a specific brain region, since different levels of staining were present throughout the MCx, FACx and Sc sections of ALS/MND and controls. Due to the variable quality of staining, quantification of this marker was not possible and a difference between groups or brain areas was not determined. Previous studies have also faced difficulties when analysing detection of SA- β -gal *in vivo* and *in vitro*, and despite its use as one of the main markers of senescence induction, its activity could be related to other cell processes, different to senescence. For instance, staining for SA- β -gal has been reported in follicles, sebaceous glands and eccrine glands in skin biopsies; this staining being independent of the age of the donors, which ranged between 20 and 90 years old (Dimri et al., 1995; Severino et al., 2000).

Recently, the study of senescence in neurones revealed a non-senescence related activity of SA- β -gal in the hippocampus of young and old mice. In this report, the number of SA- β -gal⁺ hippocampal neurones did increase with the age of the mice, a phenomenon that was related to the expansion of lysosomes as a result of oxidative stress and protein aggregation (Piechota et al., 2016). Taking this evidence into account, the possibility that increased SA- β -gal activity is, in part, associated with age or other non-senescence related cellular mechanisms cannot be excluded.

5.5.1.2. Expression of p16 and p21 in ALS/MND and control brains

5.5.1.2.1. Expression of p16 and p21 in astrocytes suggests activation of glial senescence in ALS/MND and control brains

Assessment of p16/p21 expression offers a more sensitive approach to study the activation of senescence signalling cascades in ALS/MND, compared to SA- β -gal activity detection. The current study demonstrated astroglial expression of p16 and p21, which was confirmed by co-localisation with the astrocytic marker GFAP in ALS/MND and control brains. Previous data has demonstrated that astrocytes activate senescence pathways *in vitro* and develop a SASP when exposed to different stresses, including oxidative stress (Bitto et al., 2010). Further investigation revealed accumulation of p16⁺ astrocytes as a feature of normal ageing in the human brain; additionally, the assessment of frontal cortex sections from AD patients and aged-matched controls showed a significantly higher percentage of p16⁺ astrocytes in AD patients, which suggests activation of senescence under pathological conditions (Bhat et al., 2012). More recently, expression of p16 in astrocytes has been reported in the white matter of the ageing human brain (Al-Mashhadi et al., 2015). Overall, this data correlates with the expression of p16 exclusively associated with astrocytes in ALS/MND and control donors that is described

in this chapter. The presence of p16⁺ astrocytes in control brains could suggest astrocytic senescence as a normal feature of the ageing process, which could be exacerbated by the pathology in a neurodegenerative disease such as ALS/MND.

Activation of senescence in astrocytes is further supported by the identification of p21⁺ astrocytes in ALS/MND and control brains. It is known that the p16 and the p21 pathways have a different role in the activation and maintenance of a senescent state in mitotic cells. A study conducted in human lung fibroblasts found that p21 is required for the G1-cell cycle arrest that characterises senescence in response to DNA damage, while p16 accumulation is necessary for the long-term maintenance of a senescent state (Stein et al., 1999). However, the interplay between p16 and p21 pathways is more complicated than described by Stein et al. For instance, it has been suggested that p16 is not necessary for the induction of telomere shortening dependent-senescence in human fibroblasts, but is rather dependent on the ATM-p53-p21 axis (Herbig et al., 2004). A different study described a p21-dependent cell cycle arrest in normal fibroblasts exposed to ionising radiation and replicative senescence; this pathway was affected in p53-deficient Li-Fraumeni syndrome (LFS) fibroblasts, which instead activated senescence through the p16 pathway (Mirzayans et al., 2010). Together, this evidence suggests that, apart from participating at different stages of senescence activation, the p16 or p21 senescence-effector pathways are triggered depending on the type of stress that the cells are exposed to. Expression of p16 and p21 cell cycle regulatory proteins in astrocytes of ALS/MND and control brains could reflect a pool of cells at different stages of the senescent program, a pool of cells that have entered senescence as a consequence of different types of stress, or both.

5.5.1.2.2. Expression of p21 in neurones of ALS/MND and control brains

The expression of p21 and other cell cycle regulatory proteins in post-mitotic neurones is not well understood. It has been suggested that p21 has a role in neuronal cell cycle regulation during DNA damage response and repair mechanisms. Cell cycle re-entry is necessary for neurones to repair DNA damage or to activate apoptosis (Kruman et al., 2004; Schwartz et al., 2007; Tomashevski et al., 2010). Exposure of rat cortical neurones to a sub-lethal oxidative stress causes G0 to G1 transition and triggers DNA repair through the NHEJ pathway; blocking cell cycle re-entry under these conditions does not promote NHEJ activation and the damage is left unrepaired. Moreover, suppression of p21 in the absence of DNA damage is sufficient to cause cell cycle re-entry and NHEJ activation (Tomashevski et al., 2010), which suggests that p21 is linked to maintaining neurones in the G0 phase. In a different study, induction of DNA damage using ionising radiation *in vivo* caused an increase in the mRNA and protein levels of p21 and cyclin D in sensory ganglion neurones; this increase occurred 1 day after IR exposure and persisted for 15 days before starting to gradually decrease (Casafont et al., 2011). This data demonstrates that neuronal DNA damage promotes G0 to G1 transition, confirmed by cyclin D up-regulation, but at the same, entry into S-phase and cell death is prevented by activation of the cell cycle inhibitor p21. Taking all this into consideration, it is possible that minimal basal levels of p21 are expressed in post-mitotic neurones under normal conditions in order to maintain a quiescent state; however, these levels can be altered when neurones face DNA damage and require activation of repair mechanisms. Expression of nuclear p21 in ALS/MND and control cases, in the MCx, FACx, SC and OCx, could be in part related to a normal response to age-related DNA damage that requires nuclear p21 induction to prevent aberrant S-phase transition and apoptosis.

Cell cycle and senescence are intimately related, since activation of senescent pathways is preceded by cell cycle arrest in response to a persistent DNA damage. Even though the neuronal cell cycle rests in G0 phase naturally, the fact that DNA damage promotes cell cycle re-entry suggests that, under specific circumstances of persistent unrepaired DNA damage, neurones could also activate a senescent-like response through the p21 pathway. To date, there is one report suggesting a p21-dependent senescent-like mechanism in neurones *in vivo*. Examination of brains from 1-year-old mice compared to their wild type litter mates confirmed increased γ H2AX⁺ Purkinje cells and cortical neurones, along with increased expression of p-p38MAPK and IL-6; when p21 was knocked out, a significant reduction in these senescence markers was seen, suggesting a p21-dependent activation of senescence in these cells in response to DNA damage (Jurk et al., 2012). The presence of p21⁺ neurones in ALS/MND and control brains may also indicate activation of a senescent-like state in some of these cells, which would correlate with the presence of SA- β -gal⁺ in neurones described previously.

5.5.1.2.3. Expression of senescence markers is significantly higher in the FACx of

ALS/MND brains

Interestingly, quantification of p16/p21⁺ glia and p21⁺ neurones resulted in a significantly higher percentage of positive cells only in the FACx of ALS/MND cases when compared to controls, but not in the MCx. Brettschneider et al. (2013) studied the distribution patterns of phosphorylated TDP-43 inclusions in the brain of ALS/MND cases in order to define stages that described the sequential spread of the pathology, similar to the use of Braak neurofibrillary tangle stages for AD neuropathology. This assessment revealed a sequential spread of the pTDP-43 pathology in the brain of ALS/MND cases and staging of this spread resulted in 4 main stages, with stage 1 and 2 consisting of pTDP-43

pathology in motor areas and brainstem, and stages 3 and 4 consisting of pTDP-43 spread to prefrontal cortex, striatum, post-central neocortex, temporal lobe and hippocampal formation (Brettschneider et al., 2013). Thus, the FACx in this ALS/MND cohort could be representative of the early stages of the disease that occur in the motor areas. The significantly higher expression of p16/p21⁺ glia and p21⁺ neurones could reflect DNA damage-related cell cycle dysregulation and probably a senescent-like mechanism in early stages of ALS/MND.

5.5.1.3. Oxidative DNA damage and the DNA damage response in ALS/MND

The expression of 8-OHdG, a biomarker of oxidative stress in neurodegeneration confirms that oxidative DNA damage is a prominent feature of both control and ALS/MND cases, where it localises to the nuclei and cytoplasm of pyramidal neurones, small neurones and glial cells, suggesting the oxidation of nuclear DNA, mitochondrial DNA and RNA. Several studies have identified increased oxidative stress in ALS/MND, which contributes to the pathology of the disease (Blasco et al., 2016; Chang et al., 2008; Ferrante et al., 1997; Ikawa et al., 2015; Shaw et al., 1995). The high proportion of 8-OHdG⁺ neurones in control donors may be attributed to the accumulation of ROS due to ageing and other disease processes. It remains possible that the degree of neuronal DNA oxidation could be different between ALS/MND cases and controls, but the immunohistochemical detection of 8-OHdG provides only limited, non-linear, quantification. As DNA oxidation induces a DDR, levels of γ H2AX were also investigated. No difference in the expression of γ H2AX was detected in ALS/MND compared to control donors. The phosphorylation of the histone variant H2AX at Ser139 is an important event in the initiation of the DNA repair response and correlates well with the formation of DSBs (Kinner et al., 2008). The pattern of variation in the expression of

γ H2AX was more pronounced in the MCx of ALS/MND patients but not in the FACx, where the highest levels were detected in controls. Interestingly, a significantly lower percentage of γ H2AX⁺ neurones was found in FTLD-TDP type B (all *C9orf72*⁺) cases when compared to FTLD-Minor changes/0 cases that suggests the DDR could be affected by p62 accumulation. Previous research has proposed that a defective DDR and accumulation of DNA damage could contribute to motor neuron degeneration in neuromuscular disorders such as ALS/MND (De Waard et al., 2010). Moreover, a recent study showed that *C9orf72* repeat expansion causes a defective ATM signalling in response to DNA damage through a mechanism that involves p62 accumulation and increase in R-loop structures formation (Walker et al., 2017). The DDR activated in response to DSBs involves an ATM-dependent phosphorylation of H2AX (Burma et al., 2001); a lower percentage of γ H2AX⁺ neurones in the FACx of ALS/MND could reflect ATM dysfunction and therefore, a reduction in H2AX phosphorylation. Again, the fact that this difference was only detectable in the FACx might indicate that DDR impairment could be involved from early stages of the disease. It is important to consider that the number of FTLD-TDP type B cases assessed was very low (4 cases) and so, it would be interesting to investigate expression of these markers specifically in relation to *C9orf72* in a bigger cohort.

No significant correlation was detected between the expression of 8-OHdG and γ H2AX⁺ neurones, and between 8-OHdG/ γ H2AX⁺ and p21⁺ neurones in the MCx and FACx of ALS/MND. This could be related to the heterogeneity of the cohort, which has been shown to affect the detection of neuronal γ H2AX, to the cohort size, and to the expression of high levels of both γ H2AX and nuclear 8-OHdG in neurones of control cases that could be linked to the ageing process.

5.5.1.4. No evidence of microglial activation in the FACx of ALS/MND donors

One way to examine if the higher levels of p21⁺ neurones and p16/p21⁺ glia in the FACx of ALS/MND were related to a senescence-like state was to look at the development of a SASP through the activation of a microglial response in this brain area. The SASP is characterised by the release of cytokines, chemokines, growth factors and proteases that promote inflammation and cause changes in the microenvironment of tissues (Coppé et al., 2008); in this context, activation of a SASP in the FACx of ALS/MND cases would promote recruitment of reactive microglia to this brain region. CD68, a microglial marker, is present in lysosomes and the cell membrane (Smith and Koch, 1987). Expression of CD68 aids in the identification of the microglia phenotype, as shown by Hendrickxs et al. (2017). CD68 is expressed by resting ramified microglia, amoeboid microglia and large foamy macrophages; an amoeboid phenotype in microglia indicates phagocytic reactivity (Hendrickx et al., 2017). There was no evidence of amoeboid microglia in the FACx of ALS/MND donors; detection of CD68 showed only the presence of resting ramified microglia. This result was confirmed by the detection of MHC class II, which is involved in presenting processed extracellular antigens to CD4⁺ helper T lymphocytes and is up-regulated in response to immune activation (Collawn and Benveniste, 1999). MHC class II was not up-regulated in the FACx of ALS/MND controls, and together with the CD68 data, indicated no microglial activation.

5.5.2. Microarray analysis of the transcriptome of FACx neurones in ALS/MND

An interest in the FACx neurones of ALS/MND cases was developed based on the results obtained from the immunohistochemistry experiments, which revealed a significantly

higher expression of p21⁺ neurones in this brain region. Gene profiling analysis was used to identify changes in the transcriptome of FACx neurones from ALS/MND and control donors that could relate the expression of p21 with dysregulation of cell cycle and senescence pathways.

Quality control analysis of the microarray data revealed an outlier in the control group. Removal of this array from the final analysis was done to improve the detection of differentially expressed genes. After removal, a total of 820 differentially expressed transcripts were identified in the ALS/MND FACx neurones; from these transcripts, 358 were up-regulated while 462 transcripts were down-regulated. Functional and pathway analyses did not show dysregulation of senescence or cell cycle pathways, but identified changes in the p53-signalling pathway (*GADD45*, *FAS*, *RCHY1* and *PMAIP1*). *GADD45* has been implicated in neuronal survival both *in vivo* and *in vitro*. Detection of the protein in AD brain tissue indicated expression of *GADD45* in neurones associated with the expression of the anti-apoptotic protein Bcl-2; moreover, HEK 293 cells transfected with *GADD45* are more resistant to camptothecin induced apoptosis (Torp et al., 1998). *FAS* encodes for the Fas Cell Surface Death Receptor, which participates in the activation of the extrinsic apoptosis pathway. RNA-interference silencing of this gene in SOD1-G93A mice motorneurones *in vivo* and *in vitro* significantly delays the onset of disease and promotes cell survival (Locatelli et al., 2007). Overall, these results suggest activation of apoptosis and cell survival signals in the FACx neurones of ALS/MND donors and could be linked to the expression of p21 and cell cycle reactivation in response to DNA damage.

Manual examination of the dysregulated transcripts with the higher FC values identified differential expression of mitochondrial function related genes, including up-regulation of *NDUFAF7*, *COX20*, *ENOSF1* and *AK2*, and down-regulation of *SLC25A37* and *SLC9B1*. None of these genes have been previously reported to be involved in ALS/MND pathogenesis; however, they could reflect mitochondrial alterations in the FACx neurones of ALS/MND donors, which are known to occur as part of the disease. Wiedeman et al. (2000) demonstrated reduced capacity of the ETC complexes (I, II, III and IV) in spinal cords of sporadic ALS/MND patients (Wiedemann et al., 2002) and reduced complex IV activity, specifically, has been seen in spinal cord of 17-week old symptomatic SOD1 G93A transgenic mice and in mitochondria isolated from the forebrain of presymptomatic, symptomatic and end-stage SOD1^{G93A} transgenic mice (Kirkinetzos, 2005; Mattiazzi et al., 2002)- Contrary to these reports, increased mitochondrial activity has also been detected *in vivo*. Increased complex I activity is found in the frontal cortex of fALS cases with a SOD1 AV4 mutation (Bowling et al., 1993); this complex I hyperactivity has also been reported in the forebrain of SOD1 G93 transgenic mice (Browne et al., 1998). It is possible that the changes in mitochondrial function indicating increased or impaired activity depend on the stage of the disease, as well as on the mutations involved and the model of study. Up-regulation of *NDUFAF7* and *COX20* in the FACx neurones of ALS/MND donors would suggest increased ETC activity, however, it could also reflect a mechanism of compensation in the case of impaired mitochondrial activity. Down-regulation of *SLC25A37* and *SLC9B1* points to mitochondrial defective solute transport. *SLC25A37* encodes for mitoferrin-2, a solute carrier that transports iron into the mitochondrial matrix and that is necessary for the proper functioning of other mitochondrial enzymes (Haitina et al., 2006).

Overall, transcriptome analysis of FACx neurones from ALS/MND patients revealed up-regulation of apoptotic pathways and alteration of mitochondrial function. qRT-PCR validation of *GADD45*, *COX20* and *SLC25A37* did not confirm these findings. These results could be related to a number of limitations. Ideally, validation would have been performed in at least 3 enriched neuronal RNA samples obtained by LCM from each of the control and ALS/MND cases available. This was not done due to time constraints and tissue availability. Validation could have also been affected by the case-to-case variability of the ALS/MND and control cases within the cohort, especially in the control group, which was composed of both diseased and non-diseased cases due to limited availability of the latter. qRT-PCR results showing a high variability in the expression of *GADD45*, *COX20* and *SLC25A37* within the controls could reflect changes linked to pathological changes in the diseased-controls. And finally, RNA quality could have been compromised by storage conditions; even though all samples were tested for RNA quality, this factor could still have an effect on gene expression and validation experiments.

Aging itself promotes activation of senescence in mitotic cells as a result of mechanisms such as telomere shortening, DNA damage and oxidative stress; however, an extra burden of senescent cells could be generated under certain pathological conditions characterised by increased ROS production, increased DNA damage and protein aggregation, for example. The identification of SA- β -gal⁺ neurones in the frontal association cortex of ageing brains and its weak correlation with DNA damage markers suggested a possible senescent-like state in these cells that could be contributing to neuronal dysfunction (Simpson et al., 2015). Based on this, we decided to look for senescent neurones in a neurodegenerative disease, such as ALS/MND, which is characterised by stresses that are known to trigger senescence in mitotic cells. However, immunohistochemical and

transcriptomic analysis of controls *vs* ALS/MND cases evidenced several limitations of the study, including the identification of dysregulated pathways linked to the disease itself, rather than to a mechanism that could be linked to senescence. The heterogeneity of the cohort could have also affected the results, since it included young and old donors, and both sALS and fALS cases. To avoid these interferences, it would have been better to start by analysing the transcriptomic neuronal signature of young and old donors. This would have given us the opportunity to identify dysregulated pathways in LCM neurones from old brains and a higher probability of identifying changes linked to cellular senescence and cell cycle regulation.

5.6. Main conclusions

Expression of the senescence markers SA- β -gal, p16 and p21 was detected in control and ALS/MND brains. Expression of p16 was exclusively seen in glial cells, mainly astrocytes, while p21 was found in both neurones and glia. The expression of p16 and p21 in astrocytes of ALS/MND and control donors could reflect activation of senescence pathways related to ageing. However, a significantly higher percentage of p16/p21⁺ glia in the FACx of ALS/MND patients could indicate a contributing role of this mechanism to the disease. Further assessment of the contribution of senescent astrocytes in ALS/MND would be required.

Transcriptome analysis of FACx neurones from ALS/MND patients did not show dysregulation of senescent pathways; however, a more general mechanism of apoptosis and mitochondrial dysregulation was revealed in these cells. This could explain in part the significantly higher percentage of p21⁺ neurones detected in FACx, which could reflect cell cycle dysregulation in response to DNA damage. Even though transcriptomic analysis

did not reveal dysregulation of “classical” senescence pathways, we cannot discard that some level of neuronal p21 may be linked to senescence.

A significantly higher expression of p21⁺ neurones and p26/p21⁺ glia in the FACx of ALS/MND suggests the FACx is a brain area of importance to investigate early pathological changes in ALS/MND.

Chapter 6. General discussion

6.1. Summary of major findings and limitations of the study

The neuronal dysfunction that characterises neurodegenerative diseases is caused by a myriad of mechanisms, whose interactions remain poorly understood. One of the most studied mechanisms that participate in the pathophysiology of neurodegenerative diseases is the accumulation of ROS and the alteration of antioxidant mechanisms that result in oxidative stress. Neurones are highly vulnerable to imbalances in redox states; one of the many consequences of oxidative stress is the formation of lesions at the DNA level. Neurones detect oxidative DNA damage through finely orchestrated mechanisms that lead to either activation of repair signalling pathways or apoptosis. Recently, a third option has been proposed to occur in response to persistent genotoxic stress in neurones; this suggested mechanism known as senescence, could contribute to neurodegeneration via the development of a toxic secretory phenotype in neurones exposed to persistent DNA damage, resulting in cellular propagation of injury. Even though evidence of senescent neurones has been shown in ageing mice and in ageing human brain tissue (Jurk et al., 2012; Simpson et al., 2014), the mechanisms through which senescence is induced in post-mitotic neurones and its relevance to neurodegeneration is yet to be revealed. In the current study, activation of senescence was investigated in human neurones *in vitro* that were exposed to persistent oxidative DNA damage. At the same time, evidence of neuronal senescence in neurodegeneration was studied *in vivo*, in ALS/MND brains.

The first part of this study focused on the development of a robust model to investigate oxidative DNA damage in human neurones *in vitro*. LUHMES have several advantages

over primary rat cortical neurones or cancer-derived cell lines: their human origin, the ability of these cells to remain in a proliferative state, and their relatively short and simple differentiating protocol. Nevertheless, working with LUHMES also has some disadvantages. LUHMES are very vulnerable to cell culture stress; besides, cell density, pH and temperature changes can alter LUHMES proliferation, differentiation and neurite development. For toxicity assays, cell density is determinant in the effect that the toxic substance/condition will cause in differentiated LUHMES. This was confirmed when different densities of differentiated LUHMES were exposed to various H₂O₂ concentrations: sub-confluent cultures were more vulnerable to oxidative stress, and were able to clear extracellular H₂O₂ less efficiently compared to confluent differentiated LUHMES.

Assessment of different concentrations of H₂O₂ suggested 50 µM H₂O₂ as the best concentration to cause repairable DNA damage in differentiated LUHMES. DNA damage was tracked through the detection of γH2AX foci formation, which resulted in DNA damage repair 24 hours after the cells were incubated with H₂O₂. This discovery posed a new challenge in the attempt to study senescence activation in response to a persistent DNA damage, since a single H₂O₂ challenge caused an acute response rather than chronic damage in differentiated LUHMES. Consequently, a different approach was used to induce a persistent neuronal DNA damage, which involved the exposure of already stressed LUHMES to a second dose of H₂O₂. Results presented in Chapter 2 demonstrate that this second challenge causes oxidative DNA damage in the form of DSBs in differentiated LUHMES that can be detected 96 hours post-H₂O₂ incubation. The election of H₂O₂ was based on different studies that have evaluated the oxidative effects of H₂O₂ in primary neurons in culture (Morelli et al., 2014; Park et al., 2016; Tomashevski et al.,

2010; Whittemore et al., 1995). These reports suggested a simple method to induce detectable oxidative DNA damage in neurones in culture using H₂O₂ concentrations ranging from 5 µM to 1 mM with different results in terms of cell viability. One of the drawbacks of using H₂O₂ is its relatively low stability in solution; this, added to the normal processing of extracellular H₂O₂ by the LUHMES, could have certainly caused a gradual decrease of its initial concentration after a few hours. The gradual decrease of extracellular H₂O₂ concentration was demonstrated by the clearance assays, and could have had an effect on the level of DNA damage that was caused with a single dose of 50 µM H₂O₂.

Confirmation of a persistent oxidative DNA damage in differentiated LUHMES was followed by the detection of SA-β-gal and H3K9me3 as a marker for SAHF formation. SA-β-gal detection revealed variable staining in differentiated LUHMES under normal conditions. This unexpected finding questioned the validity of SA-β-gal for the identification of senescent cells *in vitro* and *in vivo*. Several reports have expressed concerns regarding the use of SA-β-gal as a universal marker of senescence (Piechota et al., 2016; Severino et al., 2000; Yegorov et al., 1998). Although the lysosomal origin of SA-β-gal has been characterised and up-regulation of mRNA levels and enzymatic activity have been seen in human fibroblasts in culture, it is yet not known if SA-β-gal plays a role in the induction of senescence. Most importantly, it is not known if its activity reflects activation of senescent pathways in all cell types. In this study, detection of SA-β-gal activity in normal LUHMES suggests that the increased activity of this enzyme could be involved in other mechanisms in neurones; interestingly, staining for SA-β-gal in ALS/MND and control brains was not localised to all neuronal cells. This could be due to the enzyme activity being affected by the conditions used to collect and

store the brain tissue. It is known that poor storage conditions and cycles of freezing and defrosting can alter the activity of several enzymes and SA- β -gal might not be the exception (Meijer et al., 1977). However, it is also probable that SA- β -gal activity is altered by the conditions under which LUHMES are differentiated and maintained in culture, and that increased SA- β -gal activity does not reflect the normal behaviour of the enzyme *in vivo*. It would be interesting to evaluate SA- β -gal at different levels, including its activity, protein and mRNA expression, in normal proliferating and differentiating LUHMES. This would help to establish whether the stress caused by the differentiation process, cell density or days in culture, for example, have an effect on SA- β -gal activity in this cell model.

H3K9me3 expression in control and SS/DS LUHMES also suggested a different role for this marker in post-mitotic cells. Methylation of H3K9 occurs as part of several chromatin modifications in senescent cells that have a role in cell cycle arrest and that can be detected in the form of nuclear foci known as SAHF (Aird and Zhang, 2013; Zhang et al., 2005, 2007). Previous data suggested SAHF formation in mice neurones *in vivo*, which correlates with accumulation of DNA damage, increases SA- β -gal activity and IL-6 secretion (Jurk et al., 2012). In contrast, detection of SAHF in SS/DS LUHMES did not indicate activation of senescence and suggested that chromatin organisation in response to DNA damage in neurones could participate in prevention of aberrant cell cycle re-entry and cell death. These results suggest that SAHF components could have specific functions in the neuronal DDR although it is not clear if they reflect activation of classical senescence.

Gene expression profiling of SS and DS LUHMES identified novel changes at the mRNA level that were linked to the oxidative DNA damage caused by single and double incubation of LUHMES in H₂O₂. Microarray analysis did not reveal up-regulation of senescence genes in the LUHMES model of persistent DNA damage, but showed dysregulation of DDR and cell cycle regulation pathways, as well as mitochondrial dysfunction and immune response activation. Dysregulation of ATR signalling and APC/C complex related genes in DS-LUHMES shows the effect that persistent oxidative DNA damage has on neuronal cell cycle regulation. It is possible that cell cycle events, as part of the neuronal DDR, are triggered just moments after DNA lesions are caused by oxidation; however, it is noteworthy that these changes are still detectable at the mRNA level 96 hours after stress. These findings have a potential implication in neuronal dysfunction *in vivo*, since they suggest that a persistent DNA damage can induce changes in neuronal cell cycle that can also persist for a longer period of time, compared to an acute stress. These abnormal cell cycle events in neurones exposed to an oxidative environment could contribute to neurodegeneration.

Even though microarray analysis in DS-LUHMES did not confirm up-regulation of classical senescence pathways, this does not exclude the possibility of neurones being capable of activating a senescent-like state under chronic DNA damage conditions. Evaluation of the transcriptome of 96 hours DS-LUHMES could have excluded valuable information concerning the neuronal response to oxidative stress occurring prior to this time-point; at the same time, limiting the H₂O₂ incubation time of SS and DS-LUHMES to 96 hours might not have been sufficient to cause induction of a senescent-like phenotype. Moreover, stressed LUHMES/GFP-LUHMES co-cultures suggested the development of a cell-to-cell contact-dependent toxic phenotype in DS-LUHMES, which

could resemble the SASP seen in mitotic cells. In this regard, microarray analysis did not confirm up-regulation of SASP molecules; however, as with other senescence markers assessed in this study, it is possible that the components of the toxic phenotype in neurones are not necessarily the same as the ones linked to the SASP.

Detection of senescence markers in neurones *in vivo* revealed significantly higher expression of p21⁺ neurones and p16/p21⁺ glial cells in the FACx of ALS/MND cases. These results suggest that alteration of the levels of both p21 and p16 could be linked to the pathological process in ALS/MND; they do not confirm, however, senescence induction in these cells, specially considering that there was no correlation between the expression of senescence markers and 8-OHdG/ γ H2AX expression in neurones of ALS/MND cases. An important point to reflect on is the probability of p16 and p21 cell cycle regulators having differential roles in neurones compared to mitotic cells. There is not much information available on how these two proteins are regulated in post-mitotic neurones, which limits the conclusions that can be drawn from studies showing neuronal expression of these markers. Characterisation of the role of p16 and p21 in neurones under normal conditions would help in the interpretation of these results and would aid in the study of senescence in neurones *in vivo* and *in vitro*. The FACx in ALS/MND represents a brain area with minimal no end-stage pathology. Findings in the FACx could reflect changes that occur early in the disease in motor areas and propose the FACx as a relevant region to understand early pathology in ALS/MND, although more evidence is needed to support these findings.

Several limitations should be acknowledged from the *in vivo* study. First, the ALS/MND group was composed of familial and sporadic ALS/MND cases, which could have had an

impact on the results. A relatively small cohort likely restricted the information that was obtained from the immunohistochemistry experiments; however, analysis of effect size, which is not dependent on sample size, revealed a medium to high effect of the differential expression of neuronal p21 and glial p16/p21 in the FACx of ALS/MND donors when compared to controls, thus confirming that the results obtained are statistically significant and of such a size as to be of likely biological relevance.

The use of LCM to isolate neurons from ALS/MND and control frozen sections has some limitations as well. Even though it is feasible to obtain samples with enriched neuronal populations using this technique, some level of contamination with glial cells, specifically astrocytes, was demonstrated by the detection of GFAP transcripts in 3 of the 6 samples obtained by LCM. Nevertheless, enrichment of neuronal cells still enables significant information on transcriptomic changes in neurones to be identified.

6.2. Conclusions

The current study describes the successful implementation of an *in vitro* model of persistent oxidative DNA damage in human neurones. Changes related to the APC/C:Cdh1 cell cycle regulatory complex, to the ATR-mediated DDR and to oxidative phosphorylation were linked to the effects caused by this persistent oxidative DNA damage. No evidence of classical senescence was shown in this model, as assessed by SA- β -gal activity and SAHF formation, but a toxic phenotype, similar to a SASP, may be developed under these conditions.

The study also demonstrated increased expression of nuclear p21 in neurones and of p21 and p16 in glial cells in the FACx of ALS/MND patients. Microarray analysis did not

suggest p21 neuronal expression to be linked to up-regulation of classical senescent pathways. However, expression of p21 in neurones could be part of a general response to DNA damage in these cells. *In vivo* results also propose the FACx as a brain area of importance in the study of early pathological changes in ALS/MND.

6.3. Future work

6.3.1. Characterisation of the ATR and the APC/C:Cdh1 complex in DS-LUHMES

Dysregulation of the ATR signalling pathway and of the APC/C:Cdh1 complex in DS-LUHMES could have implications in neuronal function *in vivo*, and could have a role in neurodegeneration. Further characterisation of these pathways in the DS-LUHMES model would provide valuable information in the mechanisms implicated in the neuronal response to a persistent DNA damage. Had time allowed, the ATR signalling pathway and the APC/C:Cdh1 complex activation would have been assessed at the mRNA and protein levels in SS/DS-LUHMES at different time-points, under the time frame of 96 hours . Tracking their kinetics would provide a better understanding of their role in the neuronal DNA damage response mechanisms. Moreover, it would provide new and valuable information on the function of the APC/C:Cdh1 complex in neurones, which is not yet fully understood.

6.3.2. Investigating a toxic secretory phenotype in DS-LUHMES

Evidence of an effect of DS-LUHMES on healthy differentiated GFP-LUHMES was observed, and it suggested that a secretory phenotype could be developed by neurones exposed to persistent oxidative DNA damage. Nevertheless, microarray results did not reveal dysregulation of senescence-linked immune response transcripts, except for

DDX58, which was not validated. However, it is important to take into account that transcripts identified by the microarray does not always relate to translation. Thus, detection of specific cytokines and chemokines using a cytokine array would help to confirm at the protein level whether these molecules, for instance IL-6 and IL-8, are up-regulated by DS-LUHMES in response to a persistent DNA damage or not.

6.3.3. Confirmation of qRT-PCR validation results for the in vivo study

Limited time and the limited availability of suitable frozen samples did not allow for qRT-PCR validation to be conducted in a larger cohort and in triplicate. In order to confirm the findings presented in this work, qRT-PCR validation of the candidate genes *GADD45A*, *COX20* and *SLC25A37* should be conducted in enriched neuronal samples obtained by LCM to complete an N of 3 and if possible in an extended cohort of a minimum of 10 cases, given the case-to-case variation of human subjects. Expression of these genes would be evaluated in samples from the FACx and the MCx of ALS/MND and control donors. This would allow an interesting comparison of the mechanisms altered in neurones from both brain regions in ALS/MND.

6.3.4. Investigating the origin of p21 expression in ALS/MND

Expression of nuclear p21 in neurones in ALS/MND could result from cell cycle changes linked to a DNA damage response. In order to advance this hypothesis, immunohistochemical detection of cell cycle re-entry markers could be conducted in the ALS/MND and control cases. Expression of cell proliferation markers, such as Ki67, and proteins implicated in the G0-G1 and G1-S transitions, such as cyclin D and cyclin E, would inform whether cell cycle re-entry occurs in ALS/MND neurones and would partly explain the presence of p21⁺ neurones. The same approach could be taken to determine if

some level of neuronal p21 expression in ALS/MND could result from the activation of the p21 senescence pathway. Double staining for p21 and p53, ATM and CHK2, three proteins that are involved in p21-dependent senescence, would suggest induction of this pathway in neurones in ALS/MND brains.

6.3.5. Investigating astrocyte senescence in ALS/MND

Expression of p16 and p21, as well as increased SA- β -gal activity in the cytoplasm of glial cells, suggests the presence of senescent glia in ALS/MND cases. Further investigation of these findings could inform on the involvement of glial senescence in the progression of the disease. Using immunohistochemistry and LCM we could determine whether p16/p21⁺ astrocytes are linked to increased expression of DDR and senescence signalling pathway proteins, such as ATM and p53 at the protein and mRNA levels. Also, assessment of cell cycle arrest in these cells could be investigated through the expression of cell cycle regulation and proliferation markers. Finally, based on available data on astrocyte senescence and the SASP (Mombach et al., 2015; Salminen et al., 2011) the expression candidates SASP-related genes could be investigated in LMC astrocyte enriched samples.

6.3.6. Directly reprogrammed human neurones to study ageing and senescence in vitro

The embryonic nature of LUHMES proved to be a limitation in the identification of age related changes in neurones *in vitro*, including the activation of a senescent-like state under persistent DNA damage conditions. For future studies on senescence and ageing, the use of directly reprogrammed human neurones (iNs) from fibroblasts of different aged donors would be a more appropriate model of study, since iNs retain the donor's ageing signature. It would be of interest to characterise and study changes in cell cycle control in

iNs from young and old donors, as well as changes in the DNA damage response mechanisms, to identify the effect that normal ageing can have in these pathways in neurones and if these effects relate to senescence.

6.3.7. Transcriptomic analysis of LCM neurones from young and old donors

Gene expression profiling of control and ALS/MND LCM neurones revealed changes linked to the pathology but not directly related to senescence. A better way to analyse activation of senescence in neurones would be by comparing changes in the transcriptome of neurones isolated from young and old brains. Data obtained from this analysis could be compared to the data obtained from iNs *in vitro*, which would allow for a more efficient identification of changes in neurones related to ageing, and could provide better evidence on whether neurones can activate a senescent-like state or not.

References

Acosta, J.C., O’Loughlen, A., Banito, A., Guijarro, M. V., Augert, A., Raguz, S., Fumagalli, M., Da Costa, M., Brown, C., Popov, N., et al. (2008). Chemokine Signaling via the CXCR2 Receptor Reinforces Senescence. *Cell* *133*, 1006–1018.

Acosta, J.C., Banito, A., Wuestefeld, T., Georgilis, A., Janich, P., Morton, J.P., Athineos, D., Kang, T.-W., Lasitschka, F., Andrulis, M., et al. (2013). A complex secretory program orchestrated by the inflammasome controls paracrine senescence. *Nat. Cell Biol.* *15*, 978–990.

Agostini, M., Romeo, F., Inoue, S., Niklison-Chirou, M. V, Elia, A.J., Dinsdale, D., Morone, N., Knight, R.A., Mak, T.W., and Melino, G. (2016). Metabolic reprogramming during neuronal differentiation. *Cell Death Differ.* *23*, 1502–1514.

Aird, K.M., and Zhang, R. (2013). Detection of senescence-associated heterochromatin foci (SAHF). *Methods Mol. Biol.* *965*, 185–196.

Aksenova, M. V, Aksenov, M.Y., Mactutus, C.F., and Booze, R.M. (2005). Cell culture models of oxidative stress and injury in the central nervous system. *Curr. Neurovasc. Res.* *2*, 73–89.

Al-Chalabi, A., Kwak, S., Mehler, M., Rouleau, G., Siddique, T., Strong, M., and Leigh, P.N. (2013). Genetic and epigenetic studies of amyotrophic lateral sclerosis. *Amyotroph. Lateral Scler. Frontotemporal Degener.* *14 Suppl 1*, 44–52.

Al-Mashhadi, S., Simpson, J.E., Heath, P.R., Dickman, M., Forster, G., Matthews, F.E., Brayne, C., Ince, P.G., Wharton, S.B., and Medical Research Council Cognitive Function and Ageing Study (2015). Oxidative Glial Cell Damage Associated with White Matter Lesions in the Aging Human Brain. *Brain Pathol.* *25*, 565–574.

Alimonti, A., Nardella, C., Chen, Z., Clohessy, J.G., Carracedo, A., Trotman, L.C., Cheng, K., Varmeh, S., Kozma, S.C., Thomas, G., et al. (2010). A novel type of cellular senescence that can be enhanced in mouse models and human tumor xenografts to suppress prostate tumorigenesis. *J. Clin. Invest.* *120*, 681–693.

Almeida, A., Bolaños, J.P., and Moreno, S. (2005). Cdh1/Hct1-APC is essential for the survival of postmitotic neurons. *J. Neurosci.* *25*, 8115–8121.

Alvira, D., Yeste-Velasco, M., Folch, J., Casadesus, G., Smith, M.A., Pallas, M., and Camins, A. (2007). Neuroprotective effects of caffeine against complex I inhibition-induced apoptosis are mediated by inhibition of the ATM/p53/E2F-1 path in cerebellar granule neurons. *J. Neurosci. Res.* *85*, 3079–3088.

Ameziane-El-Hassani, R., and Dupuy, C. (2017). Detection of Reactive Oxygen Species in Cells Undergoing Oncogene-Induced Senescence BT - Oncogene-Induced

Senescence: Methods and Protocols. M.A. Nikiforov, ed. (New York, NY: Springer New York), pp. 139–145.

Aravinthan, A., Mells, G., Allison, M., Leathart, J., Kotronen, A., Yki-Jarvinen, H., Daly, A.K., Day, C.P., Anstee, Q.M., and Alexander, G. (2014). Gene polymorphisms of cellular senescence marker p21 and disease progression in non-alcohol-related fatty liver disease. *Cell Cycle* 13, 1489–1494.

Baker, D.J., Wijshake, T., Tchkonina, T., Lebrasseur, N.K., Childs, B.G., Van De Sluis, B., Kirkland, J.L., and Van Deursen, J.M. (2011). Clearance of p16 Ink4a-positive senescent cells delays ageing-associated disorders. *Nature* 479, 232–236.

Barascu, A., Le Chalony, C., Pennarun, G., Genet, D., Imam, N., Lopez, B., and Bertrand, P. (2012). Oxidative stress induces an ATM-independent senescence pathway through p38 MAPK-mediated lamin B1 accumulation. *EMBO J.* 31, 1080–1094.

Barber, S.C., and Shaw, P.J. (2010). Oxidative stress in ALS: Key role in motor neuron injury and therapeutic target. *Free Radic. Biol. Med.* 48, 629–641.

Bartkova, J., Rezaei, N., Liontos, M., Karakaidos, P., Kletsas, D., Issaeva, N., Vassiliou, L.V.F., Kolettas, E., Niforou, K., Zoumpourlis, V.C., et al. (2006). Oncogene-induced senescence is part of the tumorigenesis barrier imposed by DNA damage checkpoints. *Nature* 444, 633–637.

Bassermann, F., Frescas, D., Guardavaccaro, D., Busino, L., Peschiaroli, A., and Pagano, M. (2008). The Cdc14B-Cdh1-Plk1 Axis Controls the G2 DNA-Damage-Response Checkpoint. *Cell* 134, 256–267.

Bensimon, A., Schmidt, A., Ziv, Y., Elkon, R., Wang, S.Y., Chen, D.J., Aebersold, R., and Shiloh, Y. (2010). ATM-dependent and -independent dynamics of the nuclear phosphoproteome after DNA damage. *Sci. Signal.* 3.

Berkenkamp, B., Susnik, N., Baisantry, A., Kuznetsova, I., Jacobi, C., Sørensen-Zender, I., Broecker, V., Haller, H., Melk, A., and Schmitt, R. (2014). In vivo and in vitro analysis of age-associated changes and somatic cellular senescence in renal epithelial cells. *PLoS One* 9.

Berridge, M.V., and Tan, A.S. (1993). Characterization of the Cellular Reduction of 3-(4,5-dimethylthiazol-2-yl)-2,5-diphenyltetrazolium bromide (MTT): Subcellular Localization, Substrate Dependence, and Involvement of Mitochondrial Electron Transport in MTT Reduction. *Arch. Biochem. Biophys.* 303, 474–482.

Berridge, M. V., Herst, P.M., and Tan, A.S. (2005). Tetrazolium dyes as tools in cell biology: New insights into their cellular reduction. *Biotechnol. Annu. Rev.* 11, 127–152.

Bhat, R., Crowe, E.P., Bitto, A., Moh, M., Katsetos, C.D., Garcia, F.U., Johnson, F.B., Trojanowski, J.Q., Sell, C., and Torres, C. (2012). Astrocyte Senescence as a Component of Alzheimer's Disease. *PLoS One* 7.

BINDER, L.I., FRANKFURTER, A., and REBHUN, L.I. (1986). Differential Localization of MAP τ and Tau in Mammalian Neurons in Situ. *Ann. N. Y. Acad. Sci.* 466, 145–166.

Biran, A., Zada, L., Abou Karam, P., Vadai, E., Roitman, L., Ovadya, Y., Porat, Z., and Krizhanovsky, V. (2017). Quantitative identification of senescent cells in aging and disease. *Aging Cell* 16, 661–671.

Birben, E., Sahiner, U.M., Sackesen, C., Erzurum, S., and Kalayci, O. (2012). Oxidative stress and antioxidant defense. *World Allergy Organ. J.* 5, 9–19.

Bitto, A., Sell, C., Crowe, E., Lorenzini, A., Malaguti, M., Hrelia, S., and Torres, C. (2010). Stress-induced senescence in human and rodent astrocytes. *Exp. Cell Res.* 316, 2961–2968.

Blasco, H., Garcon, G., Patin, F., Veyrat-Durebex, C., Boyer, J., Devos, D., Vourc'h, P., Andres, C.R., Corcia, P., Andersen, P.M., et al. (2016). Panel of Oxidative Stress and Inflammatory Biomarkers in ALS: A Pilot Study. *Can. J. Neurol. Sci. / J. Can. Des Sci. Neurol.* 6, 1–6.

Bochman, M.L., and Schwacha, A. (2008). The Mcm2-7 Complex Has In Vitro Helicase Activity. *Mol. Cell* 31, 287–293.

Bodnar, A.G., Ouellette, M., Frolkis, M., Holt, S.E., Chiu, C.P., Morin, G.B., Harley, C.B., Shay, J.W., Lichtsteiner, S., and Wright, W.E. (1998). Extension of life-span by introduction of telomerase into normal human cells. *Science* (80-.). 279, 349–352.

Bogdanov, M., Brown, R.H., Matson, W., Smart, R., Hayden, D., O'Donnell, H., Flint Beal, M., and Cudkowicz, M. (2000). Increased oxidative damage to DNA in ALS patients. *Free Radic. Biol. Med.* 29, 652–658.

Bogefors, J., Kvarnhammar, A.M., Latif, L., Petterson, T., Uddman, R., and Cardell, L.O. (2011). Retinoic acid-inducible gene 1-like receptors in the upper respiratory tract. *Am. J. Rhinol. Allergy* 25.

Bottenstein, J.E., and Sato, G.H. (1979). Growth of a rat neuroblastoma cell line in serum-free supplemented medium. *Proc. Natl. Acad. Sci.* 76, 514–517.

BOURGES, I., RAMUS, C., MOUSSON de CAMARET, B., BEUGNOT, R., REMACLE, C., CARDOL, P., HOFHAUS, G., and ISSARTEL, J.-P. (2004). Structural organization of mitochondrial human complex I: role of the ND4 and ND5 mitochondria-encoded subunits and interaction with prohibitin. *Biochem. J.* 383, 491–499.

Bowling, a C., Schulz, J.B., Brown, R.H., and Beal, M.F. (1993). Superoxide dismutase activity, oxidative damage, and mitochondrial energy metabolism in familial and sporadic amyotrophic lateral sclerosis. *J. Neurochem.* 61, 2322–2325.

Braig, M., Lee, S., Loddenkemper, C., Rudolph, C., Peters, A.H.F.M., Schlegelberger, B., Stein, H., Dörken, B., Jenuwein, T., and Schmitt, C.A. (2005). Oncogene-induced

senescence as an initial barrier in lymphoma development. *Nature* 436, 660–665.

Brandl, A., Meyer, M., Bechmann, V., Nerlich, M., and Angele, P. (2011). Oxidative stress induces senescence in human mesenchymal stem cells. *Exp. Cell Res.* 317, 1541–1547.

Brettschneider, J., Del Tredici, K., Toledo, J.B., Robinson, J.L., Irwin, D.J., Grossman, M., Suh, E., Van Deerlin, V.M., Wood, E.M., Baek, Y., et al. (2013). Stages of pTDP-43 pathology in amyotrophic lateral sclerosis. *Ann. Neurol.* 74, 20–38.

Browne, S.E., Bowling, a C., Baik, M.J., Gurney, M., Brown, R.H., and Beal, M.F. (1998). Metabolic dysfunction in familial, but not sporadic, amyotrophic lateral sclerosis. *J. Neurochem.* 71, 281–287.

Bryson, B.L., Junk, D.J., Cipriano, R., and Jackson, M.W. (2017). STAT3-mediated SMAD3 activation underlies Oncostatin M-induced Senescence. *Cell Cycle* 16, 319–334.

Budnik, V., and Salinas, P.C. (2011). Wnt signaling during synaptic development and plasticity. *Curr. Opin. Neurobiol.* 21, 151–159.

Burma, S., Chen, B.P., Murphy, M., Kurimasa, A., and Chen, D.J. (2001). ATM phosphorylates histone H2AX in response to DNA double-strand breaks. *J. Biol. Chem.* 276, 42462–42467.

Buttitta, L.A., and Edgar, B.A. (2007). Mechanisms controlling cell cycle exit upon terminal differentiation. *Curr. Opin. Cell Biol.* 19, 697–704.

Caceres, A., Banker, G., Steward, O., Binder, L., and Payne, M. (1984). MAP2 is localized to the dendrites of hippocampal neurons which develop in culture. *Dev. Brain Res.* 13, 314–318.

Capell, B.C., Drake, A.M., Zhu, J., Shah, P.P., Dou, Z., Dorsey, J., Simola, D.F., Donahue, G., Sammons, M., Rai, T.S., et al. (2016). MLL1 is essential for the senescence-associated secretory phenotype. *Genes Dev.* 30, 321–336.

Casafont, I., Palanca, A., Lafarga, V., Berciano, M.T., and Lafarga, M. (2011). Effect of ionizing radiation in sensory ganglion neurons: Organization and dynamics of nuclear compartments of DNA damage/repair and their relationship with transcription and cell cycle. *Acta Neuropathol.* 122, 481–493.

Cavill, R., Kamburov, A., Ellis, J.K., Athersuch, T.J., Blagrove, M.S.C., Herwig, R., Ebbels, T.M.D., and Keun, H.C. (2011). Consensus-phenotype integration of transcriptomic and metabolomic data implies a role for metabolism in the chemosensitivity of tumour cells. *PLoS Comput. Biol.* 7.

Chan, K.T., Paavolainen, L., Hannan, K.M., George, A.J., Hannan, R.D., Simpson, K.J., Horvath, P., and Pearson, R.B. (2016). Combining High-Content Imaging and Phenotypic Classification Analysis of Senescence-Associated Beta-Galactosidase Staining to Identify Regulators of Oncogene-Induced Senescence. *Assay Drug Dev. Technol.* 14, 416–428.

Chang, B.D., Watanabe, K., Broude, E. V, Fang, J., Poole, J.C., Kalinichenko, T. V, and Roninson, I.B. (2000). Effects of p21Waf1/Cip1/Sdi1 on cellular gene expression: implications for carcinogenesis, senescence, and age-related diseases. *Proc Natl Acad Sci U S A* 97, 4291–4296.

Chang, L., Zhang, Z., Yang, J., McLaughlin, S.H., and Barford, D. (2015). Atomic structure of the APC/C and its mechanism of protein ubiquitination. *Nature* 522, 450–454.

Chang, Y., Kong, Q., Shan, X., Tian, G., Ilieva, H., Cleveland, D.W., Rothstein, J.D., Borchelt, D.R., Wong, P.C., and Lin, C.L.G. (2008). Messenger RNA oxidation occurs early in disease pathogenesis and promotes motor neuron degeneration in ALS. *PLoS One* 3.

Chen, S., Sayana, P., Zhang, X., and Le, W. (2013). Genetics of amyotrophic lateral sclerosis: An update. *Mol. Neurodegener.* 8.

Chen, X., Vinade, L., Leapman, R.D., Petersen, J.D., Nakagawa, T., Phillips, T.M., Sheng, M., and Reese, T.S. (2005a). Mass of the postsynaptic density and enumeration of three key molecules. *Proc. Natl. Acad. Sci.* 102, 11551–11556.

Chen, X., Nelson, C.D., Li, X., Winters, C.A., Azzam, R., Sousa, A.A., Leapman, R.D., Gainer, H., Sheng, M., and Reese, T.S. (2011). PSD-95 Is Required to Sustain the Molecular Organization of the Postsynaptic Density. *J. Neurosci.* 31, 6329–6338.

Chen, Z., Trotman, L.C., Shaffer, D., Lin, H.K., Dotan, Z.A., Niki, M., Koutcher, J.A., Scher, H.I., Ludwig, T., Gerald, W., et al. (2005b). Crucial role of p53-dependent cellular senescence in suppression of Pten-deficient tumorigenesis. *Nature* 436, 725–730.

Chernova, T., Nicotera, P., and Smith, A.G. (2006). Heme deficiency is associated with senescence and causes suppression of N-Methyl-D-aspartate receptor subunits expression in primary cortical neurons. *Mol. Pharmacol.* 69, 697–705.

Chien, Y., Scuoppo, C., Wang, X., Fang, X., Balgley, B., Bolden, J.E., Premsrirut, P., Luo, W., Chicas, A., Lee, C.S., et al. (2011). Control of the senescence-associated secretory phenotype by NF- κ B promotes senescence and enhances chemosensitivity. *Genes Dev.* 25, 2125–2136.

Childs, B.G., Durik, M., Baker, D.J., and van Deursen, J.M. (2015). Cellular senescence in aging and age-related disease: from mechanisms to therapy. *Nat. Med.* 21, 1424–1435.

Choi, J., Rees, H.D., Weintraub, S.T., Levey, A.I., Chin, L.S., and Li, L. (2005). Oxidative modifications and aggregation of Cu,Zn-superoxide dismutase associated with alzheimer and Parkinson diseases. *J. Biol. Chem.* 280, 11648–11655.

Ciccia, A., and Elledge, S.J. (2010). The DNA Damage Response: Making It Safe to Play with Knives. *Mol. Cell* 40, 179–204.

Cisowski, J., Sayin, V.I., Liu, M., Karlsson, C., and Bergo, M.O. (2016). Oncogene-

induced senescence underlies the mutual exclusive nature of oncogenic KRAS and BRAF. *Oncogene* 35, 1328–1333.

Cohen, J. (1988). Statistical power analysis for the behavioral sciences. *Stat. Power Anal. Behav. Sci.* 2nd, 567.

Cohen, J., D'Agostino, L., Wilson, J., Tuzer, F., and Torres, C. (2017). Astrocyte Senescence and Metabolic Changes in Response to HIV Antiretroviral Therapy Drugs. *Front. Aging Neurosci.* 9, 1–12.

Coleman, P.R., Chang, G., Hutás, G., Grimshaw, M., Vadas, M.A., and Gamble, J.R. (2013). Age-associated stresses induce an anti-inflammatory senescent phenotype in endothelial cells. *Aging (Albany, NY)*. 5, 913–924.

Collawn, J.F., and Benveniste, E.N. (1999). Regulation of MHC class II expression in the central nervous system. *Microbes Infect.* 1, 893–902.

Coombes, E., Jiang, J., Chu, X.-P., Inoue, K., Seeds, J., Branigan, D., Simon, R.P., and Xiong, Z.-G. (2011). Pathophysiologically Relevant Levels of Hydrogen Peroxide Induce Glutamate-Independent Neurodegeneration That Involves Activation of Transient Receptor Potential Melastatin 7 Channels. *Antioxid. Redox Signal.* 14, 1815–1827.

Coppé, J.-P., Patil, C.K., Rodier, F., Sun, Y., Muñoz, D.P., Goldstein, J., Nelson, P.S., Desprez, P.-Y., and Campisi, J. (2008). Senescence-Associated Secretory Phenotypes Reveal Cell-Nonautonomous Functions of Oncogenic RAS and the p53 Tumor Suppressor. *PLoS Biol.* 6, e301.

Coppé, J.-P., Rodier, F., Patil, C.K., Freund, A., Desprez, P.-Y., and Campisi, J. (2011). Tumor suppressor and aging biomarker p16(INK4a) induces cellular senescence without the associated inflammatory secretory phenotype. *J. Biol. Chem.* 286, 36396–36403.

Coppé, J.P., Patil, C.K., Rodier, F., Krtolica, A., Beauséjour, C.M., Parrinello, S., Hodgson, J.G., Chin, K., Desprez, P.Y., and Campisi, J. (2010). A human-like senescence-associated secretory phenotype is conserved in mouse cells dependent on physiological oxygen. *PLoS One* 5.

Crowe, E.P., Tuzer, F., Gregory, B.D., Donahue, G., Gosai, S.J., Cohen, J., Leung, Y.Y., Yetkin, E., Nativio, R., Wang, L.-S., et al. (2016). Changes in the Transcriptome of Human Astrocytes Accompanying Oxidative Stress-Induced Senescence. *Front. Aging Neurosci.* 8, 208.

Davalli, P., Mitic, T., Caporali, A., Lauriola, A., and D'Arca, D. (2016). ROS, Cell Senescence, and Novel Molecular Mechanisms in Aging and Age-Related Diseases. *Oxid. Med. Cell. Longev.* 2016.

Deas, E., Cremades, N., Angelova, P.R., Ludtmann, M.H.R., Yao, Z., Chen, S., Horrocks, M.H., Banushi, B., Little, D., Devine, M.J., et al. (2016). Alpha-Synuclein Oligomers Interact with Metal Ions to Induce Oxidative Stress and Neuronal Death in Parkinson's Disease. *Antioxid. Redox Signal.* 24, 376–391.

Debacq-Chainiaux, F., Erusalimsky, J.D., Campisi, J., and Toussaint, O. (2009). Protocols to detect senescence-associated beta-galactosidase (SA- β gal) activity, a biomarker of senescent cells in culture and in vivo. *Nat. Protoc.* 4, 1798–1806.

DeJesus-Hernandez, M., Mackenzie, I.R., Boeve, B.F., Boxer, A.L., Baker, M., Rutherford, N.J., Nicholson, A.M., Finch, N.C.A., Flynn, H., Adamson, J., et al. (2011). Expanded GGGGCC Hexanucleotide Repeat in Noncoding Region of C9ORF72 Causes Chromosome 9p-Linked FTD and ALS. *Neuron* 72, 245–256.

Demaria, M., Ohtani, N., Youssef, S.A., Rodier, F., Toussaint, W., Mitchell, J.R., Laberge, R.M., Vijg, J., VanSteeg, H., Doll, M.E.T., et al. (2014). An essential role for senescent cells in optimal wound healing through secretion of PDGF-AA. *Dev. Cell* 31, 722–733.

Demaria, M., O’Leary, M.N., Chang, J., Shao, L., Liu, S., Alimirah, F., Koenig, K., Le, C., Mitin, N., Deal, A.M., et al. (2017). Cellular senescence promotes adverse effects of chemotherapy and cancer relapse. *Cancer Discov.* 7, 165–176.

Demidenko, Z.N., Korotchkina, L.G., Gudkov, A. V., and Blagosklonny, M. V. (2010). Paradoxical suppression of cellular senescence by p53. *Proc. Natl. Acad. Sci.* 107, 9660–9664.

Dimri, G.P., Lee, X., Basile, G., Acosta, M., Scott, G., Roskelley, C., Medrano, E.E., Linskens, M., Rubelj, I., and Pereira-Smith, O. (1995). A biomarker that identifies senescent human cells in culture and in aging skin in vivo. *Proc. Natl. Acad. Sci.* 92, 9363–9367.

Dong, W., Cheng, S., Huang, F., Fan, W., Chen, Y., Shi, H., and He, H. (2011). Mitochondrial dysfunction in long-term neuronal cultures mimics changes with aging. *Med. Sci. Monit.* 17, BR91-6.

Dosemeci, A., Makusky, A.J., Jankowska-Stephens, E., Yang, X., Slotta, D.J., and Markey, S.P. (2007). Composition of the synaptic PSD-95 complex. *Mol. Cell. Proteomics* 6, 1749–1760.

Dou, Z., Ghosh, K., Vizioli, M.G., Zhu, J., Sen, P., Wangenstein, K.J., Simithy, J., Lan, Y., Lin, Y., Zhou, Z., et al. (2017). Cytoplasmic chromatin triggers inflammation in senescence and cancer. *Nature* 550.

Dringen, R., Kussmaul, L., Gutterer, J.M., Hirrlinger, J., and Hamprecht, B. (1999). The glutathione system of peroxide detoxification is less efficient in neurons than in astroglial cells. *J. Neurochem.* 72, 2523–2530.

Dringen, R., Pawlowski, P.G., and Hirrlinger, J. (2005). Peroxide detoxification by brain cells. In *Journal of Neuroscience Research*, pp. 157–165.

Dungan, C., Kosmac, K., Peck, B., McCarthy, J., and Peterson, C. (2017). p16 and γ H2AX as Markers of Cellular Senescence in Young and Old Human Skeletal Muscle. *FASEB J.* 31, 713.9-713.9.

Erickson, R.I., Paucar, A.A., Jackson, R.L., Visnyei, K., and Kornblum, H. (2008). Roles of insulin and transferrin in neural progenitor survival and proliferation. *J. Neurosci. Res.* *86*, 1884–1894.

Farr, J.N., Fraser, D.G., Wang, H., Jaehn, K., Ogrodnik, M.B., Weivoda, M.M., Drake, M.T., Tchkonina, T., LeBrasseur, N.K., Kirkland, J.L., et al. (2016). Identification of Senescent Cells in the Bone Microenvironment. *J. Bone Miner. Res.* *31*, 1920–1929.

Ferrante, R.J., Browne, S.E., Shinobu, L. a, Bowling, a C., Baik, M.J., MacGarvey, U., Kowall, N.W., Brown, R.H., and Beal, M.F. (1997). Evidence of increased oxidative damage in both sporadic and familial amyotrophic lateral sclerosis. *J. Neurochem.* *69*, 2064–2074.

Fischer, R., Maier, O., Siegemund, M., Wajant, H., Scheurich, P., and Pfizenmaier, K. (2011). A TNF receptor 2 selective agonist rescues human neurons from oxidative stress-induced cell death. *PLoS One* *6*.

Fitzgerald, A.L., Osman, A.A., Xie, T.-X., Patel, A., Skinner, H., Sandulache, V., and Myers, J.N. (2015). Reactive oxygen species and p21Waf1/Cip1 are both essential for p53-mediated senescence of head and neck cancer cells. *Cell Death Dis.* *6*, e1678.

Flanary, B.E., and Streit, W.J. (2003). Telomeres shorten with age in rat cerebellum and cortex in vivo. *J. Anti. Aging. Med.* *6*, 299–308.

Flanary, B.E., and Streit, W.J. (2004). Progressive Telomere Shortening Occurs in Cultured Rat Microglia, but Not Astrocytes. *Glia* *45*, 75–88.

Freischmidt, A., Wieland, T., Richter, B., Ruf, W., Schaeffer, V., Müller, K., Marroquin, N., Nordin, F., Hübers, A., Weydt, P., et al. (2015). Haploinsufficiency of TBK1 causes familial ALS and fronto-temporal dementia. *Nat. Neurosci.* *18*, 631–636.

Freischmidt, A., Müller, K., Ludolph, A.C., Weishaupt, J.H., and Andersen, P.M. (2016). Association of Mutations in TBK1 With Sporadic and Familial Amyotrophic Lateral Sclerosis and Frontotemporal Dementia. *JAMA Neurol.* 3–6.

Freund, A., Patil, C.K., and Campisi, J. (2011). p38MAPK is a novel DNA damage response-independent regulator of the senescence-associated secretory phenotype. *EMBO J.* *30*, 1536–1548.

Friedman, J. (2011). Why Is the Nervous System Vulnerable to Oxidative Stress? In *Oxidative Stress and Free Radical Damage in Neurology*, pp. 19–27.

Fritz, C.O., Morris, P.E., and Richler, J.J. (2012). Effect size estimates: current use, calculations, and interpretation. *J. Exp. Psychol. Gen.* *141*, 2–18.

Fuchsberger, T., Martínez-Bellver, S., Giraldo, E., Teruel-Martí, V., Lloret, A., and Viña, J. (2016). A β Induces Excitotoxicity Mediated by APC/C-Cdh1 Depletion That Can Be Prevented by Glutaminase Inhibition Promoting Neuronal Survival. *Sci. Rep.* *6*.

Fukuyama, R., Hatanpää, K., Rapoport, S.I., and Chandrasekaran, K. (1996). Gene expression of ND4, a subunit of complex I of oxidative phosphorylation in mitochondria, is decreased in temporal cortex of brains of Alzheimer's disease patients. *Brain Res.* *713*, 290–293.

Fumagalli, M., Rossiello, F., Clerici, M., Barozzi, S., Cittaro, D., Kaplunov, J.M., Bucci, G., Dobрева, M., Matti, V., Beausejour, C.M., et al. (2012). Telomeric DNA damage is irreparable and causes persistent DNA-damage-response activation. *Nat. Cell Biol.* *14*, 355–365.

Funayama, R., Saito, M., Tanobe, H., and Ishikawa, F. (2006). Loss of linker histone H1 in cellular senescence. *J. Cell Biol.* *175*, 869–880.

Galluzzi, L., Aaronson, S.A., Abrams, J., Alnemri, E.S., Andrews, D.W., Baehrecke, E.H., Bazan, N.G., Blagosklonny, M. V, Blomgren, K., Borner, C., et al. (2009). Guidelines for the use and interpretation of assays for monitoring cell death in higher eukaryotes. *Cell Death Differ.* *16*, 1093–1107.

Gao, S.G., Zeng, C., Li, L.J., Luo, W., Zhang, F.J., Tian, J., Cheng, C., Tu, M., Xiong, Y.L., Jiang, W., et al. (2016). Correlation between senescence-associated beta-galactosidase expression in articular cartilage and disease severity of patients with knee osteoarthritis. *Int. J. Rheum. Dis.* *19*, 226–232.

Geng, Y.Q., Guan, J.T., Xu, X.H., and Fu, Y.C. (2010). Senescence-associated beta-galactosidase activity expression in aging hippocampal neurons. *Biochem. Biophys. Res. Commun.* *396*, 866–869.

Gerland, L.M., Peyrol, S., Lallemand, C., Branche, R., Magaud, J.P., and Ffrench, M. (2003). Association of increased autophagic inclusions labeled for β -galactosidase with fibroblastic aging. *Exp. Gerontol.* *38*, 887–895.

Gille, J.J.P., and Joenje, H. (1992). Cell culture models for oxidative stress: superoxide and hydrogen peroxide versus normobaric hyperoxia. *Mutat. Res. DNAAging* *275*, 405–414.

Going, J.J., Stuart, R.C., Downie, M., Fletcher-Monaghan, A.J., and Keith, W.N. (2002). "Senescence-associated" beta-galactosidase activity in the upper gastrointestinal tract. *J. Pathol.* *196*, 394–400.

Gueguen, N., Desquiret-Dumas, V., Leman, G., Chupin, S., Baron, S., Nivet-Antoine, V., Vessières, E., Ayer, A., Henrion, D., Lenaers, G., et al. (2015). Resveratrol directly binds to mitochondrial complex i and increases oxidative stress in brain mitochondria of aged mice. *PLoS One* *10*.

Guest, J., Grant, R., Mori, T.A., and Croft, K.D. (2014). Changes in oxidative damage, inflammation and [NAD(H)] with age in cerebrospinal fluid. *PLoS One* *9*.

Haitina, T., Lindblom, J., Renström, T., and Fredriksson, R. (2006). Fourteen novel human members of mitochondrial solute carrier family 25 (SLC25) widely expressed in

the central nervous system. *Genomics* 88, 779–790.

Han, X., Aslanian, A., Fu, K., Tsuji, T., and Zhang, Y. (2014). The interaction between checkpoint kinase 1 (Chk1) and the minichromosome maintenance (MCM) complex is required for DNA damage-induced Chk1 phosphorylation. *J. Biol. Chem.* 289, 24716–24723.

Harada, A., Teng, J., Takei, Y., Oguchi, K., and Hirokawa, N. (2002). MAP2 is required for dendrite elongation, PKA anchoring in dendrites, and proper PKA signal transduction. *J. Cell Biol.* 158, 541–549.

Harrill, J.A., Freudenrich, T.M., Machacek, D.W., Stice, S.L., and Mundy, W.R. (2010). Quantitative assessment of neurite outgrowth in human embryonic stem cell-derived hN2TM cells using automated high-content image analysis. *Neurotoxicology* 31, 277–290.

Hayflick, L. (1965). The limited in vitro lifetime of human diploid cell strains. *Exp. Cell Res.* 37, 614–636.

Hayflick, L., and Moorhead, P.S. (1961). The serial cultivation of human diploid cell strains. *Exp. Cell Res.* 25, 585–621.

Hendrickx, D.A.E., van Eden, C.G., Schuurman, K.G., Hamann, J., and Huitinga, I. (2017). Staining of HLA-DR, Iba1 and CD68 in human microglia reveals partially overlapping expression depending on cellular morphology and pathology. *J. Neuroimmunol.* 309, 12–22.

Herbig, U., Jobling, W.A., Chen, B.P.C., Chen, D.J., and Sedivy, J.M. (2004). Telomere shortening triggers senescence of human cells through a pathway involving ATM, p53, and p21CIP1, but not p16INK4a. *Mol. Cell* 14, 501–513.

Hernandez-Segura, A., de Jong, T. V., Melov, S., Guryev, V., Campisi, J., and Demaria, M. (2017). Unmasking Transcriptional Heterogeneity in Senescent Cells. *Curr. Biol.* 27, 2652–2660.e4.

Herrero-Mendez, A., Almeida, A., Fernández, E., Maestre, C., Moncada, S., and Bolaños, J.P. (2009). The bioenergetic and antioxidant status of neurons is controlled by continuous degradation of a key glycolytic enzyme by APC/C-Cdh1. *Nat. Cell Biol.* 11, 747–752.

Hewitt, G., Jurk, D., Marques, F.D.M., Correia-Melo, C., Hardy, T., Gackowska, A., Anderson, R., Taschuk, M., Mann, J., and Passos, J.F. (2012). Telomeres are favoured targets of a persistent DNA damage response in ageing and stress-induced senescence. *Nat. Commun.* 3.

Hirao, A., Cheung, A., Duncan, G., Girard, P.-M., Elia, A.J., Wakeham, A., Okada, H., Sarkissian, T., Wong, J.A., Sakai, T., et al. (2002). Chk2 Is a Tumor Suppressor That Regulates Apoptosis in both an Ataxia Telangiectasia Mutated (ATM)-Dependent and an ATM-Independent Manner. *Mol. Cell Biol.* 22, 6521–6532.

Höglinger, G.U., Breunig, J.J., Depboylu, C., Rouaux, C., Michel, P.P., Alvarez-Fischer, D., Boutillier, A., Degregori, J., Oertel, W.H., Rakic, P., et al. (2007). The pRb/E2F cell-cycle pathway mediates cell death in Parkinson's disease. *Proc. Natl. Acad. Sci. U. S. A.* *104*, 3585–3590.

Hohnholt, M.C., Blumrich, E.M., and Dringen, R. (2015). Multiassay analysis of the toxic potential of hydrogen peroxide on cultured neurons. *J. Neurosci. Res.* *93*, 1127–1137.

Hoshimaru, M., Ray, J., Sah, D.W., and Gage, F.H. (1996). Differentiation of the immortalized adult neuronal progenitor cell line HC2S2 into neurons by regulatable suppression of the v-myc oncogene. *Proc. Natl. Acad. Sci.* *93*, 1518–1523.

Hsu, J., Hsu, M., Sorger, T., Herlyn, M., Levine, E.M., Kimmel, S., and Row, A. (1999). Heparin/endothelial cell growth supplement regulates matrix gene expression and prolongs life span of vascular smooth muscle cells through modulation of Interleukin-1. *Vitr. Cell. Dev. Biol.* *35*, 647–654.

Huang, D.W., Sherman, B.T., and Lempicki, R.A. (2009a). Systematic and integrative analysis of large gene lists using DAVID bioinformatics resources. *Nat. Protoc.* *4*, 44–57.

Huang, D.W., Sherman, B.T., and Lempicki, R.A. (2009b). Bioinformatics enrichment tools: Paths toward the comprehensive functional analysis of large gene lists. *Nucleic Acids Res.* *37*, 1–13.

Hubackova, S., Krejcikova, K., Bartek, J., and Hodny, Z. (2012). IL1-and TGFβ-Nox4 signaling, oxidative stress and DNA damage response are shared features of replicative, oncogene-induced, and drug-induced paracrine “Bystander senescence.” *Aging (Albany, NY).* *4*, 932–951.

Hughes, M.A., Brennan, P.M., Bunting, A.S., Cameron, K., Murray, A.F., and Shipston, M.J. (2014). Patterning human neuronal networks on photolithographically engineered silicon dioxide substrates functionalized with glial analogues. *J. Biomed. Mater. Res. - Part A* *102*, 1350–1360.

Ikawa, M., Okazawa, H., Tsujikawa, T., Matsunaga, A., Yamamura, O., Mori, T., Hamano, T., Kiyono, Y., Nakamoto, Y., and Yoneda, M. (2015). Increased oxidative stress is related to disease severity in the ALS motor cortex: A PET study. *Neurology* *84*, 2033–2039.

Ilieva, M., Della Vedova, P., Hansen, O., and Dufva, M. (2013). Tracking neuronal marker expression inside living differentiating cells using molecular beacons. *Front. Cell. Neurosci.* *7*.

Itahana, K., Itahana, Y., and Dimri, G.P. (2013). Colorimetric detection of senescence-associated ?? galactosidase. *Methods Mol. Biol.* *965*, 143–156.

Ivanova, I.A., D'Souza, S.J., and Dagnino, L. (2006). E2F1 stability is regulated by a novel-PKC/p38beta MAP kinase signaling pathway during keratinocyte differentiation. *Oncogene* *25*, 430–437.

Ivanova, I.A., Vespa, A., and Dagnino, L. (2007). A novel mechanism of E2F1 regulation via nucleocytoplasmic shuttling: Determinants of nuclear import and export. *Cell Cycle* 6, 2186–2195.

Iwanaga, R., Komori, H., Ishida, S., Okamura, N., Nakayama, K., Nakayama, K.I., and Ohtani, K. (2006). Identification of novel E2F1 target genes regulated in cell cycle-dependent and independent manners. *Oncogene* 25, 1786–1798.

Jiang, T., Sun, Q., and Chen, S. (2016). Oxidative stress: A major pathogenesis and potential therapeutic target of antioxidative agents in Parkinson's disease and Alzheimer's disease. *Prog. Neurobiol.* 147, 1–19.

Jin, G., Omori, N., Li, F., Sato, K., Nagano, I., Manabe, Y., Shoji, M., and Abe, K. (2002). Activation of cell-survival signal Akt by GDNF in normal rat brain. *Brain Res.* 958, 429–433.

Jurk, D., Wang, C., Miwa, S., Maddick, M., Korolchuk, V., Tsolou, A., Gonos, E.S., Thrasivoulou, C., Jill Saffrey, M., Cameron, K., et al. (2012). Postmitotic neurons develop a p21-dependent senescence-like phenotype driven by a DNA damage response. *Aging Cell* 11, 996–1004.

Kamburov, A., Cavill, R., Ebbels, T.M.D., Herwig, R., and Keun, H.C. (2011). Integrated pathway-level analysis of transcriptomics and metabolomics data with IMPaLA. *Bioinformatics* 27, 2917–2918.

Kang, C., Xu, Q., Martin, T.D., Li, M.Z., Demaria, M., Aron, L., Lu, T., Yankner, B.A., Campisi, J., and Elledge, S.J. (2015). The DNA damage response induces inflammation and senescence by inhibiting autophagy of GATA4. *Science* (80-.). 349, aaa5612-aaa5612.

Katlinskaya, Y. V., Katlinski, K. V., Yu, Q., Ortiz, A., Beiting, D.P., Brice, A., Davar, D., Sanders, C., Kirkwood, J.M., Rui, H., et al. (2016). Suppression of Type I Interferon Signaling Overcomes Oncogene-Induced Senescence and Mediates Melanoma Development and Progression. *Cell Rep.* 15, 171–180.

Kato, H., Sato, S., Yoneyama, M., Yamamoto, M., Uematsu, S., Matsui, K., Tsujimura, T., Takeda, K., Fujita, T., Takeuchi, O., et al. (2005). Cell type-specific involvement of RIG-I in antiviral response. *Immunity* 23, 19–28.

Kiernan, M.C., Vucic, S., Cheah, B.C., Turner, M.R., Eisen, A., Hardiman, O., Burrell, J.R., and Zoing, M.C. (2011). Amyotrophic lateral sclerosis. *Lancet* 377, 942–955.

Kim, C.S., Park, H.S., Kawada, T., Kim, J.H., Lim, D., Hubbard, N.E., Kwon, B.S., Erickson, K.L., and Yu, R. (2006). Circulating levels of MCP-1 and IL-8 are elevated in human obese subjects and associated with obesity-related parameters. *Int. J. Obes.* 30, 1347–1355.

Kim, Y.Y., Jee, H.J., Um, J.H., Kim, Y.M., Bae, S.S., and Yun, J. (2017). Cooperation between p21 and Akt is required for p53-dependent cellular senescence. *Aging Cell* 16,

1094–1103.

Kinner, A., Wu, W., Staudt, C., and Iliakis, G. (2008). Gamma-H2AX in recognition and signaling of DNA double-strand breaks in the context of chromatin. *Nucleic Acids Res.* *36*, 5678–5694.

Kirkinezos, I.G. (2005). Cytochrome c Association with the Inner Mitochondrial Membrane Is Impaired in the CNS of G93A-SOD1 Mice. *J. Neurosci.* *25*, 164–172.

Kitchens, D.L., Snyder, E.Y., and Gottlieb, D.I. (1994). FGF and EGF are mitogens for immortalized neural progenitors. *J. Neurobiol.* *25*, 797–807.

Kodama, R., Kato, M., Furuta, S., Ueno, S., Zhang, Y., Matsuno, K., Yabe-Nishimura, C., Tanaka, E., and Kamata, T. (2013). ROS-generating oxidases Nox1 and Nox4 contribute to oncogenic Ras-induced premature senescence. *Genes to Cells* *18*, 32–41.

Kojima, H., Kunimoto, H., Inoue, T., and Nakajima, K. (2012). The STAT3-IGFBP5 axis is critical for IL-6/gp130-induced premature senescence in human fibroblasts. *Cell Cycle* *11*, 730–739.

Konishi, Y. (2004). Cdh1-APC Controls Axonal Growth and Patterning in the Mammalian Brain. *Science* (80-.). *303*, 1026–1030.

Korotchkina, L.G., Leontieva, O. V., Bukreeva, E.I., Demidenko, Z.N., Gudkov, A. V., and Blagosklonny, M. V. (2010). The choice between p53-induced senescence and quiescence is determined in part by the mTOR pathway. *Aging* (Albany, NY). *2*, 344–352.

Kosar, M., Bartkova, J., Hubackova, S., Hodny, Z., Lukas, J., and Bartek, J. (2011). Senescence-associated heterochromatin foci are dispensable for cellular senescence, occur in a cell type- And insult-dependent manner, and follow expression of p16ink4a. *Cell Cycle* *10*, 457–468.

Kozlov, S. V., Waardenberg, A.J., Engholm-Keller, K., Arthur, J.W., Graham, M.E., and Lavin, M. (2016). Reactive Oxygen Species (ROS)-Activated ATM-Dependent Phosphorylation of Cytoplasmic Substrates Identified by Large-Scale Phosphoproteomics Screen. *Mol. Cell. Proteomics* *15*, 1032–1047.

Kraft, C., Vodermaier, H.C., Maurer-Stroh, S., Eisenhaber, F., and Peters, J.M. (2005). The WD40 propeller domain of Cdh1 functions as a destruction box receptor for APC/C substrates. *Mol. Cell* *18*, 543–553.

Kramer, E.R., Scheuringer, N., Podtelejnikov, A. V., Mann, M., and Peters, J.-M. (2000). Mitotic Regulation of the APC Activator Proteins CDC20 and CDH1. *Mol. Biol. Cell* *11*, 1555–1569.

Krishnamurthy, J., Torrice, C., Ramsey, M.R., Kovalev, G.I., Al-Regaiey, K., Su, L., and Sharpless, N.E. (2004). Ink4a/Arf expression is a biomarker of aging. *J. Clin. Invest.* *114*, 1299–1307.

Kruman, I.I., Wersto, R.P., Cardozo-Pelaez, F., Smilenov, L., Chan, S.L., Chrest, F.J., Emokpae, R., Gorospe, M., and Mattson, M.P. (2004). Cell Cycle Activation Linked to Neuronal Cell Death Initiated by DNA Damage. *Neuron* 41, 549–561.

Kuilman, T., and Peeper, D.S. (2009). Senescence-messaging secretome: SMS-ing cellular stress. *Nat. Rev. Cancer* 9, 81–94.

Kuilman, T., Michaloglou, C., Vredeveld, L.C.W., Douma, S., van Doorn, R., Desmet, C.J., Aarden, L.A., Mooi, W.J., and Peeper, D.S. (2008). Oncogene-Induced Senescence Relayed by an Interleukin-Dependent Inflammatory Network. *Cell* 133, 1019–1031.

Kurowska, Z., Brundin, P., Schwab, M.E., and Li, J.Y. (2014). Intracellular Nogo-A facilitates initiation of neurite formation in mouse midbrain neurons in vitro. *Neuroscience* 256, 456–466.

Kurz, D.J. (2004). Chronic oxidative stress compromises telomere integrity and accelerates the onset of senescence in human endothelial cells. *J. Cell Sci.* 117, 2417–2426.

Kurz, D.J., Decary, S., Hong, Y., and Erusalimsky, J.D. (2000). Senescence-associated (beta)-galactosidase reflects an increase in lysosomal mass during replicative ageing of human endothelial cells. *J. Cell Sci.* 113 (Pt 2, 3613–3622.

Lawless, C., Wang, C., Jurk, D., Merz, A., Zglinicki, T. von, and Passos, J.F. (2010). Quantitative assessment of markers for cell senescence. *Exp. Gerontol.* 45, 772–778.

Lee, A.C., Fenster, B.E., Ito, H., Takeda, K., Bae, N.S., Hirai, T., Yu, Z.X., Ferrans, V.J., Howard, B.H., and Finkel, T. (1999). Ras proteins induce senescence by altering the intracellular levels of reactive oxygen species. *J. Biol. Chem.* 274, 7936–7940.

Lee, B.Y., Han, J.A., Im, J.S., Morrone, A., Johung, K., Goodwin, E.C., Kleijer, W.J., DiMaio, D., and Hwang, E.S. (2006). Senescence-associated β -galactosidase is lysosomal β -galactosidase. *Aging Cell* 5, 187–195.

Lee, C.T., Yu, L.E., and Wang, J.Y. (2016a). Nitroxide antioxidant as a potential strategy to attenuate the oxidative/nitrosative stress induced by hydrogen peroxide plus nitric oxide in cultured neurons. *Nitric Oxide - Biol. Chem.* 54, 38–50.

Lee, H.-K., Velazquez Sanchez, C., Chen, M., Morin, P.J., Wells, J.M., Hanlon, E.B., and Xia, W. (2016b). Three Dimensional Human Neuro-Spheroid Model of Alzheimer's Disease Based on Differentiated Induced Pluripotent Stem Cells. *PLoS One* 11, e0163072.

Lee, J., Kumagai, A., and Dunphy, W.G. (2003). Claspin, a Chk1-regulatory protein, monitors DNA replication on chromatin independently of RPA, ATR, and Rad17. *Mol. Cell* 11, 329–340.

Lee, S., Tong, M., Hang, S., Deochand, C., and de la Monte, S. (2013). CSF and Brain Indices of Insulin Resistance, Oxidative Stress and Neuro-Inflammation in Early versus

Late Alzheimer's Disease. *J. Alzheimer's Dis. Park.* 3, 128.

Lees-Miller, S.P., and Meek, K. (2003). Repair of DNA double strand breaks by non-homologous end joining. *Biochimie* 85, 1161–1173.

Lehtinen, M.K., and Bonni, A. (2006). Modeling oxidative stress in the central nervous system. *Curr. Mol. Med.* 6, 871–881.

Li, Q., Spencer, N.Y., Pantazis, N.J., and Engelhardt, J.F. (2011). Alsin and SOD1 G93A proteins regulate endosomal reactive oxygen species production by glial cells and proinflammatory pathways responsible for neurotoxicity. *J. Biol. Chem.* 286, 40151–40162.

Li, Y., Nichols, M.A., Shay, J.W., and Xiong, Y. (1994). Transcriptional repression of the D-type cyclin-dependent kinase inhibitor p16 by the retinoblastoma susceptibility gene product pRb. *Cancer Res.* 54, 6078–6082.

Liao, E.-C., Hsu, Y.-T., Chuah, Q.-Y., Lee, Y.-J., Hu, J.-Y., Huang, T.-C., Yang, P.-M., and Chiu, S.-J. (2014). Radiation induces senescence and a bystander effect through metabolic alterations. *Cell Death Dis.* 5, e1255.

Liu, E., Lee, A.Y.L., Chiba, T., Olson, E., Sun, P., and Wu, X. (2007). The ATR-mediated S phase checkpoint prevents rereplication in mammalian cells when licensing control is disrupted. *J. Cell Biol.* 179, 643–657.

Liu, F., Wu, S., Ren, H., and Gu, J. (2011). Klotho suppresses RIG-I-mediated senescence-associated inflammation. *Nat. Cell Biol.* 13, 254–262.

Liu, Q., Guntuku, S., Cui, X.S., Matsuoka, S., Cortez, D., Tamai, K., Luo, G., Carattini-Rivera, S., DeMayo, F., Bradley, A., et al. (2000). Chk1 is an essential kinase that is regulated by Atr and required for the G2/M DNA damage checkpoint. *Genes Dev.* 14, 1448–1459.

Liu, S., Bekker-Jensen, S., Mailand, N., Lukas, C., Bartek, J., and Lukas, J. (2006). Claspin Operates Downstream of TopBP1 To Direct ATR Signaling towards Chk1 Activation. *Mol. Cell. Biol.* 26, 6056–6064.

Loaiza, N., and Demaria, M. (2016). Cellular senescence and tumor promotion: Is aging the key? *Biochim. Biophys. Acta - Rev. Cancer* 1865, 155–167.

Locatelli, F., Corti, S., Papadimitriou, D., Fortunato, F., Del Bo, R., Donadoni, C., Nizzardo, M., Nardini, M., Salani, S., Ghezzi, S., et al. (2007). Fas small interfering RNA reduces motoneuron death in amyotrophic lateral sclerosis mice. *Ann. Neurol.* 62, 81–92.

Loeffen, J., Smeitink, J., Triepels, R., Smeets, R., Schuelke, M., Sengers, R., Trijbels, F., Hamel, B., Mullaart, R., and van den Heuvel, L. (1998). The First Nuclear-Encoded Complex I Mutation in a Patient with Leigh Syndrome. *Am. J. Hum. Genet.* 63, 1598–1608.

Lopez-Gonzalez, R., Lu, Y., Gendron, T.F., Karydas, A., Tran, H., Yang, D., Petrucelli, L., Miller, B.L., Almeida, S., and Gao, F.B. (2016). Poly(GR) in C9ORF72-Related ALS/FTD Compromises Mitochondrial Function and Increases Oxidative Stress and DNA Damage in iPSC-Derived Motor Neurons. *Neuron* 92, 383–391.

López-Otín, C., Blasco, M.A., Partridge, L., Serrano, M., and Kroemer, G. (2013). The hallmarks of aging. *Cell* 153.

Lotharius, J. (2005). Progressive Degeneration of Human Mesencephalic Neuron-Derived Cells Triggered by Dopamine-Dependent Oxidative Stress Is Dependent on the Mixed-Lineage Kinase Pathway. *J. Neurosci.* 25, 6329–6342.

Lotharius, J., Barg, S., Wiekop, P., Lundberg, C., Raymon, H.K., and Brundin, P. (2002). Effect of mutant α -synuclein on dopamine homeostasis in a new human mesencephalic cell line. *J. Biol. Chem.* 277, 38884–38894.

Ludueña, R.F. (1998). Multiple forms of tubulin: different gene products and covalent modifications. *Int. Rev. Cytol.* 178, 207–275.

Lugo, R., Gabasa, M., Andriani, F., Puig, M., Facchinetti, F., Ramírez, J., Gómez-Caro, A., Pastorino, U., Fuster, G., Almendros, I., et al. (2016). Heterotypic paracrine signaling drives fibroblast senescence and tumor progression of large cell carcinoma of the lung. *Oncotarget* 7, 82324–82337.

Lui, D.X., Nath, N., Chellappan, S.P., and Greene, L.A. (2005). Regulation of neuron survival and death by p130 and associated chromatin modifiers. *Genes Dev.* 19, 719–732.

M€, A.D.M. • U.S. • A.P. • C., • oller-H. • E.H.-F. • A.A. • B.C. • H.L. uller, and Horvath, H.G. • M.S.-K. • P.F.C. • R. (2012). NDUFS8-related Complex I Deficiency Extends Phenotype from “PEO Plus” to Leigh Syndrome. *JIMD Rep.* 4, 113–116.

Maciel-Barón, L.A., Morales-Rosales, S.L., Aquino-Cruz, A.A., Triana-Martínez, F., Galván-Arzate, S., Luna-López, A., González-Puertos, V.Y., López-Díazguerrero, N.E., Torres, C., and Königsberg, M. (2016). Senescence associated secretory phenotype profile from primary lung mice fibroblasts depends on the senescence induction stimuli. *Age (Omaha).* 38, 1–14.

Mackenzie, I.R.A., Neumann, M., Baborie, A., Sampathu, D.M., Du Plessis, D., Jaros, E., Perry, R.H., Trojanowski, J.Q., Mann, D.M.A., and Lee, V.M.Y. (2011). A harmonized classification system for FTLTDP pathology. *Acta Neuropathol.* 122, 111–113.

De Magalhães, J.P., Chainiaux, F., Remacle, J., and Toussaint, O. (2002). Stress-induced premature senescence in BJ and hTERT-BJ1 human foreskin fibroblasts. *FEBS Lett.* 523, 157–162.

De Magalhães, J.P., Migeot, V., Mainfroid, V., De Longueville, F., Remacle, J., and Toussaint, O. (2004). No increase in senescence-associated β -galactosidase activity in werner syndrome fibroblasts after exposure to H₂O₂. In *Annals of the New York Academy of Sciences*, pp. 375–378.

Mak, T.W. (2000). DNA damage-induced activation of p53 by the checkpoint kinase Chk2. *Science* (80-.). 287, 1824–1827.

Manczak, M., Park, B.S., Jung, Y., and Reddy, P.H. (2004). Differential expression of oxidative phosphorylation genes in patients with Alzheimer's disease: implications for early mitochondrial dysfunction and oxidative damage. *Neuromolecular Med* 5, 147–162.

Mariotti, L.G., Pirovano, G., Savage, K.I., Ghita, M., Ottolenghi, A., Prise, K.M., and Schettino, G. (2013). Use of the γ -H2AX assay to investigate DNA repair dynamics following multiple radiation exposures. *PLoS One* 8.

Markowski, D.N., Thies, H.W., Gottlieb, A., Wenk, H., Wischnewsky, M., and Bullerdiek, J. (2013). HMGA2 expression in white adipose tissue linking cellular senescence with diabetes. *Genes Nutr.* 8, 449–456.

Martin, L.J., Liu, Z., Chen, K., Price, A.C., Yan, P., Swaby, J.A., and Golden, W.C. (2007). Motor neuron degeneration in amyotrophic lateral sclerosis mutant superoxide dismutase-1 transgenic mice: Mechanisms of mitochondriopathy and cell death. *J. Comp. Neurol.* 500, 20–46.

Massudi, H., Grant, R., Braidy, N., Guest, J., Farnsworth, B., and Guillemin, G.J. (2012). Age-associated changes in oxidative stress and NAD⁺ metabolism in human tissue. *PLoS One* 7.

Matsuoka, S., Ballif, B.A., Smogorzewska, A., McDonald, E.R., Hurov, K.E., Luo, J., Bakalarski, C.E., Zhao, Z., Solimini, N., Lerenthal, Y., et al. (2007). ATM and ATR substrate analysis reveals extensive protein networks responsive to DNA damage. *Science* (80-.). 316, 1160–1166.

Mattiazzi, M., D'Aurelio, M., Gajewski, C.D., Martushova, K., Kiaei, M., Flint Beal, M., and Manfredi, G. (2002). Mutated human SOD1 causes dysfunction of oxidative phosphorylation in mitochondria of transgenic mice. *J. Biol. Chem.* 277, 29626–29633.

Mecocci, P., Fanó, G., Fulle, S., MacGarvey, U., Shinobu, L., Polidori, M.C., Cherubini, A., Vecchiet, J., Senin, U., and Beal, M.F. (1999). Age-dependent increases in oxidative damage to DNA, lipids, and proteins in human skeletal muscle. *Free Radic. Biol. Med.* 26, 303–308.

Meijer, A.E.F.H., Benson, D., and Scholte, H.R. (1977). The influence of freezing and freeze-drying of tissue specimens on enzyme activity. *Histochemistry* 51, 297–303.

Menges, S., Minakaki, G., Schaefer, P.M., Meixner, H., Prots, I., Schlötzer-Schrehardt, U., Friedland, K., Winner, B., Outeiro, T.F., Winklhofer, K.F., et al. (2017). Alpha-synuclein prevents the formation of spherical mitochondria and apoptosis under oxidative stress. *Sci. Rep.* 7, 42942.

Meyer, P., Maity, P., Burkovski, A., Schwab, J., Ssel, C.M., Singh, K., Ferreira, F.F., Krug, L., Maier, H.J., Wlaschek, M., et al. (2017). A model of the onset of the senescence associated secretory phenotype after DNA damage induced senescence. *PLoS Comput.*

Biol. 1–30.

Di Micco, R., Fumagalli, M., Cicalese, A., Piccinin, S., Gasparini, P., Luise, C., Schurra, C., Garré, M., Giovanni Nuciforo, P., Bensimon, A., et al. (2006). Oncogene-induced senescence is a DNA damage response triggered by DNA hyper-replication. *Nature* *444*, 638–642.

Di Micco, R., Sulli, G., Dobrova, M., Liontos, M., Botrugno, O.A., Gargiulo, G., Dal Zuffo, R., Matti, V., D'Ario, G., Montani, E., et al. (2011). Interplay between oncogene-induced DNA damage response and heterochromatin in senescence and cancer. *Nat. Cell Biol.* *13*, 292–302.

Michaloglou, C., Vredeveld, L.C.W., Soengas, M.S., Denoyelle, C., Kuilman, T., Van Der Horst, C.M.A.M., Majoor, D.M., Shay, J.W., Mooi, W.J., and Peeper, D.S. (2005). BRAFE600-associated senescence-like cell cycle arrest of human naevi. *Nature* *436*, 720–724.

Minagawa, S., Araya, J., Numata, T., Nojiri, S., Hara, H., Yumino, Y., Kawaishi, M., Odaka, M., Morikawa, T., Nishimura, S.L., et al. (2011). Accelerated epithelial cell senescence in IPF and the inhibitory role of SIRT6 in TGF- β -induced senescence of human bronchial epithelial cells. *Am J Physiol Lung Cell Mol Physiol* *391*–401.

Minamino, T., Miyauchi, H., Yoshida, T., Ishida, Y., Yoshida, H., and Komuro, I. (2002). Endothelial cell senescence in human atherosclerosis: Role of telomere in endothelial dysfunction. *Circulation* *105*, 1541–1544.

Minamino, T., Orimo, M., Shimizu, I., Kunieda, T., Yokoyama, M., Ito, T., Nojima, A., Nabetani, A., Oike, Y., Matsubara, H., et al. (2009). A crucial role for adipose tissue p53 in the regulation of insulin resistance. *Nat. Med.* *15*, 1082–1087.

Mirzayans, R., Andrais, B., Scott, A., Paterson, M.C., and Murray, D. (2010). Single-cell analysis of p16INK4a and p21WAF1 expression suggests distinct mechanisms of senescence in normal human and Li-Fraumeni syndrome fibroblasts. *J. Cell. Physiol.* *223*, 57–67.

Mittal, M., Siddiqui, M.R., Tran, K., Reddy, S.P., and Malik, A.B. (2014). Reactive Oxygen Species in Inflammation and Tissue Injury. *Antioxid. Redox Signal.* *20*, 1126–1167.

Mombach, J.C.M., Vendrusculo, B., and Bugs, C.A. (2015). A model for p38MAPK-induced astrocyte senescence. *PLoS One* *10*.

Morelli, S., Piscioneri, A., Salerno, S., Al-Fageeh, M.B., Drioli, E., and De Bartolo, L. (2014). Neuroprotective effect of didymin on hydrogen peroxide-induced injury in the neuronal membrane system. *Cells Tissues Organs* *199*, 184–200.

Mori, K., Weng, S.M., Arzberger, T., May, S., Rentzsch, K., Kremmer, E., Schmid, B., Kretschmar, H.A., Cruts, M., Van Broeckhoven, C., et al. (2013). The C9orf72 GGGGCC repeat is translated into aggregating dipeptide-repeat proteins in FTLD/ALS.

Science (80-.). 339, 1335–1338.

Moullan, N., Mouchiroud, L., Wang, X., Ryu, D., Williams, E.G., Mottis, A., Jovaisaite, V., Frochaux, M. V., Quiros, P.M., Deplancke, B., et al. (2015). Tetracyclines disturb mitochondrial function across eukaryotic models: A call for caution in biomedical research. *Cell Rep.* 10, 1681–1691.

Muck, C., Micutkova, L., Zwerschke, W., and Jansen-Durr, P. (2008). Role of insulin-like growth factor binding protein-3 in human umbilical vein endothelial cell senescence. *Rejuvenation Res.* 11, 449–453.

Muñoz-Espín, D., Cañamero, M., Maraver, A., Gómez-López, G., Contreras, J., Murillo-Cuesta, S., Rodríguez-Baeza, A., Varela-Nieto, I., Ruberte, J., Collado, M., et al. (2013). Programmed cell senescence during mammalian embryonic development. *Cell* 155, 1104–1118.

Murata, T., Ohtsuka, C., and Terayama, Y. (2008). Increased mitochondrial oxidative damage and oxidative DNA damage contributes to the neurodegenerative process in sporadic amyotrophic lateral sclerosis. *Free Radic. Res.* 42, 221–225.

Nagano, T., Nakano, M., Nakashima, A., Onishi, K., Yamao, S., Enari, M., Kikkawa, U., and Kamada, S. (2016). Identification of cellular senescence-specific genes by comparative transcriptomics. *Sci. Rep.* 6.

Nagase, M., Yamamoto, Y., Miyazaki, Y., and Yoshino, H. (2016). Increased oxidative stress in patients with amyotrophic lateral sclerosis and the effect of edaravone administration. *Redox Rep.* 1–9.

Narita, M., Núñez, S., Heard, E., Narita, M., Lin, A.W., Hearn, S.A., Spector, D.L., Hannon, G.J., and Lowe, S.W. (2003). Rb-mediated heterochromatin formation and silencing of E2F target genes during cellular senescence. *Cell* 113, 703–716.

Narita, M., Narita, M., Krizhanovsky, V., Núñez, S., Chicas, A., Hearn, S.A., Myers, M.P., and Lowe, S.W. (2006). A Novel Role for High-Mobility Group A Proteins in Cellular Senescence and Heterochromatin Formation. *Cell* 126, 503–514.

Narita, M., Young, A.R.J., Arakawa, S., Samarajiwa, S.A., Nakashima, T., Yoshida, S., Hong, S., Berry, L.S., Reichelt, S., Ferreira, M., et al. (2011). Spatial coupling of mTOR and autophagy augments secretory phenotypes. *Science* (80-.). 332, 966–970.

Nazmi, A., Dutta, K., and Basu, A. (2011). RIG-I mediates innate immune response in mouse neurons following Japanese encephalitis virus infection. *PLoS One* 6.

Nelson, D.M., McBryan, T., Jeyapalan, J.C., Sedivy, J.M., and Adams, P.D. (2014). A comparison of oncogene-induced senescence and replicative senescence: implications for tumor suppression and aging. *Age (Dordr).* 36, 9637.

Niccoli, T., and Partridge, L. (2012). Ageing as a risk factor for disease. *Curr. Biol.* 22.

Ogrunc, M., Di Micco, R., Lontos, M., Bombardelli, L., Mione, M., Fumagalli, M., Gorgoulis, V.G., and D'Adda Di Fagagna, F. (2014). Oncogene-induced reactive oxygen species fuel hyperproliferation and DNA damage response activation. *Cell Death Differ.* *21*, 998–1012.

Olsen, C.L., Gardie, B., Yaswen, P., and Stampfer, M.R. (2002). Raf-1-induced growth arrest in human mammary epithelial cells is p16-independent and is overcome in immortal cells during conversion. *Oncogene* *21*, 6328–6339.

Otsuka, Y., Tanaka, T., Uchida, D., Noguchi, Y., Saeki, N., Saito, Y., and Tatsuno, I. (2004). Roles of cyclin-dependent kinase 4 and p53 in neuronal cell death induced by doxorubicin on cerebellar granule neurons in mouse. *Neurosci Lett* *365*, 180–185.

Oubaha, M., Miloudi, K., Dejda, A., Guber, V., Mawambo, G., Germain, M.A., Bourdel, G., Popovic, N., Rezende, F.A., Kaufman, R.J., et al. (2016). Senescence-associated secretory phenotype contributes to pathological angiogenesis in retinopathy. *Sci. Transl. Med.* *8*.

Özcan, S., Alessio, N., Acar, M.B., Mert, E., Omerli, F., Peluso, G., and Galderisi, U. (2016). Unbiased analysis of senescence associated secretory phenotype (SASP) to identify common components following different genotoxic stresses. *Aging (Albany, NY)*. *8*, 1316–1329.

Pacelli, C., Giguère, N., Bourque, M.J., Lévesque, M., Slack, R.S., and Trudeau, L.É. (2015). Elevated Mitochondrial Bioenergetics and Axonal Arborization Size Are Key Contributors to the Vulnerability of Dopamine Neurons. *Curr. Biol.* *25*, 2349–2360.

Park, J.H., Kim, C.K., Lee, S.B., Lee, K.H., Cho, S.W., and Ahn, J.Y. (2016). Akt attenuates apoptotic death through phosphorylation of H2A under hydrogen peroxide-induced oxidative stress in PC12 cells and hippocampal neurons. *Sci. Rep.* *6*.

Parker, W.D., Boyson, S.J., and Parks, J.K. (1989). Abnormalities of the electron transport chain in idiopathic Parkinson's disease. *Ann. Neurol.* *26*, 719–723.

Parrinello, S., Samper, E., Krtolica, A., Goldstein, J., Melov, S., and Campisi, J. (2003). Oxygen sensitivity severely limits the replicative lifespan of murine fibroblasts. *Nat. Cell Biol.* *5*, 741–747.

Passos, J.F., Nelson, G., Wang, C., Richter, T., Simillion, C., Proctor, C.J., Miwa, S., Olijslagers, S., Hallinan, J., Wipat, A., et al. (2010). Feedback between p21 and reactive oxygen production is necessary for cell senescence. *Mol. Syst. Biol.* *6*.

Paull, T.T., Rogakou, E.P., Yamazaki, V., Kirchgessner, C.U., Gellert, M., and Bonner, W.M. (2000). A critical role for histone H2AX in recruitment of repair factors to nuclear foci after DNA damage. *Curr. Biol.* *10*, 886–895.

Petermann, E., and Caldecott, K.W. (2006). Evidence that the ATR/Chk1 pathway maintains normal replication fork progression during unperturbed S phase. *Cell Cycle* *5*, 2203–2209.

Piechota, M., Sunderland, P., Wysocka, A., Nalberczak, M., Sliwinska, M.A., Radwanska, K., and Sikora, E. (2016). Is senescence-associated β -galactosidase a marker of neuronal senescence?

Pole, A., Dimri, M., and P. Dimri, G. (2016). Oxidative stress, cellular senescence and ageing. *AIMS Mol. Sci.* 3, 300–324.

Präbst, K., Engelhardt, H., Ringgeler, S., and Hübner, H. (2017). Basic colorimetric proliferation assays: MTT, WST, and resazurin. In *Methods in Molecular Biology*, pp. 1–17.

Procaccio, V., and Wallace, D.C. (2004). Late-onset Leigh syndrome in a patient with mitochondrial complex I *NDUFS8* mutations. *Neurology* 62, 1899–1901.

Radio, N.M., Breier, J.M., Shafer, T.J., and Mundy, W.R. (2008). Assessment of chemical effects on neurite outgrowth in PC12 cells using high content screening. *Toxicol. Sci.* 105, 106–118.

Ray, P.D., Huang, B.-W., and Tsuji, Y. (2012). Reactive oxygen species (ROS) homeostasis and redox regulation in cellular signaling. *Cell. Signal.* 24, 981–990.

Renton, A.E., Majounie, E., Waite, A., Simón-Sánchez, J., Rollinson, S., Gibbs, J.R., Schymick, J.C., Laaksovirta, H., van Swieten, J.C., Myllykangas, L., et al. (2011). A hexanucleotide repeat expansion in *C9ORF72* is the cause of chromosome 9p21-linked ALS-FTD. *Neuron* 72, 257–268.

Riss, T.L., Moravec, R.A., Niles, A.L., Duellman, S., Benink, H.A., Worzella, T.J., and Minor, L. (2013). *Cell Viability Assays*. *Assay Guid. Man.* [Internet] 114, 785–796.

Rodier, F., Coppé, J.-P., Patil, C.K., Hoeijmakers, W.A.M., Muñoz, D.P., Raza, S.R., Freund, A., Campeau, E., Davalos, A.R., and Campisi, J. (2009). Persistent DNA damage signalling triggers senescence-associated inflammatory cytokine secretion. *Nat. Cell Biol.* 11, 973–979.

Rogakou, E.P., Pilch, D.R., Orr, A.H., Ivanova, V.S., and Bonner, W.M. (1998). DNA double-stranded breaks induce histone H2AX phosphorylation on serine 139. *J. Biol. Chem.* 273, 5858–5868.

Rosen, D.R., Siddique, T., Patterson, D., Figlewicz, D.A., Sapp, P., Hentati, A., Donaldson, D., Goto, J., O'Regan, J.P., and Deng, H.X. (1993). Mutations in *Cu/Zn* superoxide dismutase gene are associated with familial amyotrophic lateral sclerosis. *Nature* 362, 59–62.

Safaiyan, S., Kannaiyan, N., Snaidero, N., Brioschi, S., Biber, K., Yona, S., Edinger, A.L., Jung, S., Rossner, M.J., and Simons, M. (2016). Age-related myelin degradation burdens the clearance function of microglia during aging. *Nat. Neurosci.* 19, 995–998.

Sainath, R., and Gallo, G. (2014). Cytoskeletal and signaling mechanisms of neurite formation. *Cell Tissue Res.* 359, 267–278.

Salminen, A., Ojala, J., Kaarniranta, K., Haapasalo, A., Hiltunen, M., and Soininen, H. (2011). Astrocytes in the aging brain express characteristics of senescence-associated secretory phenotype. *Eur. J. Neurosci.* *34*, 3–11.

Santa-Gonzalez, G.A., Gomez-Molina, A., Arcos-Burgos, M., Meyer, J.N., and Camargo, M. (2016). Distinctive adaptive response to repeated exposure to hydrogen peroxide associated with upregulation of DNA repair genes and cell cycle arrest. *Redox Biol.* *9*, 124–133.

Sazanov, L.A. (2015). REVIEWS A giant molecular proton pump: structure and mechanism of respiratory complex I. *Nat. Publ. Gr.* *16*, 375–388.

Schafer, M.J., White, T.A., Iijima, K., Haak, A.J., Ligresti, G., Atkinson, E.J., Oberg, A.L., Birch, J., Salmonowicz, H., Zhu, Y., et al. (2017). Cellular senescence mediates fibrotic pulmonary disease. *Nat. Commun.* *8*.

Schägger, H., and Pfeiffer, K. (2001). The Ratio of Oxidative Phosphorylation Complexes I-V in Bovine Heart Mitochondria and the Composition of Respiratory Chain Supercomplexes. *J. Biol. Chem.* *276*, 37861–37867.

Schapira, A.H., Cooper, J.M., Dexter, D., Clark, J.B., Jenner, P., and Marsden, C.D. (1990). Mitochondrial complex I deficiency in Parkinson's disease. *J. Neurochem.* *54*, 823–827.

Scheff, S.W., Ansari, M.A., and Mufson, E.J. (2016). Oxidative stress and hippocampal synaptic protein levels in elderly cognitively intact individuals with Alzheimer's disease pathology. *Neurobiol. Aging* *42*, 1–12.

Schieber, M., and Chandel, N.S. (2014). ROS function in redox signaling and oxidative stress. *Curr. Biol.* *24*.

Schildknecht, S., Pörtl, D., Nagel, D.M., Matt, F., Scholz, D., Lotharius, J., Schmiege, N., Salvo-Vargas, A., and Leist, M. (2009). Requirement of a dopaminergic neuronal phenotype for toxicity of low concentrations of 1-methyl-4-phenylpyridinium to human cells. *Toxicol. Appl. Pharmacol.* *241*, 23–35.

Schildknecht, S., Karreman, C., Pörtl, D., Efrémova, L., Kullmann, C., Gutbier, S., Krug, A., Scholz, D., Gerding, H.R., and Leist, M. (2013). Generation of genetically-modified human differentiated cells for toxicological tests and the study of neurodegenerative diseases. *ALTEX* *30*, 427–444.

Scholz, D., Pörtl, D., Genewsky, A., Weng, M., Waldmann, T., Schildknecht, S., and Leist, M. (2011). Rapid, complete and large-scale generation of post-mitotic neurons from the human LUHMES cell line. *J. Neurochem.* *119*, 957–971.

Schriner, S.E. (2005). Extension of Murine Life Span by Overexpression of Catalase Targeted to Mitochondria. *Science* (80-.). *308*, 1909–1911.

Schulte, U., Haupt, V., Abelmann, A., Fecke, W., Brors, B., Rasmussen, T., Friedrich, T.,

and Weiss, H. (1999). A reductase/isomerase subunit of mitochondrial NADH:ubiquinone oxidoreductase (complex I) carries an NADPH and is involved in the biogenesis of the complex. *J. Mol. Biol.* 292, 569–580.

Schwartz, E.I., Smilenov, L.B., Price, M.A., Osredkar, T., Baker, R.A., Ghosh, S., Shi, F.D., Vollmer, T.L., Lencinas, A., Stearns, D.M., et al. (2007). Cell cycle activation in postmitotic neurons is essential for DNA repair. *Cell Cycle* 6, 318–329.

Sedelnikova, O.A., Horikawa, I., Zimonjic, D.B., Popescu, N.C., Bonner, W.M., and Barrett, J.C. (2004). Senescing human cells and ageing mice accumulate DNA lesions with unreparable double-strand breaks. *Nat. Cell Biol.* 6, 168–170.

Serrano, M., Lin, A.W., McCurrach, M.E., Beach, D., and Lowe, S.W. (1997). Oncogenic ras provokes premature cell senescence associated with accumulation of p53 and p16(INK4a). *Cell* 88, 593–602.

Severino, J., Allen, R.G., Balin, S., Balin, a, and Cristofalo, V.J. (2000). Is beta-galactosidase staining a marker of senescence in vitro and in vivo? *Exp. Cell Res.* 257, 162–171.

Sharma, A., Singh, K., and Almasan, A. (2012). Histone H2AX phosphorylation: A marker for DNA damage. *Methods Mol. Biol.* 920, 613–626.

Sharma, N., Timmers, C., Trikha, P., Saavedra, H.I., Obery, A., and Leone, G. (2006). Control of the p53-p21CIP1 axis by E2f1, E2f2, and E2f3 is essential for G1/S progression and cellular transformation. *J. Biol. Chem.* 281, 36124–36131.

Shaw, P.J., Ince, P.G., Falkous, G., and Mantle, D. (1995). Oxidative damage to protein in sporadic motor neuron disease spinal cord. *Ann. Neurol.* 38, 691–695.

Shelton, D.N., Chang, E., Whittier, P.S., Choi, D., and Funk, W.D. (1999). Microarray analysis of replicative senescence. *Curr. Biol.* 9, 939–945.

Shu, Z., Heimfeld, S., Gao, D., and Hutchinson, F. (2015). Dynamic monitoring of oxidative DNA double strand break and repair in cardiomyocytes. *49*, 469–476.

Silva, A.R., Santos, A.C., Farfel, J.M., Grinberg, L.T., Ferretti, R.E., Campos, A.H., Cunha, I.W., Begnami, M.D., Rocha, R.M., Carraro, D.M., et al. (2014). Repair of oxidative DNA damage, cell-cycle regulation and neuronal death may influence the clinical manifestation of Alzheimer's disease. *PLoS One* 9, e99897.

Simpson, J.E., Ince, P.G., Haynes, L.J., Theaker, R., Gelsthorpe, C., Baxter, L., Forster, G., Lace, G.L., Shaw, P.J., Matthews, F.E., et al. (2010). Population variation in oxidative stress and astrocyte DNA damage in relation to Alzheimer-type pathology in the ageing brain. *Neuropathol Appl Neurobiol* 36, 25–40.

Simpson, J.E., Ince, P.G., Matthews, F.E., Shaw, P.J., Heath, P.R., Brayne, C., Garwood, C., Higginbottom, A., and Wharton, S.B. (2014). A neuronal DNA damage response is detected at the earliest stages of Alzheimer's neuropathology and correlates with

cognitive impairment in the MRC-CFAS ageing brain cohort. *Neuropathol. Appl. Neurobiol.* 1–28.

Singh, M., Jensen, M.D., Lerman, A., Kushwaha, S., Rihal, C.S., Gersh, B.J., Behfar, A., Tchkonina, T., Thomas, R.J., Lennon, R.J., et al. (2016). Effect of Low-Dose Rapamycin on Senescence Markers and Physical Functioning in Older Adults with Coronary Artery Disease: Results of a Pilot Study. *J. Frailty Aging* 5, 204–207.

Smirnova, L., Harris, G., Delp, J., Valadares, M., Pamies, D., Hogberg, H.T., Waldmann, T., Leist, M., and Hartung, T. (2015). A LUHMES 3D dopaminergic neuronal model for neurotoxicity testing allowing long-term exposure and cellular resilience analysis. *Arch. Toxicol.* 1–19.

Smith, M.J., and Koch, G.L. (1987). Differential expression of murine macrophage surface glycoprotein antigens in intracellular membranes. *J. Cell Sci.* 87 (Pt 1), 113–119.

Smith, K.D., Fu, M.A., and Brown, E.J. (2009). Tim-Tipin dysfunction creates an indispensable reliance on the ATR-Chk1 pathway for continued DNA synthesis. *J. Cell Biol.* 187, 15–23.

Sobecki, M., Mrouj, K., Camasses, A., Parisis, N., Nicolas, E., Llères, D., Gerbe, F., Prieto, S., Krasinska, L., David, A., et al. (2016). The cell proliferation antigen Ki-67 organises heterochromatin. *Elife* 5.

Sobecki, M., Mrouj, K., Colinge, J., Gerbe, F., Jay, P., Krasinska, L., Dulic, V., and Fisher, D. (2017). Cell-cycle regulation accounts for variability in Ki-67 expression levels. *Cancer Res.* 77, 2722–2734.

Soltani, M.H., Pichardo, R., Song, Z., Sangha, N., Camacho, F., Satyamoorthy, K., Sanguenza, O.P., and Setaluri, V. (2005). Microtubule-associated protein 2, a marker of neuronal differentiation, induces mitotic defects, inhibits growth of melanoma cells, and predicts metastatic potential of cutaneous melanoma. *Am. J. Pathol.* 166, 1841–1850.

Sørensen, C.S., Hansen, L.T., Dziegielewska, J., Syljuåsen, R.G., Lundin, C., Bartek, J., and Helleday, T. (2005). The cell-cycle checkpoint kinase Chk1 is required for mammalian homologous recombination repair. *Nat. Cell Biol.* 7, 195–201.

Stefanatos, R., and Sanz, A. (2017). The role of mitochondrial ROS in the aging brain. *FEBS Lett.* 1–16.

Stein, G.H., Drullinger, L.F., Soulard, A., and Dulić, V. (1999). Differential roles for cyclin-dependent kinase inhibitors p21 and p16 in the mechanisms of senescence and differentiation in human fibroblasts. *Mol. Cell. Biol.* 19, 2109–2117.

Stępkowski, T.M., Męczyńska-Wielgosz, S., and Kruszewski, M. (2017). mitoLUHMES: An Engineered Neuronal Cell Line for the Analysis of the Motility of Mitochondria. *Cell. Mol. Neurobiol.* 37, 1055–1066.

Stockert, J.C., Blázquez-Castro, A., Cañete, M., Horobin, R.W., and Villanueva, Á.

(2012). MTT assay for cell viability: Intracellular localization of the formazan product is in lipid droplets. *Acta Histochem.* *114*, 785–796.

Storer, M., Mas, A., Robert-Moreno, A., Pecoraro, M., Ortells, M.C., Di Giacomo, V., Yosef, R., Pilpel, N., Krizhanovsky, V., Sharpe, J., et al. (2013). XSenescence is a developmental mechanism that contributes to embryonic growth and patterning. *Cell* *155*.

Sudo, T., Ota, Y., Kotani, S., Nakao, M., Takami, Y., Takeda, S., and Saya, H. (2001). Activation of Cdh1-dependent APC is required for G1 cell cycle arrest and DNA damage-induced G2 checkpoint in vertebrate cells. *EMBO J.* *20*, 6499–6508.

Taddei, M.L., Giannoni, E., Raugei, G., Scacco, S., Sardanelli, A.M., Papa, S., and Chiarugi, P. (2012). Mitochondrial Oxidative Stress due to Complex I Dysfunction Promotes Fibroblast Activation and Melanoma Cell Invasiveness. *J. Signal Transduct.* *2012*, 1–10.

Takeuchi, S., Takahashi, A., Motoi, N., Yoshimoto, S., Tajima, T., Yamakoshi, K., Hirao, A., Yanagi, S., Fukami, K., Ishikawa, Y., et al. (2010). Intrinsic cooperation between p16INK4a and p21Waf1/Cip1 in the onset of cellular senescence and tumor suppression in vivo. *Cancer Res* *70*, 9381–9390.

Thornton, B.R., Ng, T.M., Matyskiela, M.E., Carroll, C.W., Morgan, D.O., and Toczyski, D.P. (2006). An architectural map of the anaphase-promoting complex. *Genes Dev.* *20*, 449–460.

Tomashevski, a, Webster, D.R., Grammas, P., Gorospe, M., and Kruman, I.I. (2010). Cyclin-C-dependent cell-cycle entry is required for activation of non-homologous end joining DNA repair in postmitotic neurons. *Cell Death Differ.* *17*, 1189–1198.

van Tonder, A., Joubert, A.M., and Cromarty, A. (2015). Limitations of the 3-(4,5-dimethylthiazol-2-yl)-2,5-diphenyl-2H-tetrazolium bromide (MTT) assay when compared to three commonly used cell enumeration assays. *BMC Res. Notes* *8*, 47.

Tong, Z. Bin, Hogberg, H., Kuo, D., Sakamuru, S., Xia, M., Smirnova, L., Hartung, T., and Gerhold, D. (2017). Characterization of three human cell line models for high-throughput neuronal cytotoxicity screening. *J. Appl. Toxicol.* *37*, 167–180.

Torp, R., Su, J.H., Deng, G.M., and Cotman, C.W. (1998). Gadd45 is induced in Alzheimer's disease, and protects against apoptosis in vitro. *Neurobiol. Dis.* *5*, 245–252.

Traxinger, K., Kelly, C., Johnson, B.A., Lyles, R.H., and Glass, J.D. (2013). Prognosis and epidemiology of amyotrophic lateral sclerosis Analysis of a clinic population, 1997-2011. *Neurol. Clin. Pract.* *3*, 313–320.

Uday Bhanu, M., Mandraju, R.K., Bhaskar, C., and Kondapi, A.K. (2010). Cultured cerebellar granule neurons as an in vitro aging model: Topoisomerase II?? as an additional biomarker in DNA repair and aging. *Toxicol. Vitro.* *24*, 1935–1945.

Vázquez, P., Arroba, A.I., Cecconi, F., de la Rosa, E.J., Boya, P., and de Pablo, F. (2012).

Atg5 and Ambra1 differentially modulate neurogenesis in neural stem cells. *Autophagy* 8, 187–199.

Venkatachalam, G., Surana, U., and Clément, M.V. (2017). Replication stress-induced endogenous DNA damage drives cellular senescence induced by a sub-lethal oxidative stress. *Nucleic Acids Res.* 45, 10564–10582.

Vodermaier, H.C., Gieffers, C., Maurer-Stroh, S., Eisenhaber, F., and Peters, J.M. (2003). TPR subunits of the anaphase-promoting complex mediate binding to the activator protein CDH1. *Curr. Biol.* 13, 1459–1468.

De Waard, M.C., Van Der Pluijm, I., Zuiderveen Borgesius, N., Comley, L.H., Haasdijk, E.D., Rijksen, Y., Ridwan, Y., Zondag, G., Hoeijmakers, J.H.J., Elgersma, Y., et al. (2010). Age-related motor neuron degeneration in DNA repair-deficient *Ercc1* mice. *Acta Neuropathol.* 120, 461–475.

Wade Harper, J., Adami, G.R., Wei, N., Keyomarsi, K., and Elledge, S.J. (1993). The p21 Cdk-interacting protein *Cip1* is a potent inhibitor of G1 cyclin-dependent kinases. *Cell* 75, 805–816.

Waga, S., Hannon, G.J., Beach, D., and Stillman, B. (1994). The p21 inhibitor of cyclin-dependent kinases controls DNA replication by interaction with PCNA. *Nature* 369, 574–578.

Wagner, B.A., Witmer, J.R., van't Erve, T.J., and Buettner, G.R. (2013). An assay for the rate of removal of extracellular hydrogen peroxide by cells. *Redox Biol.* 1, 210–217.

Walker, C., Herranz-Martin, S., Karyka, E., Liao, C., Lewis, K., Elsayed, W., Lukashchuk, V., Chiang, S.C., Ray, S., Mulcahy, P.J., et al. (2017). *C9orf72* expansion disrupts ATM-mediated chromosomal break repair. *Nat. Neurosci.* 20, 1225–1235.

Wang, Z., Wei, D., and Xiao, H. (2013). Methods of cellular senescence induction using oxidative stress. *Methods Mol. Biol.* 1048, 135–144.

Ward, I.M., and Chen, J. (2001). Histone H2AX Is Phosphorylated in an ATR-dependent Manner in Response to Replicational Stress. *J. Biol. Chem.* 276, 47759–47762.

Ward, N.P., Poff, A.M., Koutnik, A.P., and D'Agostino, D.P. (2017). Complex I inhibition augments dichloroacetate cytotoxicity through enhancing oxidative stress in VM-M3 glioblastoma cells. *PLoS One* 12.

Weng, M. (2014). The role of chromatin organization and structure in neuronal differentiation. Universität Konstanz.

Wharton, S.B., Chan, K.K., Anderson, J.R., Stoeber, K., and Williams, G.H. (2001). Replicative *Mcm2* protein as a novel proliferation marker in oligodendrogliomas and its relationship to Ki67 labelling index, histological grade and prognosis. *Neuropathol. Appl. Neurobiol.* 27, 305–313.

- Whittemore, E.R., Loo, D.T., Watt, J.A., and Cotmans, C.W. (1995). A detailed analysis of hydrogen peroxide-induced cell death in primary neuronal culture. *Neuroscience* *67*, 921–932.
- Wiedemann, F.R., Manfredi, G., Mawrin, C., Flint Beal, M., and Schon, E.A. (2002). Mitochondrial DNA and respiratory chain function in spinal cords of ALS patients. *J. Neurochem.* *80*, 616–625.
- Woodbine, L., Brunton, H., Goodarzi, A.A., Shibata, A., and Jeggo, P.A. (2011). Endogenously induced DNA double strand breaks arise in heterochromatic DNA regions and require ataxia telangiectasia mutated and Artemis for their repair. *Nucleic Acids Res.* *39*, 6986–6997.
- Wu, J., Luo, X., Thangthaeng, N., Sumien, N., Chen, Z., Rutledge, M.A., Jing, S., Forster, M.J., and Yan, L.J. (2017). Pancreatic mitochondrial complex I exhibits aberrant hyperactivity in diabetes. *Biochem. Biophys. Reports* *11*, 119–129.
- Wu, L., Timmers, C., Maiti, B., Saavedra, H.I., Sang, L., Chong, G.T., Nuckolls, F., Giangrande, P., Wright, F.A., Field, S.J., et al. (2001). The E2F1–3 transcription factors are essential for cellular proliferation. *Nature* *414*, 457–462.
- Xiang, W., Schlachetzki, J.C.M., Helling, S., Bussmann, J.C., Berlinghof, M., Schäffer, T.E., Marcus, K., Winkler, J., Klucken, J., and Becker, C.M. (2013). Oxidative stress-induced posttranslational modifications of alpha-synuclein: Specific modification of alpha-synuclein by 4-hydroxy-2-nonenal increases dopaminergic toxicity. *Mol. Cell. Neurosci.* *54*, 71–83.
- Yamamoto, H., Demura, T., Morita, M., Banker, G.A., Tanii, T., and Nakamura, S. (2012). Differential neurite outgrowth is required for axon specification by cultured hippocampal neurons. *J. Neurochem.* *123*, 904–910.
- Yegorov, Y.E., Akimov, S.S., Hass, R., Zelenin, A. V., and Prudovsky, I.A. (1998). Endogenous beta-galactosidase activity in continuously nonproliferating cells. *Exp. Cell Res.* *243*, 207–211.
- Yoneyama, M., Kikuchi, M., Natsukawa, T., Shinobu, N., Imaizumi, T., Miyagishi, M., Taira, K., Akira, S., and Fujita, T. (2004). The RNA helicase RIG-I has an essential function in double-stranded RNA-induced innate antiviral responses. *Nat. Immunol.* *5*, 730–737.
- Yoshii, A., and Constantine-Paton, M. (2014). Postsynaptic localization of PSD-95 is regulated by all three pathways downstream of TrkB signaling. *Front. Synaptic Neurosci.* *6*.
- Yoshii, A., Murata, Y., Kim, J., Zhang, C., Shokat, K.M., and Constantine-Paton, M. (2011). TrkB and Protein Kinase M {zeta} Regulate Synaptic Localization of PSD-95 in Developing Cortex. *J. Neurosci.* *31*, 11894–11904.
- Zeng, M., and Zhou, J.-N. (2008). Roles of autophagy and mTOR signaling in neuronal

differentiation of mouse neuroblastoma cells. *Cell. Signal.* 20, 659–665.

Zhang, Q., Wan, H., Huang, S., Zhang, Y., Wang, Y., Guo, X., He, P., and Zhou, M. (2014a). Critical role of RIG-I-like receptors in inflammation in chronic obstructive pulmonary disease. *Clin. Respir. J.* n/a-n/a.

Zhang, R., Poustovoitov, M. V., Ye, X., Santos, H.A., Chen, W., Daganzo, S.M., Erzberger, J.P., Serebriiskii, I.G., Canutescu, A.A., Dunbrack, R.L., et al. (2005). Formation of macroH2A-containing senescence-associated heterochromatin foci and senescence driven by ASF1a and HIRA. *Dev. Cell* 8, 19–30.

Zhang, R., Chen, W., and Adams, P.D. (2007). Molecular Dissection of Formation of Senescence-Associated Heterochromatin Foci. *Mol. Cell. Biol.* 27, 2343–2358.

Zhang, X., Yin, M., and Zhang, M. (2014b). Cell-based assays for Parkinson's disease using differentiated human LUHMES cells. *Acta Pharmacol. Sin.* 35, 945–956.

Zhang, Y., Unnikrishnan, A., Deepa, S.S., Liu, Y., Li, Y., Ikeno, Y., Sosnowska, D., Van Remmen, H., and Richardson, A. (2017). A new role for oxidative stress in aging: The accelerated aging phenotype in *Sod1* mice is correlated to increased cellular senescence. *Redox Biol.* 11, 30–37.

Zhang, Z., Yang, J., Kong, E.H., Chao, W.C.H., Morris, E.P., da Fonseca, P.C.A., and Barford, D. (2013). Recombinant expression, reconstitution and structure of human anaphase-promoting complex (APC/C). *Biochem. J.* 449, 365–371.

Zheng, S., Gray, E.E., Chawla, G., Porse, B.T., O'Dell, T.J., and Black, D.L. (2012). PSD-95 is post-transcriptionally repressed during early neural development by PTBP1 and PTBP2. *Nat. Neurosci.* 15, 381–388.

Zou, L. (2003). Sensing DNA Damage Through ATRIP Recognition of RPA-ssDNA Complexes. *Science* (80-.). 300, 1542–1548.

Appendices

Appendix A. Solutions

All chemicals were obtained from Sigma-Aldrich (St Louis, MO, USA) unless stated.

BSA Blocking solution for immunocytochemistry

3% Bovine serum albumin, lyophilized powder, crystallized, $\geq 98.0\%$

0.01% Tween 20

1x PBS

Blocking solution for immunohistochemistry

1.5% (v/v) normal goat serum or 15% (v/v) normal horse serum (Vector Laboratories UK, antibody dependent)

50mM TBS

DEPC water

0.1% Diethylpyrocarbonate (DEPC)

1 L distilled water

3% H₂O₂/methanol solution

1% (v/v) H₂O₂

50mM Methanol

Hoechst staining solution

10 mg/ml Bisbenzimidazole H 33342 trihydrochloride

Distilled water

Hydrogen peroxide solutions

0.1 M 30% w/w hydrogen peroxide (H₂O₂)

1x sterile PBS

Ethylenediaminetetraacetic acid (EDTA) (x1) pH 8

10 mM Tris-base

1.26 mM EDTA

0.1% Tween-20

EThD-1 solution

2 μ M Ethidium homodimer, suitable for fluorescence, ~90%

Sterile distilled water

MTT solution

5 mg/ml 3-(4,5- Dimethyl-2- thiazolyl)-2,5- diphenyl-2H- tetrazolium bromide

1x PBS

Nuclear Fast Red

0.1% nuclear fast red,

5% aluminium sulphate

Deionized water

4% Paraformaldehyde

95% powder paraformaldehyde

1x PBS

Permeabilising Solution

0.03% Triton – X100

1x PBS

Poly-L-ornithine and fibronectin coating solution

50 μ g/ml poly-L-ornithine hydrobromide

1 μ g/ml fibronectin from human plasma

Sterile distilled water

50mM Phosphate buffered saline (PBS) pH 7.4

3.2mM Na₂HPO₄

0.5mM KH₂PO₄

1.3mM KCl

135mM NaCl, pH 7.4

SDS/DMF solution

20% Sodium dodecyl sulphate, purity >99% (SDS; Melford Laboratories Ltd, UK)

50% N, N-dimethylformamide, pH 4.7 (DMF; Acros Organics, NJ, USA)

Stopping solution (clearance assays)

20 ml HBSS

20 µl 1 M 4-(2- hydroxyethyl)-1- piperazineethansulfonic acid (HEPES), pH7.2-7.5

10 mg sodium bicarbonate (NaHCO₃, 3mM)

5 mg para-hydrophenilacetic acid (pHPA, 0.8mM)

2 mg horseradish peroxidase (HRP)

50 mM Tris-buffered saline (TBS) pH 7.6

50 mM Tris

150 mM NaCl

TE buffer, pH 8

10 mM Tris,

0.1 mM EDTA

Tetracycline

1 µg/ml tetracycline

Sterile distilled water

Trisodium Citrate buffer (TSC) pH 6.5

3 g of Na₃C₆H₅O₇

Deionized water (1 L)

Appendix B. Ethical approval form for the current study.

FOR SBTB OFFICE USE

Project no. 14/001

**AUTHORISATION TO USE TISSUE RESOURCE FROM THE
SHEFFIELD BRAIN TISSUE BANK (SBTB)**

FOLLOWING CONSIDERATION BY THE SBTB MANAGEMENT BOARD:

Proposed Study Title

**NEURONAL SENESCENCE AS A CONTRIBUTOR TO NEURODEGENERATION
IN MOTOR NEURONE DISEASE**

SECTION A: PROJECT STAFF DETAILS

Head of proposed study

Title DR Initials SB

Surname WHARTON

Position READER

Organisation SHEFFIELD UNIVERSITY

Address Sheffield Institute for Translational Neuroscience
University of Sheffield
385A Glossop Road
Sheffield S10 2HQ

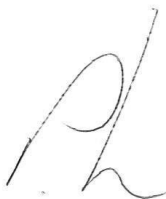
Telephone No 0114 22 22235 Fax No 0114 22 22290

Email s.wharton@sheffield.ac.uk.

SBTB PROJECT REQUEST NUMBER: 14/001

This project was reviewed by the SBTB Management Board and approval to release tissue under REC **08/MRE00/103** was granted.

Professor P G Ince
Director SBTB



Date: 28 January 2014

SBTB tissue authority / ver1: 01/02/2008

Appendix C.

The lists of dysregulated transcripts obtained from the LUHMES microarray analysis are attached in the electronic version of this work under the name “LUHMES.microarray.data”.

The list of dysregulated transcripts obtained from the microarray analysis on the FACx neurones from ALS/MND and control donors is attached in the electronic version of this work under the name “ALS/MND.microarray.data”.